VOL. 696 NO. 1 7 APRIL 1995

JOURNAL OF CHROMATOGRAPHY A

INCLUDING ELECTROPHORESIS AND OTHER SEPARATION METHODS

ELSEVIER

JOURNAL OF CHROMATOGRAPHY A

INCLUDING ELECTROPHORESIS AND OTHER SEPARATION METHODS

Scope. The *Journal of Chromatography A* publishes papers on all aspects of **chromatography, electrophoresis** and related methods. Contributions consist mainly of research papers dealing with chromatographic theory, instrumental developments and their applications. In the *Symposium volumes*, which are under separate editorship, proceedings of symposia on chromatography, electrophoresis and related methods are published. *Journal of Chromatography B: Biomedical Applications* —This journal, which is under separate editorship, deals with the following aspects: developments in and applications of chromatographic and electrophoretic techniques related to clinical diagnosis or alterations during medical treatment; screening and profiling of body fluids or tissues related to the analysis of active substances and to metabolic disorders; drug level monitoring and pharmacokinetic studies; clinical toxicology; forensic medicine; veterinary medicine; occupational medicine; results from basic medical research with direct consequences in clinical practice.

Submission of Papers. The preferred medium of submission is on disk with accompanying manuscript (see *Electronic manuscripts* in the Instructions to Authors, which can be obtained from the publisher, Elsevier Science B.V., P.O. Box 330, 1000 AH Amsterdam, Netherlands). Manuscripts (in English; *four* copies are required) should be submitted to: Editorial Office of *Journal of Chromatography A*, P.O. Box 681, 1000 AR Amsterdam, Netherlands, Telefax (+31-20) 485 2304, or to: The Editor of *Journal of Chromatography B: Biomedical Applications*, P.O. Box 681, 1000 AR Amsterdam, Netherlands. Review articles are invited or proposed in writing to the Editors who welcome suggestions for subjects. An outline of the proposed review should first be forwarded to the Editors for preliminary discussion prior to preparation. Submission of an article is understood to imply that the article is original and unpublished and is not being considered for publication elsewhere. For copyright regulations, see below.

Publication information. *Journal of Chromatography A* (ISSN 0021-9673): for 1995 Vols. 683–714 are scheduled for publication. *Journal of Chromatography B: Biomedical Applications* (ISSN 0378-4347): for 1995 Vols. 663–674 are scheduled for publication. Subscription prices for *Journal of Chromatography A*, *Journal of Chromatography B: Biomedical Applications* or a combined subscription are available upon request from the publisher. Subscriptions are accepted on a prepaid basis only and are entered on a calendar year basis. Issues are sent by surface mail except to the following countries where air delivery via SAL is ensured: Argentina, Australia, Brazil, Canada, China, Hong Kong, India, Israel, Japan, Malaysia, Mexico, New Zealand, Pakistan, Singapore, South Africa, South Korea, Taiwan, Thailand, USA. For all other countries airmail rates are available upon request. Claims for missing issues must be made within six months of our publication (mailing) date. Please address all your requests regarding orders and subscription queries to: Elsevier Science B.V., Journal Department, P.O. Box 211, 1000 AE Amsterdam, Netherlands. Tel.: (+31-20) 485 3642; Fax: (+31-20) 485 3598. Customers in the USA and Canada wishing information on this and other Elsevier journals, please contact Journal Information Center, Elsevier Science Inc., 655 Avenue of the Americas, New York, NY 10010, USA, Tel. (+1-212) 633 3750, Telefax (+1-212) 633 3764.

Abstracts/Contents Lists published in Analytical Abstracts, Biochemical Abstracts, Biological Abstracts, Chemical Abstracts, Chemical Titles, Chromatography Abstracts, Current Awareness in Biological Sciences (CABS), Current Contents/Life Sciences, Current Contents/Physical, Chemical & Earth Sciences, Deep-Sea Research/Part B: Oceanographic Literature Review, Excerpta Medica, Index Medicus, Mass Spectrometry Bulletin, PASCAL-CNRS, Referativnyi Zhurnal, Research Alert and Science Citation Index.

US Mailing Notice. *Journal of Chromatography A* (ISSN 0021-9673) is published weekly (total 52 issues) by Elsevier Science B.V., (Sara Burgerhartstraat 25, P.O. Box 211, 1000 AE Amsterdam, Netherlands). Annual subscription price in the USA US$ 5389.00 (US$ price valid in North, Central and South America only) including air speed delivery. Second class postage paid at Jamaica, NY 11431. **USA POSTMASTERS**: Send address changes to *Journal of Chromatography A*, Publications Expediting, Inc., 200 Meacham Avenue, Elmont, NY 11003. Airfreight and mailing in the USA by Publications Expediting.

See inside back cover for Publication Schedule, Information for Authors and information on Advertisements.

0021-9673/95/$09.50

Printed in the Netherlands

CONTENTS

(Abstracts/Contents Lists published in Analytical Abstracts, Biochemical Abstracts, Biological Abstracts, Chemical Abstracts, Chemical Titles, Chromatography Abstracts, Current Awareness in Biological Sciences (CABS), Current Contents/Life Sciences, Current Contents/Physical, Chemical & Earth Sciences, Deep-Sea Research/Part B: Oceanographic Literature Review, Excerpta Medica, Index Medicus, Mass Spectrometry Bulletin, PASCAL-CNRS, Referativnyi Zhurnal, Research Alert and Science Citation Index)

REGULAR PAPERS

Column Liquid Chromatography

Gas Chromatography

Planar Chromatography

(Continued overleaf)

Contents (continued)

JOURNAL OF CHROMATOGRAPHY A

VOL. 696 (1995)

JOURNAL OF CHROMATOGRAPHY A

INCLUDING ELECTROPHORESIS AND OTHER SEPARATION METHODS

ELSEVIER

Amsterdam – Lausanne – New York – Oxford – Shannon – Tokyo

J. Chromatogr. A, Vol. 696 (1995)

0021-9673/95/$09.50

Printed in the Netherlands

ELSEVIER

Journal of Chromatography A, 696 (1995) 1–18

JOURNAL OF CHROMATOGRAPHY A

NMR imaging of the chromatographic process Migration and separation of bands of gadolinium chelates

Ulrich Tallarek, Edgar Baumeister, Klaus Albert, Ernst Bayer, Georges Guiochon*

Institut für Organische Chemie, Universität Tübingen, Auf der Morgenstelle 18, D-72076 Tübingen, Germany

First received 27 September 1994; revised manuscript received 13 December 1994; accepted 14 December 1994

Abstract

The presence of gadolinium nuclei accelerates the relaxation of protons in their neighborhood. Using the imaging techniques of nuclear magnetic resonance developed for medical diagnosis, it is possible to observe the chromatographic bands of Gadolinium compounds which appear in shades of grey turning lighter with increasing gadolinium concentration. The existence of unexpectedly wide distributions of the local mobile phase velocity and the local height equivalent to a theoretical plate in an efficient chromatographic column is illustrated. The formation and resorption of fissured and/or compact zones in the column where the external porosity appears lower or higher than average is documented for the first time.

1. Introduction

Liquid chromatography is the most important method of laboratory-scale separations, whether for analytical or preparative purposes, because of the flexibility of this technique, the number of its applications and the variety of fields where it is encountered. Nevertheless, the structure of the column packing and the relationship between the column performance and this structure have been poorly studied and is still generally unknown. From a theoretical viewpoint, Giddings [1] drew the attention on the importance of the radial homogeneity of the column height equivalent to a theoretical plate (HETP) and the very harsh penalty in terms of efficiency loss caused by any long distance fluctuation of the local mobile phase velocity. Recently, Yun and Guiochon [2] have shown that considerable band spreading should arise in non-linear chromatography if even minor deviations from piston flow take place across the column and if the velocity at the column axis differs from the velocity at the column wall by a few percent.

Long ago, Knox and co-workers [3–5] studied the radial distribution of mobile phase flow velocity and local HETP in analytical columns. He showed that there are important, systematic variations. The mobile phase is somewhat faster along the column wall than in the axis, probably because dry packing causes a radial discrimination of the particles, with the larger falling closer to the wall. He also reported the existence of a region extending about 30 particle diameters from the wall, which is less homogeneous and exhibits a markedly lower efficiency. These re-

* Corresponding author. Present address: Department of Chemistry, University of Tennessee, Knoxville, TN 37996-1600, USA.

0021-9673/95/$09.50
SSDI 0021-9673(94)01231-8

sults were confirmed by Eon [6] who determined separately the axial and radial dispersion coefficients and showed that these parameters vary to a large extent across the column. The influence of bed homogeneity together with the problem of radial distribution of the sample at column inlet has been discussed by Skea [7] but without new experimental data. Recently, Baur et al. [8] and Farkas et al. [9] also obtained similar results confirming systematic variations of the flow velocity and local HETP across LC columns. However, using slurry-packed columns, they found the mobile phase velocity to be lower at the wall than in the center, by up to 8% [9], with a ridge of maximum velocity at about 2/3 of the radius from the center. The local HETP at the wall is nearly three times as high as that in the center. These results are in agreement with the conclusions of investigations of packed beds used as heat exchangers in chemical engineering [10,11], where the velocity of the stream is found to be significantly higher at the wall. They are also in agreement with observations which were made in preparative gas chromatography by Huyten et al. [12] and were explained theoretically and experimentally by Giddings and Fuller [13], documenting the particle size segregation in dry packing for the first time.

The problem has been generally ignored by the analytical community, as illustrated by the small number of relevant references. On the one hand, columns having reduced plate heights in the range between two and three are routinely produced and there is a widespread belief, albeit one unsupported by any fundamental or practical tenet, that 2 is a magic threshold and that it would not be possible to prepare columns with an HETP below twice the average particle diameter. As a matter of fact, values as low as 0.6 have been demonstrated by Knox and Parcher [3]. Furthermore, improvements on the performance of standard columns does not appear to be a high priority. On the other hand, there is no simple conceptual framework for the investigation of the structure of column packing and experimental studies require rather complex determinations of local concentrations which cannot be made using standard LC instrumentation. Previous measurements were made at the column exit, using electrochemical methods and very fine electrodes [3–6,8,9]. Using current techniques, it is difficult to acquire simultaneously measurements of the local concentrations of an analyte in a sufficiently large number of points of the column outlet cross-section to acquire the detailed representation needed of the distribution of the average residence times of the sample molecules in the column and of the variances of this distribution.

Although the importance of column homogeneity and packing density distribution appears to be minor in modern analytical HPLC, the problem is quite important in the preparative-scale applications of the method. This is essentially due to the much larger size of the column used, the possibility of large-scale fluctuations of the packing density which cause excessive losses in column performance, the direct relationship between column efficiency, recovery yield and cost, and the preeminent importance of economic considerations in the optimization of the process. However, if work is in progress on the assessment of the relationships between band profiles in non-linear chromatography and the velocity distribution inside the column [2,14], there are no data available on the distribution of packing density in large preparative columns, although the importance of achieving near plug flow has been stressed [7,15,16]. A discussion of the possible mechanisms through which non-plug flow could affect band profiles in the column and their warping or which could explain the injection of non-planar bands in a column [4,17] has been given by Skea [7]. The examination of colored bands immobilized inside columns after a certain time [15,18] provides information regarding only the band boundary and a few selected sections. It fails to provide a comprehensive picture of the band profile across the whole column. Other invasive approaches, such as the cutting of columns [19] or the insertion of thermocouples [20] has given only limited insights because of the very low spacial resolution of these techniques.

Clearly, progress in this area requires the use of more powerful investigative methods. The techniques developed for nuclear magnetic resonance imaging (NMR imaging, MRI) [21–23]

offer considerable potential for detailed investigations of local column properties [24] or for the monitoring in real time of the migration and dispersion of a band in a chromatographic column [25,26]. During the last decade, NMR imaging has become a powerful tool for medical diagnosis [27] and is now used also for non-medical imaging applications [28]. Combining the use of conventional NMR spectroscopy and of a magnetic field gradient this method yields images of any desired volume element or slide in a non-metallic object, be it a human body or the packing of a chromatographic column, provided the column tubing be non-metallic and a sufficient contrast can be achieved. In the present paper, we report on the use of a rapid imaging sequence (fast low-angle shot or FLASH) to monitor continuously the chromatographic separation of a mixture of gadolinium complexes. The same method permits the investigation of phenomena related to the introduction of the sample band inside the column.

We present here results obtained under non-satisfactory chromatographic conditions, in cases where the injection was not performed properly, the inlet filter was dirty, or the column inlet was damaged. This is more illustrative of the chromatographic process and of the possibilities to understand it better that are offered by the in situ, real-time imaging of the bands migrating along the column than results obtained under conditions of nominal performance [23]. The results reported here will clarify some of the reasons for the poor band profiles previously reported [22]. They should explain the importance of some aspects of chromatographic instrumentation which has been felt for a long time by chromatographers but have never been completely understood.

2. Theory of the method

2.1. Principle

The idea of using magnetic field gradient to enscribe in data obtained by NMR spectroscopy a code giving their location is nearly as old as NMR spectroscopy itself [29,30]. It is only in the 1970s, however, that Damadian [31], Lauterbur [32] and Mansfield and Grannell [33] independently showed how to operate space-resolved NMR spectroscopy. To the main, homogeneous, static magnetic field, $\boldsymbol{B}_0$, a much smaller, time-dependent linear gradient field, $\boldsymbol{G}(\boldsymbol{r},t)$, is superimposed. A proton resonates at the Larmor frequency and we have the following relationship between this frequency and the location [34–37]

$$\boldsymbol{B}(\boldsymbol{r},t) = \boldsymbol{B}_0 + \boldsymbol{G}(\boldsymbol{r},t) \tag{1a}$$

$$\omega(\boldsymbol{r},t) = \gamma\boldsymbol{B}(\boldsymbol{r},t) = \omega_0 + \gamma\boldsymbol{G}\boldsymbol{r} \tag{1b}$$

This last equation expresses the fundamental principle of NMR Imaging. It is illustrated in Fig. 1 in the case of a one-dimensional gradient, for the sake of simplicity [38]. $\boldsymbol{G}$ is the gradient of the pulsed gradient field, $\boldsymbol{G}(\boldsymbol{r},t)$, parallel to the main magnetic field [34] and γ is the gyromagnetic ratio, specific of the nuclei considered [$\gamma(^1\mathrm{H}) = 2.675 \cdot 10^8\ \mathrm{T}^{-1}\ \mathrm{s}^{-1}$]. $\boldsymbol{G}$ has for its components $G_x = \partial B_z/\partial x$, $G_y = \partial B_z/\partial y$ and $G_z = \partial B_z/\partial z$. As a consequence, the frequency spreads, hence the spatial resolution achieved are directly proportional to the pulse gradient strength and to the dimension of the object, with $\Delta\omega = \gamma\boldsymbol{G} \cdot \Delta\boldsymbol{r}$.

The goal in imaging methods is to derive from the signal acquired the distribution of the structural density of the object, $\rho(\boldsymbol{r})$. In NMR imaging this function is the local nuclear spin density. The basic imaging scheme is illustrated in Fig. 2 [39]. It is obvious from this figure that the signal, $S(\boldsymbol{k})$ where $\boldsymbol{k}$ is the reciprocal space vector, and the local spin density, $\rho(\boldsymbol{r})$, are related by Fourier transform and inverse Fourier transform. The concept of reciprocal space vector in MRI was introduced by Mansfield and Grannell [40,41]. It is related to the magnetic field gradient by

$$\boldsymbol{k} = (2\pi)^{-1}\gamma\boldsymbol{G}t \tag{2}$$

and

$$S(t) = \iiint(\boldsymbol{r})\ \exp\ (i\gamma\boldsymbol{G}\boldsymbol{r}t)\mathrm{d}\boldsymbol{r} \tag{3}$$

Thus, both $\boldsymbol{G}$ and t are involved in the study of the reciprocal space or $\boldsymbol{k}$ space. $\boldsymbol{G}$ determines also the direction that is followed in any move-

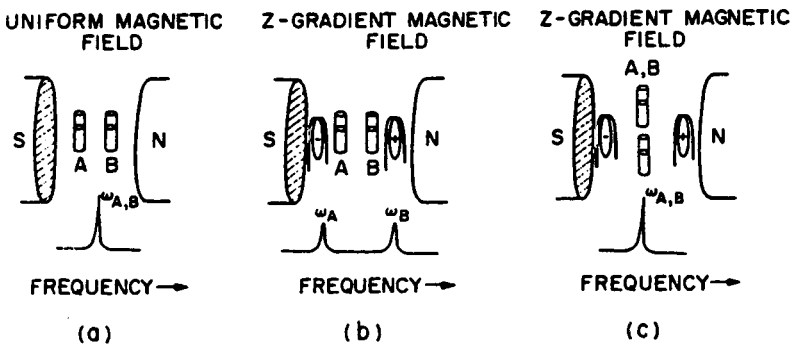

Fig. 1. Resonance frequencies of water in two capillaries placed in a magnetic field. (a) Uniform magnetic field, $\omega_A = \omega_B = \gamma B_0$. (b, c) Linear field gradient in the main field axis, $\omega_A = \gamma(B_0 + z_A G_z)$, $\omega_B = \gamma(B_0 + z_B G_z)$ and $\Delta\omega = \gamma(z_A - z_B)G_z$ [38]. The Fourier transform of the FID gives a one-dimensional projection of the integral spin density on a line parallel to the direction of the applied gradient.

ment through the k space. For reconstruction of the image, the k space is sampled systematically by varying the magnitude of the magnetic field gradient or by moving in time [37,42–44]. A Fourier transform is then performed on the data acquired. In practice, this is done by sampling the NMR signal [i.e., the free induction decay (FID) or an echo of the spins] in the time domain because the reciprocal space and the image space correspond to the time and frequency domains, respectively. By choosing the direction of the magnetic field gradient, it is possible to select the slice of the column which will be imaged.

2.2. Implementation

The visualization of the chromatographic process requires a contrast between the region of the column where the band is located and the upstream and downstream regions where the solute concentration is negligibly small. Several approaches are possible. For example, we could observe in ^{19}F NMR bands of bis-trifluorobenzene derivatives eluted in conventional reversed-phase chromatography [45]. The fluorine signal would give the required information. The converse approach, the elution of an alkyl derivative by a fluorinated solvent would be more difficult to implement, since it would require the use of a non-protonated adsorbent. The chemical shift of ^1H is insufficient to permit both the rejection of the signals for the uninteresting protons and a satisfactory signal/noise ratio. We decided for a different approach, permitting both the use of the ^1H NMR signal and of conventional chromatographic conditions. It is well known that the gadolinium ion, Gd^{3+}, considerably reduces the

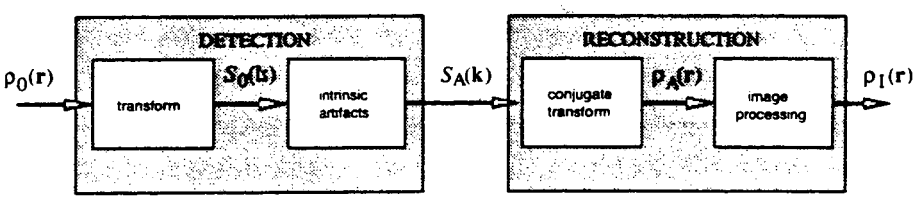

$$S(\mathbf{k}) = \iiint \rho(\mathbf{r}) \exp[i2\pi\mathbf{k}\cdot\mathbf{r}]\, d\mathbf{r} \qquad \rho(\mathbf{r}) = \iiint S(\mathbf{k}) \exp[-i2\pi\mathbf{k}\cdot\mathbf{r}]\, d\mathbf{k}$$

Fig. 2. Schematic representation of the imaging process [39].

relaxation times of the nearby protons. This ion has seven unshared electrons, is in the configuration f^7 ($\mu_{eff} = 8.0$ B.M. [46]), and gives strong electron–nucleus dipole–dipole interactions [47–51]. Thus, Gd^{3+} or its complexes can be visualized indirectly by the relaxation time differences of the mobile phase protons which they induce locally. One advantage of the approach is that it is possible to find different Gd^{3+} chelates which can be separated by chromatography and yet their response factors will be the same, allowing for the direct use of relative response in our investigations.

3. Experimental

3.1. Liquid chromatography

A Merck (Darmstadt, Germany) Superformance glass column (2.6 cm I.D. × total length 50 cm with fittings and connecting tubes, bed length, 15 cm) was used. The column was packed with LiChrospher RP-18 (Merck), 15 μm average particle size. The bed packing was achieved by permitting a concentrated slurry of the adsorbent to settle in the column over a period of several days. The actual bed length was only 13.5 cm. The system was completed by a SYKAM S 1100 pump (Gilching, Germany), a Rheodyne sampling valve (Cotati, CA, USA) and a Linear UVIS 204 detector (Reno, NV, USA). These devices were connected to the column by plastic tubing since the amount of non-magnetic metal brought inside the scanner must be small and located as far from the column as possible, not to perturb the image. Because the pump and the sampling valve are weakly magnetic, they have to be placed far enough from the column, at ca. 1.5 m. A 0.8 mm I.D. PTFE tubing was used for the connection. This causes a significant extra-column contribution to band broadening. The mobile phase was a buffer solution (see below). Neither the water used nor the buffer solution were filtered before use, contrary to standard analytical practice, which explains some of the illustrative results.

Chromatograms obtained under (i) conventional analytical conditions (connecting tubes having the same diameter but 30 cm long) before the beginning of the imaging experiments, (ii) after the second series of imaging experiments and (iii) after repair of the column, respectively, are shown in Fig. 3. They illustrate the variation in performance and should be compared to the images of the band discussed later. Note that the reduced HETP of the last peak of the chromatogram, *n*-butylbenzene, is 2.1, a value which is usually considered to be very good, in Fig. 3a, 12.0 in Fig. 3b, and 5.1 in Fig. 3c.

3.2. NMR system

The column was first placed inside an 8 cm I.D. solenoid coil (transmitter/receiver coil length, 10 cm) and this assembly was positioned horizontally in the middle of the superconducting whole body imager (Magnetom 63; Siemens, Erlangen, Germany) of the University of Tübingen. This imager operates at 1.5 T, corresponding to a frequency of approximately 63.6 MHz for proton imaging. The gradient system consists of three mutually orthogonal coil groups that can produce any desired gradient, in any direction respective to the axis of the main magnetic field. The entire system is schematized in Fig. 4. The maximum gradient strength is 9.6 mT/m. The column and the solenoid which surrounds it are positioned orthogonal to the tunnel axis, i.e., to the direction of the main magnetic field. The system permits the acquisition of images of the concentration distribution of the gadolinium concentration in any planar direction. For example, it is possible to scan slices and measure the distribution of Gd concentration in any section of the column parallel or perpendicular to its axis. The direction of this plane is chosen by setting the magnetic field gradient in the appropriate direction. The image can be updated every 7 s. In most cases (and unless stated otherwise in the figure caption), the image of the column cross-section (26 × 135 mm) is included in a 166 × 166 mm field of view, given as a 256 × 256 matrix Thus, the individual pixel corresponds to a rectangle of column packing having 0.65 × 0.61 mm. In the construction of the image, the signal is averaged over a thickness of ca 1 mm.

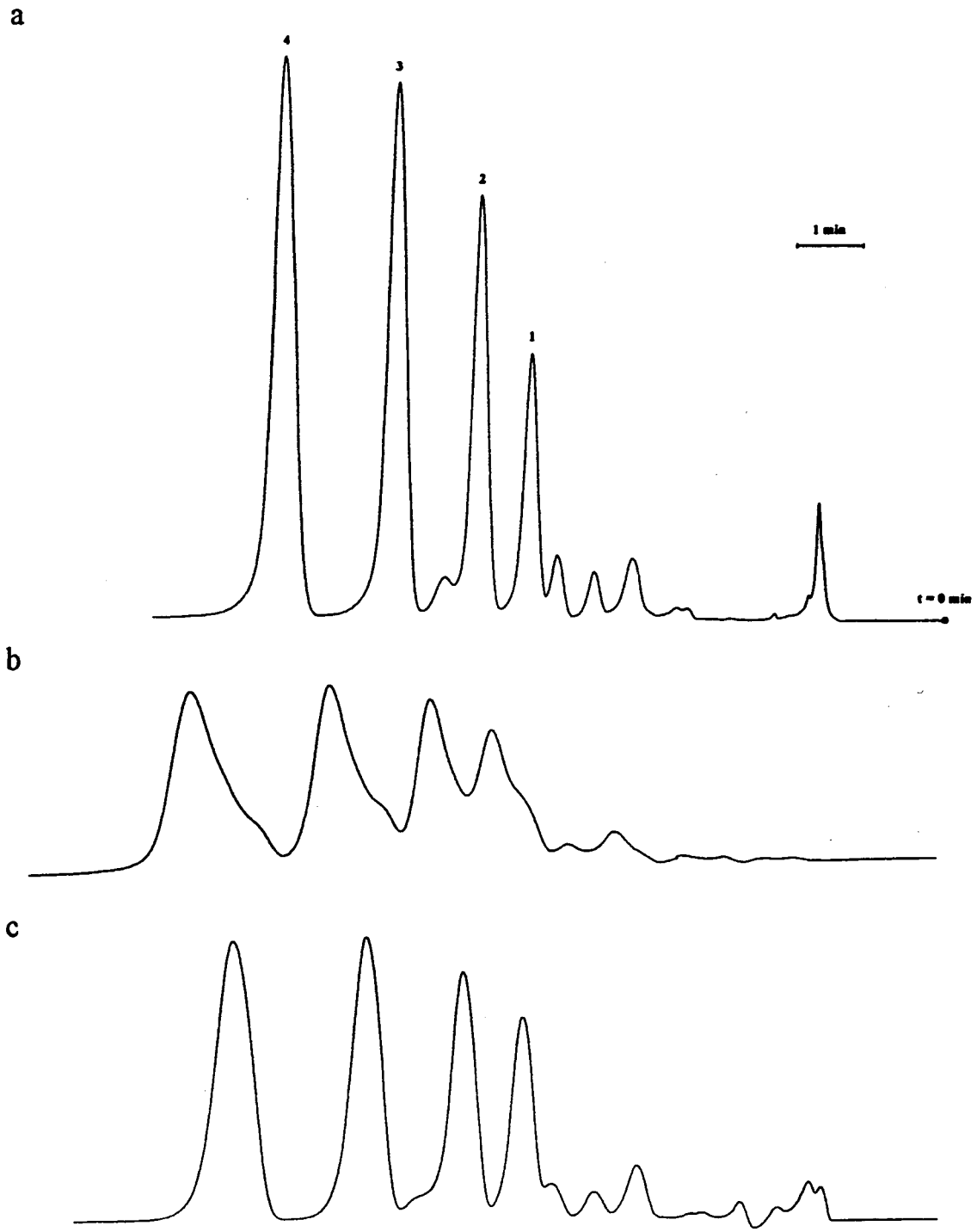

Fig. 3. Chromatogram of a test mixture. Peaks: 1 = toluene; 2 = ethylbenzene; 3 = *n*-propylbenzene; 4 = *n*-butylbenzene. (a) Beginning of the imaging experiments; (b) after the second series of imaging experiments (i.e., between Figs. 18 and 19); (c) after repair of the column. Mobile phase, water–acetonitrile (15:85), 6 ml/min, UV detection at 254 nm.

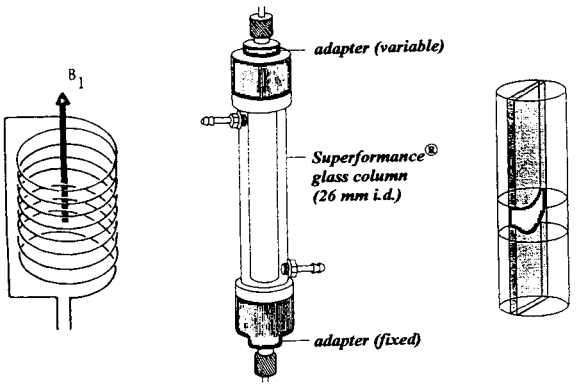

Fig. 4. Schematic representation of the imaging of a band in the chromatographic column. Left, transmitter/receiver solenoid inside which is located the column. Center, preparative glass column. Right, schematic illustration of the concentration distribution of the gadolinium complex in an axial slice of the column bed selected by an appropriate choice of the magnetic field gradient.

One of the difficulties of the experiment is the non-linear behavior of the signal which is not proportional to the gadolinium concentration. A calibration curve of ^{57}Gd in pure water is shown in Fig. 5 [52]. Above a certain concentration (approximately 1 mM), the response decreases with increasing concentration and beyond about 6 mM, it is lower than with no gadolinium. As a consequence, the regions where there is no gadolinium appear dark grey. Certain regions of the column may appear black because the local concentration of gadolinium is too high. This situation is avoided as much as possible by using small samples.

3.3. Choice of the analytes

The signal intensity of the pixels of the images obtained for different column slices depend on the spin-lattice relaxation times, T_1, and the spin–spin relaxation times, T_2, the spin density, the flow velocity, the intensity of some diffusion phenomena and the chemical shift of the nuclei present [53]. Local differences between the values of these parameters cause image contrast under selected conditions. Arranging for the proper contrast permits the acquisition of certain selected information. The visualization of a chromatographic separation requires the use of a soluble, stable compound.

Gadolinium gives stable complexes of Gd^{3+} with various organic ligands [54,55]. These chelates were used for the visualization of the chromatographic process as explained in a previous section. They were separated by reversed-phase ion-pair chromatography, a mode which permits an easy selection of experimental conditions allowing suitable retention of these chelates as anions [56]. The mobile phase was a

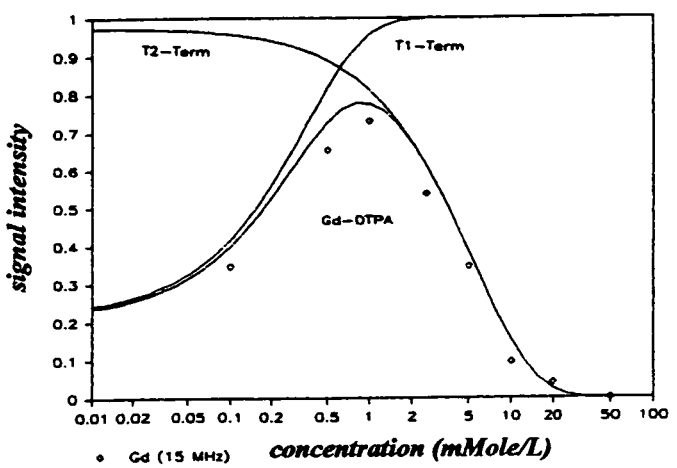

Fig. 5. Calibration curve. Plot of the signal observed versus the concentration in Gadolinium. Solid line, calculated response. Symbols, experimental data.

solution of water and acetonitrile (85:15), containing 5 m*M* KH_2PO_4 and 4 m*M* *n*-octylamine, at a pH of 5. Chelates of ethylenediaminetetraacetic acid (EDTA), *trans*-1,2-cyclohexanediaminetetraacetic acid (CDTA), ethyleneglycolbis(aminoethyl)tetraacetic acid (EGTA) and diethylenetriaminepentaacetic acid (DTPA) were prepared following classical procedures. Their structures are shown in Fig. 6. At pH 5, these complexes are completely deprotonated [57–59] and exist in solution as the anions $Gd(EDTA)^-$, $Gd(CDTA)^-$, $Gd(EGTA)^-$ and $Gd(DTPA)^{2-}$, respectively.

Saturated solutions of the complexes were freshly prepared and filtered before use. They were mixed and diluted to the proper concentration immediately prior to the experiments.

4. Results and discussion

Fig. 7 is an attempt to represent a three-dimensional image of a chelate band [60]. It shows a series of images giving the distribution of Gd concentration in 26 horizontal planes equally spaced. The distance between two successive such planes is approximately 1 mm. The images 1 and 26 correspond approximately to the planes tangent to the top and bottom of the column. Images 13 and 14 are 0.5 mm above and below the column axis, respectively. The combination of these images permits a reconstitution of the three-dimensional concentration distribution in the band at a migration distance of approximately 45 mm (see Fig. 4). These images were obtained with a rapid imaging sequence

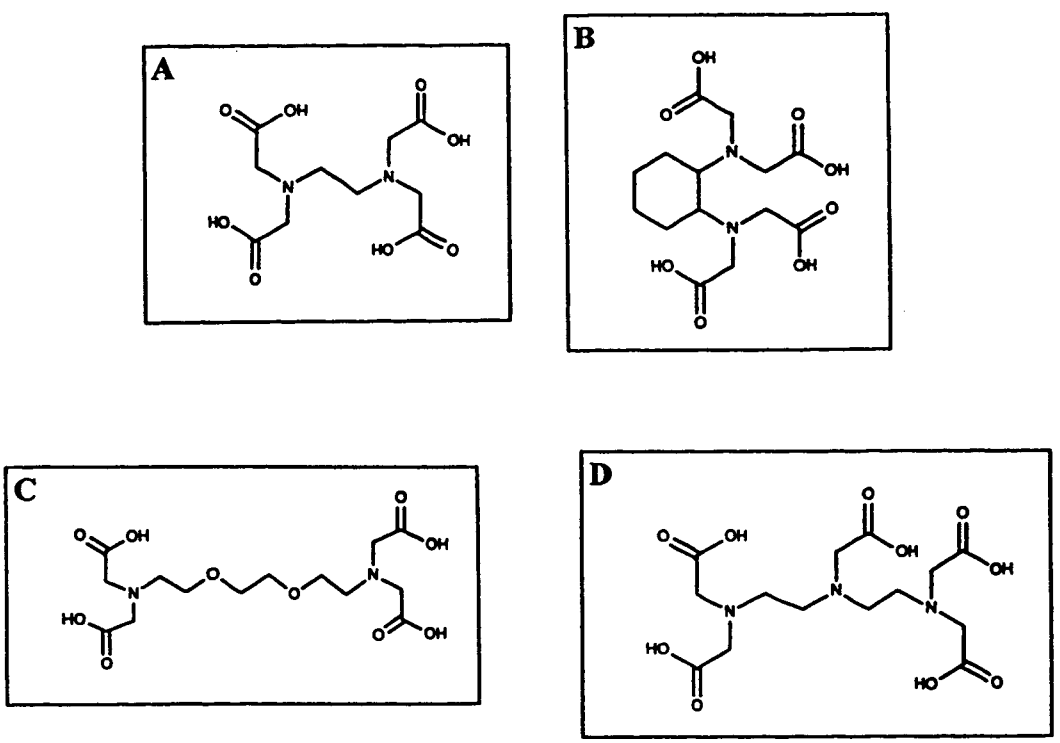

Fig. 6. Structures of the organic ligands of the gadolinium chelates used. (A) Ethylenediaminetetraacetic acid (EDTA); (B) *trans*-1,2-cyclohexanediaminetetraacetic acid (CDTA); (C) ethyleneglycolbis(aminoethyl)tetraacetic acid (EGTA); (D) diethylenetriaminepentaacetic acid (DTPA).

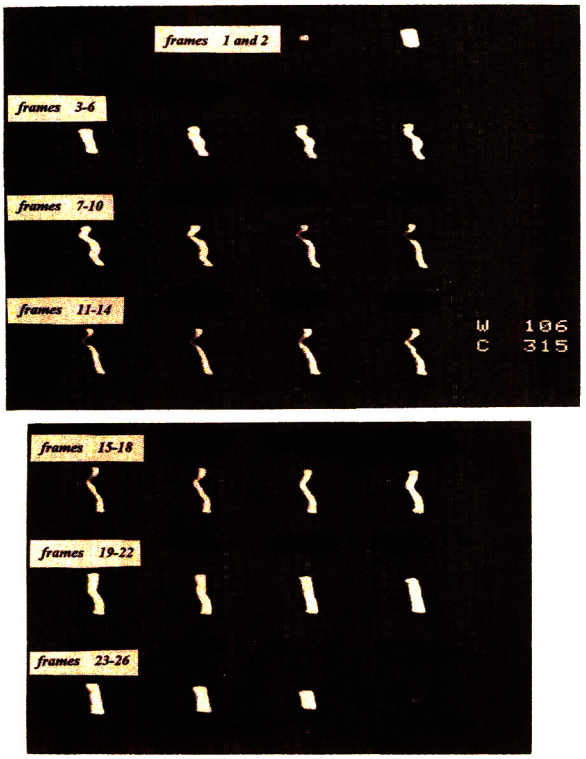

Fig. 7. Series of three-dimensional FLASH images [50] of a band of Gd(DTPA) in the chromatographic column. These images give the three-dimensional distribution of Gd concentration at a given time, corresponding to a migration distance of approximately 45 mm. Flip angle (FA), 90°; repetition time (T_R), 0.04 s; echo time (T_E), 10 ms; slice thickness (SL), 1 mm; matrix size, 128 × 128; flow from left to right. The 26 images correspond to the concentration distribution in as many sections of the column by horizontal planes (i.e., parallel to the column axis).

(FLASH [61,62]), using short repetition times (0.04 s). This procedure gives signals only for protons which have relaxed sufficiently during the repetition time, i.e., those which are in the vicinity of Gd atoms: the relaxation rate enhancement is proportional to R^{-6}, with R distance between Gd and proton. Thus, the chelates are indirectly visualized as bright zones (T_1 contrast).

We note in Fig. 7 that the pattern of the concentration distribution is far from uniform. Since injection was done with a sampling valve, its front should be flat. The important deviations from a planar distribution observed in images 6–19 suggest a strong gradient of migration velocity across the column. This, in turn, can be explained by a non-homogeneous distribution of the retention factors or of the mobile phase velocity (or both). The latter is the more important, as local fluctuations of the packing density of the column result in larger fluctuations of the local external column porosity, hence much larger fluctuations of the flow velocity, than of the retention factor. The retention factor is proportional to the local density of stationary phase, $(1-\epsilon_e)\rho_a$, where ϵ_e is the external porosity (ratio of the volume available to the mobile phase stream around the particles to the geometrical volume of the column, of the order of 0.35 to 0.40) and ρ_a is the apparent density of the particles of adsorbent. A fluctuation of packing density resulting in a relative change of the porosity $\Delta\epsilon_e/\epsilon_e$ will cause a relative change in

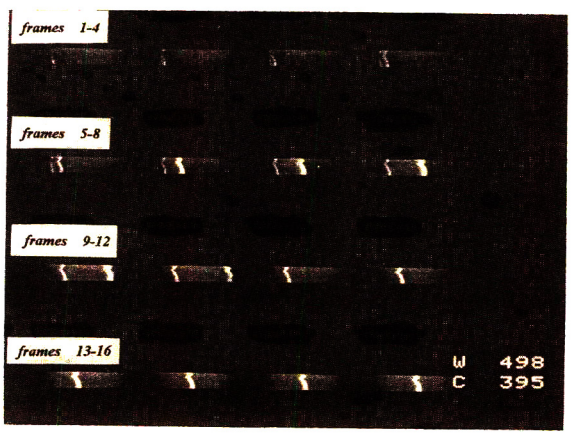

Fig. 8. Two-dimensional FLASH images from the separation of bands of Gd(EGTA) and Gd(DTPA). These images were taken at different times and are all cross-section of the concentration distribution by the horizontal plane through the column axis. Flow-rate, 6 ml/min, from left to right. Same experimental conditions as in Fig. 7, except $T_R = 0.03$ s, SL = 4 mm and matrix size, 256 × 256.

the local retention factor nearly 1.6 times lower (value of the ratio $(1-\epsilon_e)/\epsilon_e$) and, because of the Blake–Kozeny equation relating the external porosity and the permeability, a relative change in the permeability 4.5 time larger, hence a 7 times larger effect on the flow velocity than on the retention time.

Indeed, the band profile does not correspond to what would be expected under plug flow conditions and could be interpreted as suggesting an important variation of the permeability in the radial direction. We note, however, that the distribution is not cylindrical, nor even symmetrical as reported by previous workers [3–6,8,9] and expected for a cylindrical column packed by sedimentation. A careful examination of Figs. 8 and 9 shows that the velocity is nearly the same everywhere and that the profiles propagate nearly unchanged, except for some axial spreading (apparent axial dispersion [24]). These observations suggest an alternate explanation, the obstruction of the inlet filter of a region of the packing at the column inlet, interfering with the introduction of the band into the column without causing differential migration of parts of the profile. This possibility will be further discussed later.

The planar section of the three-dimensional band profiles shown in Fig. 7 were obtained all at the same time for a single component band [Gd(DTPA)]. Fig. 8 shows sections of the band profiles of Gd(EGTA) and Gd(DTPA) during their progressive separation by an horizontal plane through the column axis at different times. Gd(EGTA) is eluted first [26]. The first four frames in this figure are shown enlarged in Fig. 9. Comparison with frame 13 in Fig. 7 shows that the flow velocity distribution in the column has not changed much in the mean time. Note that the Gd(EGTA) band disappears after frame 10 because the resolution becomes too large to keep it in the figure. In Fig. 10, we show the con-

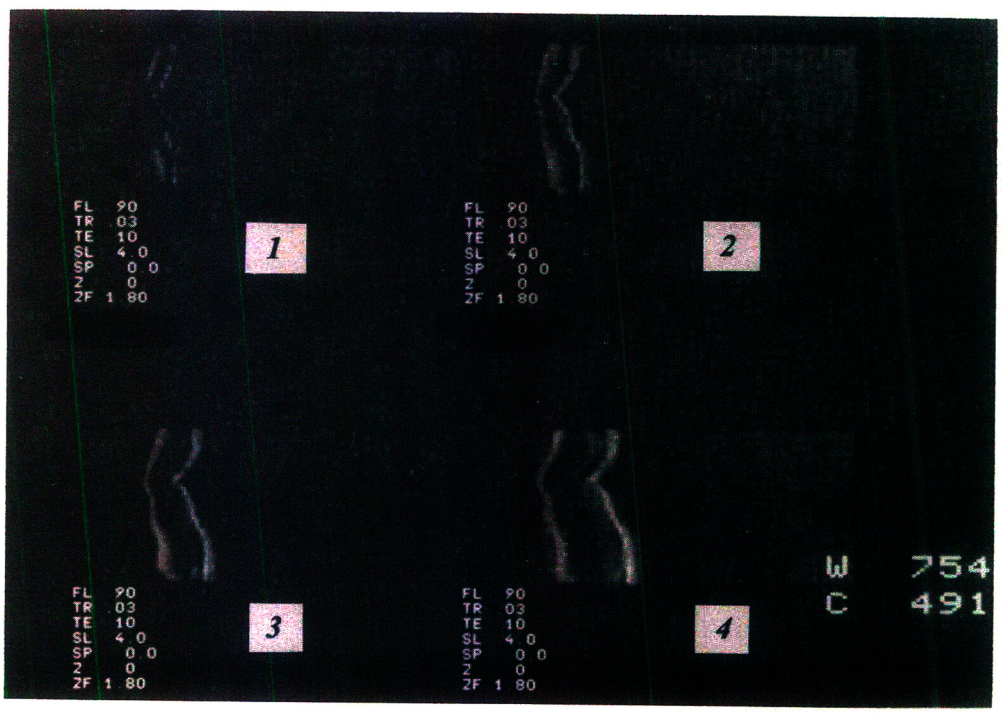

Fig. 9. Two-dimensional FLASH images of the progressive separation of bands of Gd(EGTA) and Gd(DTPA). Enlargement of the first four images in Fig. 8.

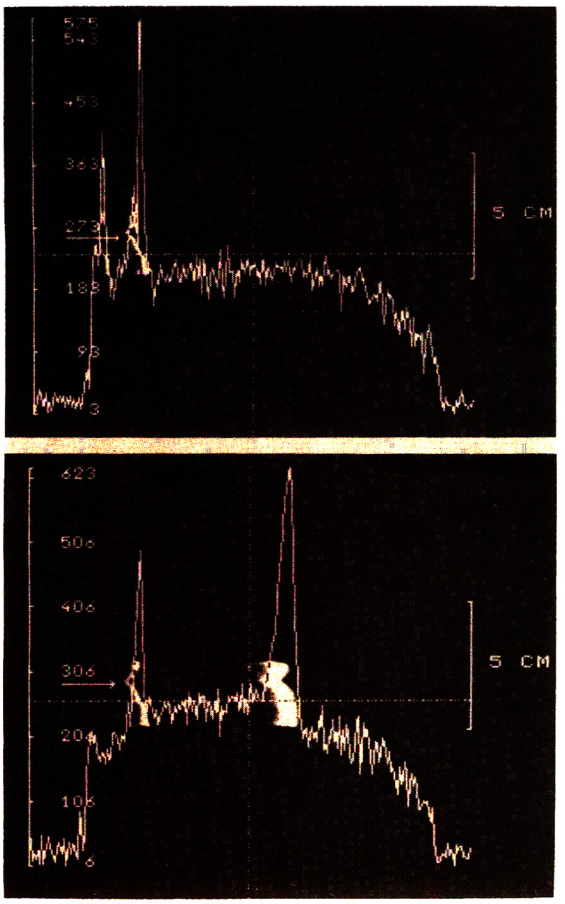

Fig. 10. Signal intensity profiles of the two bands of gadolinium complexes in Fig. 8 (frame 8) along the column axis.

centration profile along a parallel to the column axis for frame 8. The profiles are narrow and nearly symmetrical. Fig. 11 shows the two-dimensional planar section of the band profiles of Gd(EGTA), Gd(CDTA) and Gd(DTPA), eluted in this order [26]. The time evolved between frames 1 and 16 is approximately 2.8 min. The band profiles obtained are very similar to those shown above and to illustrations of the difficulties associated with separations of closely eluted bands when the plug flow condition is not satisfied (e.g., Ref. [7], Fig. 12.15). Note that while the column efficiency corresponded to a value of

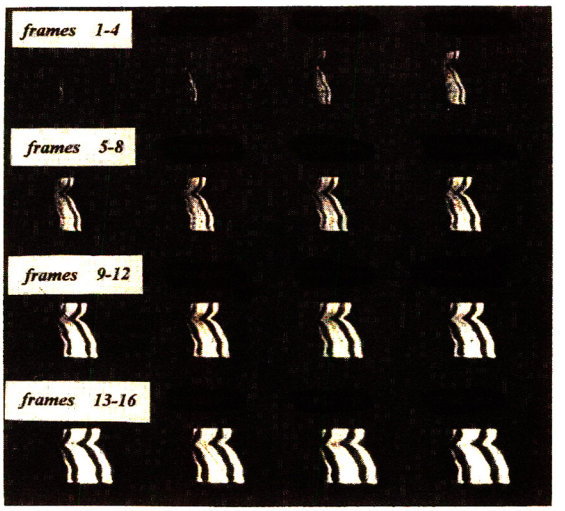

Fig. 11. Two-dimensional FLASH images of the bands of Gd(EGTA), Gd(CDTA) and Gd(DTPA) during their separation. Same conditions as for Fig. 8.

the reduced plate height of 2.1 at the beginning of the experiments (Fig. 3a), the efficiency calculated from the width of the zone in the direction parallel to its axis corresponds to a reduced plate height of 1.0 to 1.2, even though the column is connected to the injection valve through a 150 cm long tubing. The three bands in Fig. 11 are clearly well resolved in frame 6; they are most probably separated earlier. However, because the column is longer than the solenoid coil, the images of its ends are somewhat darker, obscuring the early separation. Obviously, the resolution achieved in frame 16 will be seriously degraded upon elution of the band system, the part of the bands along the right wall eluting earlier than the part along the left one.

The question then arises, what causes the band profile to assume a Λ-shape in the radial direction (Fig. 7, frames 9–17 and Figs. 8 to 11)? Figs. 12 and 13 demonstrate an increase in the extent of the band spreading or apparent axial dispersion for both Gd(EGTA) and Gd(DTPA) after one day of operation. In the same time, the permeability of the column decreases, forcing a reduction in the flow-rate used for the experi-

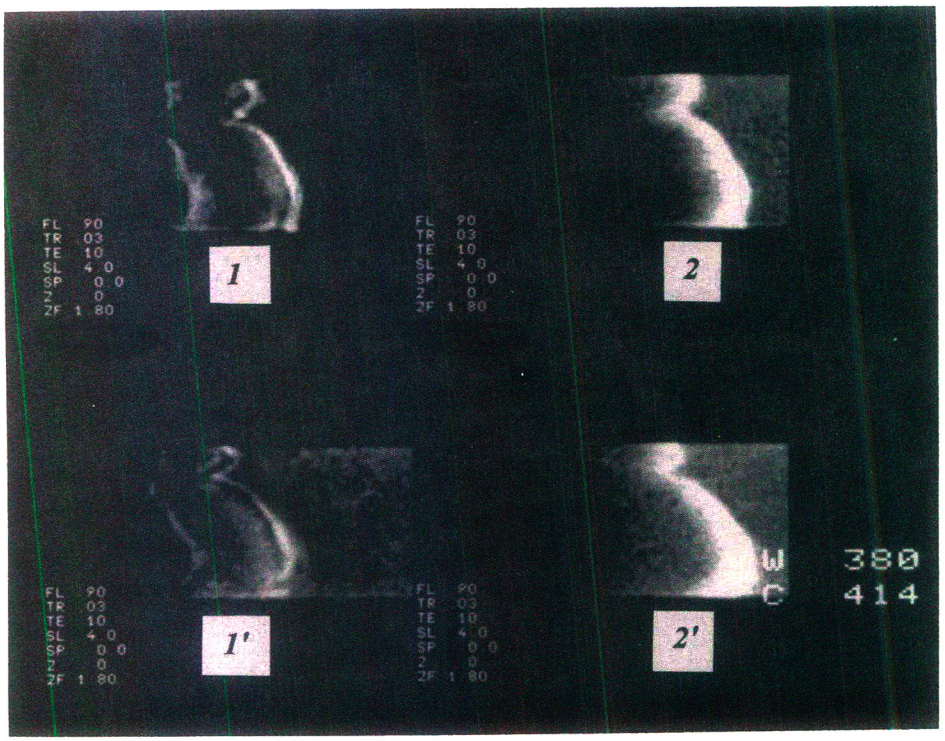

Fig. 12. Aging of a column. Comparison of the two-dimensional FLASH images of the bands of Gd(EGTA) and Gd(DTPA) after 5 min (1, 1′) and of the bands of Gd (DTPA) after 30 min (2, 2′) obtained at one day interval. Same selected slice, same NMR conditions as in Fig. 8, same time interval after injection. Flow-rate, 4 ml/min, left to right.

ments (from 6 to 4 ml/min). Progressive obstruction of the column inlet takes place. To investigate the origin and mechanism of this phenomenon, horizontal spin echo images of the column inlet were taken as well as FLASH images of its inlet, using a three-dimensional spin echo sequence [37]. They are presented in Fig. 14.

Fig. 14a shows sections of the column by several horizontal planes, below the column axis (frames 1 and 2), through the column axis (frame 3) and above this axis (frame 4). They all reveal a dark zone at the beginning of the column, much darker than observed normally. This result is explained by the presence of a significant amount of a metal which, like gadolinium, enhances the spin relaxation of ^{1}H. The amount is so large that no signal is observed under normal imaging conditions (this is known as the T_2 effect). The concentration of the deposits has to decay very sharply along the column, otherwise there would be a bright white band turning to grey just after the black band, see Fig. 5). Fig. 14b shows sections of the column by planes perpendicular to its axis and equidistant by about 2 mm. The first section is at the column inlet (i.e., in the filter, frame 1). They show that the column plugging is not homogeneous (frames 2–4). A dark spot is noticed off center in frame 2. Its position shows that it corresponds to the origin of the band perturbation (Figs. 7–13) and demonstrates that this perturbation took place at injection.

The direction of flow was then reversed in the column, which is against recommended laboratory practice in chromatography. The first injection, after the column has been flushed for about 15 min, gave the images in Figs. 15 and 16. Note that the flow direction being reversed, it now

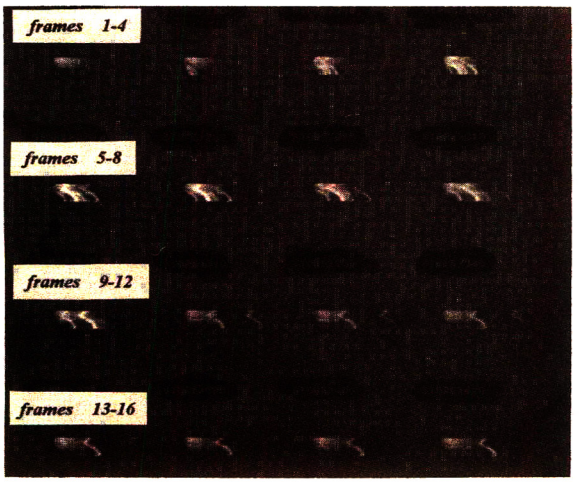

Fig. 13. Two-dimensional FLASH images of the separation of the three gadolinium chelates (see Fig. 11) after degradation of the column performance caused by partial plugging of the inlet frit. Conditions: flow-rate, 3 ml/min, left to right. FL = 90°; T_R = 0.03 s; T_E = 10 ms; SL = 4 mm; matrix size, 256 × 256.

goes from right to left in the Figs. 15–18. Obviously, a small hole and a zone of high permeability has formed against the left wall and the injected band has migrated much faster in this part of the column. In the rest of the column, the packing seems to be quite homogeneous. Like in the former case, the mobile phase velocity seems to be nearly constant outside the perturbed area at the inlet, giving near plug-flow migration of the distorted band (cf. Fig. 7). Horizontal spin echo (Fig. 17) and vertical FLASH images (Fig. 18) of the column inlet regions were taken as in the previous case (Figs. 15 and 16). Their interpretation requires some more information regarding the nature of the NMR signal.

Since the relaxation times T_1 and T_2 are differently influenced by the experimental conditions, namely by the factors which influence the interactions of the protons with their local environment, it is possible to adjust the signal so as to have either a static or a dynamic view of the column. In the former case, the influence of the mobile phase velocity is reduced to a minimum and the image describes the distribution of the concentrations of ^{1}H, of gadolinium, and of paramagnetic ions. In the latter case, channels where the mobile phase flows appear darker than stagnant pools and some estimate of relative velocities is possible. The comparison of different images permit the recognition of differences in packing density, channel patterns, degree of wetting of the stationary phase, and mobile phase velocity in channels. A crack in the column bed can be visualized because the protons in this channel relax more slowly than those in the small spaces between or inside particles. Accordingly, they appear to be darker.

Figs. 17 and 18 show images which confirm the presence of a crack at the beginning of the packing. The occurrence of the T_2 effect is underlined by arrows in Fig. 17b (frame 5). After a certain migration distance, the complexes dilute and become visible through the T_1 effect (e.g., compare frames 3 and 4, Fig. 15). The band profile results from the combination of very fast migration along the crack and slower, quasi plug-flow migration everywhere else. Fig. 17a illustrates clearly why the presence of a hole at the inlet of a column is so damaging for its efficiency. The hole observed in this case is rather important, however, as seen in Fig. 18 and conclusions regarding the influence of the size of small holes cannot be drawn. Frames 6–9 show its horizontal cross-section. The arrow in frame 6 indicates the beginning of the hole. Another observation to be made in Figs. 17 and 18 is the abundance of black spots at this end of the column compared to the other end (Figs. 7–14). Since the column has been packed by sedimentation, it is expected that the metallic particles, denser than silica fall earlier to the bottom. They are made visible by the considerable reduction that they cause in the relaxation time of the neighbor water protons. Physical examination of the column confirmed, as expected, the presence of particles, some of them metallic or oxides, on the inlet filter and of a hole at the other end, along the column wall.

After replacing the flow distributor, the filter, and the first 1.5 cm of packing and filling the hole, the column was replaced in the scanner and operated with the mobile phase flowing in the

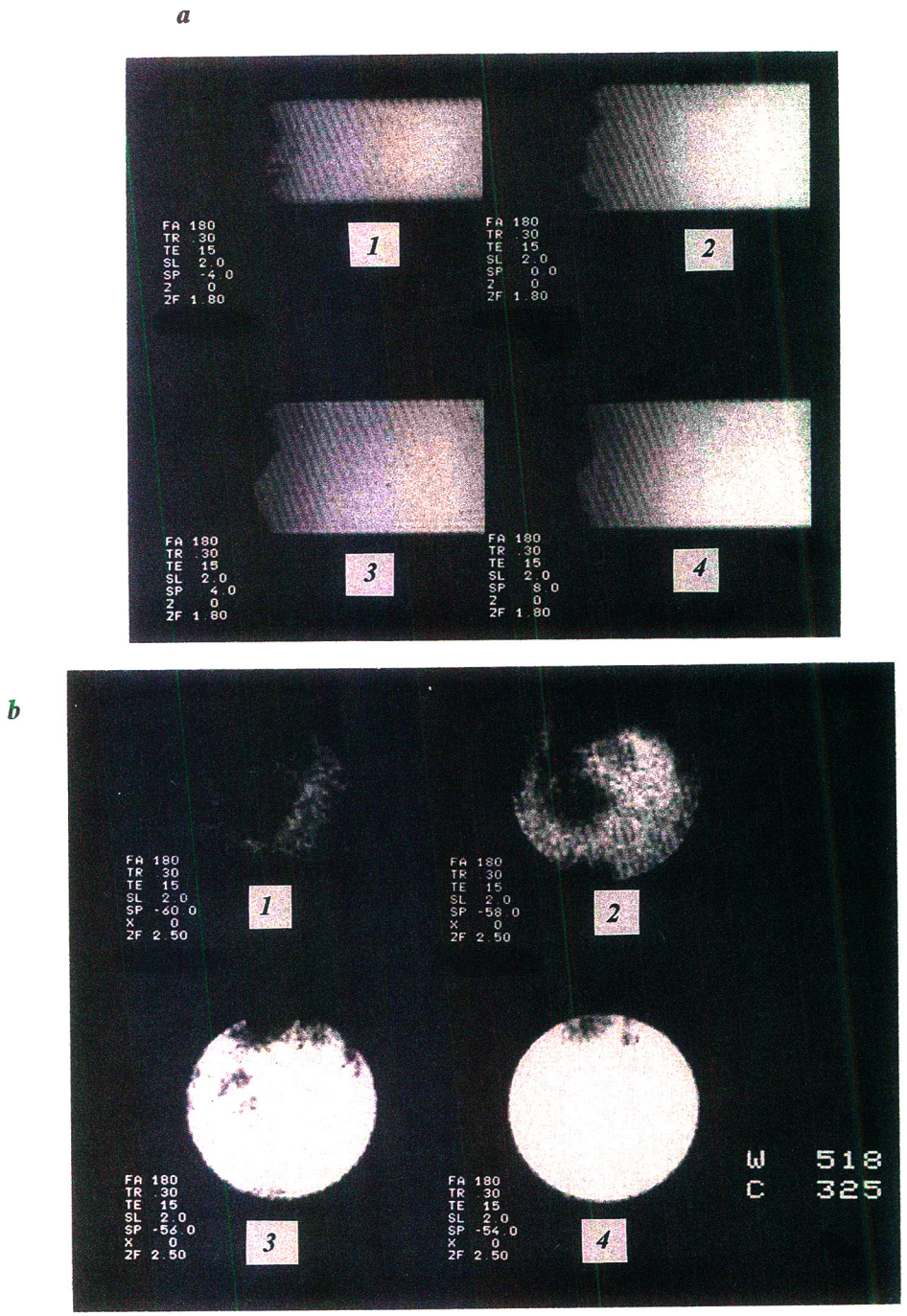

Fig. 14. Three-dimensional spin-echo images of the beginning of the column. (a) Series of parallel slices, 2 mm apart, around the middle of the column. (b) Series of vertical slices, starting from the filter and 2 mm apart.

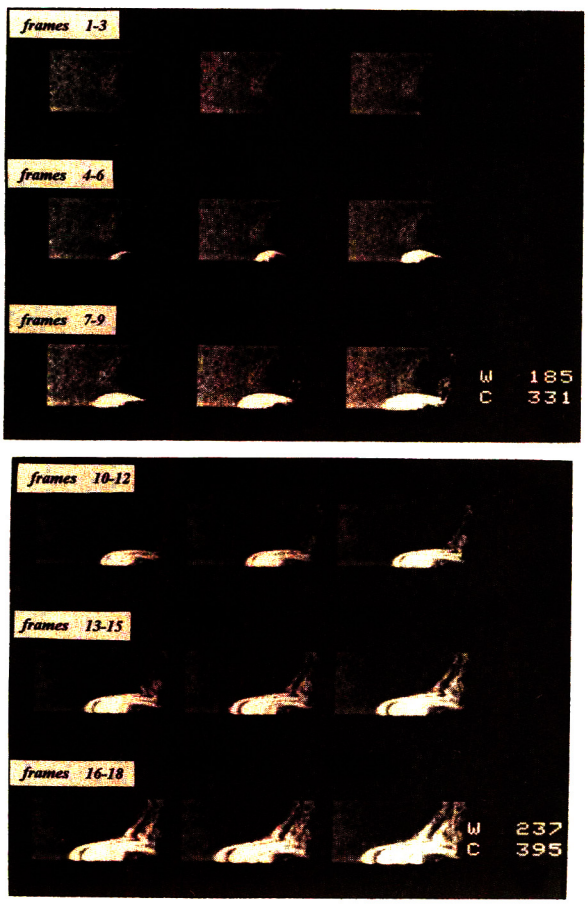

Fig. 15. Two-dimensional FLASH images of the bands of Gd(EGTA), Gd(CDTA) and Gd(DTPA) during their separation. Same NMR conditions as for Fig. 13. Flow-rate, 6 ml/min, right to left.

initial direction. The images of the band profiles obtained (Figs. 19 and 20) show a considerable improvement in the general shape, although the bands are slightly wider and diffuse. The curvature of the three bands in Fig. 19a suggests that either the top of the new packing was not flat, or its density was slightly higher along the wall than in the center. However, there is again near plug-flow migration. In Fig. 20, the bands are nearly flat, showing that the repair has been satisfactory. However, the bands are now more diffuse than in Figs. 7–9, in agreement with the reduced

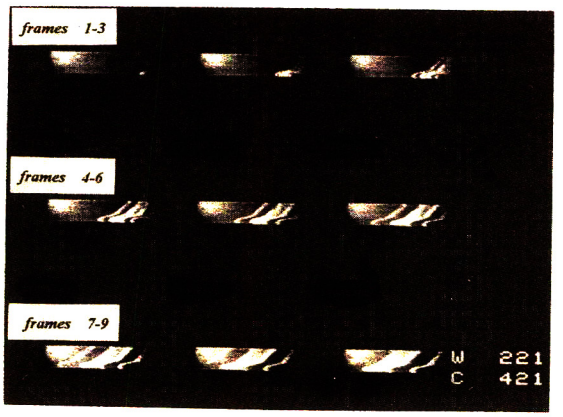

Fig. 16. Two-dimensional FLASH images of the bands of Gd(EGTA), Gd(CDTA) and Gd(DTPA) during their separation. Same as Fig. 15, but extending over longer migration distance. Frames 1 and 2 are frames 6 and 15 in Fig. 15.

column efficiency. The reduced HETP increases from 2.1 to 5.1, suggesting that the new packing is not as regular and homogeneous as the original one.

5. Conclusions

The results described in this work may appear to contradict previous reports in the literature regarding the lack of homogeneity of packed chromatographic columns. We note, however, that, while authors using dry-packing [3–6,10–13] or slurry-packing methods [8,9] find the bed to be radially heterogeneous, with a lower permeability in the center (dry packing, particle size discrimination) or along the wall (slurry packing, probably an effect of the Poiseuille flow profile in the slurry), we find the bed to be extremely homogeneous, with near plug-flow everywhere except in some regions near the column inlet. NMR images show that the reduced HETP in the bed can be as low as 1.0. The column performance is easily degraded, however mainly related to phenomena taking place when the injected band of sample enters the column. Chromatographers have always felt that performing a "correct" injection was a most critical

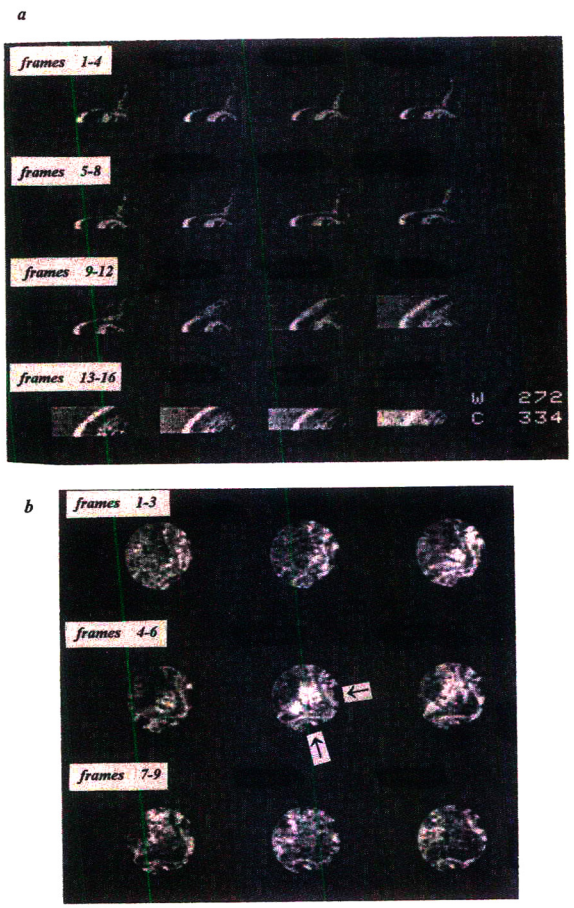

Fig. 17. Three-dimensional FLASH images of the bands of Gd(EDTA) and Gd(DTPA) ca. 2.5 min after injection. FL = 90°; T_R = 0.04 s; T_E = 10 ms; SL = 1 mm; matrix size, 256 × 256. (a) Horizontal slices starting from its middle (frame 1) and going to its top (frame 16), ca. 0.8 mm apart. (b) Vertical slices, starting ca. 12 mm inside the column (frame 1) and going toward the inlet (frame 9).

step in achieving high column efficiency [7] but have always lacked a clear illustration of the difficulties associated with it.

Obstruction of the inlet frit or cracks resulting from uneven consolidation of the bed cause considerable deformation of the band profile, the sample zone moving much faster when entering some parts of the bed than in others. Thus, not filtering the mobile phase before it enters the chromatographic system is dangerous for the column, resulting in performance rapidly ruined. Similarly, the direction of flow in a column should not be reversed. Consolidation of the packing is a slow process, not fully understood. The apparent density of the packing may vary by 10 to 20% depending on the conditions under which it is packed and the procedures used to compress it [63]. The mobile phase flows through the packing, so the pressure gradient, the local velocity and the friction stress applied by the liquid stream to the packing are constant in an homogeneous bed, and this results in an homogeneous contribution to consolidation. Nevertheless, since the bed does not move, there is a static compression pressure applied to the packing, which is equal to the inlet pressure less the friction of the bed along the wall (friction which explains why it is not possible to empty some columns from their packing just by taking off the end frit). This pressure causes uneven consolidation and results in a bed which is denser at the inlet than at the outlet [63]. Reversing the flow direction in the bed causes consolidation to proceed again in the opposite direction and, even in a conventional analytical column, there are no reasons for this consolidation to take place homogeneously. The formation of holes or zones of higher local permeability is quite possible as a result of the collapse of local vaults in the packing.

Finally, our results also confirm that the local separations achieved are often much better than the apparent separations recorded with a bulk detector. As already remarked by Horne et al. [5] and confirmed by Baur et al. [8] and Farkas et al. [9], considerable improvements in the resolution achieved in analytical applications would be obtained if bulk detectors were replaced by local detectors.

Acknowledgement

We thank the Alexander von Humboldt Stiftung (Bonn, Germany) for the Research Award received by G.G.

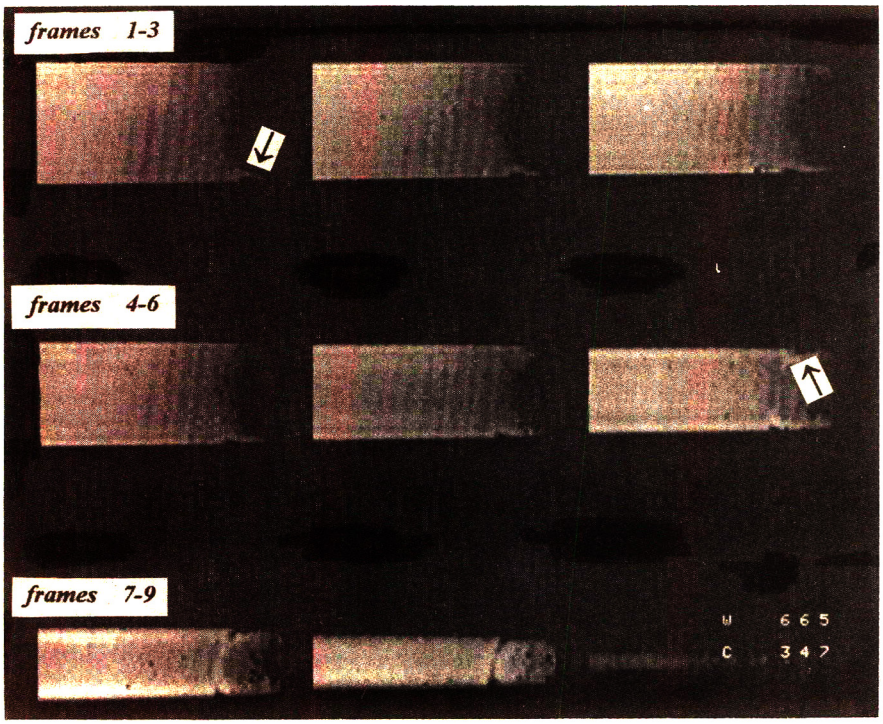

Fig. 18. Three-dimensional spin-echo images of the initial part of the column bed. FL = 90°; T_R = 0.03 s; T_E = 10 ms; SL = 4 mm; matrix size, 256 × 256. The crack which is at the origin of the gross deformation of the band profile is indicated by arrows. In frame 8 it extends over both sides of the column and in frame 9 it occupies the entire section.

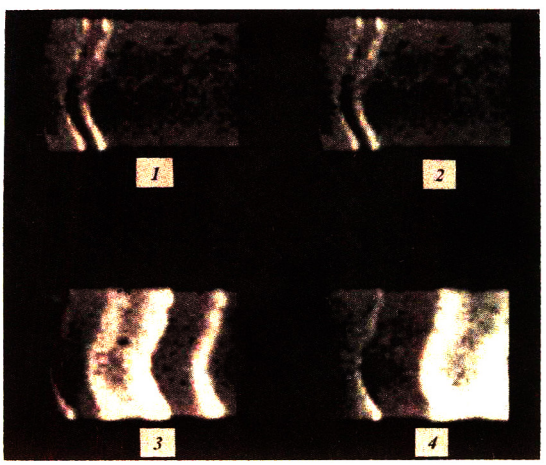

Fig. 19. Two-dimensional FLASH images of the bands of Gd(EGTA), Gd(CDTA) and Gd(DTPA) during their separation on the repaired column. Flow-rate, 6 ml/min, left to right. Same NMR conditions as for Fig. 13.

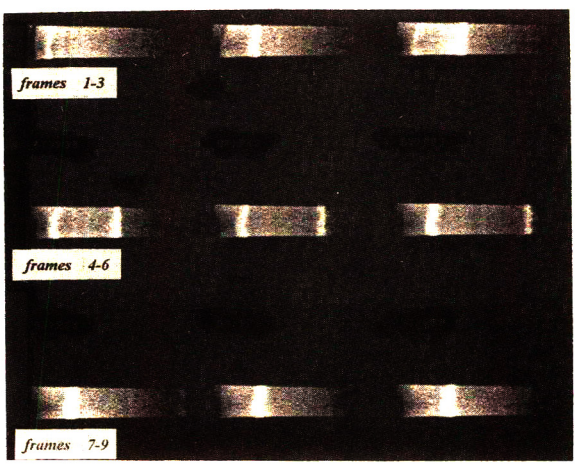

Fig. 20. Two-dimensional FLASH images of the bands of Gd(EDTA) and Gd(DTPA) during their separation on the repaired column. Same experimental conditions as for Fig. 19.

References

[1] J.C. Giddings, *J. Gas Chromatogr.*, 1 (1963) 12.
[2] T. Yun and G. Guiochon, *J. Chromatogr.*, in press.
[3] J.H. Knox and J. Parcher, *Anal. Chem.*, 41 (1969) 1599.
[4] J.H. Knox, G.R. Laird and P.A. Raven, *J. Chromatogr.*, 122 (1976) 129.
[5] D.S. Horne, J.H. Knox and L. McLaren, *Sep. Sci.*, 1 (1966) 531.
[6] C. Eon, *J. Chromatogr.*, 149 (1978) 29.
[7] W.M. Skea, in P.R. Brown and R.A. Hartwick (Editors), *High Performance Liquid Chromatography*, Wiley, New York, 1989, p. 496.
[8] J.E. Baur, E.W. Kristensen and R.M. Wightman, *Anal. Chem.*, 60 (1988) 2338.
[9] T. Farkas, J.Q. Chambers and G. Guiochon, *J. Chromatogr.*, in press.
[10] R.A. Bernard and R.H. Wilhelm, *Chem. Eng. Progr.*, 46 (1950) 233.
[11] C.E. Schwartz and J.M. Smith, *Ind. Eng. Chem.*, 45 (1953) 1209.
[12] F.H. Huyten, W. van Beersum and G.W.A. Rijnders, in R.P.W. Scott (Editor), *Gas Chromatography 1960*, Butterworths, London, 1960, p. 224.
[13] J.C. Giddings and E.N. Fuller, *J. Chromatogr.*, 7 (1962) 255.
[14] T. Yun and G. Guiochon, in preparation.
[15] H. Colin, P. Hilaireau and J. de Tournemire, *LC·GC*, 3 (1990) 40.
[16] H. Colin, in G. Ganetsos and P.E. Barker (Editors), *Preparative and Production Scale Chromatography*, Marcel Dekker, New York, 1993, p. 11.
[17] M.J. Golay and J.G. Atwood, *J. Chromatogr.*, 186 (1979) 353.
[18] M. Sarker and G. Guiochon, *LC·GC*, 12 (1994) 300.
[19] E.B. Byrne and L. Lapidus, *J. Am. Chem. Soc.*, 77 (1955) 6506.
[20] G. Hesse and H. Engelhardt, *J. Chromatogr.*, 21 (1966) 223.
[21] E. Bayer, W. Müller, M. Ilg and K. Albert, *Angew. Chem., Int. Ed. Engl.*, 28 (1989) 1029.
[22] M. Ilg, J. Maier-Rosenkranz, W. Müller, K. Albert, E. Bayer and D. Höpfel, *J. Magn. Reson.*, 96 (1992) 335.
[23] M. Ilg, J. Maier-Rosenkranz, W. Müller. and E. Bayer, *J. Chromatogr.*, 517 (1990) 263.
[24] E. Baumeister, U. Klose, K. Albert, E. Bayer and G. Guiochon, *J. Chromatogr.*, in press.
[25] E. Baumeister, *Dissertation*, Universität Tübingen, Tübingen, 1994.
[26] U. Tallarek, *M.Sc. Dissertation*, Universität Tübingen, Tübingen, 1994.
[27] F.W. Wehrli, D. Shaw and J.B. Kneeland (Editors), *Biomedical Magnetic Resonance Imaging*, VCH, New York, 1988.
[28] R.A. Komoroski, *Anal. Chem.*, 65 (1993) 1068A.
[29] H.V. Carr and E.M. Purcell, *Phys. Rev.*, 94 (1954) 630.
[30] R. Bradford, C. Clay and E. Strick, *Phys. Rev.*, 84 (1954) 157.
[31] R. Damadian, *Science*, 171 (1971) 1151.
[32] P.C. Lauterbur, *Nature*, 242 (1973) 190.
[33] P. Mansfield and P.K. Grannell, *J. Phys.*, C6 (1973) 422.
[34] P. Mansfield and P.G. Morris, in *Advances in Magnetic Resonance*, Academic Press, New York, 1982, Ch. 3.
[35] W. Kuhn, *Angew. Chem., Int. Ed. Engl.*, 29 (1990) 1.
[36] G.D. Fullerton, *Magn. Reson. Imag.*, 1 (1982) 39.
[37] P.T. Callaghan, *Principles of Nuclear Magnetic Resonance Microscopy*, Clarendon, New York, 1991, Ch. 3.
[38] F.A. Bovey, *Nuclear Magnetic Resonance Spectroscopy*, Academic Press, New York, 1988, p. 492.
[39] P.T. Callaghan, *Principles of Nuclear Magnetic Resonance Microscopy*, Clarendon, New York, 1991, p. 5.
[40] P. Mansfield and P.K. Grannell, *Phys. Rev.*, 12 (1975) 3618.
[41] P. Mansfield, *J. Phys.*, E21 (1988) 18.
[42] A. Kumar, D. Welti and R.R. Ernst, *J. Magn. Reson.*, 18 (1975) 69.
[43] W.A. Edelstein, J.M.S. Hutchison, G. Johnson, T.W. Redpath and L.M. Eastwood, *Phys. Med. Biol.*, 25 (1980) 751.
[44] G. Johnson, J.M.S. Hutchison, T.W. Redpath, L.M. Eastwood, *J. Magn. Reson.*, 54 (1983) 374.
[45] E. Baumeister, K. Albert and E. Bayer, in preparation.
[46] Ch. Kittel, *Introduction to Solid State Physics*, Wiley, New York, 1986, Ch. 14.
[47] R.B. Lauffer, *Chem. Rev.*, 87 (1987) 901.
[48] D.G. Gadian, J.A. Payne, D.J. Bryant, I.R. Young, D.H. Carr and G.M. Bydder. *J. Comput. Assist. Tomogr.*, 9 (1985) 242.
[49] S.H. Koenig and R.D. Brown, *Magn. Reson. Med.*, 1 (1984) 478.
[50] S.H. Koenig, C. Baglin, R.D. Brown and C.F. Brewer, *Magn. Reson. Med.*, 1 (1984) 496.
[51] C.D. Barry, A.C.T. North, J.A. Glasel, R.J.P. Williams and A.V. Xavier, *Nature*, 232 (1971) 236.
[52] W. Grodd and R.C. Brasch, *Fortschr. Röntgenstr.*, 145 (1986) 130.
[53] P.T. Callaghan, *Principles of Nuclear Magnetic Resonance Microscopy*, Clarendon, New York, 1991, Ch. 5.3.
[54] G. Sosnovsky and N.U.M. Rao, *Eur. J. Med. Chem.*, 23 (1988) 517.
[55] H.J. Weinmann, R.C. Brasch, W.R. Press and G.E. Wesley, *Am. J. Roentgenol.*, 142 (1984) 619.
[56] M.M. Vora, S. Wukovnig, R.D. Finn, A.M. Emran, T.E. Boothe and P.J. Kotari, *J. Chromatogr.*, 369 (1986) 187.
[57] T. Moeller and L.C. Thompson, *J. Inorg. Nucl. Chem.*, 24 (1962) 499.
[58] E. Merciny and J. Fuger, *Anal. Chim. Acta*, 160 (1984) 87.
[59] R.S. Kolat and J.E. Powell, *Inorg. Chem.*, 1 (1962) 485.
[60] D. Matthaei, J. Frahm and A. Haase, *Magn. Reson. Imag.*, 4 (1986) 381.
[61] A. Haase, J. Frahm, D. Matthaei, W. Hänicke and K.-D. Merboldt, *J. Magn. Reson.*, 67 (1986) 258.
[62] V.M. Runge (Editor), *Enhanced Magnetic Resonance Imaging*, Mosby, St. Louis, MO, 1989, Ch. 5.
[63] G. Guiochon and M. Sarker, in preparation.

ELSEVIER

Journal of Chromatography A, 696 (1995) 19–30

JOURNAL OF CHROMATOGRAPHY A

Utilization of the dry impact blending method to prepare irregularly shaped particles for high-performance liquid chromatographic column packings

Futaba Honda[a,*], Hirotaka Honda[b], Masumi Koishi[b]

[a]*PHD Inc., 2-49-24, Nakamichi, Hakodate-shi, Hokkaido 041, Japan*

[b]*Faculty of Industrial Science and Technology, Science University of Tokyo, 102-1, Tomino, Oshamanbe-cho, Yamakoshi-gun, Hokkaido 049-35, Japan*

First received 21 June 1994; revised manuscript received 6 December 1994; accepted 7 December 1994

Abstract

The use of the dry impact blending method to prepare various materials for HPLC column packings that might otherwise be unsuitable is proposed. Crystalline hydroxyapatite (HA) was adopted as a model of a useful but fragile, irregularly shaped material and was embedded on the surface of polyethylene beads by impact blending. The resulting HA composites were evaluated for the crystallinity of the HA, the ability to adsorb and desorb proteins and performance as an HPLC column packing for proteins. Non-specific irreversible adsorption of proteins was observed. This adsorption could be saturated, however, and subsequently the HA composites performed satisfactorily in the HPLC of proteins.

1. Introduction

In high-performance liquid chromatographic (HPLC) separations, for good results it is necessary that the particles of the column packings have regular shapes, for example, spherical with uniform size in the range 3–10 μm in diameter [1]. Methods for the preparation of particles that satisfy these conditions have been established for silica gel and some organic polymers. For that reason, a number of packings have been prepared by chemically modifying the surface of spherical silica gel with alkyl groups, ion-exchange groups, etc. They demonstrate high performance, and a number of solutes have been determined with their use with good results. Silica gel has disadvantages, however; its uncoated surface is dissolved by alkaline solution and bonds to alkyl groups tend to be cleaved by acidic solution. Further, the unique adsorption characteristics of some other materials offer advantages for the separation of substances with which satisfactory results have not yet been obtained with silica-based materials. Examples of such alternative materials include titania [2–4], zirconia [2–7] and polypeptides [8]. Only a few such materials have been used as HPLC column packings because it is difficult to shape

* Corresponding author. Present address: Faculty of Industrial Science and Technology, Science University of Tokyo, 102-1, Tomino, Oshamanbe-cho, Yamakoshi-gun, Hokkaido 049-35, Japan.

0021-9673/95/$09.50
SSDI 0021-9673(94)01216-4

many of them into spheres which are rigid and have a proper uniform size.

The preparation of composite particles by combinations of diverse particles has been developed in the pharmaceutical field [9–11]. The technique is called dry impact blending. Powder particles are suspended in a high-speed air stream and vigorously blended. The impact forces that attend the collision between the particles or between the particles and striking pins in a machine makes the diverse particles adhere. For example, when 5–200 μm polymer particles and inorganic ultramicroparticles under 1 μm are blended with the impact method, we can obtain composite particles that have the inorganic ultramicroparticles densely packed on the surface of the polymer particles. It has been confirmed experimentally that small particles are fixed on large particle surfaces when the ratio of the diameter of the large particle to that of the small particle is larger than 10:1.

We have previously prepared composite particles consisting of 0.3–0.9-μm silica ultramicrospheres (with an ODS coating) and 5–10-μm polyethylene microspheres for HPLC column packings [12]. The particles were useful for separating proteins of high molecular mass. The study indicated that the ultramicrospheres, which could not be utilized directly for HPLC column packings, could be used as a composite as a stationary phase in HPLC with acceptable flow-rates of the mobile phase.

In this paper, we describe the preparation and utilization of composite particles prepared from irregularly shaped particles as HPLC column packings. We selected crystalline hydroxyapatite as a model of an irregularly shaped particle. It exhibits characteristic adsorption of proteins and has well known chromatographic properties. Although crystalline hydroxyapatite has frequently been employed for the purification of antibodies in column chromatography, it must be processed by sintering or by being packed with a special method when it is used as an HPLC column packing [13–18], since the intact crystal is so fragile that it cannot resist high pressures. We anticipated that forming crystalline hydroxyapatite into composite particles would solve this problem.

2. Experimental

2.1. Chemicals and reagents

Low-density spherical polyethylene (PE) beads (average diameter 10 μm) as core particles of the composite were supplied by Sumitomo Seika (Osaka, Japan). Crystalline hydroxyapatite (HA) was prepared from Na_2HPO_4 and $CaCl_2$ according to the Tiselius method [19]. Na_2HPO_4, $CaCl_2$, NaOH, KH_2PO_4, K_2HPO_4, trifluoroacetic acid (TFA), Triton X-100 [polyoxyethylene(10)octyl phenyl ether] and acetonitrile of analytical-reagent grade were purchased from Wako (Osaka, Japan). Albumin (from bovine serum), cytochrome *c* (type III, from horse heart), lysozyme (grade I, from chicken egg white), ribonuclease A (type III, from bovine pancreas) and myoglobin (from horse skeletal muscle) were purchased from Sigma (St. Louis, MO, USA). For the determination of proteins, a Simpack CLC-ODS column (150 mm × 6.0 mm I.D.), purchased from Shimadzu (Kyoto, Japan), was used. Empty columns (50 mm × 2.0 mm and 4.6 mm I.D.) were purchased from Nihon Chromato (Tokyo, Japan). A spherical HA-packed column (KB column, 135 mm × 7.8 mm I.D.) from Koken (Tokyo, Japan) was used for comparison with the HA composite column.

2.2. Apparatus

For the preparation of HA composite particles, an O.M. Dizer and a Hybridizer (NHS-0; Nara Machinery, Tokyo, Japan) were used. HA and HA composite particles were observed by scanning electron microscopy (SEM) (JSM-T220; JEOL, Tokyo, Japan) after being sputter coated with gold with an ion sputtering apparatus (JFC-1100; JEOL).

All chromatographic tests were performed on an LC-6A gradient system with a Rheodyne

Model 7125 injection valve, connected to an SPD-6A UV spectrophotometric detector and a Chromatopac C-R6A integrator (Shimadzu).

2.3. Dry impact blending method

Details of the machines and the method were described in previous papers [9–12]. PE and HA powders were blended (1400 rpm for 10 min) with the O.M. Dizer; three kinds of mixtures, which contained 30, 40 or 50% (w/w) of HA, were prepared and the total amount was fixed at 15 g. The resulting mixtures were treated by the dry impact blending method using the Hybridizer, with a rotational speed of 16 000 rpm and a treatment time of 10 min. The vessel was cooled by circulation of water through the jacket during the treatment.

2.4. Evaluation of HA composite particles by X-ray diffractometry

To evaluate HA, PE and HA composite particles containing 30% HA (30% HA composite), X-ray powder diffraction patterns were measured using an MXP^3 System computer-controlled X-ray diffractometer (Mac Science, Tokyo, Japan). CuKα radiation patterns were recorded from 5 to 90° (2θ) in steps of 0.020°.

2.5. Measurement of maximum amounts of protein adsorbed

A 10-mg amount of HA or a 20 mg amount of HA composite particles was suspended in 500 μl of 1 m*M* potassium phosphate buffer [an equimolar mixture of K_2HPO_4 and KH_2PO_4 (pH $\approx$ 6.8) (KPB)]. A 500-μl volume of the BSA solution which contained 2 or 1 mg/ml of BSA in 1 m*M* KPB was added. After mixing, the mixture was allowed to stand for 30 min at room temperature. A 200-μl volume of the supernatant was withdrawn and its protein content was determined by RP-HPLC. A 800-μl volume of 400 m*M* KPB was added to the sedimented HA composite; after mixing, the mixture was allowed to stand for 30 min at room temperature. The protein content of the supernatant was determined by RP-HPLC. The sample volume was 20 μl and Shim-pack CLC-ODS was used as an analytical column. Elution was carried out with a linear gradient in 15 min from 25% to 50% of acetonitrile in 0.1% TFA at a flow-rate of 1 ml/min and the eluate was monitored at 220 nm. The maximum amount of BSA adsorbed on HA and HA composite particles from 1 m*M* KPB solution was calculated from the protein contents of both supernatants.

2.6. Adsorption–desorption behaviour of HA and HA composite particles

A 20-mg amount of HA or HA composite particles was suspended in 500 μl of 5 m*M* KPB. A 20-μl volume of a protein mixture was added, containing 1 mg/ml each of BSA, cytochrome *c*, lysozyme and ribonuclease A. After mixing, the mixture was allowed to stand for 30 min at room temperature for adsorption. A 500-μl volume of KPB of the appropriate strength was added to adjust the KPB concentration of the suspensions to 5, 25, 50, 100, 150 and 200 m*M*. After mixing, the mixtures were allowed to stand for 30 min at room temperature for desorption. The protein contents of the supernatants were determined by RP-HPLC. The sample volume was 200 μl and analysis was performed in a manner similar to that described above.

2.7. Separation of proteins

Composites with 30% or 50% HA were slurry-packed into stainless-steel columns with 5 m*M* KPB. A volume of 10 μl or 20 μl of the protein mixture solution, which contained 1 mg/ml of each protein, was applied to the columns. Linear gradient elution was employed with KPB from 5 to 202.5 m*M* at a flow-rate of 0.5 ml/min and the eluate was monitored at 220 nm.

3. Results and discussion

3.1. Observation of HA composite particles

Typical SEM photographs of HA and HA composite particles are shown in Figs. 1 and 2, respectively. As can be seen in Fig. 1, HA consisted of plate-like flakes. In HA composite particles, large HA particles are absent and PE coated with superfine fragments was observed. We consider that HA was fractured into many superfine fragments by the strong impact forces which arose from mutual collisions between different particles or between particles and the striking pins attached to the rotor.

When the physical appearance of the surface was compared for HA composite particles with different HA contents, 30% HA had a relatively smooth surface which was densely coated with rounded fragments of HA having a uniform size of ca. 0.1 μm. As the HA content increased, particularly with 50% HA, several larger sized unfractured fragments were clearly observed, and thus the fragment sizes became varied. As a result, 30% and 40% HA had a homogeneous coating layer with fine HA fragments, whereas 50% HA was rough because of the partially overlaid layer of HA fragments. Further, 50% HA was also observed to contain many irregularly shaped particles of about 1 μm, which were considered to be aggregates of excess HA.

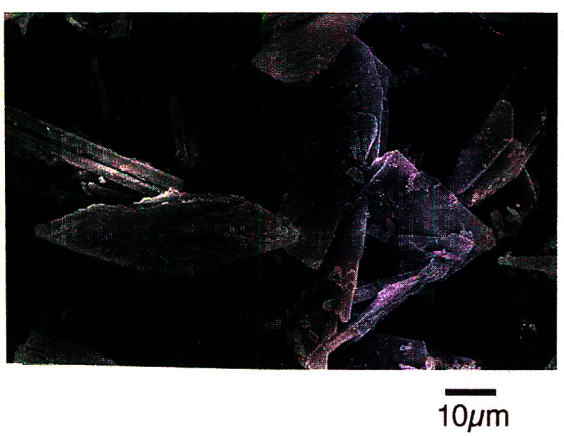

Fig. 1. Typical SEM photograph of HA.

These observations suggested that the process of forming the HA coating layer was as follows. When a small amount of HA was added, HA was well fractured and fixed on the PE surface immediately through dry impact blending. However, if a larger amount of HA than the required amount was added, it was difficult to fix all the HA on PE homogeneously. Repeated collisions could also lead to enlarged HA aggregates which subsequently might be fixed on the HA layer of composite particles. The result was irregularly shaped particles and partial overlaid layers at 50% HA.

When HA fragments are assumed to be spheres of 0.1 μm, the amount of HA required to cover the whole surfaces of PE beads is calculated to be about 11% of the total mass (see Appendix). In 30% HA, almost all HA particles were regarded as adhering to PE surfaces because an excess of HA which was not fixed on HA composite particles was hardly observed. Therefore, it is considered that HA fragments, although they seemed to form a monolayer coating, were fixed on PE with about a double-layer thickness, that is, the HA coating layer was about 0.2 μm thick.

3.2. Evaluation of crystallinity of HA and HA composite particles

The following mechanism has been proposed for the separation of proteins on HA [13]. Two types of vertical main surface appear on an HA, called the a (or b) surface and the c surface. The a or b surface has C sites, which adsorb carboxyl groups, whereas the c surface has P sites, which adsorb basic groups. Protein molecules can be adsorbed using a number of different local molecular surfaces, each of which can face the crystal surface and can orient in different directions on the crystal surface. Hence a specific chromatographic separation can be obtained on the HA column based on subtle differences in the geometrical arrangement of the adsorption groups on a protein.

Mechanical effects such as trituration, friction and compression change the physico-chemical properties of some crystals, such as crystal form

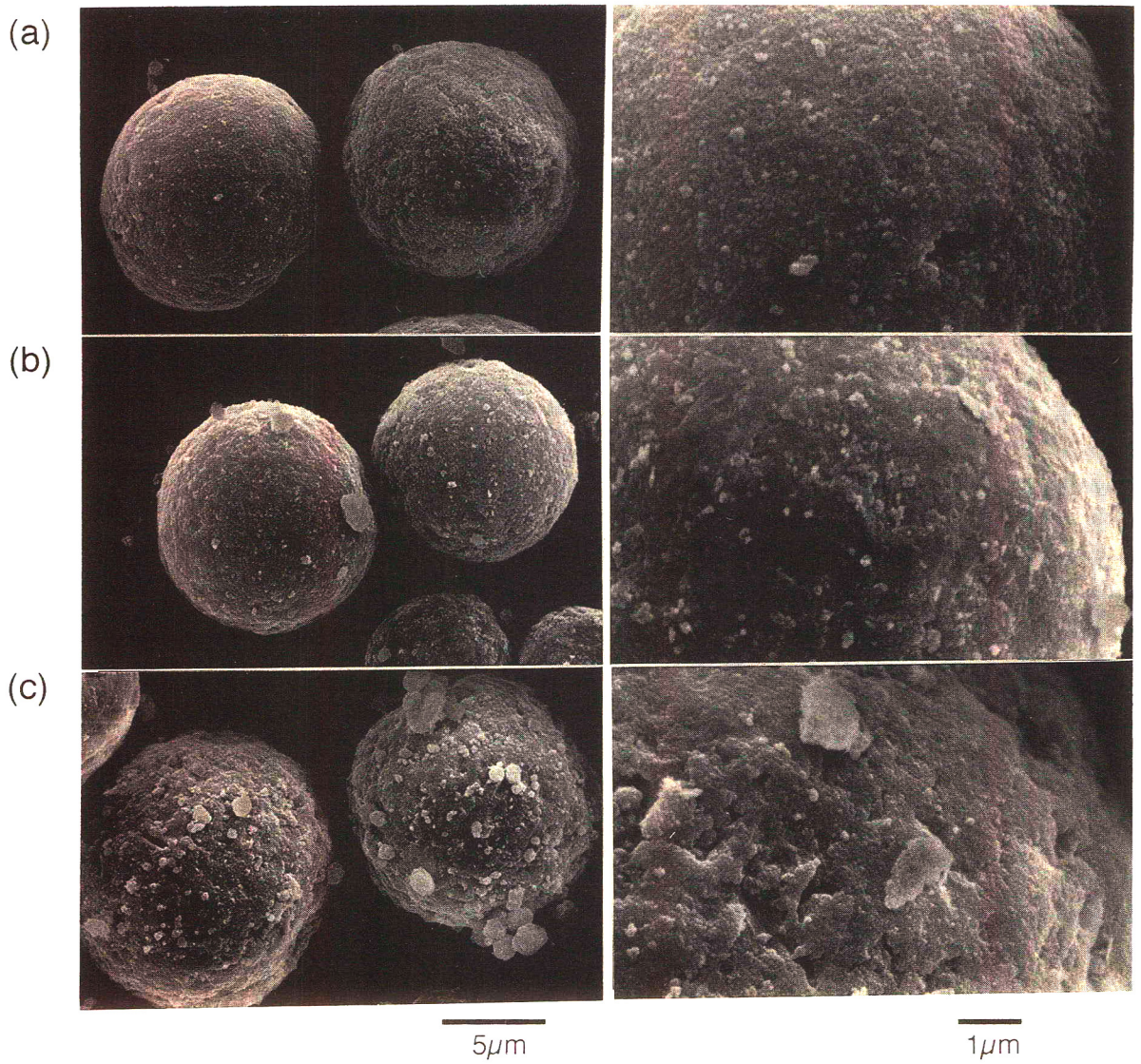

Fig. 2. Typical SEM photographs of HA composite particles: (a) 30% HA; (b) 40% HA; (c) 50% HA.

and reactivity. This phenomenon is termed mechanochemistry. It has been reported that some powders changed their forms from crystalline to amorphous when they were fixed on large particles by dry impact blending [20,21]. The changes were regarded as mechanochemistry. In the work cited, the change was utilized to improve the dissolution properties of slightly soluble drugs. In this study, however, if the crystalline form of HA is changed by dry impact blending, then the chromatographic properties of HA composite particles may differ from those of intact HA.

The crystallinity of HA composite particles was compared with that of HA by powder X-ray diffractometry. The diffraction patterns of HA, PE and 30% HA are shown in Fig. 3. The diffraction pattern of HA matches the pattern of

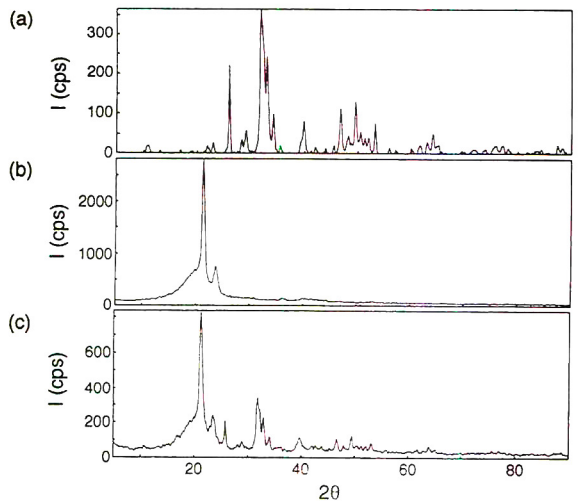

Fig. 3. X-ray powder diffractograms of (a) HA, (b) PE and (c) 30% HA composite particles.

synthetic hydroxyapatite [$Ca_5(PO_4)_3(OH)$] (diffraction data from the Joint Committee in Powder Diffraction Standards). When the diffraction pattern of the 30% HA was compared with that of HA, the main peaks of both patterns agreed completely, except for some broad peaks on HA-composite particles which were distributed around $2\theta = 21°$ derived from PE. This indicates that the crystalline form of HA is maintained after dry impact blending.

3.3. Maximum amounts of protein adsorbed

The maximum amount of BSA adsorbed was independent of the HA content of the HA composite particles, the maximum amounts adsorbed in 1 m*M* KPB being 68.6, 5.70, 5.67 and 6.09 mg/g for HA and 30%, 40% and 50% HA adsorbents, respectively. The results suggest that the specific surface area of HA on all the HA composite particles is approximately equal. Hence, when the maximum amount of BSA adsorbed on HA composite particles is compared with that of HA, it is considerably smaller than the values that are expected from the HA content. Therefore, an increase in the content of HA is not effective in increasing the maximum amount of proteins adsorbed. Roughly estimated, it is considered that more than half of the HA surface area is inaccessible because HA fragments are embedded in PE, adhere to PE or aggregate with each other.

3.4. Adsorption–desorption properties of proteins

The adsorption–desorption properties of proteins on HA composite particles in KPB solution were evaluated and the results are shown in Fig. 4. With intact HA, all proteins were adsorbed in 5 m*M* KPB, then desorbed between 25 and 200 m*M*, except for cytochrome *c*. Cytochrome *c* was not desorbed completely below 400 m*M* KPB (data not shown). This indicates that a certain amount of cytochrome *c* is adsorbed by HA extremely strongly.

Next, adsorption–desorption properties of proteins on HA composite particles were compared with those on HA (Fig. 4). In 5 m*M* KPB, every HA composite particle adsorbed almost all proteins. In contrast with HA, some adsorbed proteins were not desorbed completely from HA

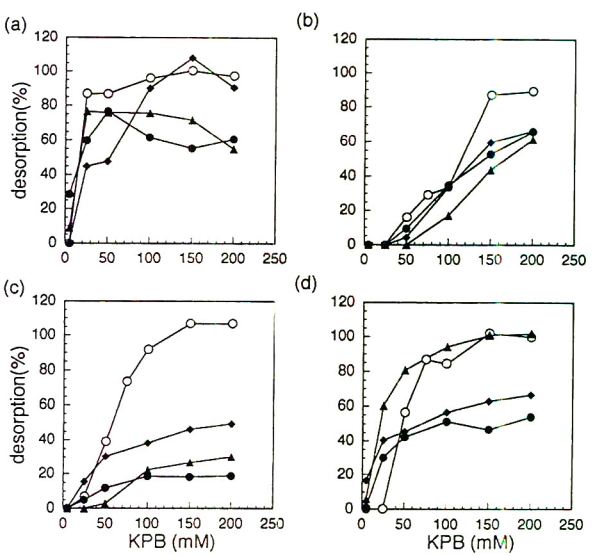

Fig. 4. Adsorption–desorption behaviour in KPB for (a) BSA, (b) cytochrome *c*, (c) lysozyme and (d) ribonuclease A of (○) HA and (●) 30%, (▲) 40% and (◆) 50% HA composite particles.

composites, in spite of using KPB concentrations up to 200 m*M*. Although the desorption curves for different HA composites showed similar patterns for individual proteins, there was no simple relationship between the degree of desorption with 200 m*M* KPB and the HA content or the kind of protein. This seems to indicate that with HA composites, protein adsorption is due in part to forces other than ionic interactions.

An explanation for the incomplete desorption is that HA was fractured into fine fragments during dry impact blending. Crystal sections that hardly appeared on the surface of large crystals are thereby abundantly exposed, and this plane might adsorb proteins more strongly. To investigate the influence of fracture, the fractured HA that was obtained by the dry impact blending treatment with only HA was applied to the adsorption–desorption test. Irreversible adsorption was not increased compared with intact HA (Fig. 5), and therefore fracturing HA did not influence its adsorption of proteins.

As an alternative explanation, the incomplete desorption is due to the hydrophobic interaction of proteins with exposed surfaces of the PE used as the core particle for the composite. In an attempt to prevent any hydrophobic interaction, KPB containing 0.1% (v/v) Triton X-100 was used as an adsorption–desorption medium. The desorption curves showed similar patterns to crystalline HA for individual proteins, and further, almost all proteins were desorbed from HA composite particles below 200 m*M* KPB (Fig. 6). The results suggest that the hydrophobic interaction of proteins is responsible for incomplete desorption from HA composites. Also, it is avoidable by adding Triton X-100 without losing the ionic interaction with proteins.

We further investigated in the adsorption of proteins by HA composites by hydrophobic interaction how the adsorption influenced the adsorption–desorption behaviour by ionic interactions. The degree of adsorption and desorption of proteins was measured again with HA composite particles that had been used for the adsorption–desorption test once and had already adsorbed a certain amount of proteins hydrophobically. The used HA composite particles were suspended in 500 μl of 5 m*M* KPB after they had been washed twice with 400 and 5 m*M* KPB, respectively. The correlation between protein desorption and KPB concentration is shown in Fig. 7. Almost all proteins were desorbed from HA composite particles below 200 m*M* KPB. The irreversible adsorption of proteins seems to have reached saturation during the first

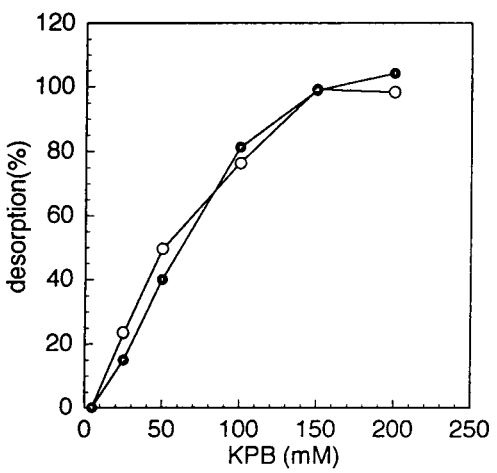

Fig. 5. Adsorption–desorption behaviour in KPB for total proteins of (○) HA and (●) crushed HA.

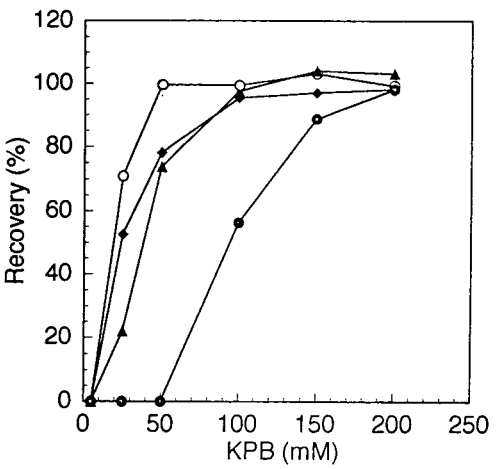

Fig. 6. Adsorption–desorption behaviour in KPB containing 0.1% (v/v) Triton X-100 for (○) BSA, (●) cytochrome *c*, (▲) lysozyme and (◆) ribonuclease A of 30% HA.

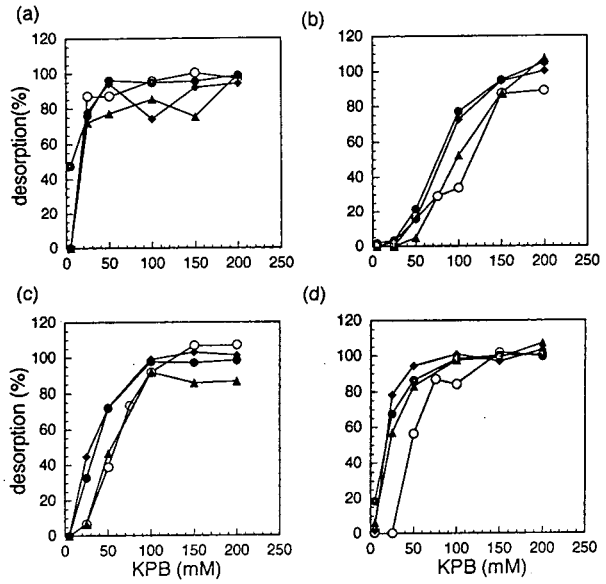

Fig. 7. Adsorption–desorption behaviour in KPB for (a) BSA, (b) cytochrome *c*, (c) lysozyme and (d) ribonuclease A of (○) HA and (●) 30%, (▲) 40% and (◆) 50% HA composite particles, which for the adsorption-desorption test once.

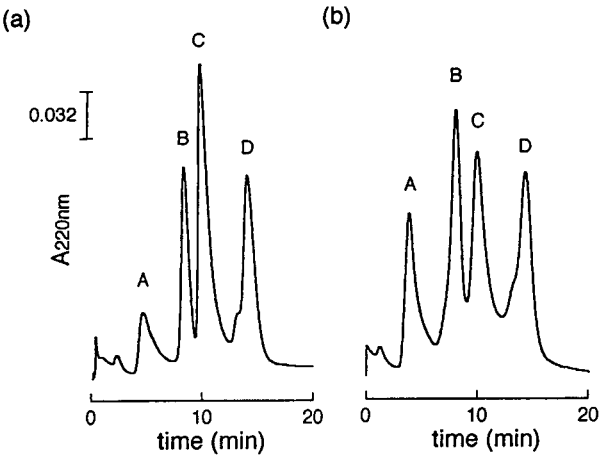

Fig. 8. Separation of standard proteins on the columns of (a) 30% and (b) 50% HA composite particles. Conditions: column, 50 mm × 2.0 mm I.D.; elution, 15-min linear gradient from 5 to 202.5 m*M* KPB; flow-rate, 0.5 ml/min; detection, UV at 220 nm. Peaks: A = BSA; B = ribonuclease A; C = lysozyme; D = cytochrome *c*.

test, and further irreversible adsorption did not occur. Each of the proteins that were adsorbed on each HA composite particle in 5 m*M* KPB now showed a characteristic desorption behaviour that was dependent on KPB concentration.

Consequently, HA composite particles demonstrated adsorption–desorption properties based on ionic interactions similar to crystalline HA.

3.5. Protein separation

The 30% and 50% HA composites were packed into columns (50 mm × 2.0 mm I.D.), which were used for the separation of a protein standard mixture. The back-pressures of the columns were 2.94 and 5.49 MPa for 30% and 50% HA, respectively, when 5 m*M* KPB was used as the mobile phase at a flow-rate of 0.5 ml/min. From the observations of HA composite particles by SEM, 50% HA contains a number of irregularly shaped small particles that resemble aggregates of HA fragments. We speculate that the back-pressure was higher than that for 30% HA because the flow path in the 50% HA column was plugged with the small particles.

Fig. 8 the results of protein separation. Both of the columns were able to separate model proteins with a linear gradient of KPB concentration. The 50% HA column exhibited relatively broad peaks and could not separate each peak to the baseline.

The 30% HA column exhibited a relatively favourable separation under the same conditions. When the column bed volume was increased, five proteins could be separated (Fig. 9). When the two chromatograms obtained from the 30% HA column (Fig. 9) and a conventional spherical HA-packed column (Fig. 10) were compared, they agreed in the elution order of proteins, and cytochrome *c* was resolved into two peaks, corresponding to the oxidized and the photoreduced forms [14] on both columns. Therefore, it is indicated that these proteins were recognized by the 30% HA column similarly to the conventional spherical HA-packed column. Although the 30% HA column totally eluted proteins at a lower concentration of KPB than the spherical HA-packed column, this is thought to be due to the feature of the crystalline

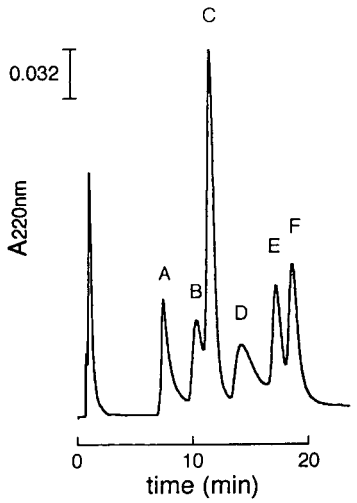

Fig. 9. Separation of standard proteins on the 30% HA column. Conditions: column, 50 mm × 4.6 mm I.D.; elution, 15-min linear gradient from 5 to 202.5 m*M* KPB; flow-rate, 0.5 ml/min; detection, UV at 220 nm. Peaks: A = BSA; B = myoglobin; C = ribonuclease A; D = lysozyme; E = cytochrome *c* (reduced); F = cytochrome *c* (oxidized).

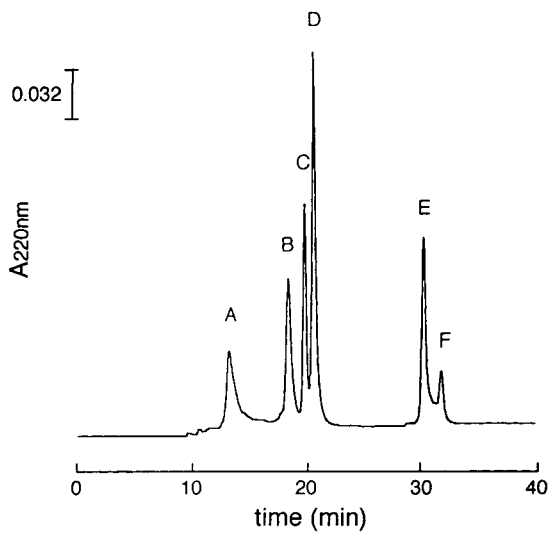

Fig. 10. Separation of standard proteins on a conventional spherical HA-packed column. Conditions: column, 135 mm × 7.8 mm I.D.; elution, 30-min linear gradient from 5 to 300 m*M* KPB; flow-rate, 1.0 ml/min; detection, UV at 220 nm. Peaks: A = BSA; B = myoglobin; C = ribonuclease A; D = lysozyme; E = cytochrome *c* (reduced); F = cytochrome *c* (oxidized).

HA used as the material, because the HA composite particles demonstrated adsorption–desorption abilities similar to those of the crystalline HA.

Irreversible adsorption of proteins on the HA composite columns was also observed in chromatographic usage with the first injection of the protein mixture. However, after 100 μg of protein had been applied, the irreversible adsorption disappeared. The irreversible adsorption could also be avoided in the presence of Triton X-100 (Fig. 11). The chromatogram of KPB containing Triton X-100 was well matched with the chromatogram without Triton X-100 in the KPB elution concentration of proteins.

The performance of the HA composite column (30% HA was employed) was evaluated by different types of examination.

Plots of plate height H vs. linear flow velocity u for tryptophan ($k' = 0.45$) with isocratic chromatography are shown in Fig. 12. The H values increase linearly with increasing velocity. When the relationship is applied to the Knox equation ($h = Av^{1/3} + B/v + Cv$; $h = H/d_p$, $v = ud_p/D$;

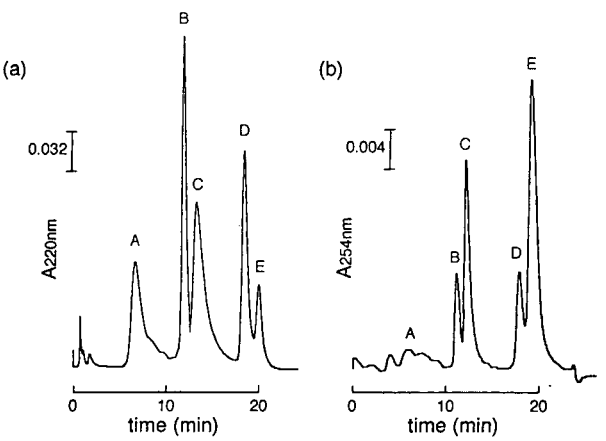

Fig. 11. Separation of standard proteins on the 30% HA column in the absence or presence of triton X-100. (a) Conditions: column, 50 mm × 4.6 mm I.D.; elution, 19-min linear gradient from 5 to 202.5 m*M* KPB; flow-rate, 0.5 ml/min; detection, UV at 220 nm. (b) Conditions: elution, 19-min linear gradient from 5 to 202.5 m*M* KPB containing 0.1% (v/v) Triton X-100; detection UV at 254 nm (a longer wavelength was employed because the absorbance by Triton X-100 was very strong at 220 nm); other conditions as in (a). Peaks: A = BSA; B = ribonuclease A; C = lysozyme; D = cytochrome *c* (reduced); E = cytochrome *c* (oxidized).

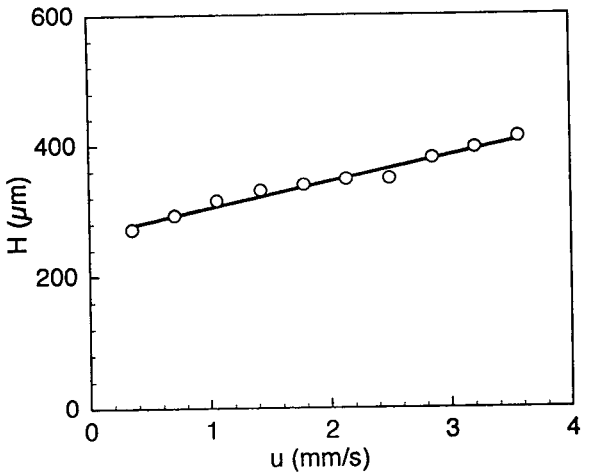

Fig. 12. Plots of plate height for tryptophan ($k' = 0.45$) on the 30% HA column as a function of the mobile phase velocity. Conditions as in Fig. 9.

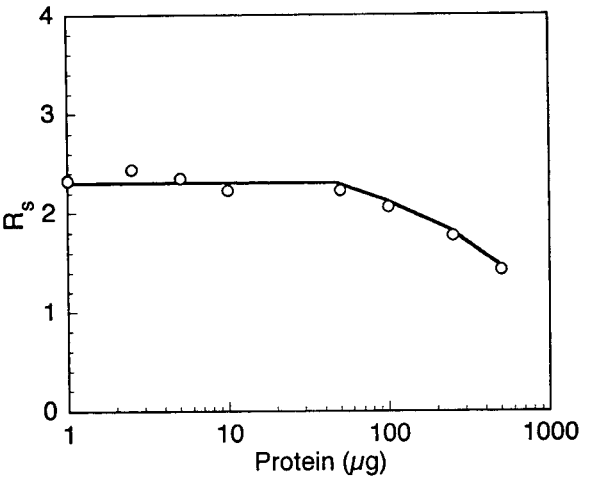

Fig. 13. Dependence of the peak resolution on sample loading of the 30% HA column. Conditions as in Fig. 9.

d_p = particle diameter of the packing, D = diffusion coefficient of solute), it is clear that coefficients A and C, that is, diffusion at inter-particles and dispersion from slow mass transfer of solute molecules, are the main reasons for band spreading on the column. As the size of the particles is relatively large, this may be responsible for the diffusion and dispersion.

The effect of sample loading was evaluated from the peak resolution under linear gradient conditions. Various concentrations of the protein solutions that contained BSA and myoglobin in the ratio 5:2, in order to be equal in peak height, were separated on the column, then total protein amount vs. resolutions (R_s) were plotted (Fig. 13). R_s remained constant at loadings up to 50 μg and then decreased with further increase in the sample loading. Accordingly, the maximum sample load resulting in the highest resolution with closed peaks is 50 μg as total amount.

The reproducibility of the HA composite particles was examined by comparing R_s on each of the columns packed with particles from five separate batches. These batches were derived from one batch of PE and two batches of crystalline HA. The R_s of BSA and myoglobin peaks was measured five times for each column using the conditions indicated in Fig. 13 and the average values obtained were 2.26, 2.24, 2.21, 2.29 and 2.49. The HA composite particles prepared by the treatment thus demonstrated good reproducibility.

After usage as an HPLC column packing for 3 weeks continuously, the particles were removed from the column and observed with SEM (Fig. 14). Elimination of the HA layer is hardly observed and the surface appearance of the used particles is the same as that of the particles before use. This confirms that HA composite particles are stable when employed continuously as HPLC column packings for at least 3 weeks.

In conclusion, the HA composite column could separate proteins using a gradient of KPB concentration, and then the reproducibility and the mechanical stability of the HPLC column packings has been demonstrated.

4. Conclusions

This study demonstrated that the dry impact blending method could produce an HPLC column packing from irregularly shaped materials too fragile for direct use in HPLC. Dry impact blending is also potentially capable of producing HPLC packings reproducibly on a large scale.

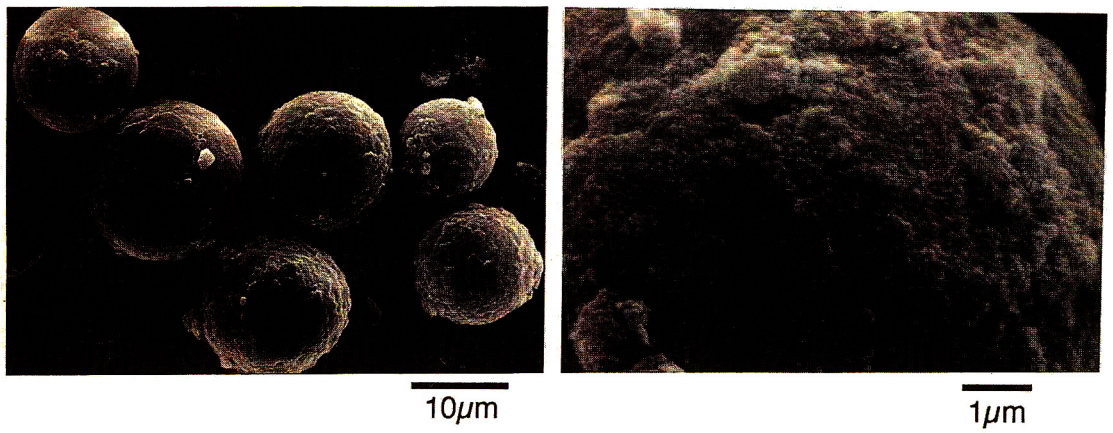

Fig. 14. Typical SEM photographs of HA composite particles after use as an HPLC column packing for 3 weeks continuously.

Appendix

If the shapes of a core and a wall particle are spherical, the optimum mixing ratio for coating the core particles with a dense monolayer of the wall particles is calculated as follows.

The maximum number of the wall particles that are arranged on the core particle can be approximated by small circles which are placed on a unit sphere in a closest-packing array. Therefore, if the radii of the core and the wall particle are R and r, respectively, the number of wall particles for coating the core particle (A) is calculated as follows [12]:

$$A \approx \frac{4\pi[R + r(1-2k)]^2}{\pi r^2} \cdot \frac{\pi}{\sqrt{12}}$$

where k is the ratio of embedded depth of the wall particle to its diameter and $\pi/\sqrt{12}$ is the approximation of the maximum coating ratio of the sphere surface due to the circles. The approximation applies when the number of fixed circles is significantly large [22]. The optimum mixing ratio of the wall particle (M) is then calculated as follows:

$$M\ (\%) = \frac{Ar^3\rho_r}{R^3\rho_R + Ar^3\rho_r} \cdot 100$$

where ρ_R and ρ_r are the specific gravity of the core particle and the wall particle, respectively.

As the densities of PE and HA are 0.92 and 3.16 g/cm^3, respectively, M for covering the 10-μm PE beads with 0.1-μm spherical HA with $k = 0$ is calculated to be ca. 11%.

References

[1] J.H. Knox and B. Kaur, in P.R. Brown and R.A. Hartwick (Editors), *High Performance Liquid Chromatography*, Wiley-Interscience, New York, 1988, p. 189.
[2] M. Kawahara, H. Nakamura and T. Nakajima, *Anal. Sci.*, 5 (1989) 485.
[3] M. Kawahara, H. Nakamura and T. Nakajima, *J. Chromatogr.*, 515 (1990) 149.
[4] U. Trüdinger, G. Müller and K.K. Unger, *J. Chromatogr.*, 535 (1990) 111.
[5] M.P. Rigny, E.F. Funkenbusch and P.W. Carr, *J. Chromatogr.*, 499 (1990) 291.
[6] J.A. Blackwell and P.W. Carr, *J. Chromatogr.*, 596 (1992) 27.
[7] J.A. Blackwell and P.W. Carr, *J. Liq. Chromatogr.*, 15 (1992) 1487.
[8] C. Hirayama, H. Ihara and X. Li, *J. Chromatogr.*, 530 (1990) 148.
[9] M. Koishi, H. Honda, T. Ishizaka, T. Matsuno, T. Katano and K. Ono, *Chim. Oggi*, 5 (1987) 43.
[10] H. Honda, K. Ono, T. Ishizaka, T. Matsuno, T. Katano and M. Koishi, *J. Soc. Powder Technol. Jpn.*, 24 (1987) 593.
[11] M. Koishi, in K. Iinoya, K. Gotoh and K. Higashitani (Editors), *Powder Technology Handbook*, Marcel Dekker, New York, 1991, p. 453.
[12] F. Honda, H. Honda and M. Koishi, *J. Chromatogr.*, 609 (1992) 49.

[13] T. Kawasaki, S. Takahashi and K. Ikeda, *Eur. J. Biochem.*, 152 (1985) 361.
[14] T. Kawasaki, W. Kobayashi, K. Ikeda, S. Takahashi and H. Monma, *Eur. J. Biochem.*, 157 (1986) 291.
[15] T. Kadoya, T. Isobe, M. Ebihara, T. Ogawa, M. Sumita, H. Kuwahara, A. Kobayashi, T. Ishikawa and T. Okuyama, *J. Liq. Chromatogr.*, 9 (1986) 3543.
[16] Y. Kato, K. Nakamura and T. Hashimoto, *J. Chromatogr.*, 398 (1987) 340.
[17] Y. Yamakawa, K. Miyasaka, T. Ishikawa, Y. Yamada and T. Okuyama, *J. Chromatogr.*, 506 (1990) 319.
[18] T. Kawasaki, M. Niikura and Y. Kobayashi, *J. Chromatogr.*, 515 (1990) 125.
[19] A. Tiselius, S. Hjertén and Ö. Levin, *Arch. Biochem. Biophys.*, 65 (1956) 132.
[20] T. Ishizaka, H. Honda, Y. Kikuchi, K. Ono, T. Katano and M. Koishi, *J. Pharm. Pharmacol.*, 41 (1989) 361.
[21] T. Ishizaka, H. Honda and M. Koishi, *J. Pharm. Pharmacol.*, 45 (1993) 770.
[22] L.F. Tóth, *Lagerungen in der Ebene, auf der Kugel und im Raum*, Springer, Heidelberg, 1972, Ch. III.

ELSEVIER

Journal of Chromatography A, 696 (1995) 31–39

JOURNAL OF CHROMATOGRAPHY A

Automated on-line trace enrichment and determination of phenolic compounds in environmental waters by high-performance liquid chromatography

E. Pocurull, G. Sánchez, F. Borrull, R.M. Marcé*

Departament de Química, Universitat Rovira i Virgili de Tarragona, Imperial Tarraco 1, 43005 Tarragona, Spain

First received 19 July 1994; revised manuscript received 1 December 1994; accepted 5 December 1994

Abstract

Automated trace enrichment of phenolic compounds on a 10 × 2.0 mm I.D. precolumn packed with PLRP-S was coupled on-line with reversed-phase column liquid chromatography and electrochemical detection. Two different eluents were used owing to the different polarities of the phenolic compounds and the difficulty of combining gradient elution with electrochemical detection. In the analysis of real samples (tap and river water), each step of the automatic method was optimized taking into account the complexity of the matrix. In tap water, the preconcentration of 4-ml samples allowed phenolic compounds to be determined at the ng l^{-1} level and the limits of detection (LODs) were between 1 and 10 ng l^{-1} (except for 2,4-dinitrophenol and 2-methyl-4,6-dinitrophenol, for which the LODs were 75 and 50 ng l^{-1}, respectively). When river water was analyzed, only 1 ml of sample could be preconcentrated because of humic and fulvic acid interference and the detection limits were about four times higher.

1. Introduction

The determination of phenol and substituted phenols is receiving increasing attention because of their toxicity. Further, the presence of chlorinated phenols, which can be present in drinking waters as a consequence of the disinfection process with chlorine, has an adverse effect on the taste and odour of water [1,2]. The maximum admissible concentration (MAC) according to EC directives for phenols in drinking water is 0.5 $\mu g\ l^{-1}$, excluding those phenols which do not react with chlorine [3].

There are various methods for determining phenols in water. The spectrophotometric method based on the reaction of 4-aminoantipyrine with phenols [4] is recommended but only the total content of phenols can be determined. Another much used method is based on gas chromatography with derivatization and electron-capture detection, which is the standard EPA method [5].

Recently, these compounds have been determined by RPLC using mainly UV [6–8] or amperometric detection [9–11], although other detection techniques such as mass spectrometry [12], fluorescence or chemiluminescence after derivatization [13] have also been described.

When amperometric detection is used, it is necessary to develop the chromatographic sepa-

* Corresponding author.

0021-9673/95/$09.50
SSDI 0021-9673(94)01202-4

ration by isocratic elution to avoid baseline distortion. In this case, when isocratic elution is used, the main problem in the separation is the different polarities of the compounds, which results in long analysis times and the appearance of broader peaks for the last-eluted compounds, with a consequent loss of sensitivity.

Although amperometric detection is very sensitive, the low concentration allowed in drinking water by EC regulations implies a preconcentration process. Liquid–liquid extraction has been the most often used technique, but in the last few years solid–phase extraction (SPE) has become more popular [14,15]. Various packing materials with different selectivity such as octadecyl-bonded silica, styrene–divinylbenzene copolymer and graphitized carbon black are currently available. Some of them have been applied to the determination of phenolic compounds [16–19], with varying results. On-line solid-phase extraction procedures involve better sensitivity, lower sample volume, lower consumption of organic solvents, higher automation potential and better reproducibility [20–25].

In this paper, the eleven phenolic compounds considered as priority pollutants by the EPA were determined using a liquid chromatographic system with an electrochemical detector. Isocratic elution was selected and two eluents had to be used. In order to decrease the limit of detection, an automatic on-line preconcentration system with a styrene–divinylbenzene copolymer precolumn and with the addition of the ion-pair reagent tetrabutylammonium bromide (TBA) to the sample was developed. The performance of the total system was checked with tap and river water.

2. Experimental

2.1. Equipment

Chromatographic experiments were performed using a Shimadzu (Tokyo, Japan) LC-9A pump with an HP-1049A electrochemical detector (Hewlett-Packard, Palo Alto, CA, USA). The temperature of the column was controlled by a Bio-Rad (Veenendaal, Netherlands) oven and chromatographic data were collected and recorded using an HP-3365 Series II Chemstation, which was controlled by Windows 3.1 (Microsoft). The separation was performed using a 250×4 mm I.D. Spherisorb ODS-2 column with a particle size of 5 μm.

The sample was injected through a Rheodyne valve with a 20-μl loop or with an automatic method using a Must column-switching device (Spark-Holland, Emmen, Netherlands) that allowed the sample to be injected after the preconcentration process. To carry out the solid-phase extraction, a precolumn (10×2 mm I.D.) packed with a styrene–divinylbenzene copolymer (PLRP-S) (15–25 μm particle size) (Spark Holland) and a Waters (Milford, MA, USA) M45 pump to deliver the sample were used.

2.2. Reagents and standards

Phenol (Ph), 4-nitrophenol (4-NP), 2,4-dinitrophenol (2,4-DNP), 2-chlorophenol (2-CP), 2-nitrophenol (2-NP), 2,4-dimethylphenol (2,4-DMP), 2-methyl-4,6-dinitrophenol (2-M-4,6-DNP), 4-chloro-3-methylphenol (4-C-3-MP), 2,4-dichlorophenol (2,4-DCP) and 2,4,6-trichlorophenol (2,4,6-TCP) were obtained from Aldrich Chemie (Beerse, Belgium) and pentachlorophenol (PCP) from Janssen Chemie (Geel, Belgium). Standard solutions (2000 mg l^{-1} of each compound) were prepared in methanol–water (50:50). If stored in a refrigerator, the solutions were stable for several months. A mixture of all phenolic compounds was prepared weekly by diluting the standard solution in water obtained with a Milli-Q system (Millipore, Bedford, MA, USA), and more diluted working solutions were prepared every day by diluting the solution with Milli-Q-purified, tap and river water.

HPLC-grade methanol (Scharlau, Barcelona, Spain) and Milli-Q quality water were used in the preparation of the eluent and in the solid-phase extraction system.

The pH values of the eluent were adjusted with sulphuric acid (Panreac, Barcelona, Spain) and acetate buffer (Merck, Darmstadt, Germany). To adjust the ionic strength of the

eluent, potassium nitrate (Probus, Badalona, Spain) and potassium chloride (Probus) were added. The tetrabutylammonium bromide used as an ion-pair reagent in the extraction process was supplied by Fluka (Buchs, Switzerland).

2.3. Chromatographic conditions and detection

Two eluents with different solvent strength were used. For the separation of the nine most polar compounds studied, the eluent used was methanol–water (45:55) acidified to pH 3.0 with H_2SO_4 and containing KCl and KNO_3 at final concentrations of 0.05 and 2 g l^{-1}, respectively (eluent A). The eluent used for the separation of 2,4,6-TCP and PCP was methanol–water (65:35) adjusted at pH 4.7 with acetic acid–sodium acetate buffer and KCl and KNO_3 at final concentrations of 0.05 and 2 g l^{-1}, respectively (eluent B). In both instances, the flow-rate was 1 ml min^{-1}, the column temperature was kept at 50°C and the volume of sample for direct injection was 20 μl.

The potential values used in the electrochemical detector were 1.1 V for the nine most polar compounds and 0.8 V for 2,4,6-TCP and PCP. The electrochemical detector worked in the amperometric mode with a glassy carbon electrode. A solid-state Ag–AgCl reference electrode was used, so the eluents had to contain KCl (0.05 g l^{-1}). The electrochemical cleaning technique was used every twenty injections to correct the electrodeposition on the surface of the electrode, applying a cyclic treatment with alternate potentials. The working electrode was polished in the conventional way every 60 injections [8,26].

2.4. On-line trace enrichment

The on-line solid-phase extraction process was carried out using a 10×2 mm I.D. precolumn packed with the styrene–divinylbenzene copolymer (PLRP-S). The pH of the samples was adjusted at about 9.0 and TBA was added at a concentration of 5 m*M*. The addition of TBA to the sample meant an increase in breakthrough volumes, mainly for the most polar compounds, as had been shown previously [27].

Fig. 1 shows a diagram of the programmable delivery system used for automatic preconcentration. Two switching valves were used in order to clean up the tubes, activate the precolumn and measure more accurately the sample volume to be preconcentrated. Table 1 shows the programme followed in the extraction process. The flow-rate was 2 ml min^{-1} in all processes. First,

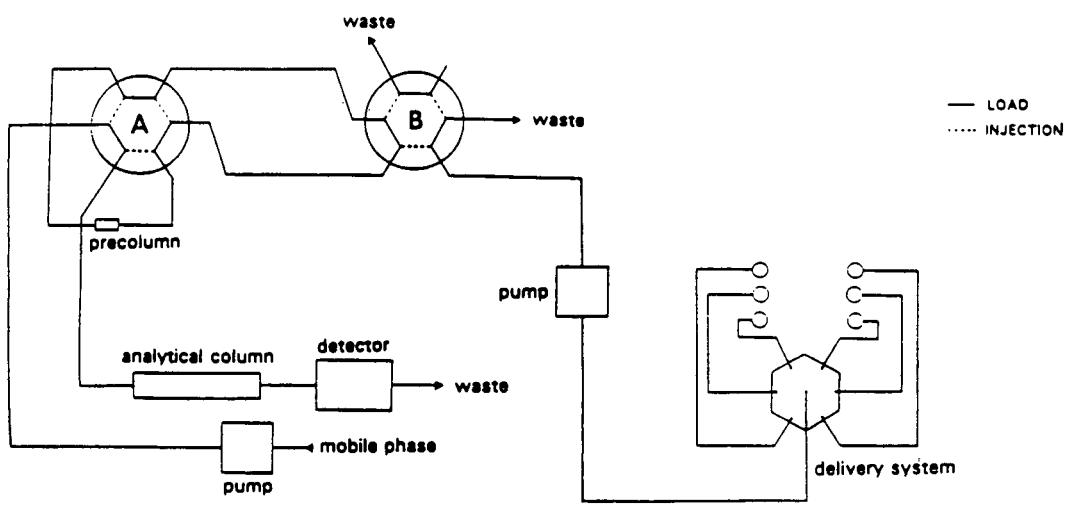

Fig. 1. Set up for automated preconcentration of sample.

Table 1
Programme for the extraction process

Step	Time (min)	Event	Valve A	Valve B
1	0	Washing tubes with methanol	Load	Load
2	2	Conditioning cartridge with methanol	Load	Inject
3	8	Washing tubes with water–TBA	Load	Load
4	10	Activation of cartridge with water–TBA	Load	Inject
5	11	Washing tubes with sample	Load	Load
6	13	Sample preconcentration	Load	Inject
7[a]	15	Washing tubes with water–TBA	Load	Load
8[a]	17	Clean-up with water–TBA	Load	Inject
9	15/18.5	Analyte desorption	Inject	Inject

[a] Only applied when river water was analysed.

the preconcentration system was washed with methanol for 2 min to remove all the solvents between the delivery system and the pump delivering sample. Then, in step 2, the cartridge was cleaned up and conditioned with methanol for 6 min. Another step (3) was introduced to remove the methanol with a 5 m*M* solution of TBA. After activating the cartridge with the TBA solution for 1 min and cleaning the tubes with the sample for 2 min, the preconcentration step started (at 13 min). The length of this step can be changed depending on the matrix sample (2 min for standard solution and tap water or 0.5 min for river water). In the next step, the analytes trapped on the precolumn were desorbed in the backflush mode and transferred on-line to the analytical column.

When river water was analysed, prior to the injection of the sample two additional steps were introduced in the programme to remove humic and fulvic acids, which may introduce an important distortion peak at the beginning of the chromatogram. In this case, two steps (7 and 8) to clean up the tubes and the cartridge were included in the programme.

3. Results and discussion

As mentioned above, two eluents were optimized to carry out the isocratic separation: one to separate the nine most polar phenolic compounds studied (eluent A, which contains 45% methanol) and another, with a higher solvent strength (eluent B, with 65% of methanol), to separate 2,4,6-TCP and PCP, which are the least polar compounds studied. The best results for the more polar compounds were obtained at pH 3.0, but for the other compounds (eluent B), the pH had to be increased in order to shorten the analysis time, because the retention time of PCP is highly pH dependent, although the retention time of 2,4,6-TCP does not change very much with pH. Of the different pH values tested, between 3 and 5, pH 4.7 allowed the separation of both compounds in less than 10 min. Although some workers used gradient elution [11], lower sensitivity was obtained because of the baseline drift and two runs are preferred [8].

In order to select the best working potential, different potential values were tested and for eluent A the potential had to be fixed at 1.1 V, because at lower potentials nitrophenols had a very low response in the range of concentrations studied and a considerable background appeared in the chromatogram at higher potential values, which meant that it took a longer time to stabilize the detector. On the other hand, for 2,4,6-TCP and PCP, with the eluent specified previously, the highest signal was obtained at 0.8 V.

The electrochemical ratios of the peak areas at different voltages for each phenolic compound were determined under the experimental conditions used so that they could be used as confirmation data when real samples were ana-

Table 2
Electrochemical ratios of the peak areas at different voltages

Compound	0.8/1.1 V	0.9/1.1 V	1.0/1.1 V	0.7/0.8 V	1.0/0.8 V	1.1/0.8 V
Ph	0.05	0.28	0.71			
4-NP	0.00	0.00	0.11			
2,4-DNP	0.00	0.02	0.08			
2-CP	0.13	0.44	0.74			
2-NP	0.00	0.01	0.29			
2,4-DMP	0.51	0.74	0.91			
2-M-4,6-DNP	0.00	0.00	0.07			
4-C-3-MP	0.27	0.60	0.76			
2,4-DCP	0.41	0.77	0.88			
2,4,6-TCP				0.89	0.94	0.91
PCP				0.29	0.86	0.81

lysed. The results are given in Table 2 and the relative standard deviations of the values ($n = 4$) were between 1.5 and 7.9%.

Fig. 2 shows the chromatograms obtained after a 20-μl injection of a standard solution of 20 μg l^{-1} of each phenol except 2-M-4,6-DNP (40 μg l^{-1}) and 2,4-DNP (200 μg l^{-1}) with the two optimum eluents. Good resolution between the different peaks was observed. The linearity of the response was checked for different ranges depending on the sensitivity of each compound and in all instances good linearity was achieved. The detection limits of the chromatographic method were determined for a signal-to-noise ratio of about 3, and the results of linearity ranges and limits of detection are given in Table 3.

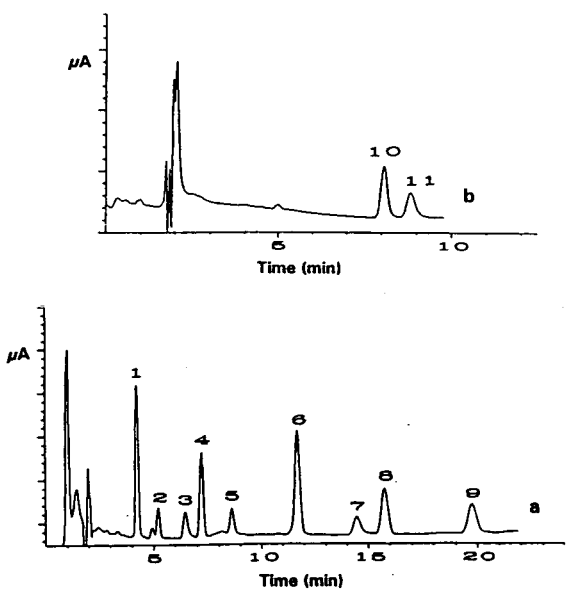

Fig. 2. Chromatograms obtained under optimum conditions for a standard solution of phenols of 20 μg l^{-1}, except 2-methyl-4,6-dinitrophenol (40 μg l^{-1}) and 2,4-dinitrophenol (200 μg l^{-1}). (a) Eluent A; (b) eluent B. 1 = phenol; 2 = 4-nitrophenol; 3 = 2,4-dinitrophenol; 4 = 2-chlorophenol; 5 = 2-nitrophenol; 6 = 2,4-dimethylphenol; 7 = 2-methyl-4,6-dinitrophenol; 8 = 4-chloro-3-methylphenol; 9 = 2,4-dichlorophenol; 10 = 2,4,6-trichlorophenol; 11 = pentachlorophenol.

In order to determine lower concentrations of phenols, a preconcentration system was required. On-line trace enrichment systems improve the limit of detection as all of the preconcentrated sample is injected into the chromatographic system whereas only an aliquot is injected when an off-line system is used.

Different packing materials were used for on-line SPE. In a previous paper [17] the off-line SPE of phenolic compounds was studied and it was shown that a styrene–divinylbenzene copolymer meant a higher breakthrough volume than C_{18} or cyclohexyl and the addition of an ion-pair reagent such as TBA also increased the breakthrough volumes of phenolic compounds. Some workers [20] recommend the use of two precolumns in series, one with PLRP-S for all phenolic compounds except for phenol, because of the low breakthrough volume, for which they recommended a non-ionic styrene–divinylbenzene copolymer with a large number of active aromatic sites (ENVI-Chrom P) and, conse-

Table 3
Linearity ranges, R^2 and limits of detection of phenolic compounds by direct injection and with on-line trace enrichment of 4 ml of Milli-Q-purified water adjusted to pH 9 and with TBA added

Compound	Direct injection			On-line trace enrichment		
	Linear range ($\mu g\ l^{-1}$)	R^2	LOD ($\mu g\ l^{-1}$)	Linear range ($\mu g\ l^{-1}$)	R^2	LOD ($ng\ l^{-1}$)
Ph	1–20	0.9990	0.1	0.01–1.0	0.9996	2
4-NP	5–25	0.9984	1	0.025–5.0	0.9982	10
2,4-DNP	25–200	0.9996	10	0.1–10.0	0.9984	75
2-CP	1–20	0.9994	0.5	0.01–1.0	0.9996	5
2-NP	5–25	0.9986	1	0.025–5.0	0.9986	10
2,4-DMP	1–20	0.9994	0.1	0.01–1.0	0.9996	2
2-M-4,6-DNP	5–25	0.9990	2	0.075–5.0	0.9980	50
4-C-3-MP	1–20	0.9990	0.5	0.01–1.0	0.9990	5
2,4-DCP	1–20	0.9980	0.5	0.01–1.0	0.9980	5
2,4,6-TCP	1–50	0.9990	0.1	0.01–1.0	0.9978	1
PCP	1–50	0.9988	0.1	0.01–1.0	0.9962	1

quently, a higher retention of phenolic compounds. In a recent paper [27], on-line SPE of phenolic compounds was studied and the influence of the different parameters, including the addition of TBA to the sample, on the breakthrough volumes was studied. Most compounds had breakthrough volumes considerably higher with PLRP-S than with other precolumns, whereas for the most polar compounds, mainly phenol, the breakthrough volumes were low and were considerably increased by the addition of TBA to the sample.

According to the values obtained, 4 ml of sample with TBA added was chosen as the volume for preconcentration, mainly determined by the phenol breakthrough volume. It should also be pointed out that higher sample volumes would cause overlap of the phenol peak with the peak that appeared at the beginning of the chromatogram and owing to the polar compounds retained in the precolumn.

Fig. 3 shows the chromatograms of 4 ml of Milli-Q-purified water spiked at 0.1 $\mu g\ l^{-1}$ with each phenolic compound, except 0.2 $\mu g\ l^{-1}$ for 2-M-4,6-DNP and 1 $\mu g\ l^{-1}$ for 2,4-DNP when the on-line trace-enrichment process was used. Good resolution between the different peaks can be observed, in addition to the presence of several unknown peaks with different retention times from the peaks of the compounds studied. Only slight peak broadening was observed for the compounds when the automatic on-line preconcentration method was used.

The linearity of the response for the total

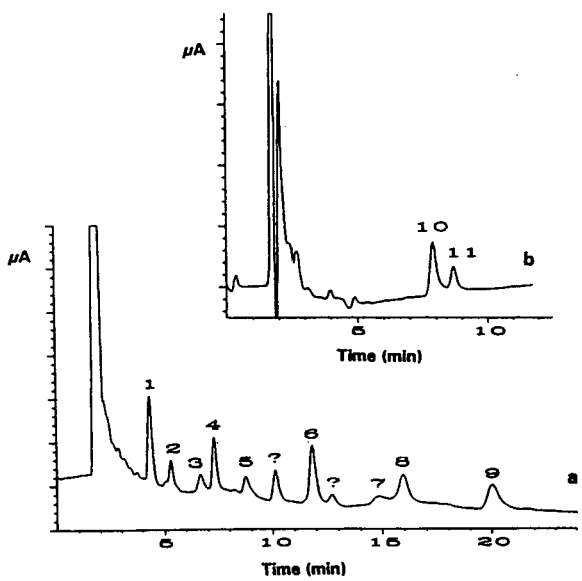

Fig. 3. Chromatograms obtained by on-line trace enrichment of 4 ml of Milli-Q-purified water spiked at 0.1 $\mu g\ l^{-1}$ with each phenolic compound, except 2-methyl-4,6-dinitrophenol (0.2 $\mu g\ l^{-1}$) and 2,4-dinitrophenol (1 $\mu g\ l^{-1}$). (a) Eluent A; (b) eluent B. For peak designation, see Fig. 2; ? = unknown.

analytical system, including the preconcentration step, was checked for a sample volume of 4 ml of Milli-Q-purified water spiked at different concentrations depending on the sensitivity of each phenolic compound. The results obtained for the linearity range are included in Table 3 together with the limits of detection (signal-to-noise ratio = 3). The recoveries for a sample of 0.2 $\mu g\ l^{-1}$ were >85% for all compounds except 2,4-DNP and 2-M-4,6-DNP, the recoveries of which were about 75%. The repeatability of the method was checked with a 4-ml Milli-Q-purified water sample spiked at the 0.1 $\mu g\ l^{-1}$ level and the R.S.D. were between 1.5 and 7.7% ($n = 4$).

The analytical performance of the system was tested with tap and river water. When tap water was analysed, 300 μl of a 10% solution of Na_2SO_3 were added to 100 ml of water before adding the standard solution of phenolic compounds in order to eliminate free chlorine, which could react with phenols and produce chlorophenols [13].

The linearity of the method was checked with tap water and it was essentially as good as for Milli-Q-purified water (R^2 values between 0.995 and 0.9994). Recoveries were calculated from the calibration graph including a preconcentration step with Milli-Q-purified water [28] and they were >90% for all compounds. The repeatability of the method was checked with a 4 ml of tap water sample spiked at the 0.1 $\mu g\ l^{-1}$ level. The R.S.D.s were between 1.9 and 8.2% ($n = 4$). The limits of detection were also similar to those obtained with Milli-Q-purified water and allowed pollutants to be determined at the levels required by present EC regulations.

On-line trace enrichment for river water showed a large, distorted peak at the beginning of the chromatogram, owing to the presence of humic substances in the river water. When eluent A was used, a volume of 4 ml of sample could not be preconcentrated because of interference with the first compounds eluted. It was necessary to decrease the volume for preconcentration.

A volume of 1 ml of sample was chosen to be preconcentrated. Under these conditions, a less distorted peak at the beginning of the chromatogram also appeared. Different clean-up steps were studied and the optimum one, with a decrease in the peak due to fulvic and humic acids and no decrease in the recoveries of phenolic compounds, is given in Table 1. The linearity of the response of the complete system was checked and linear ranges were found to be 0.05–5 $\mu g\ l^{-1}$ for all the compounds analysed with eluent A, except 2,4-DNP (0.5–40 $\mu g\ l^{-1}$) and 2-M-4,6-DNP (0.5–20 $\mu g\ l^{-1}$) ($R^2 = 0.994$–0.998). The repeatability of the method in river water was checked with a sample spiked at 0.5 $\mu g\ l^{-1}$ and the R.S.D.s found were between 3.2 and 8.5% ($n = 4$). The limits of detection (LOD) were between 5 and 50 ng l^{-1}, except for 2-M-4,6-DNP and 2,4-DNP (0.2 and 0.3 $\mu g\ l^{-1}$, respectively).

In Figs. 4a and b the chromatograms of a river water sample and the same sample spiked with a standard solution of the nine phenolic compounds at the 0.5 $\mu g\ l^{-1}$ level are shown. Different peaks also appeared but none of them could be assigned to any phenolic compound.

Fig. 4c shows the chromatogram obtained after the on-line preconcentration of 4 ml of tap water with the addition of Na_2SO_3. Several peaks appeared, one of them at the same retention time as phenol, which was assigned to phenol using electrochemical ratios. The concentration of phenol was 43 ng l^{-1}. The chromatogram obtained for a 4-ml tap water sample spiked with a phenolic compounds at the 0.1 $\mu g\ l^{-1}$ level with the addition of Na_2SO_3 is shown in Fig. 4d. Samples treated with Na_2SO_3 showed a larger peak at the beginning of the chromatogram.

The same study was carried out with the other two compounds and the results obtained in the analysis of 4-ml tap water sample and a 4-ml tap water sample spiked with a standard solution of 0.1 $\mu g\ l^{-1}$ and addition of sulphite solution are shown in Fig. 5a and b, respectively. It can be seen that a peak with a retention time similar to that of 2,4,6-TCP appears, but a study of the response at several potential values did not confirm the presence of this compound. It should be pointed out that the narrower peak at the beginning of the chromatogram is due to the

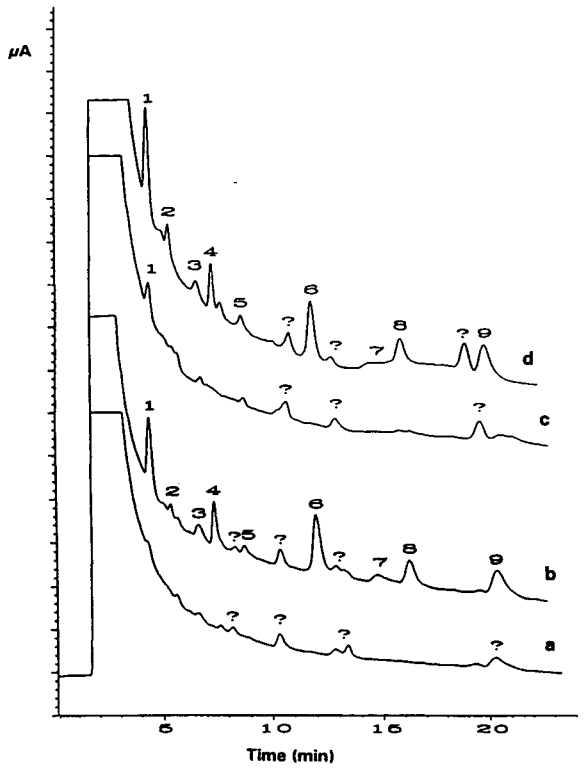

Fig. 4. Chromatograms with eluent A of (a) 1 ml of river water sample followed by the clean-up step (3 ml of water–TBA); (b) 1 ml of river water sample spiked at 0.5 $\mu g\ l^{-1}$ with each phenolic compound, except 2-M-4,6-DNP (1 $\mu g\ l^{-1}$) and 2,4-DNP (4 $\mu g\ l^{-1}$), followed by the clean-up step; (c) a 4-ml sample of tap water with Na_2SO_3 added; (d) a 4-ml sample of tap water with Na_2SO_3 added and spiked with a standard addition as in Fig. 3. For peak designation, see Fig. 2.

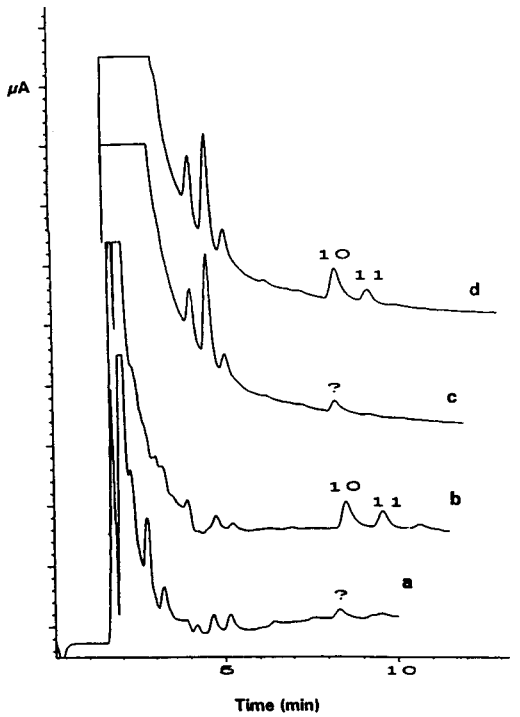

Fig. 5. Chromatogram with eluent B of (a) a 4-ml sample of tap water; (b) a 4-ml sample of tap water spiked at 0.1 $\mu g\ l^{-1}$ with 2,4,6-TCP and PCP; (c) a 4-ml river water sample; (d) a 4-ml river water sample spiked at 0.1 $\mu g\ l^{-1}$ with 2,4,6-TCP and PCP. For peak designation, see Fig. 2.

higher solvent strength of eluent B compared with eluent A.

For the determination of 2,4,6-TCP and PCP in river water, no clean-up step was required. In this instance, the volume of sample for the analysis was 4 ml and no large peak appeared at the beginning of the chromatogram, owing to the higher solvent strength. The linearity ranges for tap and river water were the same as those obtained for Milli-Q-purified water. The R.S.D.s for a 4-ml river water sample spiked at 0.1 $\mu g\ l^{-1}$ with 2,4,6-TCP and PCP were 3.2 and 5.1%, respectively ($n = 4$), and L.O.D. were 1 ng l^{-1} for both compounds. Chromatograms for a 4-ml river water sample and a 4-ml river water sample spiked at 0.1 $\mu g\ l^{-1}$ with each compound are shown in Fig. 5c and d, respectively. The peak that appeared at the same retention time as TCP was not assigned to this compound using the electrochemical ratios.

4. Conclusions

An on-line trace-enrichment–reversed-phase liquid chromatographic method with electrochemical detection has been developed for the determination of phenolic compounds in environmental waters. Two different eluents had to be optimized owing to the different polarities of the compounds studied. The addition of an ion-pair reagent to the sample allowed higher volumes of sample to be preconcentrated with

better recoveries, mainly for the most polar compounds. The preconcentration of only 4 ml of tap water allowed most compounds to be determined in the range 0.01–0.5 $\mu g\ l^{-1}$ and the LODs were at the low ng l^{-1} level. When river water samples were analysed, it was only possible to preconcentrate 1 ml of sample and the LODs were about four times higher.

References

[1] P.A. Realini, *J. Chromatogr. Sci.*, 19 (1981) 124.
[2] D.A. Baldwin and J.K. Debowski, *Chromatographia*, 26 (1988) 186.
[3] *Drinking Water Directive 80/778/EEC*, Commission of the European Communities, Brussels, 1980.
[4] *Standard Methods for the Examination of Water and Wastewater*, American Public Health Association, New York, 16th ed., 1985.
[5] *Fed. Regist.*, 233, No. 44, Dec. 3 (1979) 69464.
[6] C.P. Ong, H.K. Lee and S.F.Y. Li, *J. Chromatogr.*, 464 (1989) 405.
[7] O. Busto, J.C. Olucha and F. Borrull, *Chromatographia*, 32 (1991) 566.
[8] J. Ruana, I. Urbe and F. Borrull, *J. Chromatogr. A*, 655 (1993) 217.
[9] E. Nieminen and P. Heikkila, *J. Chromatogr.*, 464 (1989) 405.
[10] R.E. Shoup and G.S. Mayer, *Anal. Chem.*, 54 (1982) 1164.
[11] D.A. Baldwin and J.K. Debowski, *Chromatographia*, 26 (1988) 186.
[12] D.F. Hunt, J. Shabanowitz, T.M. Harvey and M. Coates, *Anal. Chem.*, 57 (1985) 525.
[13] P.J.M. Kwakman, D.A. Kamminga, U.A.Th. Brinkman and G.J. de Jong, *J. Chromatogr.*, 553 (1991) 345.
[14] I. Liska, J. Krupcík and P.A. Leclerq, *J. High Resolut. Chromatogr.*, 12 (1989) 577.
[15] B. Gawdzik, J. Gawdzik and U. Czerwinska-Bil, *J. Chromatogr.*, 509 (1990) 136.
[16] E. Pocurull, M. Calull, R.M. Marcé and F. Borrull, *Chromatographia*, 38 (1994) 579.
[17] A. Di Corcia, S. Marchese and R. Samperi, *J. Chromatogr.*, 642 (1993) 175.
[18] C. Borra, A. Di Corcia, M. Marchetti and R. Samperi, *Anal. Chem.*, 10 (1991) 317.
[19] L. Schmidt, J.J. Sun, J.S. Fritz, D.F. Hagen, C.G. Markell and E.E. Wisted, *J. Chromatogr.*, 641 (1993) 57.
[20] E.R. Brouwer and U.A.Th. Brinkman, *J. Chromatogr. A*, 678 (1994) 223.
[21] M.W. Nielen, U.A.Th. Brinkman and R.W. Frei, *Anal. Chem.*, 57 (1985) 806.
[22] I. Liska, E.R. Brouwer, H. Lingeman and U.A.Th. Brinkman, *Chromatographia*, 37 (1993) 13.
[23] P. Subra, M.C. Hennion, R. Rosset and R.W. Frei, *J. Chromatogr.*, 456 (1988) 121.
[24] U.A.Th. Brinkman, *J. Chromatogr. A*, 665 (1994) 217.
[25] M.C. Hennion, *Trends Anal. Chem.*, 10 (1991) 317.
[26] A.G. Huesgen and R. Schuster, *Selective HPLC Analysis in River Water* (*Application Note*), Hewlett-Packard, Waldbronn, 1990.
[27] E. Pocurull, R.M. Marcé and F. Borrull, *Chromatographia*, in press.
[28] V. Pichon and M.C. Hennion, *J. Chromatogr. A*, 665 (1994) 269.

ELSEVIER

Journal of Chromatography A, 696 (1995) 41–47

JOURNAL OF CHROMATOGRAPHY A

Determination of residual free epoxide in polyether polyols by derivatization with diethylammonium N,N-diethyldithiocarbamate and liquid chromatography

F. Van Damme*, A.C. Oomens

Analytical Development Department, Dow Benelux N.V., P.O. Box 48, 4530 AA Terneuzen, Netherlands

First received 22 August 1994; revised manuscript received 19 December 1994; accepted 20 December 1994

Abstract

A normal-phase liquid chromatographic method is described for the determination of epoxides and particularly residual ethylene oxide and propylene oxide in polyether polyols. The residual epoxides are derivatized with diethylammonium N,N-diethyldithiocarbamate into the corresponding 1-(N,N-diethyldithiocarbamoyl)-2-hydroxyethane and -hydroxypropane. The dithiocarbamoyl esters are extracted into chloroform and separated by normal-phase liquid chromatography. Detection is done by ultraviolet at 278 nm. Total analysis time is about 45 min. Linearity (0.1–100 ppm), detection limits (0.5 ppm), recovery from spiked samples (>95%) and interferences have been studied.

1. Introduction

Epoxides such as ethylene oxide (epoxyethane, EO) and propylene oxide (1,2-epoxypropane, PO) are important chemicals for the manufacture of polyoxyalkylene substances with a large variety of industrial and pharmaceutical applications (e.g. polyurethanes, lubricants, soaps, cosmetics). Both EO and PO are classified as toxic components. EO has shown sufficient evidence for suspected carcinogenity to animals and humans [1]. Exposure of humans to EO and PO should therefore be minimized.

The analysis of residual free epoxides can be done by gas chromatography (GC) with electron-capture detection. For this purpose, the epoxides are first reacted with hydrobromic acid followed by further derivatization of the resulting 2-bromoalkanol with heptafluorobutyrylimidazole. Application of this approach has been described for the determination of EO in air [2]. The analysis of residual epoxides in high-molecular-mass polyoxyalkylene adducts such as polyether polyols is less straightforward with GC. In this case the epoxides need to be separated from the rest of the viscous non-volatile matrix prior to analysis, or a chromatographic multicolumn switching system is necessary. The use of the purge and trap technique followed by GC–flame ionization detection had been evaluated before, but had shown to be problematic because of the presence of small volatile molecules interfering with the determination of residual EO or PO. These by-products were often present in higher concentrations than

* Corresponding author. Present address: Dow Deutschland Inc., Postfach 20, D-77834 Rheinmünster, Germany.

0021-9673/95/$09.50
SSDI 0021-9673(94)01270-9

the residual free epoxides and interfered with the quantitation because of partial or complete co-elution. Depending on the polyether production conditions applied, the concentration of these interfering substances varies from product to product. A second approach using GC could be the splitting of free epoxides with acid, followed by derivatization with acetic anhydride or trifluoroacetic anhydride. In the case of polyether polyols however, there can be some residual amounts of ethylene glycol and propylene glycol present in the samples as such. Besides the latter, vinyl ethers are present as well, which split into small carbonyl components by acid treatment. So a number of side reactions can take place, complicating the analysis. The nature of the polyol product and more importantly of some by-products, is thus such that they can interfere in the GC analysis. Therefore, a liquid chromatographic (LC) procedure in combination with the off-line derivatization procedure has proven to be more reliable in this case.

The present article describes the determination of residual epoxides in polyether polyols (molecular mass 1000–10 000 g/mol) using isocratic liquid chromatography in combination with a simple off-line derivatization reaction that converts the epoxides into UV-absorbing dithiourethanes. The use of N,N-diethyldithiocarbamate (DDTC) salts for epoxide derivatization has been reported before in the determination of 1,2:5,6-dianhydrogalactitol, a hexitol diepoxide, in blood plasma [3]. Sodium DDTC was used in this case to convert the drug into a UV absorbing species with higher hydrophobic character, in order to transfer it to water-immiscible solvents such as chloroform. After derivatization, the resultant dithiocarbamoyl ester was analyzed by LC with UV detection. The DDTC salts are most known for their chelation capabilities of heavy metal ions. Because of this property they have been applied in the analysis of bivalent ions such as Pb^{II}, Hg^{II}, Cd^{II} and Cu^{II} [4,5] and of Pt^{II} complexes [6,7]. Sodium DDTC has been used as well to preconcentrate heavy metal ions from aqueous solutions into non-polar solvents [4,8].

2. Experimental

2.1. Chemicals

All solvents (*n*-hexane, methanol, tetrahydrofuran, chloroform) used were from J.T. Baker in highest purity available (HPLC grade or equivalent). Phosphate buffer solution Ready to use at pH 7.00 was obtained from Merck. Phosphoric acid (85%) was from J.T. Baker. Propanal (99 + %) was obtained from Janssen Chimica. Acetaldehyde (99 + %) and acetone (HPLC grade) were from J.T. Baker. The derivatization agent diethylammonium DDTC (98%) was from Aldrich. The sodium salt (99%) of DDTC was obtained from Merck. EO (>99%) and PO (>99%) were obtained from the production plants in Dow Benelux (Terneuzen, Netherlands) and Dow Deutschland (Stade, Germany) respectively.

2.2. Sample preparation and derivatization procedure

As most solvents and reagents are toxic and/or flammable, all sample preparation was performed in a fumehood. Epoxides are known to react with dithiocarbamic acid salts [3] according to the scheme in Fig. 1. The resulting 1-(N,N-diethyldithiocarbamoyl)-2-hydroxyethane and

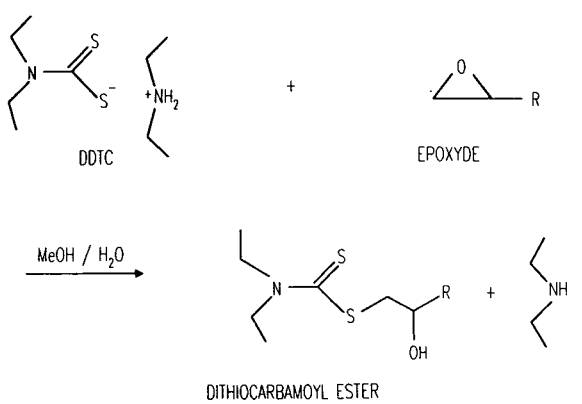

Fig. 1. Reaction of DDTC diethylammonium salt with epoxides.

-hydroxypropane (dithiourethanes) absorb UV light with a maximum at 278 nm. As an example, the UV spectrum of the epoxyethane–dithiocarbamate adduct is shown in Fig. 2.

The reagent solution was prepared by dissolving 500 mg of diethylammonium DDTC in 50 ml of buffer at pH 7.00. The solution was put in an ultrasonic batch for 5 min (the resulting solution will stay somewhat opalescent). A fresh reagent solution was made each day. The solution is stable above pH 6, below this pH rapid decomposition with carbon disulfide evolution takes place. The solid salt of DDTC was stored in a refrigerator for no longer than one month after opening.

Standard solutions containing epoxide in the amount of 1000 ppm were prepared in methanol and stored in a deep freezer. These were further diluted in methanol to obtain epoxide concentrations of 0.1 up to 50 ppm (mg/l methanol).

The standards were derivatized by mixing 5.0 ml of standard solution (in methanol) with 5.0 ml of DDTC reagent in a pressure resistant 20-ml glass vial. The vials were closed with PTFE-lined aluminum snap-caps, shaken and put in an oven at 90°C for 30 min. As safety precaution, the vials were put into a screw-capped stainless-steel container standing permanently in the oven. After this period the vials were cooled to room temperature with streaming water. Fifteen drops of 85% phosphoric acid (about 0.3 ml) were added, followed by 10.0 ml of chloroform. The vial was shaken vigorously during 1 min. After phase separation, 10 μl of the lower chloroform layer were subjected to LC analysis.

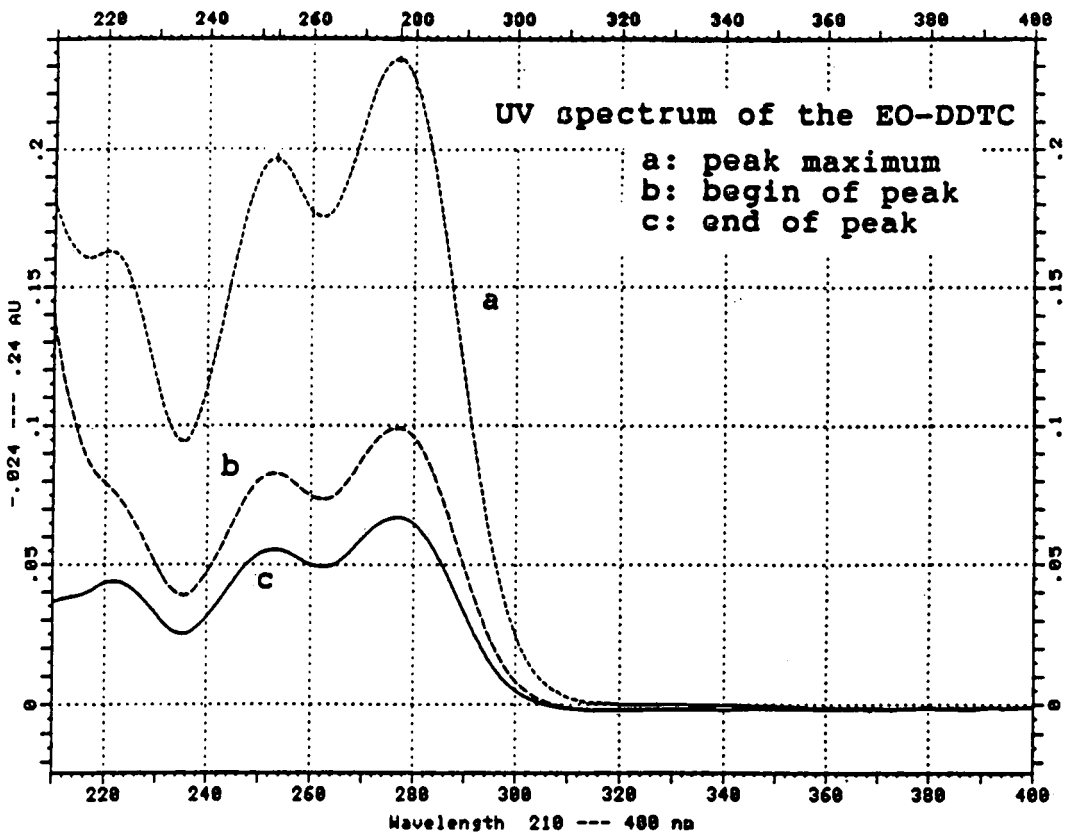

Fig. 2. UV spectrum of 1-(N,N-diethyldithiocarbamoyl)-2-hydroxyethane.

Samples were derivatized by accurately weighing approximately 500 mg of polyether polyol in a 20-ml glass vial, after which 4.5 ml of methanol and 5.0 ml of DDTC reagent were added. Further sample preparation was identical as described above. The polyether polyol distributes over the two layers giving rise to a hazy appearance of both the chloroform and methanol layer (after about half an hour, the polyether polyol has completely migrated into the methanol layer, giving a clear chloroform layer). After methanol–chloroform phase separation, 10 μl of the chloroform layer was injected into the liquid chromatograph. No chromatographic problems such as pressure increase or baseline drift were observed with this procedure for a period of at least 5 days. The blank was prepared by mixing 5.0 ml of the DDTC solution with 5.0 ml of methanol, followed by the procedure as described above.

2.3. Chromatographic conditions

A Shimadzu LC-9A pump and Shimadzu SPD-6AV UV–Vis detector (278 nm and 0.02 AUFS) were used. A 10-μl volume of the chloroform layer was injected by a Valco 6-way valve. Quantitation was done on peak area using Nelson 6000 software on a HP1000 computer. A Zorbax-NH_2 column (25 cm × 0.46 cm I.D.) from DuPont was used. The eluent consisted of 89% (v/v) of *n*-hexane, and 11% (v/v) of methanol–tetrahydrofuran (2:1). Flow-rate was set to 1.0 or 2.0 ml/min. At the end of each week the column was rinsed with about 200 ml of tetrahydrofuran to remove adsorbed polymers.

3. Results and discussion

3.1. Quantitative aspects

The precision of the derivatization and analysis procedure was studied by derivatizing and analyzing one sample 10 times spread over two successive days. The data are presented in Table 1. The relative standard deviations (R.S.D.s) on PO and EO determination were 3.2 and 5.3%, respectively (at levels of 2.9 and 1.5 ppm, respectively).

Calibration lines of concentration versus detector response were linear in the range from 0.1 to 100 ppm. These concentrations refer to the epoxide standard solutions in methanol of which 5 ml were used in the derivatization procedure. The linear regression coefficients were 0.99998 and 0.99992 for EO and PO, respectively. With the 10-μl injection, the detection limits for both epoxides were about 50 ppb (signal/noise = 3). This corresponds to a level of 0.5 ppm in the samples if 500 mg were used in the final procedure. When lower concentrations need to be determined a larger injection volume can be used.

The recovery from spiked samples was studied with different amounts of polyether taken into account. Samples were fortified with varying amounts of the standard solution prepared as described above. Low recoveries at low concentrations were measured when 1000-mg sample amounts were used. However when 500 mg of polyether polyol was used, complete recovery was observed down to sub-ppm level. The data are presented in Table 2.

Table 1
Precision of derivatization and analysis

Analysis	Day	PO counts	EO counts
1	1	9 819	5 520
2	1	9 729	5 409
3	1	9 887	5 703
4	1	10 138	5 748
5	1	10 663	6 505
6	2	9 636	5 632
7	2	9 953	5 813
8	2	10 186	6 060
9	2	9 631	5 658
10	2	9 802	5 712
Average		9 944	5 776
S.D.		314	309
R.S.D. (%)		3.2	5.3

Table 2
Ethylene oxide recovery from spiked samples

Sample amount (g)	Spike (ppm)	Counts		Recovery (%)
		Theory	Found	
0.98	1	22 432	17 501	78
1.00	4	61 984	54 830	88
0.97	10	141 088	129 446	92
0.98	20	272 928	258 507	95
0.99	40	536 608	515 260	96
0.50	0.4	6 413	6 975	109
0.50	0.8	14 023	14 365	102
0.50	1.0	18 828	18 853	100
0.50	2.0	36 853	38 939	106
0.50	10.0	188 828	208 384	110

3.2. Interferences

The possible interference of traces of small molecule aldehydes and ketones present in samples was studied. To see whether such contaminants give rise to DDTC adducts eluting at similar retention times as the epoxides, small carbonyl components such as propanal, acetone and acetaldehyde (1500, 1200 and 900 ppm in methanol, respectively) were subjected to the same derivatization procedure as described in the experimental part. No interfering peaks were observed on the position of the epoxide–DDTC adducts. Residual EO and PO were also determined in polyether polyol based on aromatic initiators (e.g. phenols). In most products coelution of the EO–and/or PO–DDTC adducts with low-molecular-mass polyether oligomers was observed. This makes the determination of residual free epoxides in such products at the above described conditions impossible.

3.3. DDTC sodium salt versus diethylammonium salt

In order to study the effect of the DDTC cation on the epoxide–dithiocarbamate reaction yield, 1% (w/v) solutions of both sodium and diethylammonium DDTC were used for the derivatization of epoxide standards. The obtained responses for EO and PO were 45 and 10%, respectively, higher when the diethylammonium salt was used, despite the higher molar concentration of the sodium DDTC reagent. Due to this higher yield, the ammonium salt was used further.

3.4. Stability of derivatized standards

After the derivatization procedure, the chloroform layer was routinely analyzed within 8 h. However, the obtained dithiocarbamoyl esters in chloroform slowly decay in time. A derivatized 1 ppm ethylene oxide solution was reanalyzed after standing 4 days at room temperature. The area counts of the adduct after this time period decreased to about 85% of its original value, directly measured after derivatization. Normally, no corrections were made on the quantitation, because samples were analyzed directly after derivatization.

3.5. Effect of derivatization temperature on reaction rate

The reaction rate and yield between the epoxide and DDTC ammonium salt was studied at 25, 70, 90 and 100°C. At room temperature the final equilibrium concentration was only reached after 24 h. At 70°C the same equilibrium con-

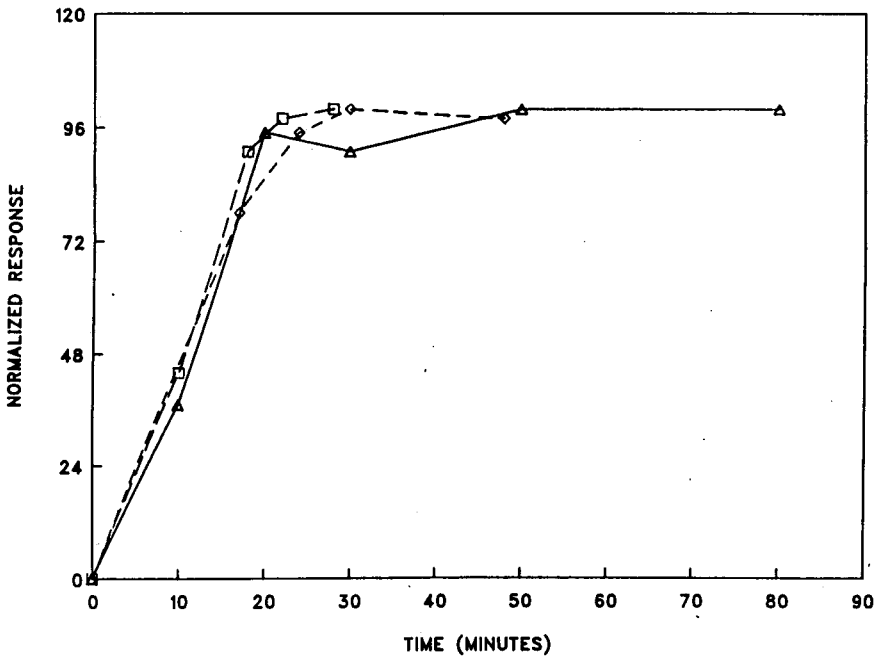

Fig. 3. Time to reach equilibrium concentration (EO) at different derivatization temperatures: △ = 70°C; ◇ = 90°C; □ = 100°C.

centration was found after about 25 min. At 90 and 100°C an identical response was measured after this same time period. As final temperature 90°C was chosen for convenience and because fluctuations in reaction time do not have an influence on the final response. The results of this equilibrium study are shown in Fig. 3.

3.6. Analysis of polyether polyols from different sources

Table 3 shows residual epoxide content in different commercially available industrial lubricants, being polyether adducts, from various manufacturers. A typical chromatogram is shown

Table 3
Residual free epoxide in commercial lubricants

Product	Epoxyethane (ppm)	Epoxypropane (ppm)
Lubricant A	2.5	3.5
Lubricant B	N.D.[a]	N.D.[a]
Lubricant C	2.3	N.D.[a]
Polyether D	2.9	5.8
Product E		
5 min after EO addition	1350	–
30 min after EO addition	150	–
45 min after EO addition	10.0	–
60 min after EO addition	3.9	–

[a]N.D. = Non-detected, detection limit 0.5 ppm.

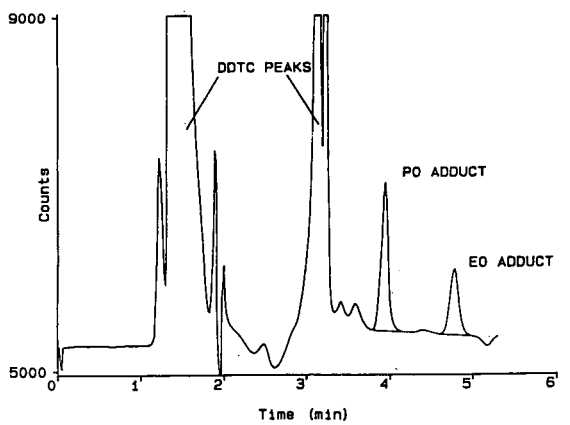

Fig. 4. Typical chromatogram of PO–DDTC and EO–DDTC adducts in a commercial sample. column: Zorbax-NH_2 (25 cm); eluent: 89% (v/v) *n*-hexane, 11% (v/v) methanol–tetrahydrofuran (2:1); flow-rate: 2 ml/min; detection: UV at 278 nm and 0.02 AUFS; injection volume: 10 μl.

in Fig. 4. The product E refers to an experiment in a pilot plant to study reaction rates. Samples were taken at different times after completion of the addition of EO to the pre-heated reaction mixture. Optimum production cycles can be established in this way.

4. Conclusions

Residual EO and PO can be determined down to sub-ppm level in polyether polyols using DDTC as an off-line derivatization agent. The methodology is simple and requires only standard LC instrumentation.

References

[1] *IARC Monographs on the Evaluation of Carcinogenic Risks to Humans: Supplement 7*, IARC, World Health Organization, Lyon, 1987.
[2] K.J. Cummins, G.R. Schultz, J.S. Lee, J.H. Nelson and J.C. Reading, *Am. Ind. Hyg. Assoc. J.*, 48 (1987) 563.
[3] D. Munger, L.A. Sternson, A.J. Repta and T. Higushi, *J. Chromatogr.*, 143 (1977) 375.
[4] H. Irth, G.J. de Jong, U.A.Th. Brinkman and R.W. Frei, *Anal. Chem.*, 59 (1987) 98.
[5] R.M. Smith, A.M. Butt and A. Thakur, *Analyst*, 110 (1985) 35.
[6] S.J. Bannister, L.A. Sternson and A.J. Repta, *J. Chromatogr.*, 173 (1979) 333.
[7] G.R. Gale, L.M. Atkins and E.M. Walker, Jr., *Ann. Clin. Lab. Sci.*, 12 (1982) 345.
[8] D. Chakraborti, W.R.A. De Jonghe, W.E. Van Mol, R.J.A. Van Cleuvenbergen and F.C. Adams, *Anal. Chem.*, 56 (1984) 2692.

ELSEVIER

Journal of Chromatography A, 696 (1995) 49–62

JOURNAL OF CHROMATOGRAPHY A

Rapid purification of cotton seed membrane-bound N-acylphosphatidylethanolamine synthase by immobilized artificial membrane chromatography

Song-Jun Cai[a], Rosemary S. McAndrew[b], Brian P. Leonard[b], Kent D. Chapman[b], Charles Pidgeon[a,*]

[a]*Department of Medicinal Chemistry, School of Pharmacy, Purdue University, West Lafayette, IN 47907, USA*
[b]*Department of Biological Sciences, University of North Texas, Denton, TX 76203, USA*

First received 22 September 1994; revised manuscript received 10 November 1994; accepted 10 November 1994

Abstract

N-Acylphosphatidylethanolamine synthase (NAPES) is a membrane-bound enzyme present in cotton seedlings at a concentration of ≤0.02% of the total protein. NAPES was purified to electrophoretic homogeneity in a single chromatographic step using immobilized artificial membrane (IAM) chromatography. The IAM column used for NAPES purification was ^{ether}IAM.PE$^{C10/C3}$ and this surface contains a monolayer of immobilized phosphatidylethanolamine (PE). Since PE is an analogue of the natural substrate for NAPES, ^{ether}IAM.PE$^{C10/C3}$ columns function as an affinity column for this enzyme. Detergent-solubilized microsomal proteins from cotton were loaded on to the ^{ether}IAM.PE$^{C10/C3}$ column and eluted with buffered mobile phases containing 0.2 m*M* dimyristoylphosphatidylethanolamine (DMPE) and 2 m*M* dodecylmaltoside. Little NAPES functional activity eluted if DMPE was removed from the mobile phase. Mobile phase DMPE is also a substrate for NAPES, and therefore both the mobile phase and IAM surface contains NAPES substrates. Mobile phase DMPE may function as both a surfactant-type affinity displacing ligand effecting protein elution and also a stabilizing factor of NAPES functional activity. The loading capacity on semi-preparative ^{ether}IAM.PE$^{C10/C3}$ (6.5 × 1.0 cm) columns was ca. 5 mg of total detergent solubilized microsomal proteins, and protein recovery was quantitative. This one-step IAM purification of NAPES resulted in a single band on silver-stained polyacrylamide gels, and 3940 fold increase in NAPES specific activity. The molecular mass of the purified NAPES protein is 64 000. ^{125}I labeled [12-(4-azidosalicyl)amino]dodecanoic acid is a photoreactive fatty acid substrate of NAPES that was used to confirm protein purity.

1. Introduction

During the postgerminative growth phase of plants, the primary amine of membrane-associated phosphatidylethanolamine (PE) may be acylated with palmitic acid and perhaps other free fatty acids. N-Acylphosphatidylethanolamine (NAPE) was initially found in cotyledons of cotton seedlings but appears to be a phospholipid found in several other plants including

* Corresponding author.

0021-9673/95/$09.50
SSDI 0021-9673(94)01113-3

soybean cotyledons, castor bean endosperm, okra cotyledons and rice cell suspensions [1]. In addition to plant cells, NAPE has also been found in animal cells. However, the presence of NAPE analogues in animal cells has always been associated with cell-stress or cell damage. For instance, NAPE has been found in degenerating epidermal cells, infarcted heart tissue, ischemic brain tissue and a few tumor cell lines (reviewed in Ref. [2]). During cell stress or tissue damage, free fatty acids are enzymatically released from membrane phospholipids and the free fatty acids destabilize healthy cell membranes [3–5]. Thus to minimize fatty acid induced cellular toxicity, an efficient fatty acid scavenger mechanisms likely exists that involves the formation of NAPE.

NAPE is enzymatically synthesized from PE and free fatty acids by NAPE synthase (NAPES) in a time-, temperature-, pH- and protein concentration-dependent manner [6,7]. NAPES was found in cotton seed microsomes [1] and partially purified by isoelectric focusing [7]. In this report, we describe the purification of this enzyme to homogeneity in one step using immobilized artificial membrane (IAM) chromatography. In addition, the enzyme was unambiguously identified using a photoreactive affinity cross-linking ligand [8].

IAM surfaces have been used for (i) enzyme immobilization [9], (ii) facilitating the coupling of polar and non polar molecules [10], (iii) predicting drug transport across human skin and other biological barriers [11–13], and (iv) predicting the pathophysiological effects of bile salts [14]. IAMs are also chromatography surfaces designed to emulate the membrane surfaces found in liposomes [15–17] and several membrane proteins have been purified using IAM chromatography: (i) cytochrome P450 [18], (ii) cholesterol transfer protein [19], (iii) phospholipase A_2 [20], and an intestinal peptide transporter protein [21]. Typically, IAM chromatography results in $\geq$70% of the contaminating proteins being removed from the target protein in one step. In this report we extend the chromatographic applications of IAM chromatography to the purification of NAPES.

2. Experimental

2.1. Chemicals

Sodium dodecyl sulfate (SDS), N,N'-methylene-bis-acrylamide (BIS), acrylamide, ammonium persulfate (APS), N,N,N',N'-tetramethylethylenediamine (TEMED) and molecular mass markers for gel electrophoresis were purchased from Bio-Rad (Hercules, CA, USA). 3-[3-(Chloroamidopropyl)dimethylammonio] - 1 - propane - sulfonate (CHAPS) was from Aldrich (Milwaukee, WI, USA). Glacial acetic acid, hydrochloric acid (concentrated), sodium phosphate (monobasic), ethylene glycol (EG), silver nitrate, 37% formaldehyde solution were obtained from Fisher Scientific. Sodium carbonate, sodium thiosulfate and sodium chloride were from J.T. Baker (Philipsburg, NJ, USA). Glycine, dodecylmaltoside (DDM), dimyristoyl phosphatidylethanolamine (DMPE), sodium deoxycholate (DOC), trichloroacetic acid (TCA), phenylmethyl sulfonyl fluoride (PMSF), pepstatin A, leupeptin, benzamidin and Tris base were ordered from Sigma (St. Louis, MO, USA). Micro bicinchoninic acid (BCA) protein assay reagent kit was obtained from Pierce (Rockford, IL, USA). Methanol was obtained from Mallinckrodt (Paris, KY, USA). Absolute ethanol was obtained from McCormick Distilling Co. (Pekin, IL, USA). Centricon and Centriprep devices were purchased from Amicon (Beverly, MA, USA). [1-^{14}C] palmitic acid (57 mCi/mmol) was obtained from DuPont NEN (Wilmington, DE, USA).

2.2. Membrane preparation and solubilization

Microsomal proteins from 1-day old cotton seedlings were prepared according to Chapman and Moore [7]. Briefly, cotyledons were homogenized in a solution containing 100 m*M* K-PO_4 (pH 7.2), 10 m*M* KCl, 1 m*M* EDTA, 1 m*M* $MgCl_2$, 400 m*M* sucrose plus a cocktail of protease inhibitors (1 m*M* PMSF, 1 m*M* benzamidin, 1 m*M* ethylene glycol-bis(β-aminoethyl ether) N,N,N',N'-tetraacetic acid (EGTA), 1 m*M* pepstatin A, 1 m*M* leupeptin). The

homogenate was filtered through four layers of cheesecloth and the filtrate centrifuged at 10 000 *g* for 20 min at 3°C. The resulting supernatant was ultracentrifuged at 150 000 *g* for 1 h at 3°C. The resulting microsomal pellet was resuspended in 400 m*M* sucrose plus protease inhibitors to a concentration of 10 mg protein/ml buffered with 20 m*M* Na-PO_4 (pH 7.2). After washing with 1 *M* NaCl, the microsomes were resuspended in buffer containing 20% glycerol, the cocktail of protease inhibitors, 0.2 m*M* DDM, 20 m*M* Na-phosphate (pH 8.0) and 1 m*M* EDTA. The critical micelle concentration of DDM is 0.14 m*M*. Detergent-extracted microsomes were subjected to centrifugation at 150 000 *g* for 1 h; the supernatant contained the target enzyme.

The supernatant containing the DDM-solubilized microsomal proteins were concentrated on Centricon-30 or Centriprep-10 device depending on the sample volume. Centricon-30 or Centriprep-10 were centrifuged at 6000 rpm (5000 *g*) for 30 min at 4°C on Sorvall RC2-B with Sorvall Type SS-34 rotor to concentrate the proteins prior to injection on IAM columns. The solubilized microsomal protein samples were concentrated as follows: 2 ml of sample to 40 μl for pilot columns, 5 ml to 900 μl for analytical columns, and 45 ml to ca. 2 ml for semi-preparative IAM columns.

2.3. IAM chromatography

Several phospholipids have been immobilized at monolayer densities to prepare IAM chromatography packing materials suitable for purifying membrane proteins [10,22]. The membrane lipids that have been immobilized include phosphatidylcholine (PC), phosphatidylglycerol (PG), phosphatidylserine (PS), phosphatidylethanolamine (PE), and phosphatidic acid (PA). Immobilized PE surfaces were used for the purification of NAPES and this IAM surface is denoted as ^{ether}IAM.PE$^{C10/C3}$ (Fig. 1). ^{ether}IAM.PE$^{C10/C3}$ was synthesized in our laboratory [10,22] and the superscript "ether" denotes an ether linkage between the alkyl chain and the glycerol backbone of the phospholipid. IAMs are routinely prepared by a three-step bonding pro-

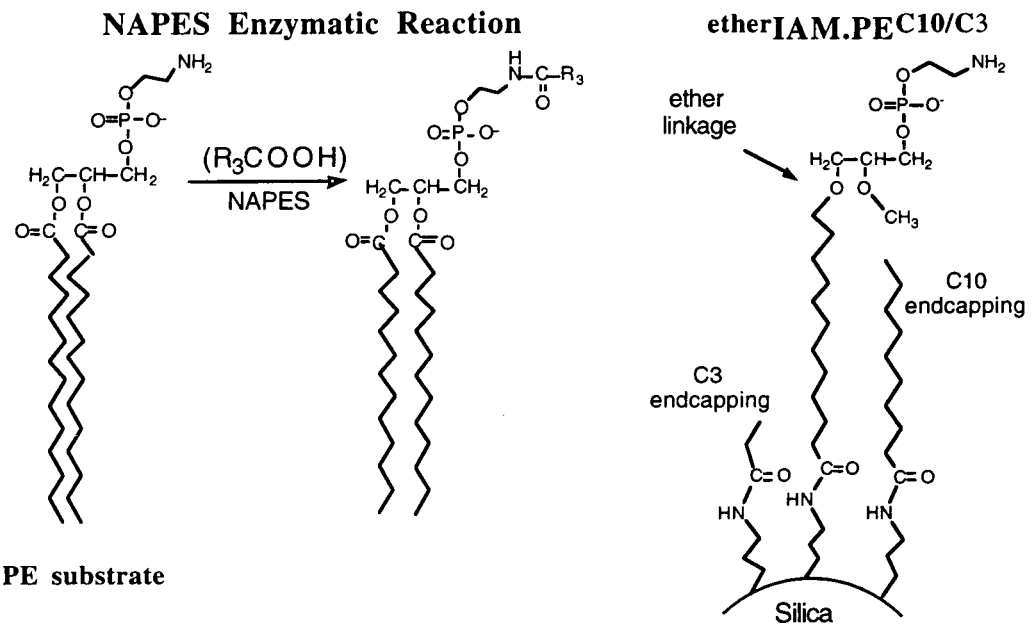

Fig. 1. Comparison of the PE lipid substrate for the NAPES enzymatic reaction to the PE lipid substrate immobilized on the IAM surface. R_3COOH is free fatty acid, for example, palmitic acid.

cess: step (i) involves phospholipid immobilization, step (ii) involves end capping with decanoic (C10) anhydrides, and then propionic (C3) anhydrides until the IAM surface is ninhydrin negative, step (iii) involves removing phospholipid protecting groups, e.g., for the ^{ether}IAM.PE$^{C10/C3}$ column, *tert.*-butoxycarbonyl from the amino group of PE. The C10 and C3 alkyl chains from the end capping reactions are shown in Fig. 1. PE was bonded to chromatographically efficient 12-μm silica propylamine particles containing 300-Å pores. The surface coverage of PE was 83 mg PE/g silica propylamine which corresponds to a surface density of ca. 66 Å^2/PE molecule on the IAM surface [10]. HPLC columns were packed at Regis (Skokie, IL, USA). Pilot size columns were 3 × 0.46 cm, analytical size columns were 15 × 0.46 cm, and semi-preparative columns were 6.5 × 1.0 cm. The IAM surface shown in Fig. 1 is very stable from pH 2 to pH 8.

Our HPLC system employs a Rainin Rabbit-HP pump and a Milton Roy Variable Wavelength UV Monitor set at 254 nm for detection. All chromatography experiments were performed at room temperature. Typically, the detector was set to a range of 0.05 and a response time of 0.05 s. The flow-rate was 1 ml/min for analytical size and semi-preparative size IAM columns and 0.2 ml/min for the pilot size column. Prior to sample loading, the IAM column was always equilibrated with at least 30 column volumes of mobile phase A. Mobile phase A contained 20 m*M* sodium phosphate (pH 8.0), 20% EG and 1 m*M* EDTA. EG was included in the mobile phase as a precautionary measure to preserve NAPES activity during protein purification [23] and EDTA was used to inhibit the inactivation of NAPES caused by divalent metal ions [7]. Mobile phase B was comprised of mobile phase A plus 0.2 m*M* DMPE and 2 m*M* DDM. To prepare mobile phase B, approximately 100 mg of DMPE powder was added to mobile phase A containing DDM and stirred for 2–3 h at room temperature. Filtration of the mobile phase through 0.2-μm nylon-66 filters (Rainin) resulted in several milligrams of non solubilized DMPE remaining on the filter. Gravimetric analysis of the non solubilized DMPE remaining on the filter was used to calculate the final concentration of DMPE in mobile phase B.

2.4. NAPES activity assay

NAPES activity was monitored by the method of Chapman and Moore [7]. Briefly, on ice, a stock solution of Na-phosphate buffer, DDM and dioleoyl phosphatidylethanolamine (DOPE) were mixed with each chromatographic fraction (usually 100 μl) to a final volume of 0.495 ml (final concentration: 20 m*M* Na-PO_4, pH 8.0, 0.2 m*M* DDM, 40 μM DOPE). Then 2.5 μl of [1-^{14}C]palmitic acid (50 μ*M* final; 10 mCi/nmol in ethanol) was added, vortexed briefly and sonicated for 2 s. The solution was placed in a 45°C water bath for 10 min with shaking at 120 rpm. The reaction was terminated by the addition of 2 ml of boiling 2-propanol followed by incubation at 70°C for 30 min. The reaction tubes were cooled in ice bath and 1 ml of chloroform was added. After intermittent vortexing for 30 min, 1 ml of chloroform and 2 ml of 1 *M* KCl were added to separate the mixture into 2 phases. The resulting mixtures were centrifuged for 10 min at 2000 rpm (325 *g*) to complete phase separation. The upper aqueous phase was aspirated and discarded and the chloroform phase containing extracted phospholipids was washed twice with 2 ml of 1 *M* KCl. The residual chloroform phase was dried under N_2 and the residue suspended in 50 μl chloroform–methanol (2:1, v/v) and separated by TLC on silica gel G-60 plates. TLC plates were developed first with hexane–ethyl ether (8:2, v/v) for 45 min, and then with chloroform–methanol–water (80:35:1, v/v/v) for 60 min in the same direction. The lipids and standards were visualized by I_2 vapor, and then radiolabeled lipids were scanned and quantified for radioactivity using a Bioscan System 200 radiometric scanner [7]. The activity was expressed as nmol of NAPE produced/h/ml.

2.5. SDS-PAGE

Chromatography fractions were subjected to TCA precipitation to concentrate the proteins prior to gel electrophoresis. The TCA precipi-

tation method involved adding 0.1 ml of 0.15% DOC to the ca. 1-ml chromatography fractions, incubating at room temperature for 10 min, and then adding 0.1 ml of 72% TCA [24]. The sample was incubated on ice for 1 h and then centrifuged at 14 000 rpm (16 000 *g*) using an Eppendorf Centrifuge (Model 5415) for 15 min. After centrifugation, the supernatant was decanted and the pellet washed with 1 *M* NaCl. The protein pellet was solubilized with 20 μl tank buffer (25 m*M* Tris, 0.2 *M* glycine, 0.1% SDS, pH 8.3) and if necessary, adjusted to pH ≈ 8 by a trace amount of dry Tris base powder. The 20 μl solubilized sample was mixed with 20 μl of twice concentrated gel electrophoresis sample treatment buffer (2 ×) that contained trace amounts of bromophenol blue indicator-dye, and then heated at 75°C for 15 min. The samples were sonicated for a few seconds, briefly vortexed and ca. 10 μl loaded onto 12% polyacrylamide gel. Gels were run at constant voltage (200 V) with cold water circulation, until the dye reached the gel front. The gels were stained with silver using the method of Merril [25].

In addition, photoreactive affinity cross-linking ligand was utilized to identify the target protein on the gel. The radiolabeled photoaffinity ligand is [12-(4-azidosalicyl)amino]dodecanoic acid (^{125}I-ASD), which is a fatty acid substrate of NAPES [8].

2.6. Protein content measurement

Protein content was measured based on the BCA method of Cu^{2+} chelation. Chromatography fractions contain EG, EDTA, lipids and detergents that may interfere with BCA protein assays. Consequently, TCA precipitation was performed according to the manufacturer's (Pierce) suggestion as follows. Each chromatography fraction (1 ml) was mixed with 200 μl of 100% TCA and incubated on ice for 1 h. Precipitated proteins were pelleted by centrifugation at 14 000 rpm for 8 min (16 000 *g*). The supernatant was decanted and the pellet was washed gently with 1 *M* NaCl solution. After the pellet was solubilized with 1 ml of 0.3 *M* phosphate buffer (pH 8.0), 1 ml of newly prepared BCA microassay working reagent was added to each sample and the samples were then incubated at 60°C for 60 min. The absorbance at 562 nm was measured on a Beckman-7 spectrophotometer against the blank. The protein concentration was calculated from a standard curve using bovine serum albumin (BSA) as the protein standard, in which, known concentrations of BSA solutions were subjected to the same TCA precipitation.

3. Results and discussion

Free fatty acids and PE are substrates for NAPES (Fig. 1). The purification strategy for NAPES was developed based on the concept that PE analogues might function as affinity surfaces for the purification of this enzyme. The IAM surface prepared from PE is denoted as ^{ether}IAM.PE$^{C10/C3}$ and the structure is depicted in Fig. 1. NAPES binding to the ^{ether}IAM.PE$^{C10/C3}$ surface requires elution with mobile phase modifiers that selectively bind and elute the enzyme from the column. Since natural diacylated phospholipids, such as DMPE, are substrates for NAPES, these compounds may function as "affinity displacing ligands" for NAPES bound to ^{ether}IAM.PE$^{C10/C3}$. The purification strategy for NAPES is thus based on both affinity ligands tethered to the chromatographic surface (e.g. PE analogues) and "affinity displacing ligands" (e.g. DMPE) in the mobile phase.

DMPE is insoluble in aqueous buffers, and therefore detergents were required to assure solubilization. For IAM chromatography, DDM was used as the mobile phase detergent for DMPE solubilization because DDM maintains NAPES activity at a weight ratio of detergent:protein of 2:1 [7]. Fig. 2 shows the chromatographic profile eluting from an ^{ether}IAM.PE$^{C10/C3}$ pilot column after injecting DDM-solubilized microsomal proteins and eluting with a DDM–DMPE detergent gradient. A 40 μl volume of the microsomal proteins (ca. 200 μg total protein) was loaded at 0.2 ml/min and after 10 min, a shallow detergent gradient from 10 to 30 min was applied to elute the proteins. Prior to the detergent gradient, two peaks eluted from the column: peak 1 at 3 min, and peak 2 at

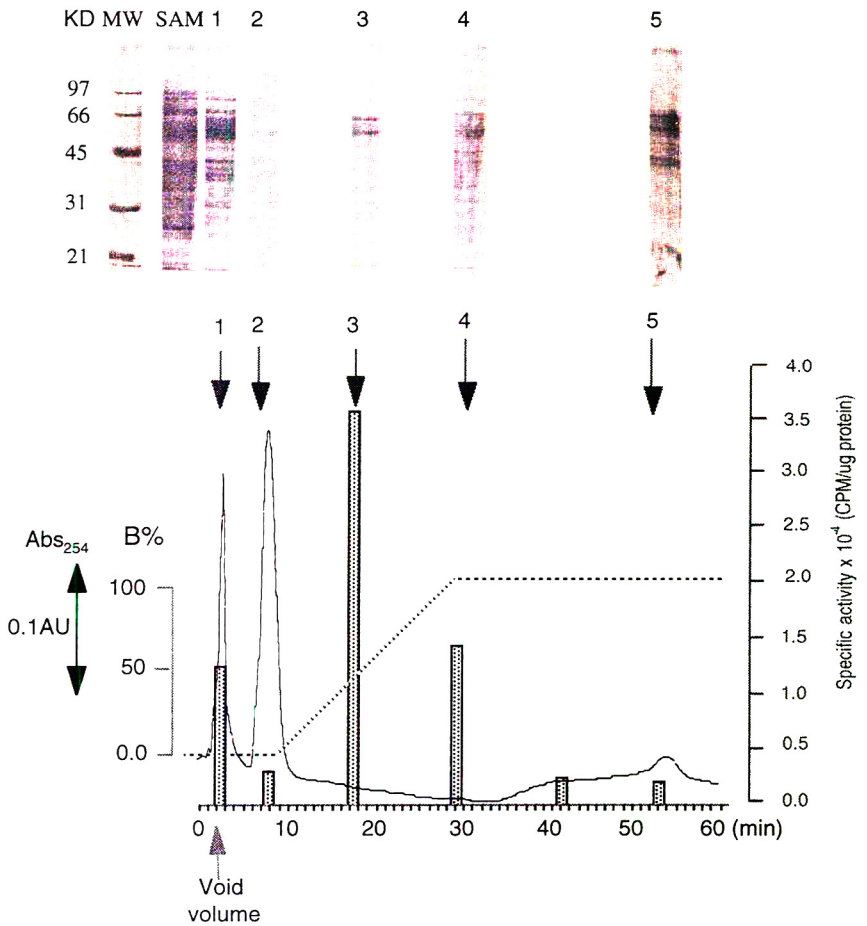

Fig. 2. ^{ether}IAM.PE$^{C10/C3}$ Chromatography on a pilot size column (3 × 0.46 cm). The flow-rate was 0.2 ml/min, and detection was at 254 nm (solid line). Prior to injecting 40 μl (0.2 mg microsomal protein), the column was equilibrated with 30 ml of mobile phase A which contained 20 m*M* sodium phosphate (pH 8.0), 20% EG and 1 m*M* EDTA. Mobile phase B was mobile phase A containing 0.2 m*M* DMPE and 2 m*M* DDM. The broken line is the detergent gradient used in the chromatography. A 20-min detergent gradient was used for this experiment. The histogram heights represent NAPES specific activity for particular chromatography fractions.

7 min. Peak 1 and peak 2 can be considered as pass-through peaks that represents either (i) column overloading, or (ii) molecules that do not have high affinity for the ^{ether}IAM.PE$^{C10/C3}$ surface.

Significant amount of proteins were only found in peak 1, but both peak 1 and peak 2 contained small amounts of NAPES activity (compare gel lanes 1 and 2 in Fig. 2). Since peak 1 contained NAPES activity, albeit very low amounts, the ^{ether}IAM.PE$^{C10/C3}$ pilot column was overloaded for this target protein under these experimental conditions. Furthermore, since there are virtually no proteins in peak 2 which eluted at 7 min, the strong absorbance at 254 nm must represent the elution of small molecular mass UV absorbing compounds that are present in the DDM solubilized sample; most likely these UV absorbing species are protease inhibitors (pepstatin, benzamidin, etc.).

Most of the NAPES activity eluted immediately after the initiation of the DDM–DMPE

detergent gradient (gel lane 3, Fig. 2). However, the NAPES activity continued to elute during the entire gradient and most of the contaminating proteins were removed from the target protein (gel lane 3–5). Thus the shallow detergent gradient used for this initial chromatography experiment removed most of the contaminating proteins in the pass-through peak, but the NAPES target protein was not purified to homogeneity. Nevertheless, we estimate that there is ca. 2.5–3 fold increased specific activity of NAPES.

Since pilot size columns could not resolve NAPES activity from contaminating proteins, larger analytical size columns were used. In addition, slightly larger amounts of protein were loaded onto the ^{ether}IAM.PE$^{C10/C3}$ column. Fig. 3 shows the elution profile after loading a 900 μl

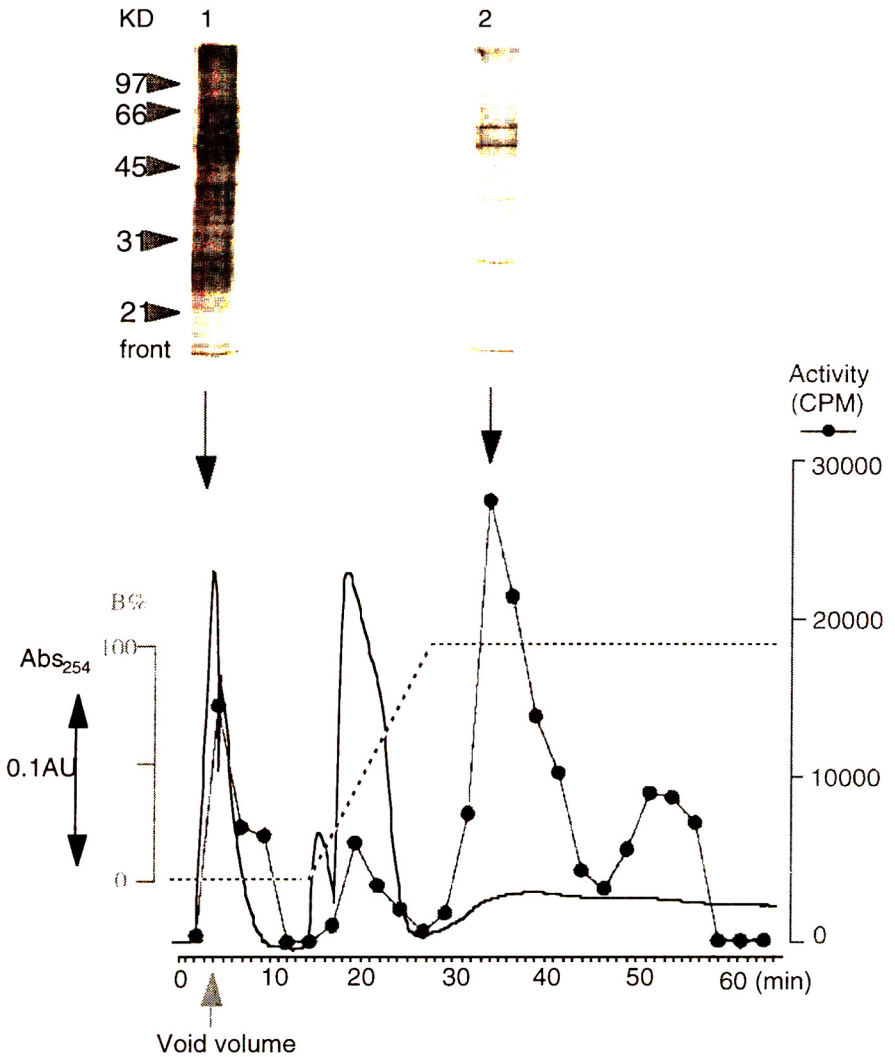

Fig. 3. ^{ether}IAM.PE$^{C10/C3}$ Chromatography on an analytical size column (15 × 0.46 cm). Mobile phases A and B are given in the legend to Fig. 2. Prior to injecting 900 μl (0.5 mg microsomal protein), the column was equilibrated with 30 ml of mobile phase A. The flow-rate was 0.4 ml/min and detection was at 254 nm. The solid line is absorbance at 254 nm eluting from the column and the broken line is the detergent gradient. The filled circles represent NAPES activity for particular chromatography fractions.

volume of the microsomal proteins (ca. 500 μg total protein) at 0.4 ml/min on a 10 × 0.46 cm analytical size ^{ether}IAM.PE$^{C10/C3}$ column. Similar to results obtained using the smaller pilot column, two peaks eluted during the loading step; however, these two peaks were better resolved because the analytical column is longer than the pilot column. Very little NAPES activity eluted prior to the DDM–DMPE detergent gradient. A steep 10-min DDM–DMPE detergent gradient resulted in the elution of NAPES activity in primarily one peak, and most importantly, very few contaminating proteins were in the sample (Fig. 3, gel lane 2).

Both Fig. 2 and Fig. 3 demonstrate that highly purified NAPES resulted from small IAM columns, but some NAPES activity eluted in the pass-through peak(s) from both experiments. A major objective during protein purification is to obtain high recovery of functional protein, and therefore, loss of the target protein in the pass-through peak should be minimized. To eliminate the NAPES activity eluting in the pass-through peak, a semi-preparative IAM column was used with elution conditions similar to that used to generate the data in Fig. 2 and Fig. 3. NAPES purification on a semi-preparative 6.5 × 1.0 cm ^{ether}IAM.PE$^{C10/C3}$ column was tested. Fig. 4 shows the elution profile after loading 2 ml of the microsomal proteins (ca. 4.5 mg total protein) at 1 ml/min. As expected, NAPE synthase activity did not elute in the pass-through peak in spite of the higher protein loading (5 mg of total protein). After 18 min of sample loading and column equilibration, a 15-min linear gradient from 0 to 100% B (containing buffered 0.2 m*M* DMPE and 2 m*M* DDM) was used to elute the proteins. Several small UV absorbing peaks were detected after elution with mobile phase B. However, the maximum NAPES activity eluted in a region of the chromatogram that had little or no UV absorbance. The key finding from Fig. 4 is that larger amounts of NAPES can be loaded on the ^{ether}IAM.PE$^{C10/C3}$ column. We estimate

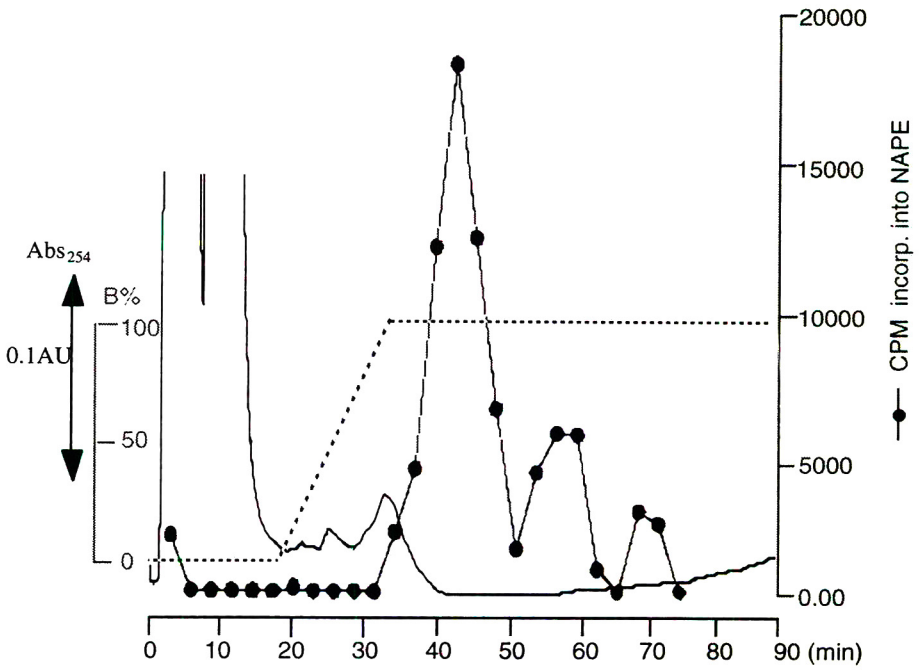

Fig. 4. ^{ether}IAM.PE$^{C10/C3}$ Chromatography on a semi-preparative column (6.5 × 1.0 cm). Mobile phases A and B are given in the legend to Fig. 2. Prior to injecting 2 ml (ca. 5 mg microsomal protein), the column was equilibrated with 30 ml of mobile phase A. The flow-rate was 1 ml/min, detection was at 254 nm (solid line), and the gradient (broken line) are shown. The solid circles represent NAPES activity for particular chromatography fractions.

that the capacity of semi-preparative ^{ether}IAM.PE$^{C10/C3}$ columns is at least 10 times the capacity of pilot columns. Although protein loading on semi-preparative columns was good (i.e., ca. 5 mg total protein loaded and no NAPES activity in the pass-through peaks), NAPES was not purified to homogeneity and other elution conditions were tested with the intent of obtaining pure NAPES.

Since shallow detergent gradients were unsuccessful at purifying NAPES, a two-step detergent gradient was tested. As shown in Fig. 5, immediately after the 7-min peak eluted, the IAM column was perfused with the first DDM–DMPE detergent gradient, a steep 10-min gradient from 0 to 0.8 m*M* DDM. After a 10-min plateau elution, a second steep DDM–DMPE detergent gradient from 0.8 m*M* to 2.0 m*M* DDM detergent was applied over 5 min. As shown in Fig. 5, this two-step detergent gradient increased the spreading of the NAPES activity eluting from the ^{ether}IAM.PE$^{C10/C3}$ column. Thus this two-step gradient did not improve the purity of NAPES and two-step gradients were not further pursued.

To validate the necessity of DMPE for NAPES elution, the chromatography in the presence and absence of DMPE was performed. Fig. 6 compares the elution of proteins from the ^{ether}IAM.PE$^{C10/C3}$ column with and without DMPE present in the DDM detergent gradient. For this comparison, a steep 15-min DDM detergent gradient was used and the flow-rate was 0.2 ml/min. This increased flow-rate and steep DDM detergent gradient was chosen because the 20-min gradient at 0.2 ml/min spread NAPES activity that eluted from the column as shown in Fig. 2. When DMPE was omitted from the detergent gradient, very little NAPES activity eluted from the ^{ether}IAM.PE$^{C10/C3}$ column (Fig. 6, open circles). However, elution with mobile phases containing both DDM and DMPE resulted in very high amounts of NAPES activity eluting from the column (Fig. 6, closed circles). This demonstrates that mobile phase DMPE increases the NAPES activity eluting from the IAM column.

All of the above chromatography experiments utilized linear detergent gradients that were maintained at a plateau detergent concentration

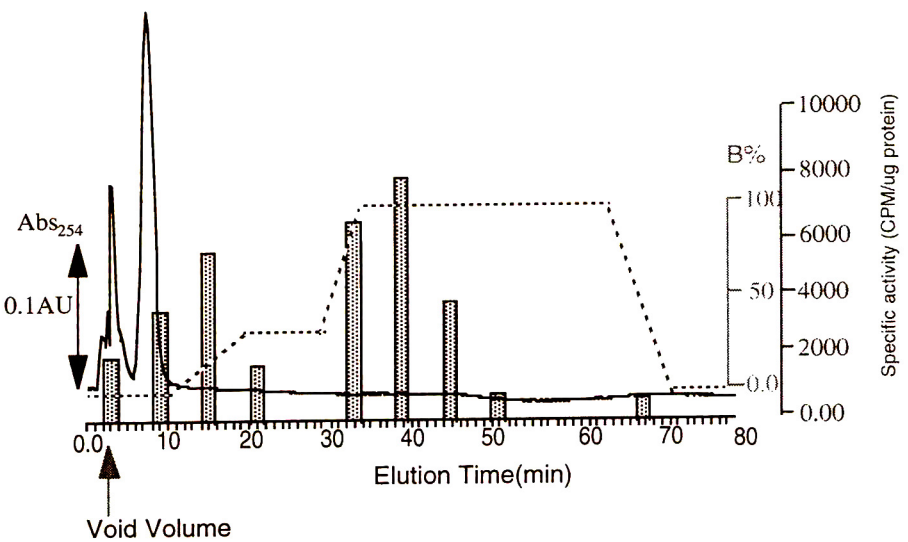

Fig. 5. Two-step gradient chromatography on an ^{ether}IAM.PE$^{C10/C3}$ pilot size column (3 × 0.46 cm). Mobile phases A and B are given in the legend to Fig. 2. Prior to injecting 40 μl (0.2 mg microsomal protein), the column was equilibrated with 30 ml of mobile phase A. The flow-rate was 0.2 ml/min, detection at 254 nm (solid line) and the detergent gradient (broken line) are shown. The solid circles represent NAPES activity for particular chromatography fractions.

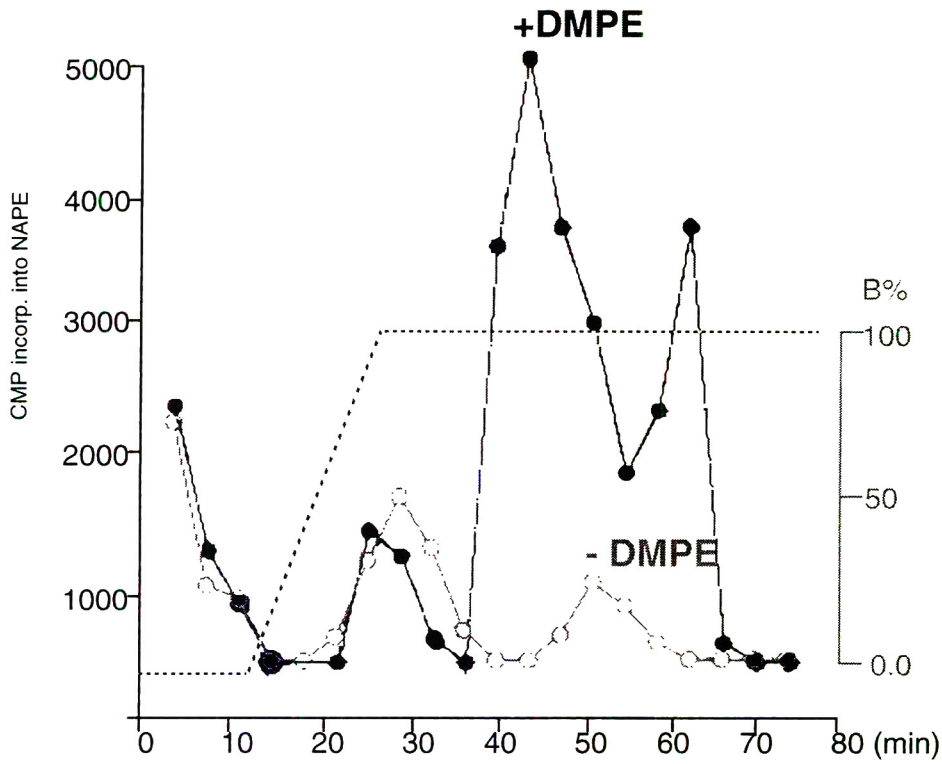

Fig. 6. Effect of DMPE on the elution of NAPES from ^{ether}IAM.PE$^{C10/C3}$. The flow-rate was 0.2 ml/min, detection at 254 nm, and a pilot size column (3 × 0.46 cm) was used. Prior to injecting 40 μl (0.2 mg microsomal protein), the column was equilibrated with 30 ml of mobile phase A. The composition of mobile phase A and B are given in the legend to Fig. 2. However, DMPE was omitted from mobile phase B in one experiment.

for ca. 30–60 min to facilitate the elution of proteins that exhibit high affinity for the ^{ether}IAM.PE$^{C10/C3}$ surface. However, polyacrylamide gel electrophoresis always showed contaminating proteins in chromatography fractions containing the NAPES activity. These contaminating proteins could not be resolved using conventional elution strategies shown in Figs. 2–6. We therefore attempted unconventional elution conditions. Preliminary studies demonstrated that bolus injections of mobile phase B (i.e., the detergent mobile phase containing DDM–DMPE) resulted in protein elution. In other words, instead of using a 10-min gradient of mobile phase B, a 1-ml pulse injection of mobile phase B resulted in the elution of a few proteins. Consequently, a "pulse gradient" was tested for eluting NAPES activity from the ^{ether}IAM.PE$^{C10/C3}$ column. A "pulse gradient" refers to a steep detergent gradient that plateaus for only a few minutes before the mobile phase concentration is reduced back to the equilibration buffer.

Using a DDM pulse gradient, Fig. 7 shows the elution profile after loading 1.6 ml of the microsomal proteins (ca. 5 mg total protein) at 1 ml/min on a 6.5 × 1.0 cm ^{ether}IAM.PE$^{C10/C3}$ column. The pulse gradient, applied 18 min after protein loading, was a steep 2-min linear gradient from 0–100%B, followed by a 9-min plateau, followed by a steep descending gradient back to the equilibration buffer A. Most interesting from this elution condition was that NAPES activity did not elute during the pulse gradient; NAPES activity eluted in fraction 10 which was collected ca. 15 min after the pulse gradient was

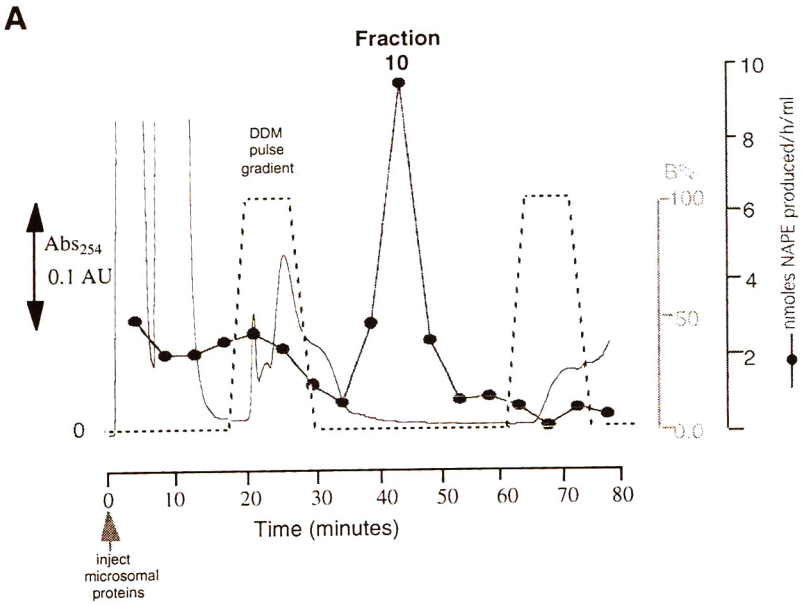

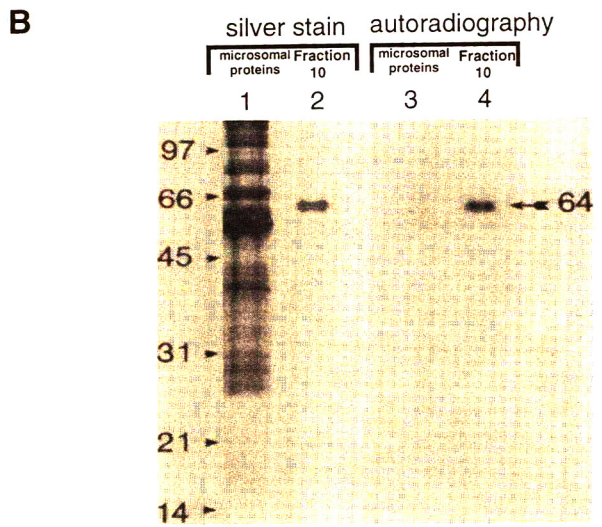

Fig. 7. (A) Purification of NAPES on a semi-preparative ^{ether}IAM.PE$^{C10/C3}$ (6.5 × 1.0 cm) column using a pulse detergent gradient system. The flow-rate was 1 ml/min, detection at 254 nm (solid line), and the two pulsed detergent gradients (broken lines) given. Prior to injecting 2 ml (5 mg microsomal protein), the column was equilibrated with 30 ml of mobile phase A. The solid circles represent NAPES activity. (B) SDS-PAGE analysis of NAPES purification on ^{ether}IAM.PE$^{C10/C3}$. Lane 1 shows the DDM-solubilized microsomal proteins (12 μg protein) mixture that was injected on to the column. Lane 2 (ca. 1 μg protein loaded on the gel) is from chromatography fraction 10. Lane 3 (DDM-solubilized microsomal proteins) and land 4 (chromatography fraction 10) are autoradiographs that contain ^{125}I-ASD (2.6 μ*M*, 2 μCi) labeling of NAPES prior to SDS-PAGE analysis.

completed. Furthermore the NAPES activity was concentrated in only 3 chromatography fractions (Fractions 9, 10, 11).

Fraction 10 eluting at ca. 42 min (Fig. 7A) was subjected to SDS-PAGE analysis (Fig. 7B). Protein visualization by silver staining showed a single intense band at 64 kilodalton indicating that NAPES was purified to homogeneity (lane 2). McAndrew et al. [8] prepared a ^{125}I photoreactive crosslinking substrate analogue of NAPES, and this photoaffinity ligand was used to confirm that the 64-kilodalton protein was NAPES (Fig. 7B, Lane 4). The single step purification of NAPES (Fig. 7A) from detergent solubilized microsomes is remarkable considering that NAPES is almost undetectable in the microsomal proteins (Fig. 7B); both autoradiographs and silver stain analysis show virtually no detectable NAPES in the detergent solubilized microsomes. The NAPES specific activity in detergent solubilized microsomes was 281 nmol/h/mg protein, and the specific activity in fraction 10 was 9890 nmol/h/mg protein. Thus NAPES was purified 3940 fold by using an ^{ether}IAM.PE$^{C10/C3}$ column.

As shown in Fig. 7A, a second DDM pulse gradient was applied to the ^{ether}IAM.PE$^{C10/C3}$ column to evaluate if additional proteins remained on the column. A few proteins eluted during the second DDM pulse gradient; however, since no NAPES activity eluted from the second DDM pulse gradient, these proteins were not further studied.

Novel elution conditions such as the DDM pulse gradient may leave residual proteins on the ^{ether}IAM.PE$^{C10/C3}$ column after chromatography. Thus the column should be washed with 1% CHAPS or other detergents to completely remove residual proteins. DDM is not used to wash the column because it is expensive relative to CHAPS. However, detergent washes leave residual detergents on ^{ether}IAM.PE$^{C10/C3}$ columns and these detergents must also be washed from the columns. Furthermore, DMPE phospholipids must also be removed from the ^{ether}IAM.PE$^{C10/C3}$ column. Thus ^{ether}IAM.PE$^{C10/C3}$ columns are routinely washed with MeOH (30–40 column volumes) after each experiment to remove residual DMPE and residual detergents.

The purification of NAPES using IAM chromatography was based on a membrane affinity concept. In our system, DMPE was intended to be used as the affinity displacing ligand to displace NAPES adsorbed to the IAM column. However, the elution of NAPES activity lagged behind the perfusion of DMPE, and in fact, when DDM pulse gradients containing DMPE were used, the NAPES activity did not elute during the detergent pulse gradient (e.g., Fig. 7). The explanation for NAPES activity lagging the DMPE mobile phase gradient may reside in the difference between small aqueous soluble displacing ligands compared to surfactant-type displacing ligands. Small aqueous soluble affinity displacing ligands are used in conventional affinity chromatography to elute target proteins that are bound to chromatography surfaces through bioaffinity interactions. In contrast, IAMs are a membrane affinity chromatography surface that requires surfactant-type displacing ligands for efficient displacement of proteins bound to the IAM surface. Water soluble displacing ligands have limited access to the protein–IAM binding site, but hydrophobic displacing ligands (e.g., DMPE) can partition into the IAM surface to facilitate protein displacement.

The hydrophobic tail of DMPE undoubtedly partitions into the immobilized PE monolayer. However, since DMPE is insoluble in aqueous media, mobile phase DDM was required for DMPE solubilization. Thus DMPE is delivered to the IAM surface via a DDM/DMPE micelle (Fig. 8). The short pulse DDM–DMPE detergent gradient contained a total of only ca. 1 mg of DMPE. The 6.5×1.0 cm ^{ether}IAM.PE$^{C10/C3}$ column (used for the purification shown in Fig. 6) contains ca. 4 g of packing material which corresponds to ca. 330 mg of immobilized PE. The 1 mg of DMPE equilibrates with the 330 mg of immobilized PE during the pulse gradient, but DMPE does not elute from the column during the pulse gradient. The key concept is that the equilibrium between detergent solubilized DMPE and immobilized

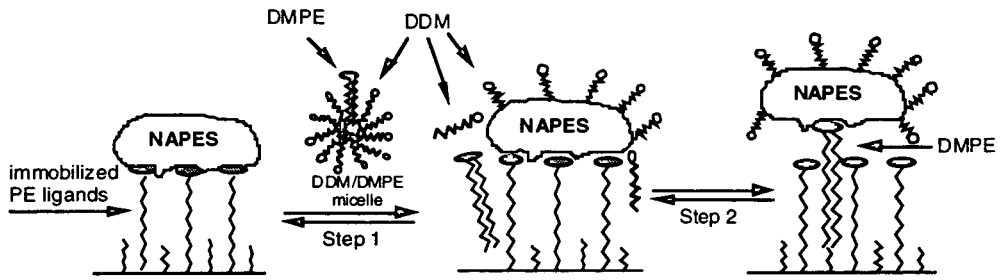

Fig. 8. NAPES purification by IAM chromatography using DDM–DMPE detergent mixtures.

PE makes the elution of DMPE lag behind the pulse gradient.

NAPES is a 64 kilodalton protein that chemically interacts with many immobilized PE ligands, but for clarity, only three immobilized PE molecules were used to depict the NAPES binding site on the ^{ether}IAM.PE$^{C10/C3}$ surface in Fig. 8. Both DDM gradients and DDM–DMPE gradients generate two NAPES peaks with little functional activity; however when DDM–DMPE detergent gradients are used, the late eluting NAPES peak has >5 fold increased functional activity (Fig. 6).

The explanation for the DMPE-induced increased NAPES activity (Fig. 6), and DMPE-induced protein purity (Fig. 7) most likely resides in the binding of DMPE with surface associated NAPES. As shown in Fig. 8, after NAPES is adsorbed to the IAM column, DDM–DMPE detergent gradients cause both DDM and DMPE to partition into the IAM surface. However, DDM is freely soluble in the mobile phase, whereas DMPE requires DDM for solubilization. Consequently, DMPE partitioning favors the IAM surface; lateral diffusion of DMPE allows DMPE to partition into the binding site of NAPES. Alternatively, DMPE in the mobile phase may partition into the NAPES active site through a micelle–protein interaction. Regardless of the DMPE diffusion path for entry into the NAPES active site, the NAPES–DMPE complex exhibits different elution and functional activity compared to the non complexed NAPES. Since no structural information is available regarding the NAPES binding site or the protein–membrane binding interactions, Fig. 8 should be considered as only a very preliminary model that is useful for discussing the chromatography of NAPES on IAM columns.

Regarding functional activity, it is known that substrates included in the mobile phase can stabilize membrane proteins and increase functional activity during the chromatographic process [26,27]. Since DMPE is a substrate of NAPES, the increased functional activity eluting from the column (Fig. 6) is caused, in part, by stabilization of NAPES–DMPE complex during IAM chromatography. Regarding protein elution, the NAPES–DMPE complex may have either higher or lower affinity for the IAM surface. Higher affinity would occur if DMPE functions as an affinity ligand as described [28], lower affinity would occur if DMPE facilitates displacement of NAPES from the IAM surface. The main peak of functional NAPES activity elutes ca. 10 min earlier when DMPE is included in the mobile phase (Fig. 6) and this suggests that the NAPES–DMPE complex increases the efficiency of DDM-induced elution of NAPES, i.e. DMPE is functioning as an affinity displacing ligand.

The utility of the pulse detergent gradient to purify NAPES to homogeneity involves the selective removal of only a few contaminating proteins. In other words, Figs. 2–4 demonstrate that steep (20 to 30 min) detergent gradients can purify NAPES to >90% purity in one step; only a few contaminating proteins are present based on SDS-PAGE analysis. The DDM–DMPE pulse gradient was able to selectively remove the few contaminating proteins from the target protein. As described above, small amounts of

DMPE in the mobile phase can initiate the formation of the NAPES–DMPE complexes, and DDM more efficiently elutes the complex from the surface. The slightly increased selectivity of mobile phase DMPE was sufficient to remove the contaminating proteins from NAPES in a single step. However, from a chromatographic point of view, the key concept is that NAPES exhibits high affinity for the IAM column; proteins that exhibit high affinity for IAM columns are usually purified >70–90% in one step as shown in Figs. 2–4.

DMPE is not an affinity surfactant as proposed by Torres et al. [28]. Affinity surfactants are custom synthesized using an analogue of the enzyme substrate linked to a surfactant, and the surfactant–substrate is non covalently coated onto C18 columns. The target enzyme exhibits increased affinity for the C18 surface by affinity interactions to the affinity surfactant. Since DMPE functioned as an affinity displacing ligand, the effect of DMPE on protein elution is distinct from affinity surfactants described by Torres et al. [28].

Acknowledgments

This work was supported in part by NIH (AI33031, and 2R446M3022-02) and NSF (CTS 9214794) to C.P., and grants from NSF (MCB-9320047) and USDA-NRICGP (agreement No. 94-37304-1230) to K.D.C.

References

[1] K.D. Chapman and T.S. Jr. Moore, *Arch. Biochem. Biophys.*, 30 (1993) 21.
[2] H.H.O. Schmid, P.C. Schmid and V. Natarajan, *Prog. Lipid Res.*, 29 (1990) 1.
[3] N.G. Bazan, *Biochim. Biophys. Acta*, 218 (1970) 1.
[4] G.Y. Sun, R. Manning and J. Strosznajder, *Neurochem. Res.*, 5 (1980) 1211.
[5] P.V. Reddy, P.C. Schmid, V. Natarajan, T. Muramatsu and H.H.O. Schmid, *Biochim. Biophys. Acta*, 795 (1984) 130.
[6] K.D. Chapman and T.S. Jr. Moore, *Plant. Physiol.*, 102 (1993) 761.
[7] K.D. Chapman and T.S. Jr. Moore, *Biochim. Biophys. Acta*, 1211 (1994) 29.
[8] R.S. McAndrew, B.P. Leopard and K.D. Chapman, *Biochim. Biophys. Acta*, (1994) submitted for publication.
[9] X.-M. Zhang and I.W. Wainer, *Tetrahedron Lett.*, 34 (1993) 4731.
[10] S. Ong, S.J. Cai, C. Bernal, D. Rhee, X. Qiu and C. Pidgeon, *Anal. Chem.*, 66 (1994) 782.
[11] F.M. Alvarez, C.B. Bottom, P. Chickale and C. Pidgeon, in T. Ngo (Editor), *Molecular Interactions in Bioseparations*, Plenum Press, New York, 1993, p. 151.
[12] S. Ong, H. Liu, X. Qiu, G. Bhat and C. Pidgeon, *Anal. Chem.*, (1994) in press.
[13] S. Ong, H. Liu, X. Qiu, M. Pidgeon, A.H. Dantzig, J. Monroe, W.J. Hornback, J.S. Kasher, L. Glunz, T. Sczczerba and C. Pidgeon, *J. Med. Chem.*, (1994) submitted for publication.
[14] D.E. Cohen, M.R. Leonard, A.R. Leonard, Donovan and M.C. Caray, *Gastroenterology*, 104 (1993) A889.
[15] C. Pidgeon and U.V. Venkatarum, *Anal. Biochem.*, 176 (1989) 36.
[16] C. Pidgeon, *U.S. Pat.*, 4 931 498 (1990).
[17] C. Pidgeon, *U.S. Pat.*, 4 927 879 (1990).
[18] C. Pidgeon, J. Stevens, S. Otto, C. Jefcoate and C. Marcus, *Anal. Biochem.*, 194 (1991) 163.
[19] H. Thurnhofer, J. Schnabel, M. Betz, G. Lipka, C. Pidgeon and H. Hauser, *Biochim. Biophys. Acta*, 1064 (1991) 275.
[20] C. Pidgeon, S.J. Cai and C. Bernal, *J. Chromatogr. A.*, (1994) submitted for publication.
[21] C. Pidgeon, unpublished results.
[22] X. Qiu, S. Ong, C. Bernal, D. Rhee and C. Pidgeon, *J. Org. Chem.*, 59 (1994) 537.
[23] M.P. Deutscher, in M.P. Deutscher (Editor), *Methods Enzymol.*, Academic Press, San Diego, CA, 1990, p. 83.
[24] G.L. Peterson, *Anal. Biochem.*, 83 (1977) 346.
[25] C.R. Merril, in M.P. Deutscher (Editor), *Methods Enzymol.*, Academic Press, San Diego, CA, 1990, p. 477.
[26] P.J. Brown and A. Schonbrunn, *J. Biol. Chem.*, 268 (1993) 6668.
[27] P.N. Moynagh and D.C. Williams, *Biochem. Pharmacol.*, 43 (1992) 1939.
[28] J.L. Torres, R. Guzman, R.G. Carbonell and P.K. Kilpatrick, *Anal. Biochem.*, 171 (1988) 411.

ELSEVIER

Journal of Chromatography A, 696 (1995) 63–74

JOURNAL OF CHROMATOGRAPHY A

On-line trace enrichment of polar pesticides in environmental waters by reversed-phase liquid chromatography–diode array detection–particle beam mass spectrometry

R.M. Marcé[a,*], H. Prosen[b], C. Crespo[a], M. Calull[a], F. Borrull[a], U.A.Th. Brinkman[c]

[a]*Department of Chemistry, Universitat Rovira i Virgili, Imperial Tarraco 1, 43005 Tarragona, Spain*
[b]*Department of Chemistry and Chemical Technology, University of Ljubljana, Aškerčeva 5, 61000 Ljubljana, Slovenia*
[c]*Department of Analytical Chemistry, Free University, De Boelelaan 1083, 1081 HV Amsterdam, Netherlands*

First received 10 October 1994; revised manuscript received 6 December 1994; accepted 7 December 1994

Abstract

The determination of a group of pesticides by RPLC–diode array detection, coupled on-line to particle beam MS, is developed for the analysis of different environmental waters. On-line trace enrichment of 100 ml of sample on a PLRP-S precolumn allows the determination of most pesticides at levels between 0.2 and 5 $\mu g\ l^{-1}$ and detection limits in the range 0.05–0.5 $\mu g\ l^{-1}$ for diode array detection and 0.02–0.5 $\mu g\ l^{-1}$ for particle beam MS. With real-life samples, a distinct matrix effect is observed in particle beam MS detection, which is caused by coeluting compounds acting as carriers. This improves analyte detectability and requires standard addition to be used for quantification. Different river and drinking waters were analysed and some pollutants were detected at sub- $\mu g\ l^{-1}$ levels.

1. Introduction

The determination of medium and highly polar pollutants in water is mainly carried out by RPLC [1–6] using a variety of detectors, the UV–visible absorbance detector being the most popular one because of its robustness and wide application range. Fluorescence and electrochemical detectors provide higher sensitivity and selectivity but, because of the latter aspect, the number of compounds that can be detected is rather limited. The lack of confirmatory power of absorbance detection is partially solved by the use of diode array detection (DAD), but the UV spectra within one compound class often are not very different and the confirmatory power of DAD is limited.

Mass spectrometric (MS) detection in LC is becoming increasingly important, because of its high confirmatory power, which is very important in environmental analysis because of the legal implications of analytical data. Different interfaces have been developed [7–10] and, although thermospray is the most popular one for the analysis of environmental pollutants [11–13] because of its high sensitivity, the advantage

* Corresponding author.

0021-9673/95/$09.50
SSDI 0021-9673(94)01217-2

of obtaining electron impact (EI) spectra when using the particle beam (PB) interface makes PB-MS very powerful in the detection and determination of pollutants. In fact, the determination of medium and highly polar pesticides by RPLC–PB-MS is reported in literature [14–16]. The possibility to obtain positive and/or negative chemical ionization spectra increases the confirmatory power of MS detection.

The poor sensitivity of the particle beam interface is quite well known. Several attempts have been made to improve it, such as the addition of a carrier to the eluent [17] or of compounds with a structure similar to that of the analytes of interest to improve transport through the interface. The use of isotopically labelled analogues of each compound has also been applied to increase the sensitivity [18,19]. Two further drawbacks for quantitation are the non-linearity of calibration plots and the enhancement of the analyte signal because of coeluting compounds acting as a carrier. However, in one recent study [20], good linearity was obtained for several compounds.

Since the detection limits typically obtained in RPLC–PB-MS do not allow to determine pesticides at the low tolerance levels of 0.1 $\mu g\ l^{-1}$ for drinking water and 1–3 $\mu g\ l^{-1}$ for surface water, a preconcentration system prior to LC is necessary. The advantages of on-line trace enrichment procedures include better sensitivity, lower consumption of organic solvents, higher automation potential and simplicity of the analysis compared with off-line procedures and are widely described in Refs. [21–24]. The applicability of on-line trace enrichment–RPLC has been demonstrated for the determination of many pesticides with DAD [1–3,24,25] and also for MS detection with the thermospray [26–28] and PB interfaces [20].

Some authors use LC–DAD for quantitative analysis because of its robustness and an additional analysis by LC–MS is carried out when any pesticide is suspected in order to confirm its presence. Although this is a proper procedure, two analytical runs are now required. Therefore, in the present paper on-line trace enrichment–RPLC–DAD–PB-MS has been used for the determination of a group of pesticides in drinking and surface water and quantitative results from DAD and PB-MS are compared.

2. Experimental

2.1. Chemicals

All pesticides were of 98–99% purity; they were obtained from Riedel-de Häen (Seelze, Germany). Stock solutions of each compound were prepared at the 1000 $\mu g\ ml^{-1}$ level in HPLC-grade methanol (Scharlau, Barcelona, Spain). If stored in a refrigerator at 8°C, the solutions were stable for several months. Working stock solutions of all pesticides at a concentration of 40 $\mu g/ml$ were prepared in methanol; they were diluted to different concentrations with methanol for calibration graph construction.

HPLC-gradient-grade methanol (Scharlau) and 0.1 *M* ammonium acetate were used to prepare the LC eluent. Ammonium acetate was from Panreac (Montcada i Reixac, Spain). An appropriate amount of the salt was dissolved in water obtained from a Milli-Q water purification system (Millipore, Bedford, MA, USA) and pH was adjusted to 5 with acetic acid (Probus, Badalona, Spain). The ammonium acetate solution was filtered through a 0.45-μm nylon filter prior to use.

Helium for the PB interface was 99.995% pure from Carburos Metalicos (Barcelona, Spain).

2.2. Instrumentation

LC was performed on a HP 1090 liquid chromatograph (Hewlett-Packard, Palo Alto, CA, USA) equipped with two pumps, a diode array detector, a six-port rotary valve and an autosampler. The system was controlled by a HP Workstation HP79994A which also performed data acquisition from DAD. Helium was used for solvent degassing. The analytical column was a 200 × 4.0 mm I.D. stainless-steel column packed with Spherisorb ODS2, 5 μm (Teknokroma, Barcelona, Spain). The precolumn consisted of a holder and a 10 × 2.0 mm cartridge packed with

15–25 μm PLRP-S styrene–divinylbenzene copolymer (Spark Holland, Emmen, Netherlands). An Applied Biosystems (Ramsey, USA) pump was used to deliver the sample and wet the precolumn.

The diode array detector was set at 240, 254 and 280 nm and spectra were recorded in the range 200–400 nm.

A Hewlett-Packard 5989 A MS Engine, equipped with a dual EI/chemical ionization source was connected to the DAD outlet via a Hewlett-Packard PB interface. All data were acquired on a HP UX 59944C data system. The ion source block and quadrupole temperatures were set at 250 and 100°C, respectively. The MS Engine was tuned to m/z 69, 219 and 502 corresponding to perfluorotributylamine. The scan range was m/z 64–400 u, in order to avoid noise due to ammonium acetate, at 2 s/scan.

Interface tuning and signal optimization were conducted by injecting solutions of 500 ng monuron by flow injection analysis using methanol–0.1 *M* ammonium acetate (60:40, v/v) as the carrier stream. The desolvation chamber temperature was set at 65°C and the helium nebulizer pressure at 50 p.s.i. (1 p.s.i. = 6894.76 Pa). Typical operating pressures were 0.5 Torr (1 Torr = 133.322 Pa) at the second-stage momentum separator and $1.5 \cdot 10^{-5}$ Torr in the ion source chamber.

After background subtraction the spectrum of each compound was compared with those in the Wiley library and good confidence levels were obtained although the reference spectra were generated using either a direct insertion probe or GC.

The area of the base peak ion for each compound extracted from the total ion chromatogram was used in the quantification procedure of PB-MS data.

2.3. Analytical procedure

The PLRP-S precolumn was flushed at 5 ml min^{-1} with 5 ml of methanol and 5 ml of methanol–ammonium acetate (pH 5.0) (30:70, v/v). Subsequently, a 100-ml sample was preconcentrated (4 ml min^{-1}) on the precolumn. The analytes trapped on the precolumn were desorbed in the backflush mode with methanol–0.1 *M* ammonium acetate (pH 5.0) (30:70, v/v) and transferred on-line to the analytical column. The actual separation of the analytes was carried out using a linear gradient of methanol–0.1 *M* ammonium acetate (pH 5.0) from 30:70 to 88:12 in 34 min. The flow-rate of the HPLC eluent was 0.4 ml min^{-1} and the column temperature was 40°C.

3. Results and discussion

3.1. RPLC–DAD–PB-MS

The scheme of the total system used is shown in Fig. 1. Firstly, chromatographic conditions

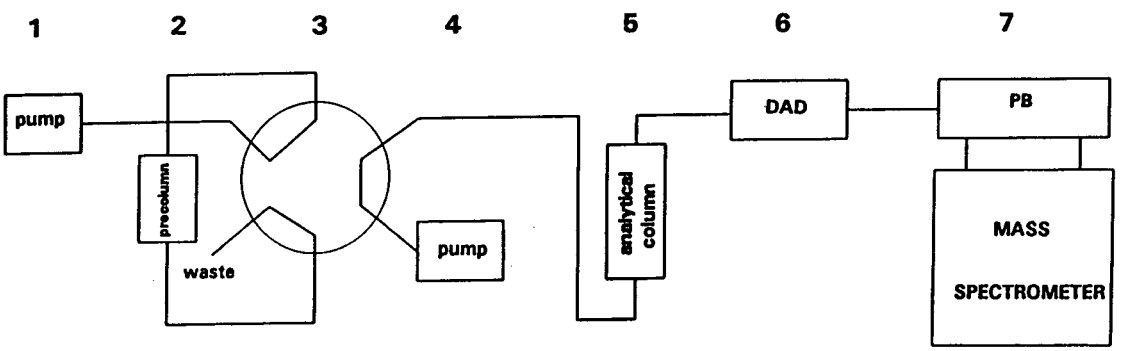

Fig. 1. Scheme of the experimental set-up. 1 = Pump delivering sample; 2 = PLRP-S precolumn; 3 = six-port rotatory valve; 4 = eluent pump; 5 = analytical column; 6 = diode array detector; 7 = particle beam interface and mass spectrometer.

were optimized based on previous results [20]. The ammonium acetate added to the eluent acts as a carrier and extends the PB-MS linear range [29]. Methanol was chosen as this is the solvent to be recommended from the PB-MS point of view. Although 2.1 mm I.D. analytical columns are preferred for PB-MS analysis, because of the relatively low flow rates which are permitted, a 4.6 mm I.D. column was selected as this implies better results when an on-line trace enrichment cartridge is connected to the column. A flow of 0.4 ml min^{-1} was selected because it is the recommended flow for the PB interface, and does not cause undue peak broadening.

A linear gradient of methanol–ammonium acetate (pH 5) from 30:70 to 88:12 in 34 min was used to carry out the separation of the analytes. The retention times of each analyte with the gradient profile are included in Table 1. As can be seen, all compounds are eluted in 30 min. Monuron and propuxur coeluted; still at low concentrations and when detecting at 280 nm they could be quantified separately. Unfortunately, at this wavelength the sensitivity was much lower than at 254 nm which is conventionally used for analytes.

For DAD chromatograms were recorded at 240, 254 and 280 nm. The wavelength used to quantify each compound is included in Table 1. Although lower wavelengths are sometimes used for some compounds, with the present eluent a serious distortion of the baseline was observed at lower wavelengths, mainly due to the presence of ammonium acetate.

Coupling PB-MS to the outlet of the DAD system did not cause noticeable additional peak broadening and satisfactory data from DAD and MS could be obtained from a single injection. As an illustration, Fig. 2 shows a total ion chromatogram obtained with PB-MS and a chromatogram using DAD after 5 μl injection of a standard solution of 40 μg ml^{-1} of each pesticide.

As regards MS detection, the base peak of each compound is included in Table 1. It must be pointed out that the m/z range for acquisition was 64–400, even though some compounds, such as linuron, have their base peak (m/z 61) at lower m/z values which implied a loss of sensitivity. The m/z range was selected in order to avoid noise caused by ammonium acetate [7].

Good linearity was obtained for all compounds from 1 to 40 μg ml^{-1} at the wavelengths shown in Table 1, with R^2 values between 0.986 and 0.9998. Calibration plots for the base peak of each compound obtained from the total ion chromatogram were constructed from 2 to 40 μg

Table 1
Name of pesticides studied, class of pesticide, retention time, λ used for measuring the absorbance and base peak used for quantification from chromatogram under full-scan acquisition conditions

Compound	Class	t_R (min)	λ_{selec} (nm)	Base peak (m/z)
Oxamyl	C	7.12	240	72
Methomyl	C	8.55	240	105
Aldicarb	C	16.87	254	68
Cyanazine	T	18.47	240	212
Monuron	P	19.84	254	72
Propoxur	C	19.84	280	110
Carbofuran	C	20.36	280	164
Simazine	T	21.14	240	201
Carbaryl	C	21.85	280	144
Fluometuron	P	22.99	240	72
Atrazine	T	25.10	240	200
Diuron	P	25.81	254	72
Linuron	P	28.12	254	161
Barban	C	28.60	240	153

C = Carbamates; P = phenylureas; T = triazines.

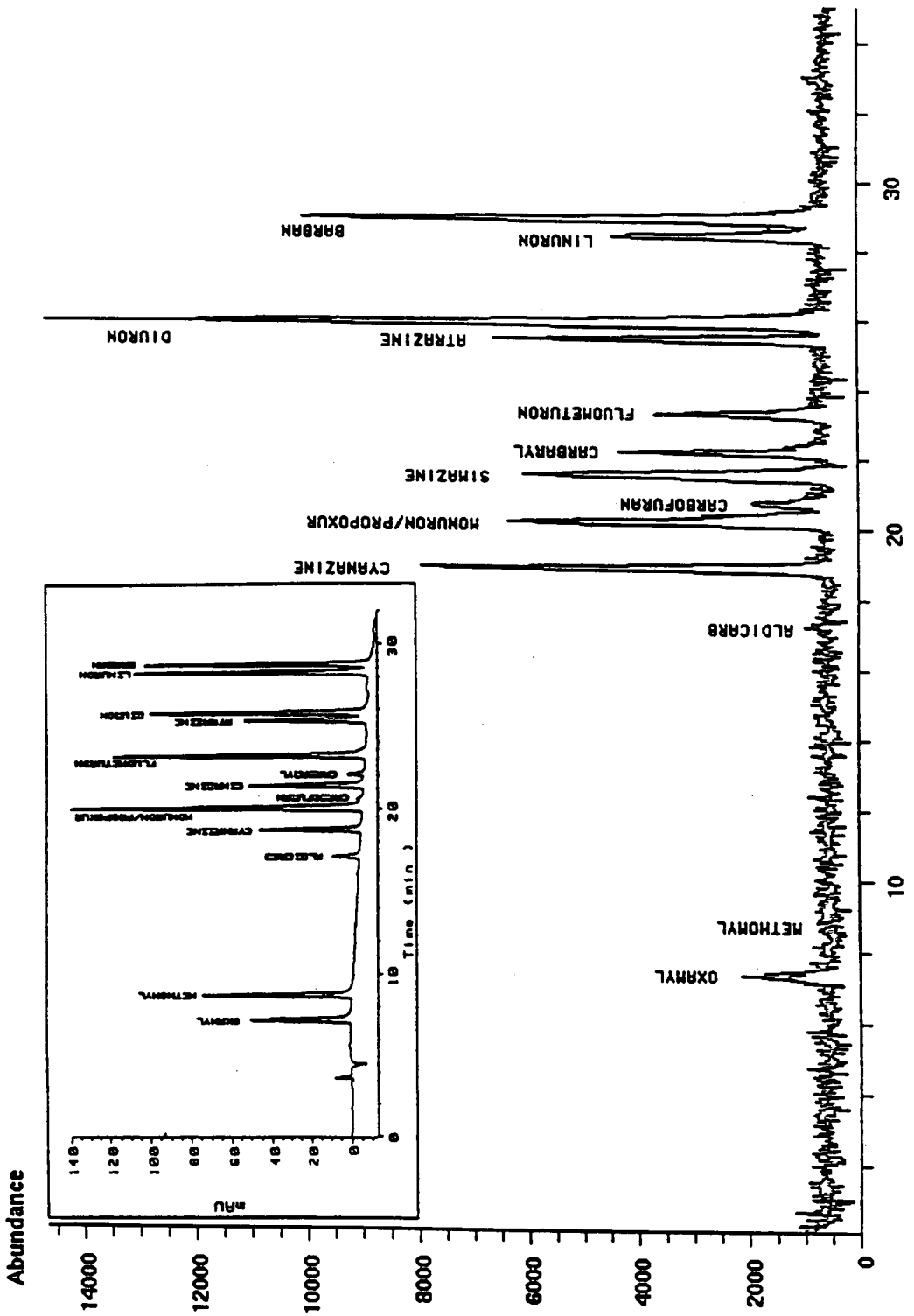

Fig. 2. RPLC–PB-MS total ion chromatogram of a standard solution of 14 pesticides at 40 $\mu g\ ml^{-1}$. The insert shows the RPLC–DAD chromatogram at wavelength 240 nm.

ml^{-1}. For most compounds the linearity was quite good (R^2 between 0.982 and 0.9990); an exponential response was obtained for compounds such as methomyl, aldicarb and simazine. Although better sensitivity could be obtained by using selected ion monitoring (SIM), full-scan acquisition was preferred since the spectrum of each pesticide can then be obtained.

3.2. Trace enrichment

Trace enrichment was carried out by using an on-line solid-phase extraction system. A highly hydrophobic styrene–divinylbenzene precolumn was selected because of the higher breakthrough volumes for most compounds studied, compared with C_{18}-bonded silica material.

Different sample volumes were preconcentrated and the recoveries for each compound were calculated using DAD (25, 50 and 100 ml of Milli-Q water, without any pH adjustment; spiking at 1 $\mu g\ l^{-1}$, see Table 2). From these results, and taking into account the level of these pesticides allowed in drinking water (0.1 $\mu g\ l^{-1}$), a volume of 100 ml was selected for further studies although with this volume, the recoveries of methomyl and oxamyl were lower than 20% due to early breakthrough.

Linearity of the response for the total analytical system, including the preconcentration step, was checked for a sample volume of 100 ml of Milli-Q water spiked at different concentrations. Good linearity was obtained from 0.2 to 5 $\mu g\ l^{-1}$ for all compounds (with the exception of methomyl, oxamyl and aldicarb) using both DAD and PB-MS. R^2 values obtained were between 0.990 and 0.9996 for DAD and between 0.984 and 0.996 for PB-MS. The early eluting compounds, methomyl and oxamyl, were not included because their recoveries were very low. The detection of aldicarb was not very sensitive with either DAD or PB-MS (Fig. 2) and linearity was therefore checked from 1 to 5 $\mu g\ l^{-1}$ (R^2 values of 0.994 and 0.990, respectively).

Fig. 3 shows a chromatogram obtained for 100 ml of Milli-Q water spiked at 1 $\mu g\ l^{-1}$ of each pesticide using DAD. Although some peak broadening is apparent it is not really detrimental for monitoring purposes.

Table 2
Recovery and relative standard deviation ($n = 4$) of pesticides at 1 $\mu g\ l^{-1}$ in Milli-Q water at different sample volumes

Compound	Sample volume (ml)					
	25		50		100	
	Recovery (%)	R.S.D. (%)	Recovery (%)	R.S.D. (%)	Recovery (%)	R.S.D. (%)
Oxamyl	38	7	45	9	20	11
Methomyl	30	10	16	9	8	14
Aldicarb	94	6	86	7	85	6
Cyanazine	86	8	90	6	92	7
Monuron	93	5	84	4	82	5
Propoxur	95	4	94	5	80	6
Carbofuran	102	3	98	4	97	4
Simazine	88	4	85	6	82	6
Carbaryl	90	5	92	3	94	4
Fluometuron	96	2	101	3	92	2
Atrazine	96	4	92	3	87	5
Diuron	92	3	87	5	85	5
Linuron	94	5	85	4	82	6
Barban	80	6	76	7	70	7

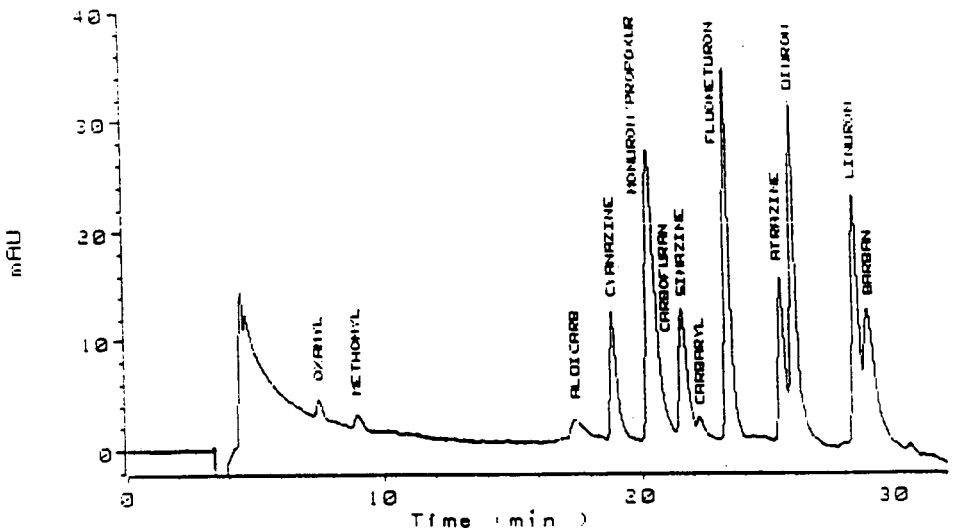

Fig. 3. On-line trace enrichment–RPLC–DAD chromatogram recorded at 240 nm of 100 ml Milli-Q water spiked with 14 pesticides at 1 $\mu g\ l^{-1}$ without any pH adjustment (pH about 6). For conditions, see text.

3.3. Performance of the total system

The analytical performance of the system was tested with tap and river water. Initially the influence of the pH of the sample solution was tested. No significant differences were found between recoveries obtained at pH 3 and at pH 6. However, adjusting the sample pH to 3 gave a larger matrix peak. We therefore preferably carried out the preconcentration at pH about 6, which actually meant that the samples could be preconcentrated without any pH adjustment. It should be point out that no clogging of the cartridge was observed with river water previously filtered through 0.45 μm.

The matrix peak which is mainly due to humic and fulvic acids did not appear in the PB-MS chromatograms. However, quantitative analyses showed a matrix effect at both pH values tested, higher responses being obtained compared with those found for preconcentration of Milli-Q water. This is due to a carrier effect [30] which is caused by the coelution of compounds acting as carriers; it was observed with both tap and surface water. This implies that quantification using PB-MS detection can not be carried out with calibration curves constructed for Milli-Q water; instead, standard addition must be used. The matrix effect caused the detection limits for some compounds in real samples to be lower than those obtained with Milli-Q water.

As regards linearity, this was essentially as good for the real-life water samples as for Milli-Q water. In the relevant ranges, the R^2 values were between 0.984 and 0.9990 for DAD (river water, 0.5–5 $\mu g\ l^{-1}$; tap water, 0.2–5 $\mu g\ l^{-1}$) and between 0.975 and 0.990 for PB-MS (0.2–5 $\mu g\ l^{-1}$ for both types of water). It should be added that, with the total analytical system, linear rather than the earlier exponential calibration plots were also observed for simazine and aldicarb.

Using DAD, it was found that the recovery for the complete on-line procedure with water samples spiked with 0.5 $\mu g\ l^{-1}$ of each pesticide was higher than 80% for both tap and river water, except for the first two eluting compounds, as was expected on the basis of the breakthrough volumes.

The repeatability of the method was checked with a 100-ml tap water sample spiked at the 1 $\mu g\ l^{-1}$ level. R.S.D. values were between 0.4

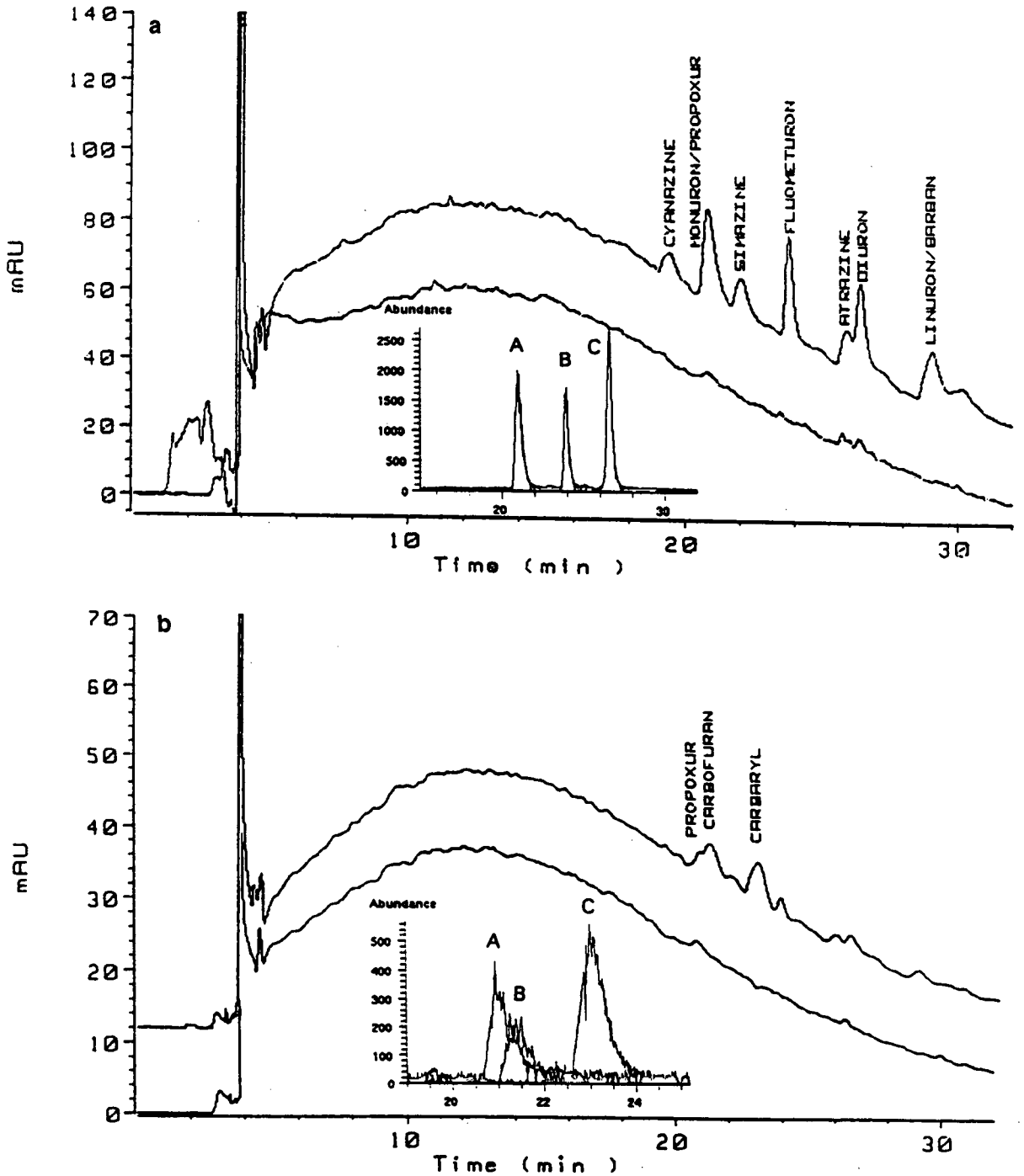

Fig. 4. On-line trace enrichment–RPLC–DAD chromatograms of 100 ml of river water and 100 ml of river water spiked with 14 pesticides at 1 μg l^{-1}. (a) Recorded at 240 nm; inset shows the PB-MS mass chromatogram of m/z 72: A = monuron, B = fluometuron, C = diuron. (b) Recorded at 280 nm; inset shows the PB-MS mass chromatograms of: A = propoxur (m/z 110), B = carbofuran (m/z 164), C = carbaryl (m/z 144).

and 9% for DAD and between 3 and 16% for PB-MS ($n = 4$). These are quite satisfactory results for the low concentration studied.

The limit of detection ($S/N = 3$) of the method varied between about 0.5 and 0.05 $\mu g\ l^{-1}$ for DAD and between about 0.5 and 0.02 $\mu g\ l^{-1}$ for PB-MS detection (full scan acquisition but quantification of highest peak), depending on the sample type and the analyte. It should again be pointed out that the matrix effect improves the response using PB-MS detection with real samples, especially for atrazine and carbofuran.

Fig. 4 shows the RPLC–DAD chromatograms of 100 ml of a river water sample (no pH adjustment) recorded at 240 nm and at 280 nm and the chromatograms for the same samples spiked with 1 $\mu g\ l^{-1}$ of each pesticide. The inserts show the RPLC–PB-MS mass chromatograms of the same sample using proper m/z values for the selective detection of several of the test analytes. The difference in both analyte detectability and selectivity is striking.

In order to further illustrate the potential of LC–PB-MS, Fig. 5 shows mass chromatograms at m/z 72, 144, 200 and 164 which were recorded after trace enrichment of 100 ml of tap water spiked with the several pesticides at the 0.1 $\mu g\ l^{-1}$ level.

3.4. Applications

Various river Ebro water samples were analysed and some pesticides were found. The mass chromatogram at m/z 72 obtained for one such sample is shown in Fig. 6. The peak which was eluted at 25.8 min could be assigned to isoproturon on the basis of a comparison with the retention time and the PB-MS spectrum of a

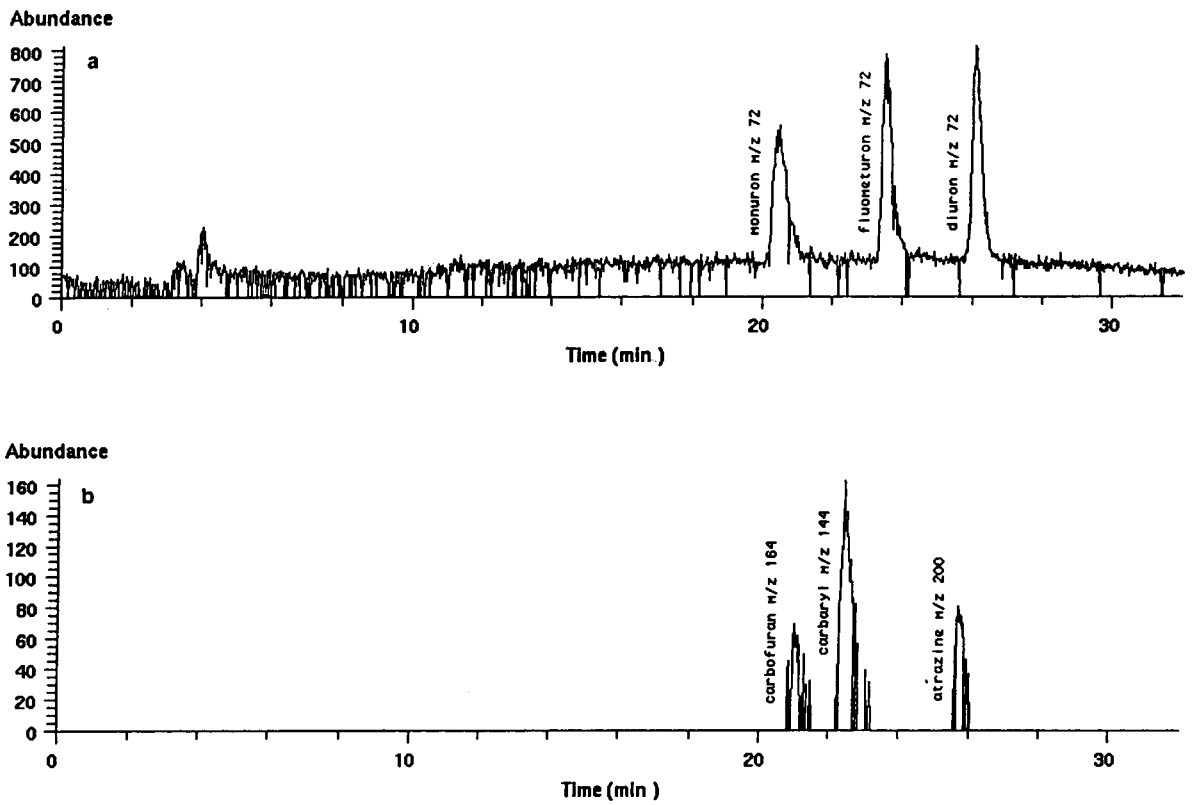

Fig. 5. On-line trace enrichment–RPLC–PB-MS extracted ion chromatogram of 100 ml tap water spiked with pesticides at 0.1 $\mu g\ l^{-1}$: (a) m/z 72; (b) m/z 164 (carbofuran), m/z 144 (carbaryl) and m/z 200 (atrazine).

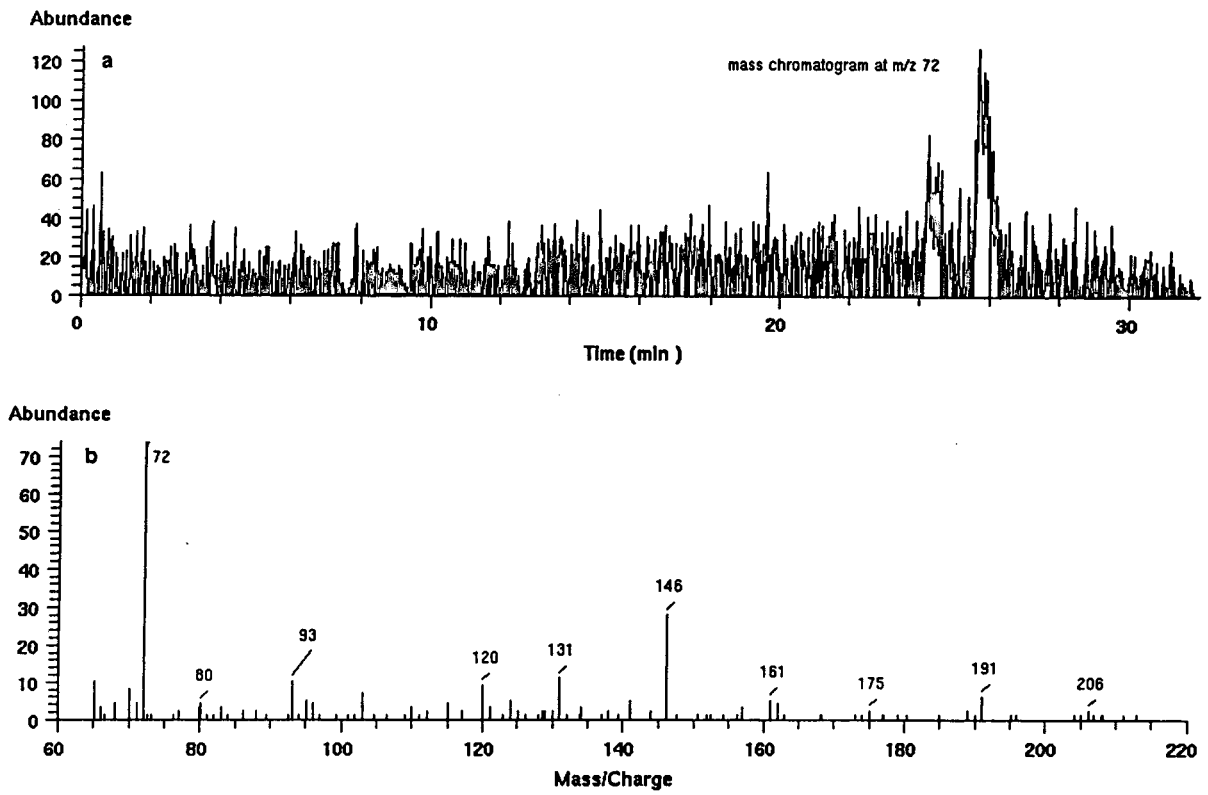

Fig. 6. (a) On-line trace enrichment–RPLC–PB-MS mass chromatogram (m/z 72) of 100 ml river Ebro water. (b) PB-MS spectrum of peak assigned to isoproturon (25.8 min). The peak at 24.3 min has not been identified as yet.

standard. It should be pointed out that although the peak intensity of the mass chromatogram was low, the spectrum showed a good match with the spectrum of the standard (95%). When using DAD instead of PB-MS detection, a small peak was observed at the proper retention time but spectral identification turned out to be impossible. After construction of PB-MS and DAD calibration curves, quantitation gave isoproturon levels of 0.074 $\mu g\ l^{-1}$ (standard addition) and 0.070 $\mu g\ l^{-1}$, respectively. The close similarity of these values is rather gratifying. Actually, in other river water samples isoproturon could be quantified by RPLC–PB-MS down to 0.05 $\mu g\ l^{-1}$; in these instances, no noticeable signal was observed with DAD.

Another example of a pollutant that was detected by means of on-line trace enrichment–RPLC with PB-MS, but not with DAD is presented in Fig. 7, which shows the mass chromatogram at m/z 77 of a 100-ml river Ebro sample, the mass spectrum of the peak of interest and the best match from the Wiley library. On this basis, the peak could be tentatively assigned to N-benzenesulfonamide which has been detected in the river Ob [20] and in water from several other rivers [31].

4. Conclusions

The present study demonstrates that on-line trace enrichment–RPLC–DAD–PB-MS presents no experimental problems and can be used for the trace-level determination of micropollutants in surface and tap water at levels of, typically, 0.2–5 $\mu g\ l^{-1}$ and 0.5–5 $\mu g\ l^{-1}$, respectively. Quantification is possible with both detection

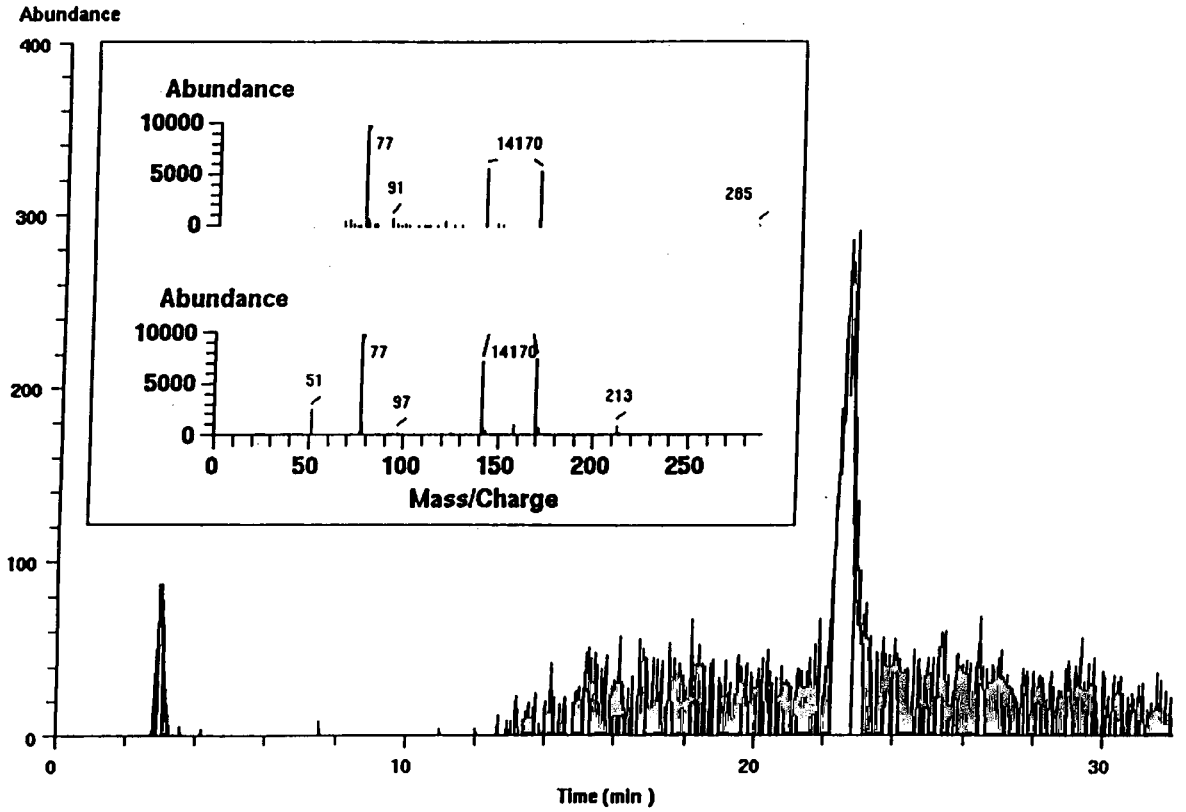

Fig. 7. Ion chromatogram at m/z 77 of 100 ml of river water and PB-MS spectrum of the peak at 22.5 min (inset, top; 22.462–22.736 min) and the PB-MS spectrum of N-benzenesulfonamide from the Wiley library (inset, bottom).

modes, although standard addition is required with PB-MS detection because of a beneficial carrier effect due to coeluting compounds in real samples. The main advantage of the present set-up is that complementary UV–Vis absorbance and EI-type mass spectral data are collected in one run. The high confirmatory power is illustrated with isoproturon and N-benzenesulfonamide as examples. It is worthwhile to add that the analyte detectability observed with PB-MS is rather better than is often assumed.

Acknowledgements

We acknowledge the mobility grant of Eurochemometrics-COMETT (Tempus project) given to H.P.

References

[1] E.R. Brouwer, I. Liska, R.B. Geerdink, P.C.M. Frintrop, W.H. Mulder, H. Lingeman and U.A.Th. Brinkman, *Chromatographia*, 32 (1991) 445.
[2] I. Liska, E.R. Brouwer, A.G.L. Ostheimer, H. Lingeman, U.A.Th. Brinkman, R.B. Geerdink and W.H. Mulder, *Intern. J. Environ. Anal. Chem.*, 47 (1992) 267.
[3] J. Slobodnik, E.R. Brouwer, R.B. Geerdink, W.H. Mulder, H. Lingeman and U.A.Th. Brinkman, *Anal. Chim. Acta*, 268 (1992) 55.
[4] C.J. Miles, *J. Chromatogr.*, 592 (1992) 283.
[5] A. Balinova, *J. Chromatogr.*, 643 (1993) 203.
[6] E. Pocurull, M. Calull, R.M. Marcé and F. Borrull, *Chromatographia*, 607 (1994) 135.
[7] W.V. Ligon and S.B. Dorn, *Anal. Chem.*, 62 (1990) 2573.
[8] D. Barceló, *Anal. Chim. Acta*, 263 (1992) 1.
[9] M.A. Brown, R.D. Stephens and I.S. Kim, *Trends Anal. Chem.*, 10 (1991) 330.
[10] E.R. Schmid, *Chromatographia*, 30 (1990) 573.

[11] D. Volmer, K. Leusen and G. Wünsch, *J. Chromatogr.*, 660 (1994) 231.
[12] H.Fr. Schröder, *J. Chromatogr.*, 554 (1991) 251.
[13] D. Barceló, G. Durand, R.J. Vreeken, G.J. de Jong, H. Lingeman and U.A.Th. Brinkman, *J. Chromatogr.*, 553 (1991) 311.
[14] T.D. Behymer, T.A. Bellar and W.L. Budde, *Anal. Chem.*, 62 (1990) 1686.
[15] C.J. Miles, D.R. Doerge and S. Bajic, *Arch. Environ. Contam. Toxicol.*, 22 (1992) 247.
[16] I.S. Kim, F.I. Sasinos, R.D. Stephens, J. Wang and M.A. Brown, *Anal. Chem.*, 63 (1991) 819.
[17] A. Apffel and M.L. Perry, *J. Chromatogr.*, 554 (1991) 103.
[18] D.R. Doerge, M.W. Burger and S. Bajk, *Anal. Chem.*, 64 (1992) 1212.
[19] J.S. Ho, T.D. Behymer, W.L. Budde and T.A. Bellar, *J. Am. Soc. Mass Spectrom.*, 3 (1992) 662.
[20] H. Bagheri, J. Slobodnik, R.M. Marcé, R.T. Ghijsen and U.A.Th. Brinkman, *Chromatographia*, 37 (1993) 159.
[21] M.C. Hennion, *Trends Anal. Chem.*, 10 (1991) 317.
[22] P. Subra, M.C. Hennion, R. Rosset and R.W. Frei, *Int. J. Environ. Anal. Chem.*, 37 (1989) 45.
[23] U.A.Th. Brinkman, *J. Chromatogr. A*, 665 (1994) 217.
[24] V. Pichon and M.C. Hennion, *J. Chromatogr. A*, 665 (1994) 269.
[25] J. Lintelmann, C. Mengel and A. Kettrup, *Fresenius' J. Anal. Chem.*, 346 (1993) 752.
[26] H. Bagheri, E.R. Brouwer, R.T. Ghijsen and U.A.Th. Brinkman, *J. Chromatogr.*, 647 (1993) 121.
[27] H. Bagheri, E.R. Brouwer, R.T. Ghijsen and U.A.Th. Brinkman, *Analusis*, 20 (1992) 475.
[28] S. Chiron, S. Dupas, P. Scribe and D. Barceló, *J. Chromatogr. A*, 665 (1994) 295.
[29] T.A. Bellar, T.D. Behymer and W.L. Budde, *J. Am. Soc. Mass Spectrom.*, 1 (1990) 92.
[30] F.R. Brown and W.M. Draper, *Biol. Mass Spectrom.*, 20 (1991) 515.
[31] L.B. Clark, R.T. Rosen, T.G. Hartman, J.B. Louis and J.D. Rosen, *Int. J. Environ. Anal. Chem.*, 45 (1991) 169.

ELSEVIER

Journal of Chromatography A, 696 (1995) 75–81

JOURNAL OF CHROMATOGRAPHY A

Determination of chiral purity of ethyl nipecotate using a Chiralcel-OG column

Abu M. Rustum

Department 41G (R13), Bioanalytical Research, Abbott Laboratories, 1401 Sheridan Road, North Chicago, IL 60064, USA

First received 4 October 1994; revised manuscript received 27 October 1994; accepted 28 October 1994

Abstract

The *R*-(−)- and *S*-(+)-enantiomers of ethyl nipecotate tartaric acid salt were separated by chiral high performance liquid chromatography on a commercially available chiral stationary phase using a non-polar mobile phase. Samples of ethyl nipecotate tartaric acid salt were analysed on a Chiralcel-OG column as the free base of ethyl nipecotate after extraction. The mobile phase was hexane–2-propanol–2-methyl-2-propanol (94:4:2, v/v/v), to which ca. 0.5 ml/l of dimethylamine was added. The method is able to separate the two enantiomers with a resolution factor (R_s) of approximately 1.3 and a selectivity factor (α) of 1.15. The limit of quantification of the *S*-(+)-enantiomer is 0.2% in the *R*-(−)-enantiomer. The method was validated by the standard addition method and determining the recovery of the *S*-(+)-enantiomer in the *R*-(−)-enantiomer. The precision of the method was determined by analysing seven individual sample preparations. The analysis was done by two analysts on different days, using different equipment and reagents.

1. Introduction

In recent years there has been renewed interest in the synthesis of pure enantiomers, specifically because of the increasing awareness of the importance of optical purity in the context of biological activity. The active enantiomer is called the eutomer and the undesirable enantiomer the distomer. Some distomers inhibit the biological activity of the eutomer and sometimes even exhibit severe adverse effects [1–4]. In the last decade, interest in the stereochemical aspects of drug development has intensified because of the more stringent regulations for the marketing of optically active compounds by the US Food and Drug Administration (FDA) and other regulatory agencies [5,6].

Gas chromatography (GC) and high-performance liquid chromatography (HPLC) have been used for the direct and indirect separation and determination of the optical isomers of pharmacologically active compounds [7–14]. The separation of enantiomers by GC or HPLC is one of the fastest growing fields in the area of separation technology. Numerous theoretical and experimental studies have been conducted by the early pioneers of chiral chromatography in order to understand the mechanism of the separation of enantiomers on chiral stationary phases [7,9,15,16]. Indirect separations of enantiomers have also been performed by derivatization of the optically active compounds with pure optically active reagents, forming diastereoisomers [17]. All commercially available chiral stationary phases have been classified by Wainer [18,19] according to the mechanism of separation of

SSDI 0021-9673(94)01060-9

chiral compounds having different functional groups. Simple, reproducible and sensitive analytical methods are required to determine, and hence control, the chiral purity of the starting materials or intermediates to ensure the desired chiral purity of the optically active drug.

Ethyl nipecotate is a cyclic β-amino acid derivative used as the starting chiral material in the synthesis of tiagabine · HCl. The structures of the free base and tartaric acid salt of ethyl nipecotate are shown in Fig. 1. Tiagabine · HCl is being developed as an antiepileptic/anticonvulsive agent and is currently in phase III clinical trials. The drug is synthesized in pure *R*-(−)-enantiomeric form because it is pharmacologically more potent than the *S*-(+)-enantiomer. However, the toxicological characteristics of the two enantiomers were found to be comparable. As the drug is synthesized and being developed in its *R*-(−)-enantiomeric form, it is critical to control the chiral purity of ethyl nipecotate in order to achieve the desired chiral purity of the final product. Ethyl nipecotate undergoes three steps/substeps in the synthesis of tiagabine · HCl prior to the isolation of the final product, and racemization of ethyl nipecotate (or its derivative) occurs in each of the three steps of synthesis. Therefore, using ethyl nipecotate with a very low *S*-(+)-enantiomer will yield the final product with good chiral purity. From historical data, it has been found that the final compound contains less than 0.5% of the *S*-(+)-enantiomer when the ethyl nipecotate used in the synthesis contained less than 0.2% of the *S*-(+)-enantiomer. Several commercially available columns were investigated during method development using both normal- and reversed-phase modes to achieve optimum resolution and sensitivity for the two enantiomers.

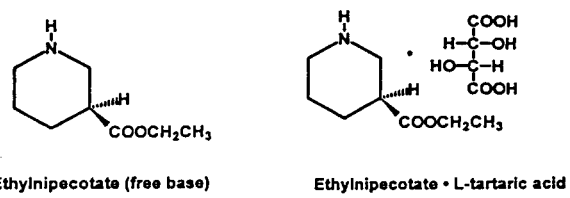

Fig. 1. Structure of ethyl nipecotate free base and ethyl nipecotate tartaric acid salt.

2. Experimental

2.1. Equipment

An HPLC solvent-delivery system (SP 8800) equipped with an injector/autosampler (SP 8780), an integrator (SP4270) and a variable-wavelength UV–visible detector (SP 8450) was used (Spectra-Physics, San Jose, CA, USA). A 25 cm × 4.6 cm I.D., Chiralcel-OG column was used in the method finally developed (Daicel Chemical). The other chiral stationary phase columns investigated were 25 cm × 4.6 mm I.D., 5 μm D-phenylglycine (Regis Chemical, Morton Grove, IL, USA), 25 cm × 4.6 mm I.D., 5 μm Cyclobond-1 β-cyclodextrin (Rainin Instrument, Woburn, MA, USA), 25 cm × 4.6 mm I.D., 5 μm phenylalanine (Jones Chromatography, Mid-Glamorgan, UK), 25 cm × 4.6 mm I.D., 10 μm Chiralcel-OJ (Daicel Chemical) and 15 cm × 7.5 mm I.D., 10 μm bovine serum albumin column (manufactured by Machery–Nagel, purchased from Alltech Associates, Deerfield, IL, USA).

2.2. Materials

HPLC-grade hexane, 2-propanol, ethyl acetate and anhydrous sodium carbonate were purchased from Fisher Scientific (Fairlawn, NJ, USA), diethylamine (analytical-reagent grade) and 2-methyl-2-propanol from Aldrich (Milwaukee, WI, USA) and a racemic mixture of *R*-(−)- and *S*-(+)-enantiomers of ethyl nipecotate from Abbott Labs. (North Chicago, IL, USA). Borosilicate scintillation vials and disposable pipettes were obtained from Baxter Scientific (Waukegan, IL, USA).

2.3. Preparation of sample

Approximately 100 mg of the samples were weighed and transferred into a scintillation vial and dissolved in 5 ml of distilled water. About 100 mg of anhydrous sodium carbonate were

added to the aqueous solution of the sample and vortex mixed for about 5 min, then ca. 5 ml of ethyl acetate were added and vortexed for about 2 minutes. The solution was allowed to settle into two layers and the ethyl acetate layer was transferred into a fresh scintillation vial with a disposable pasteur pipette. The ethyl acetate was evaporated to dryness under an air stream. The residue was reconstituted in ca. 10 ml of mobile phase and injected directly into the HPLC system.

2.4. Preparation of mobile phase

To 940 ml of hexane, 40 ml of 2-propanol, 20 ml of 2-methyl-2-propanol and 0.5 ml of diethylamine were added and mixed. This mobile phase mixture was degassed for ca. 5 min and used for analysis.

2.5. Chromatographic conditions

The final chromatographic conditions adopted were as follows: the mobile phase flow-rate was 0.8 ml/min, the samples were monitored with a UV detector at 230 nm and 0.10 AUFS and 10 μl of the sample solution were injected into the HPLC.

2.6. Calculation

Quantification of the *S*-(+)-enantiomer was based on peak-area measurement and the following equation was used for calculation:

$$S\text{-}(+)\text{-enantiomer}\ (\%) = \frac{\text{peak area of } S\text{-}(+)\text{-enantiomer}}{\text{sum of the peak areas of } S\text{-}(+)\text{- and } R\text{-}(-)\text{-enantiomers}} \cdot 100$$

2.7. Limit of quantification

Samples of *R*-(−)-ethyl nipecotate were analysed to determine the lowest level of the *S*-(+)-enantiomer that can be determined with good reproducibility (R.S.D. less than 10%). The limit of quantification (LOQ) of the method for the *S*-(+)-enantiomer was about 0.2% at a signal-to-noise ratio of 3.

3. Results and discussion

Injection of the blank (mobile phase) into the HPLC system showed no peak eluting with the same retention times as those of the *S*-(+)- and *R*-(−)-enantiomers. Fig. 2 is a typical chromatogram of the racemic mixture of ethyl nipecotate and shows that the peaks of the *S*-(+)- and *R*-(−)-enantiomers are adequately resolved from each other. The selectivity factor (enantiomeric selectivity) of the two optical isomers was 1.15. However, the resolution between the two enantiomers was ca. 1.3.

The amount of the *S*-(+)-enantiomer present in the *R*-(−)-enantiomer was determined on the basis of peak areas. The response of the UV detector at 230 nm was linear from 0.10 to 1.0 mg/ml for 10-μl injections. A typical linear regression equation for the analyte has a correlation coefficient of >0.999 and essentially passed through the origin.

Authentic reference materials of the pure *S*-(+)- and *R*-(−)-enantiomers were used to de-

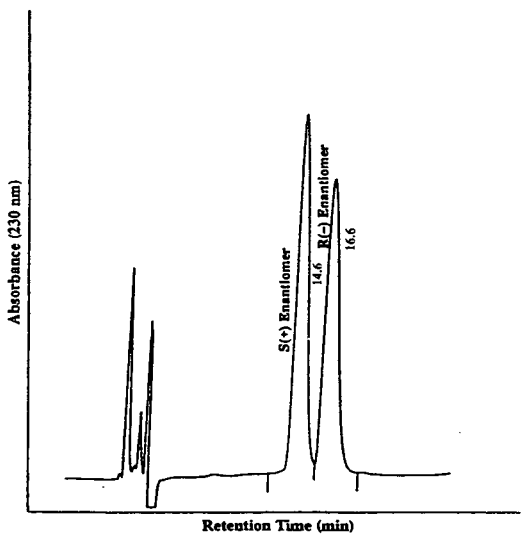

Fig. 2. Typical chromatogram of racemic mixture of ethyl nipecotate using the mobile phase described in the text.

termine the relative retention volumes and the elution order of the two enantiomers. Under the chromatographic conditions described here, the *S*-(+)-enantiomer eluted before the *R*-(−)-enantiomer. Because the *S*-(+)-form is not the enantiomer of interest, the elution of the *S*-(+)-enantiomer prior to the *R*-(−)-enantiomer makes this method ideal for trace analysis of the *S*-(+)-enantiomer present in the *R*-(−)-enantiomer of ethyl nipecotate.

The tartaric acid salt of ethyl nipecotate is used directly in the synthesis of tiagabine · HCl. Ethyl nipecotate tartaric acid salt is not soluble in the mobile phase described here. Therefore, extraction of ethyl nipecotate free base (which is soluble in the mobile phase) was necessary prior to injection of the sample into the HPLC system. The extraction of ethyl nipecotate free base was also necessary because the tartaric acid (if injected onto the chiral column) deteriorates the chiral selectivity of ethyl nipecotate and changes the chiral properties of the column. Occasional deterioration of the column properties such as selectivity factor and efficiency, observed after the injection of certain samples, may also be related to tartaric acid accumulated on the column during sample analysis. Typically, the column performance was regained after cleaning, using the procedure described below..

Experiments were conducted to obtain a mobile phase that will give optimum resolution and selectivity for the two enantiomers on the Chiralcel-OG column. The chiral stationary phase of the Chiralcel-OG column is the methylphenyl carbamate of cellulose, which is agglomerated on silica by a proprietary technique. The types and amounts of solvents that can be used in the mobile phase without damaging the chiral stationary phase of the Chiralcel-OG column are limited. Typical mobile phases are mixtures of hexane or heptane with 2-propanol (typically 10%, v/v). Other solvents such as diethylamine (<0.5%), *tert.*-butanol, 1-octanol and other long-chain alcohols can be used in trace concentrations (<1%) to improve the selectivity, resolution or efficiency of the chromatography. It was also observed that 10% ethanol with 30% 2-propanol in hexane does not deteriorate the chromatographic properties of the stationary phase of the Chiralcel-OG column.

The selectivity for and resolution of the two enantiomers of ethyl nipecotate varies with the type and amount of alcohols present in the mobile phase. Therefore, the ratios of the two alcohols in the mobile phase needs careful adjustment in order to achieve optimum resolution and selectivity. 2-Methyl-2-propanol increases the resolution of the two enantiomers from less than 1 to 1.5. The absence of 2-propanol in the mobile phase has a significant effect on the resolution of the two enantiomers. In the absence of 2-propanol, the resolution factor (R_s) of the two enantiomers remains less than 1 when the concentration of 2-methyl-2-propanol in the mobile phase varies from 0.5 to 15%. On the other hand, the selectivity factor (α) for the two enantiomers remains less than 1.1 when 2-methyl-2-propanol is not present in the mobile phase. Therefore, the optimum resolution and selectivity were obtained by using a combination of the two alcohols in the mobile phase. Experiments were conducted to determine the effect of 2-propanol and 2-methyl-2-propanol in the mobile phase on α and R_s for the two enantiomers of ethyl nipecotate by varying the percentage of one alcohol in the mobile phase and keeping the percentage of the second alcohol constant. The results of these experiments are summarized in Tables 1 and 2.

The presence of diethylamine (in a trace amount) in the mobile phase is critical to obtaining the desired resolution and chromatographic

Table 1
Effect of 2-propanol in the mobile phase on chiral selectivity (α) and resolution (R_s) of ethyl nipecotate

2-Propanol (%)[a]	α	R_s
0.5	1.23	0.45
1.0	1.18	0.89
2.0	1.16	1.10
4.0	1.14	1.28
6.0	1.10	1.37
8.0	1.06	1.58

[a] The content of 2-methyl-2-propanol in the mobile phase was kept constant at 2% (v/v).

Table 2
Effect of 2-methyl-2-propanol in the mobile phase on chiral selectivity (α) and resolution (R_s) of ethyl nipecotate

2-Methyl-2-propanol (%)[a]	α	R_s
0.5	1.31	0.80
1.0	1.27	1.11
2.0	1.21	1.33
5.0	1.16	1.42
7.0	1.08	1.53
9.0	1.01	1.62

[a] The content of 2-propanol in the mobile phase was kept constant at 4% (v/v).

efficiency. Two other amines, *N*,*N*-dimethyloctalamine and triethylamine, were also tested. Both of these amines were found to be less effective than diethylamine in decreasing the band broadening of the two enantiomers and enhancing the chromatography efficiency. It was also found that the chiral selectivity of the Chiralcel-OG column for ethyl nipecotate changed permanently when *N*,*N*-dimethyloctylamine was used in the mobile phase. The resolution of the two enantiomers was less than 1 when a Chiralcel-OC column treated with *N*,*N*-dimethyloctylamine was used for analysis. This finding demonstrates that one has to be careful in trying various trace solvent modifiers in the mobile phase during method development using the Chiralcel-OG or similar types of chiral stationary phases. Typically, 500 ml of the mobile are needed to condition a new column in order to obtain reproducible chromatographic results.

Columns packed with different chiral stationary phases were also investigated for the enantiomeric separation of ethyl nipecotate. Pirkle-type columns, such as phenylglycine and phenylalanine, and also a β-cyclodextrin column were investigated under both normal- and reversed-phase mobile phase conditions for the separation of the two enantiomers of ethyl nipecotate. For normal-phase conditions, hexane, 2-propanol, ethanol, 0.1% trifluoroacetic acid of diethylamine were used as solvents in various proportions in the mobile phase to obtain retention times from 6 to 25 min. For reversed-phase conditions, various ratios of 0.01 *M* phosphate or perchlorate buffers at different pH (2.2–7.5) with different percentages of an organic modifier such as acetonitrile, methanol or 2-propanol were used to obtain retention times ranging from 6 to 20 min. No indication of enantiomeric separation was obtained from all the experiments described above.

Protein columns such as bovine serum albumin (BSA) and α-glycoprotein (AGP-1) were also investigated using different percentages of 2-propanol (BSA column) and methanol–acetonitrile (AGP column) with 0.01 *M* aqueous phosphate buffer (pH $\approx$ 3.5–7.2). The retention time of ethyl nipecotate varied from 7 t o 20 min. These columns also gave no indication of enantiomeric separation under any of the mobile phase conditions used.

Other derivatized cellulose chiral columns such as Chiralcel-OD and Chiralcel-OJ were also investigated for the enantiomeric separation of ethyl nipecotate. Solvents such as hexane, 2-propanol, 2-methyl-2-propanol and ethanol with trace amounts (<0.1%) of trifluoroacetic acid and diethylamine were used in the mobile phase at various solvent strengths. The Chiralcel-OD column showed some indication of enantiomeric separation when a mobile phase of hexane–2-propanol (90:10) containing 0.1% trifluoroacetic acid was used. The Chiralcel-OJ column also showed some indication of chiral separation when a mobile phase of hexane–2-methyl-2-propanol–2-propanol, 94:4:2 containing 0.1% trifluoroacetic acid was used. However, the resolution of and selectivity for the analyte did not improve significantly when the ratios of the solvents (for both the columns) were varied to extreme solvent strengths. The selectivity factors (α) for the Chiralcel-OD and Chiralcel-OJ columns obtained from these experiments were 1.07 and 1.03, respectively.

Chiralcel-OG columns from different lots were tested for column-to-column reproducibility for the enantiomers of ethyl nipecotate. The resolution and chiral selectivity for the two enantiomers of ethyl nipecotate were found to be reproducible on columns having different lot numbers. However, conditioning of the new

column with an appropriate amount of mobile phase (typically 500 ml) was required to achieve satisfactory reproducibility.

Standard addition and recovery experiments were conducted to determine the accuracy of the method for the determination of the *S*-(+)-enantiomer present in the *R*-(−)-enantiomer of ethyl nipecotate. The levels of addition were approximately 2.5–25%. The recovery of the *S*-(+)-enantiomer averaged 100.5% with an R.S.D. of 0.8%. The data for the standard addition and recovery experiments are summarized in Table 3. The mean α value obtained from the chromatograms of the standard addition and recovery experiments was 1.14 ± 0.06 ($n = 6$, R.S.D. $\approx 5\%$).

The precision and short-term ruggedness were also determined by two analysts using a sample of *R*-(−)-ethyl nipecotate containing a small amount of the *S*-(+)-enantiomer. Two samples of *R*-(−)-ethyl nipecotate were prepared by each of the two analysts. The samples were analysed on two different instruments and columns and on different days. The precision of the method was found to be 7.6% (R.S.D.) at an *S*-(+)-enantiomer level of ca. 1% in *R*-(−)-ethyl nipecotate. The data from these experiments are summarized in Table 4. Fig. 3 shows a typical chromatogram for *R*-(−)-ethyl nipecotate containing ca. 1.5% of the *S*-(+)-enantiomer.

The limit of quantification of the *S*-(+)-enantiomer of ethyl nipecotate was determined by injecting samples containing trace levels of the *S*-(+)-enantiomer. The limit of quantification was ca. 0.2% of the peak area of the *R*-(−)-enantiomer at a signal-to-noise ratio of 3.

The Chiralcel-OG column used in the method to separate the two enantiomers of ethyl nipecotate was reasonably stable in terms of selectivity, efficiency, resolution and other chromatographic

Table 3
Standard addition and recovery of the *S*-(+)-enantiomer in the *R*-(−)-enantiomer of ethyl nipecotate tartaric acid salt

(*S*)-(+)-ENP[a] added (%, w/w)	(*S*)-(+)-ENP[a] found (%, w/w)	Recovery (%)
2.4	2.4	100.0
11.3	11.3	100.0
13.6	13.6	100.0
16.0	16.0	100.0
18.1	18.4	101.7
23.8	24.1	101.3
		Mean 100.5
		S.D. 0.8
		R.S.D. 0.8%

[a] ENP = Ethyl nipecotate.

Table 4
Precision data for the determination of the *S*-(+)-enantiomer in the *R*-(−)-enantiomer of ethyl nipecotate by different analysts

Analyst No.	Peak-area percentage of *S*-(+)-enantiomer
1	0.94
1	1.06
1	0.88
1	1.00
2	0.86
2	0.92
2	0.90
	Mean 0.94
	S.D. 0.071
	R.S.D. 7.6%

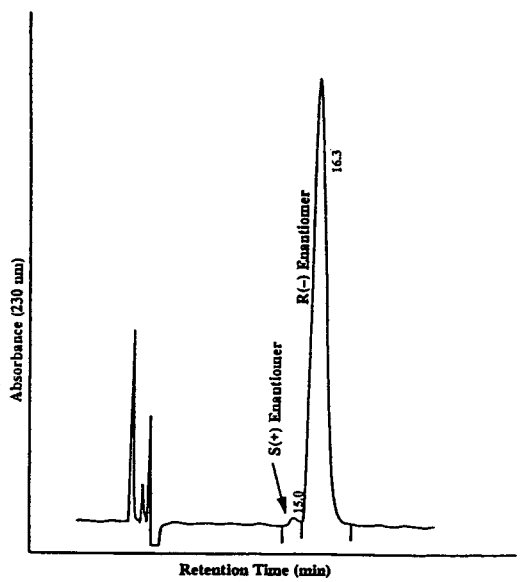

Fig. 3. Typical chromatogram of the *R*-(−)-enantiomer of ethyl nipecotate using the same mobile phase in Fig. 2.

properties. The Chiralcel-OG column did not show any significant change in chromatographic properties after ca. 400 sample injections with the following maintenance procedure applied. On at least two occasions, the selectivity and resolution deteriorated after 60–70 injections of the sample. The column was easily regenerated to its initial chromatographic efficiency, selectivity and resolution simply by washing it with ca. 100 ml of hexane–2-propanol–ethanol (60:30:10, v/v/v) at a flow-rate of 0.3 ml/min. After the cleaning, the column was reconditioned with ca. 100 ml of the mobile phase. The occasional deterioration of the chromatographic properties of the column was probably due to the accumulation of tartaric acid and some unknown impurities from the samples on the column. This column and method were also used to analyse in-process samples that typically contain multiple minor components.

4. Conclusions

Ethyl nipecotate has one chiral centre and is the starting raw material in the synthesis of tiagabine · HCl, which is being developed as an antiepileptic agent. Therefore, it is critical to control the presence of the undesired enantiomer in order to ensure the required chiral purity of the final product. The method described in this paper is rugged, reproducible and capable of providing the chiral purity information necessary to manufacture the final product with the desired quality. The separation of the two enantiomers of ethyl nipecotate was reproducible on five different columns from five different batches.

References

[1] E.J. Ariens, *Med. Res. Rev.*, 6 (1986) 451.
[2] E.J. Ariens, *Eur. Clin. Pharmacol.*, 26 (1984) 663.
[3] M. Simonyi, *Med. Res. Rev.*, 4 (1984) 359.
[4] I.W. Wainer and D.E. Drayer, *Drug Stereochemistry*, Marcel Dekker, New York, 1988.
[5] J.W. Hubbard, D. Ganes, H.K. Lim and K.K. Midha, *Clin. Biochem.*, 19 (1986) 107.
[6] D.W. Drayer, *Clin. Pharmacol. Ther.*, 40 (1986) 125.
[7] D.W. Armstrong, *Anal. Chem.*, 59 (1987) 844.
[8] N. Nimura, Y. Kasahara and T. Kinoshita, *J. Chromatogr.*, 213 (1981) 327.
[9] J.D. Morrison, *Asymmetric Synthesis*, Vol. 1, Academic Press, New York, 1983.
[10] M. Gazdag, G. Szepesi and K. Milhalyfi, *J. Chromatogr.*, 450 (1988) 145.
[11] J.D. Morrison (Editor), *Asymmetric Synthesis*, Vol. 1, Academic Press, New York, 1983.
[12] L.R. Gelber and J.L. Neumeyer, *J. Chromatogr.*, 257 (1983) 317.
[13] H. Farukawa, *Chem. Pharm. Bull.*, 23 (1975) 1625.
[14] T. Arai, H. Koike, K. Hirata and H. Oizumi, *J. Chromatogr.*, 448 (1988) 439.
[15] D.W. Armstrong, X. Xang, S.M. Han and R.A. Menges, *Anal. Chem.*, 59 (1987) 2594.
[16] M. Zief and L.J. Crane, *Chromatographic Chiral Separations*, Marcel Dekker, New York, 1988.
[17] J. Gal, *LC · GC*, 5 (1987) 106.
[18] I.W. Wainer, *Trends Anal. Chem.*, 6 (1987) 125.
[19] I.W. Wainer, *A Practical Guide to the Selection and Use of HPLC Chiral Stationary Phases*, 1988.

ELSEVIER

Journal of Chromatography A, 696 (1995) 83–92

JOURNAL OF CHROMATOGRAPHY A

Determination of codeine in human plasma by high-performance liquid chromatography with fluorescence detection☆

Brianne Weingarten*, Hou-Yeh Wang, Dale M. Roberts

The Purdue Frederick Company, Purdue Research Center, Department of Pharmacokinetics/Drug Metabolism, 99 Saw Mill River Road, Yonkers, NY 10701, USA

First received 9 May 1994; revised manuscript received 23 November 1994; accepted 6 December 1994

Abstract

A rapid, reliable and rugged assay for determining codeine in human plasma using reversed-phase high-performance liquid chromatography with fluorescence detection was developed. This analytical method utilized an ion-exchange/mixed-mode solid-phase extraction procedure. The chromatographic separation was achieved using a 150 × 4.6 mm I.D., 3-μm reversed-phase C_8 (deactivated for basic analytes) column at ambient temperature. Fluorescence detection (excitation at 214 nm and emission above 345 nm) for codeine and nalorphine allowed for a detectable limit of 5 ng/ml. The results showed that the method was linear from 10 to 300 ng/ml. The method had good reproducibility, precision, accuracy and recoveries of 91 and 90% for codeine and nalorphine, respectively. This method has been applied to study the pharmacokinetics of codeine in normal human subjects.

1. Introduction

Codeine has long been used as an analgesic and antitussive in pharmaceutical preparations. A sensitive and specific bioanalytical method is essential for studying the bioavailability of codeine from oral formulations. Many previously reported assays [1–4] for codeine utilize liquid–liquid extractions which are time consuming and solvent-usage intensive. The recoveries associated with these methods [2–4] are often below 80%, and endogenous peaks elute near the codeine or internal standard peaks [5] making quantitation at the lower limits of detection difficult. A high-performance liquid chromatographic (HPLC) method with fluorescence detection has been developed, which is both accurate and precise for the determination of codeine. This method utilizes a solid-phase extraction technique which provides clean extracts with high recoveries for codeine and the internal standard nalorphine. This method may be used in pharmacokinetic studies where monitoring of codeine in human plasma samples is required without metabolites or other compounds interfering. To date, several thousands of samples have been analyzed using this method to de-

* Corresponding author.

☆ Presented at the *18th International Symposium on Column Liquid Chromatography, Minneapolis, MN, 8–13 May 1994.*

0021-9673/95/$09.50
SSDI 0021-9673(94)01212-1

termine the bioavailability of codeine. The solid-phase extraction procedure may readily be automated using any of the commercially available sample processing workstations.

2. Experimental

2.1. Chromatographic conditions

The HPLC system consisted of Hewlett-Packard (Avondale, PA, USA) Series 1050 pump and 1050 autosampler equipped with Applied Biosystems (Ramsey, NJ, USA) Spectroflow 980 programmable fluorescence detector. The fluorescence detector was operated at a 214 nm excitation wavelength with an emission wavelength cutoff filter of 345 nm. The chromatographic separation was performed on a 150 × 4.6 mm I.D., 3-μm Basic C_8 column (YMC, Wilmington, NC, USA). The mobile phase composition consisted of acetonitrile–5 m*M* ammonium phosphate dibasic (8:92, v/v) adjusted to pH 5.8 with phosphoric acid. The flow-rate through the column at ambient temperature was 1.0 ml/min. The column provided excellent resolution of the analytes from all the endogenous peaks present in the extracted plasma. Consistent column performance was found from various lots of packing material. Typically over one thousand injections could be made on a column with no appreciable loss in performance.

2.2. Data handling

Data acquisition and calculations were performed by the Perkin-Elmer Nelson (PE Nelson) Access*Chrom chromatography data analysis system (revision 1.7; Cupertino, CA, USA).

2.3. Sample preparation

Aliquots of 1 ml of plasma were pipetted into 75 × 12 mm I.D. polypropylene test tubes to which 100 μl of the 1000 ng/ml nalorphine internal standard solution and 1.0 ml of deionized water were added. The solid-phase extractions were performed on a Varian Vac-Elut sample processing manifold. The Bond Elut Certify (Varian Sample Preparation Products, Harbor City, CA, USA) columns (3 ml capacity) were conditioned with 2.0 ml of methanol followed by 2.0 ml deionized water. The plasma samples were then transferred to the columns and drawn through at a flow-rate of 2.0 ml/min. The columns were rinsed by using 2.0 ml of water followed by 2.0 ml acetonitrile. The packing was allowed to dry for 1 min under vacuum after the acetonitrile rinse step. The codeine and nalorphine were then eluted into polypropylene test tubes using 2.0 ml of 98% of dichloromethane–isopropanol (80:20, v/v) with 2% ammonium hydroxide. The eluent was then evaporated to dryness under nitrogen at 40°C using a Zymark (Hopkinton, MA, USA) Turbo Vap LV evaporator. The residue was then reconstituted with 100 μl of mobile phase and 60 μl were injected on the HPLC column.

3. Results and discussion

3.1. Linearity and calibration

To evaluate the linearity of the method, standard curves were prepared by spiking plasma with different amounts of codeine in the range of 10 to 300 ng/ml and a constant amount of nalorphine (100 ng/ml). Linear regression analyses were performed using ratios of peak areas of drug to internal standard vs. the respective drug concentrations. To determine the inter- and intra-day accuracy and precision of the calibration curves, three seven-point calibration curves in the range of 10–300 ng/ml were assayed on three separate days. One curve was used to calibrate the other two curves. As shown in Table 1, good inter-/intra-day precision was obtained with the mean accuracy ranging from −8.00 to 2.50% over the investigated concentrations.

The accuracy was estimated by the slope (mean slope value 1.01), intercept (mean intercept value −0.0340) and correlation coefficient (e.g. 0.9999). For example, a typical least

Table 1
Accuracy and precision of codeine calibration curves

Actual concentration (ng/ml)	Calculated codeine concentration (ng/ml)			Mean (ng/ml)	Standard deviation (ng/ml)	Mean accuracy (%)	Relative standard deviation (%)
	Day 1	Day 2	Day 3				
10.0	10.1, 10.5, 11.2	10.1, 10.5, 9.32	8.63, 8.66, 9.89	9.88	0.864	−1.20	8.75
20.0	17.8, 19.2, 19.3	18.9, 18.4, 18.2	19.1, 17.3, 17.8	18.4	0.720	−8.00	3.91
30.0	29.3, 30.8, 30.5	29.8, 31.0, 29.2	29.2, 29.5, 31.0	30.0	0.786	0.00	2.62
50.0	50.9, 50.0, 49.9	48.7, 51.0, 49.2	49.6, 50.3, 49.2	49.9	0.781	−2.00	1.57
100	101, 101, 106	103, 102, 98.9	102, 101, 100	102	2.02	2.00	1.98
200	204, 204, 208	201, 204, 203	207, 210, 205	205	2.76	2.50	1.35
300	297, 306, 302	299, 309, 301	295, 312, 299	302	5.67	0.667	1.88

squares plot gives the equation $y = 0.013x + 0.0151$ with correlation coefficient of 0.9999.

3.2. Precision and accuracy

Inter- and intra-day accuracy and precision were determined by analyzing human plasma controls spiked with codeine at levels of 10.0, 50.0 and 150 ng/ml. The intra-day precision ranged from 1.35% ($n = 4$) to 16.1% ($n = 3$). The inter-day precision ranged from 2.57% ($n = 11$) to 9.75% ($n = 10$).

The accuracy was determined by comparing the measured concentrations to the expected concentrations of codeine in spiked blank human plasma. The mean deviations ranged from −11.8 to −3.20% for 10.0 ng/ml, −3.00 to −0.400% for 50.0 ng/ml and −1.33 to 2.00% for 150 ng/ml codeine in human plasma. Values for precision and accuracy are summarized in Tables 2–4.

Table 2
Precision and accuracy of 10 ng/ml codeine control

Day	Calculated concentration (ng/ml)	Mean (ng/ml)	Standard deviation (ng/ml)	Relative standard deviation (%)	Accuracy (%)
1	8.91				−10.9
	10.0				0.00
	10.2				2.00
	9.59				−4.10
		9.68	0.570	5.89	−3.20
2	9.03				−9.70
	8.21				−17.9
	9.22				−7.80
		8.82	0.537	6.09	−11.8
3	8.68				−13.2
	8.46				−15.4
	11.2				12.2
		9.45	1.52	16.1	−5.50
Overall		9.35	0.912	9.75	−6.50

Table 3
Precision and accuracy of 50 ng/ml codeine control

Day	Calculated concentration (ng/ml)	Mean (ng/ml)	Standard deviation (ng/ml)	Relative standard deviation (%)	Accuracy (%)
1	48.9				−2.20
	49.6				−0.80
	50.8				1.60
		49.8	0.961	1.93	−0.400
2	49.4				−1.20
	49.6				−0.80
	48.3				−3.40
	48.4				−3.20
		48.9	0.670	1.37	−2.20
3	48.9				−2.20
	49.0				−2.00
	45.9				−8.20
	50.1				0.200
		48.5	1.80	3.71	−3.00
Overall		49.0	1.26	2.57	−2.00

Table 4
Precision and accuracy of 150 ng/ml codeine control

Day	Calculated concentration (ng/ml)	Mean (ng/ml)	Standard deviation (ng/ml)	Relative standard deviation (%)	Accuracy (%)
1	144				−4.00
	150				0.00
	152				1.33
	147				−2.00
		148	3.50	2.37	−1.33
2	153				2.00
	151				0.667
	153				2.00
	156				4.00
		153	2.06	1.35	2.00
3	154				2.67
	150				0.00
	143				−4.67
	154				2.67
		150	5.19	3.46	0.00
Overall		151	4.06	2.69	0.667

3.3. Recovery

Absolute recovery was measured by direct comparison of peak areas of non-extracted water standards vs. plasma extracts. The recoveries of codeine and nalorphine, the internal standard, were determined separately. The recovery of codeine over the standard curve concentrations ranged from 82.7 to 108% and averaged 91.4%. The recovery of the internal standard, nalorphine at 100 ng/ml was 90.7%.

3.4. Sensitivity

The working calibration curve for this method is prepared with 10 ng/ml codeine in plasma as the lowest standard. This is considered to be the limit of quantitation of codeine which can be measured within a certain preset level of certainty. The limit of detection was 5 ng/ml, represented as the amount of sample that generates a detector response equal to twice the background noise of the system.

A representative chromatogram of blank plasma containing internal standard (nalorphine) is shown in Fig. 1. There is no chromatographic interference at the retention time of codeine (15 min). The internal standard has a retention time of 18 min. Figs. 2 and 3 are chromatograms of the minimum codeine plasma concentration which can accurately be measured (10 ng/ml) and one of a higher concentration (300 ng/ml).

3.5. Specificity/interferences

Codeine is completely resolved from the internal standard nalorphine, and there are no interferences present at either of the respective retention times. The major metabolites of codeine are morphine and norcodeine. These metabolites were assayed for any possible interferences and the chromatograms are shown in Fig. 4.

The most difficult part in applying a solid-phase extraction technique [6] is identifying a sorbent which will eliminate interfering compounds from the sample matrix. Previous work

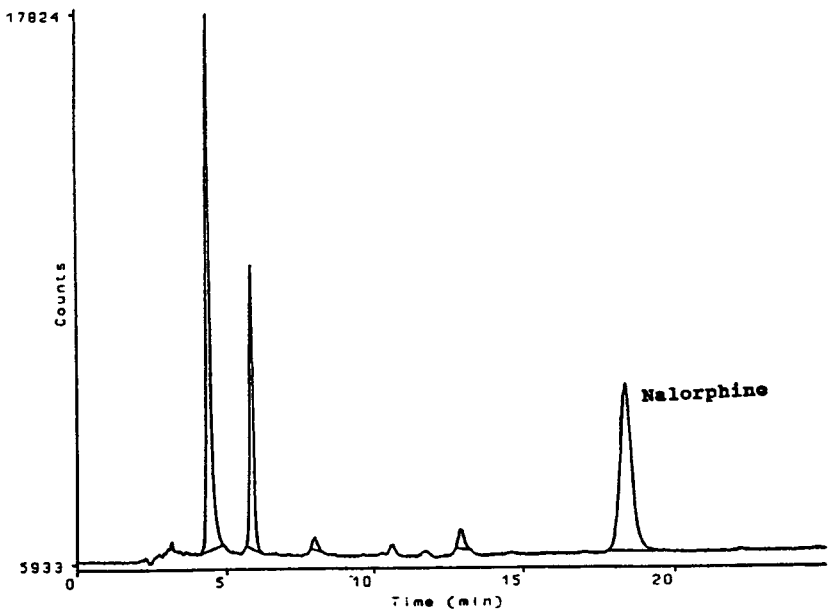

Fig. 1. Chromatogram showing extracted blank plasma spiked with 100 ng/ml nalorphine (internal standard). Chromatographic conditions: injection volume, 60 μl; extraction column, Bond Elut Certify colums (3 ml capacity); analytical column, YMC Basic C_8 (150 × 4.6 mm I.D., 3 μm); mobile phase, acetonitrile–5 m*M* ammonium phosphate dibasic (pH 5.8) (8:92); flow-rate, 1.0 ml/min; fluorometric detection (excitation wavelength 214 nm, emission above 345 nm).

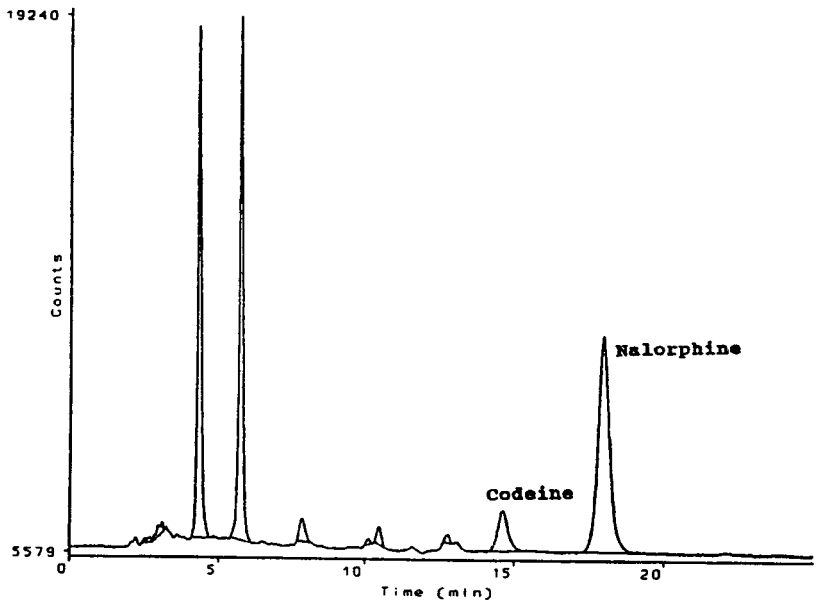

Fig. 2. Chromatogram showing extracted blank plasma spiked with 10 ng/ml of codeine and 100 ng/ml of nalorphine (internal standard). Chromatographic conditions as in Fig. 1.

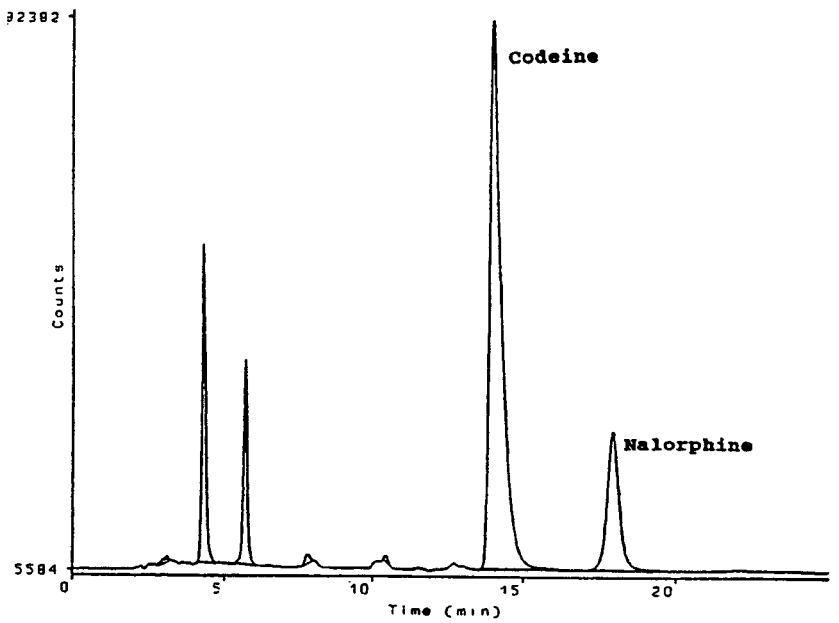

Fig. 3. Chromatogram showing extracted blank plasma spiked with 300 ng/ml of codeine and 100 ng/ml of nalorphine (internal standard). Chromatographic conditions as in Fig. 1.

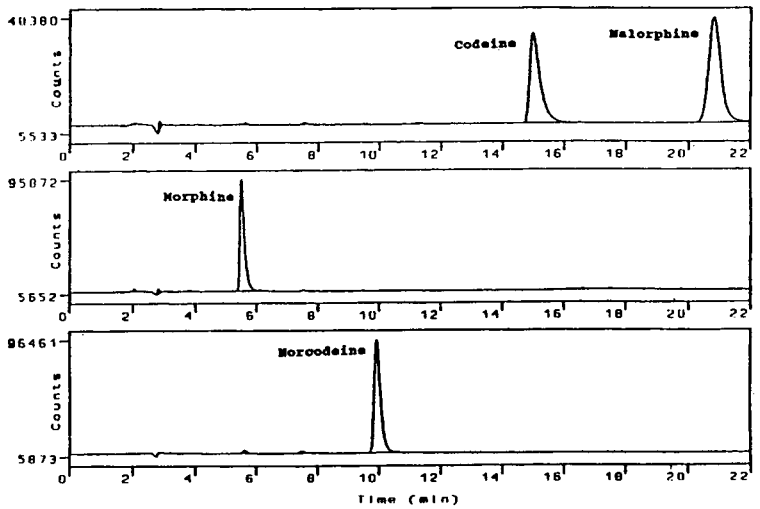

Fig. 4. Water-spiked chromatograms of pure drug compounds: codeine phosphate (500 ng/ml), nalorphine hydrochloride (1000 ng/ml), morphine sulfate (1000 ng/ml) and norcodeine hydrochloride (1000 ng/ml). The top chromatogram is codeine and nalorphine (15 and 22 min, respectively), the middle chromatogram morphine at 5.5 min and the bottom chromatogram norcodeine at 10 min. Chromatographic conditions: injection volume 60 μl; analytical column, YMC Basic C_8 (150 × 4.6 mm I.D., 3 μm); mobile phase, acetonitrile–5 m*M* ammonium phosphate dibasic (pH 5.8) (8:92); flow-rate, 1.0 ml/min; fluorometric detection (excitation wavelength 214 nm, emission above 345 nm).

on codeine was performed on a non-polar C_{18} cartridge, as well as a C_8 cartridge. The advent of the Bond-Elut Certify column (acid/base/neutral sorbent) resulted in a much cleaner plasma extract without almost any spurious peaks in the chromatogram.

3.6. Stability

The stability of codeine in plasma was determined by analyzing frozen plasma standards after one week, two weeks, three months and seven months. These frozen standard curves were compared against a freshly prepared codeine plasma standard curve in each instance. Illustrated in Table 5 are the calculated concentrations (ng/ml) of codeine from the newly prepared and frozen curves. From the results obtained (Table 5), it was concluded that codeine stored frozen in plasma is stable for at least seven months.

3.7. Freeze and thaw

To assess the instability of the analytes due to the number of quantitative freeze thaw cycles, a stock plasma solution of 50 ng/ml concentration of codeine was made and 1-ml aliquots from this stock were pipetted into 10 tubes. Each tube was subjected to different cycles (Table 6) of freezing and thawing. Tube 1 was frozen and thawed once while tube 10 was frozen and thawed ten times. After the cycles were completed the concentration of codeine in these samples were measured against freshly prepared codeine standard curves. The results are illustrated in Table 6.

4. Application

This method has been utilized to assay over 3800 plasma samples from a bioequivalence study in normal volunteers. After obtaining Institutional Review Board approval and Informed Consent, subjects received two formulations of codeine (100 mg) both administered under fed and fasted conditions in a four-way randomized crossover study. As can be seen from Figs. 5 and 6, the 10 and 150 ng/ml quality

Table 5
Stability of codeine in plasma

Actual concentration (ng/ml)	calculated codeine concentration (ng/ml)							
	One week		Two weeks		Three months		Seven months	
	New curve	Frozen curve	New curve	Frozen curve	New curve	Frozen curve	New curve	Frozen curve
10.0	8.87	9.35	9.19	9.55	9.44	11.4	11.6	9.82
20.0	19.3	20.2	19.9	19.5	19.5	18.4	22.3	19.4
30.0	28.8	29.8	28.7	29.7	32.0	28.8	27.5	27.0
50.0	51.9	51.3	50.9	50.0	50.0	47.5	44.1	45.2
100	103	99.1	104	102	99.3	92.8	102	94.0
200	198	198	197	203	198	188	207	190
300	300	308	301	308	301	291	296	287
Linear regression equations	$y = 0.013x + 0.0071$ $r = 0.9999$	$y = 0.013x - 0.0081$ $r = 0.9995$	$y = 0.013x + 0.0153$ $r = 0.9996$	$y = 0.013x + 0.0002$ $r = 1.000$	$y = 0.014x + 0.0195$ $r = 0.9999$	$y = 0.014x + 0.0085$ $r = 0.9994$	$y = 0.013x + 0.0361$ $r = 0.9992$	$y = 0.013x + 0.0207$ $r = 0.9999$

r = Correlation coefficient.

Table 6
Freeze and thaw

Day	Codeine concentration (ng/ml)
1	46.9
2	46.2
3	50.2
4	49.4
5	50.3
6	50.8
7	48.6
8	49.4
9	48.9
10	49.4

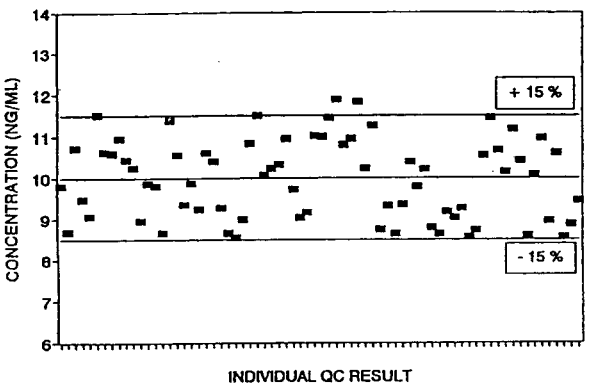

Fig. 5. Results from quality control (QC) samples (concentration 10 ng/ml) during the time course of the pharmacokinetic study.

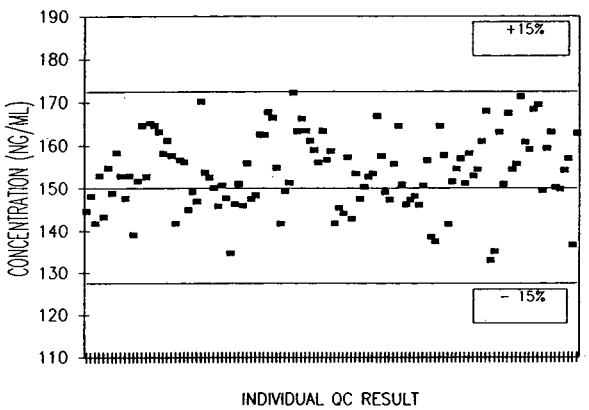

Fig. 6. Results from quality control samples (concentration 150 ng/ml) during the time course of the pharmacokinetic study.

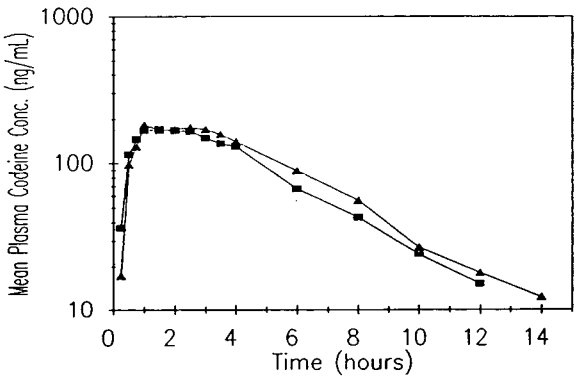

Fig. 7. Semilogarithmic plot of mean plasma concentration versus time profile for codeine after a single dose of 100 mg codeine phosphate liquid fed (▲) and fasted (□) in human volunteers.

control data demonstrate the good overall inter/intra-day accuracy and precision of the method under routine conditions obtained during the 3 month analysis period. Fig. 7 shows mean plasma concentrations of codeine following a single 100-mg dose of codeine phosphate liquid with and without food. The terminal half-life of codeine was 2.5 h.

5. Conclusions

The analysis of codeine in human plasma by HPLC with fluorescence detection is a rapid, sensitive and specific assay. This analytical method is capable of quantitating and monitoring the levels of codeine in plasma following an ion-exchange/mixed-mode solid-phase extraction procedure.

The use of the YMC Basic C_8 column resulted in excellent separation of codeine and nalorphine (internal standard) as well as good peak shape. There were no interferences with the analytes from extracted endogenous fluorogenic substances.

Combining both the extraction technique and detection method has resulted in a method suitable for determining the plasma codeine concentrations in pharmacokinetic studies.

References

[1] S.S. Mohammed, M. Butschkau and H. Derendorf, *J. Lig. Chromatogr.*, 16 (1993) 2325.
[2] D.E. Easterling, W.R. deTorres and R.K. Desiraju, *Pharm. Res.*, 3 (1986) 45.
[3] Z.R. Chen, F. Bochner and A. Somogyi, *J. Chromatogr.*, 491 (1989) 367.
[4] I.W. Tsina, M. Fass, J.A. Debban and S.B. Matin, *Clin. Chem.*, 28 (1982) 1137.
[5] G. Chari, A. Gulati, R. Bhat and I.R. Tebbett, *J. Chromatogr.*, 571 (1991) 263.
[6] *Application Notes, Opiate Extraction Procedure*, Varian Sample Preparation Products, Harbor City, CA, 1989.

ELSEVIER

Journal of Chromatography A, 696 (1995) 93–99

JOURNAL OF CHROMATOGRAPHY A

High-performance liquid chromatography of the fluorescent dyes Fura-2 and Mag-Fura Stability in organic solvents

Mickey Castle*, Els Neuteboom

Department of Pharmacology, Eastern Virginia Medical School, P.O. Box 1980, Norfolk, VA 23501, USA

First received 30 August 1994; revised manuscript received 24 November, 1994; accepted 7 December 1994

Abstract

The fluorescent dye indicators Fura-2/AM and Mag-fura are used to estimate changes in intracellular concentrations of calcium and magnesium, respectively. HPLC, coupled to fluorescence and ultraviolet detectors, indicated that these dyes are unstable when dissolved in methanol and are especially unstable in glass containers compared to plastic. Both dyes were very stable in acetonitrile and dimethyl sulfoxide. The glass vials used in these studies appear to contain an unidentified substance which causes changes in the spectral intensities of these fluorescent dyes in the presence of methanol but not other solvents. With Fura-2/AM, there was an initial two fold increase in fluorescence during the first four hours in methanol and glass with no change in retention time, peak shape or ultraviolet absorption. With Mag-fura, no increase in fluorescence was observed but instead there was a reduction of more than 90% in both fluorescence and ultraviolet absorption within 30 min, indicating that significant decomposition occurs under these conditions. These results confirm previous studies which suggest that acetonitrile is preferable to methanol for sample preparation and chromatographic analysis of Fura-2 and Mag-Fura. These data also indicate that glass vials contain an extractable substance which markedly enhances the spectral intensities of Fura-2/AM.

1. Introduction

Fluorescent dye indicators have provided a means of quantitating intracellular free ion concentrations for several cations which are known to play important roles in cell signaling [1,2]. Two of the most significant cations in this respect are calcium and magnesium. The measurement of intracellular free calcium involves introduction into the cell of a fluorescent dye which exhibits different fluorescent spectra in the presence and absence of calcium [3]. The fluorescent properties of Fura-2 have been widely used to estimate intracellular free calcium ion concentrations [1,2]. Fura-2 acid exhibits a maximum fluorescence at 360 nm when not bound to calcium ions. In the presence of calcium ions, fluorescence is enhanced and the fluorescence maximum shifts to 340 nm. The ratio of the fluorescence intensity at these two wavelengths is used as an estimate of changes in the intracellular free calcium ion concentration. Since Fura-2 is polar and thus unable to cross biological membranes, an esterified form, the pentaacetox-

* Corresponding author.

0021-9673/95/$09.50
SSDI 0021-9673(94)01215-6

ymethyl ester (Fura-2/AM), is required to introduce the ion indicator into cells. Once inside the cell, Fura-2/AM is converted by cellular esterases to Fura-2 acid which becomes trapped inside the cell and combines with free calcium ions. Fura-2/AM does not bind calcium ions and has a different fluorescence maximum than does Fura-2 acid.

There are few studies which have addressed the rate of conversion of the ester to the acid or the concentrations of the ester and acid within the cell. One such study used HPLC with fluorescence detection to separate and quantitate Fura-2 acid and Fura-2/AM [4]. These investigators were able to estimate the rate of hydrolysis of the ester in several cell types after extraction with organic solvents. The authors noted that extraction of cells with methanol resulted in significant breakdown of Fura-2/AM and produced numerous peaks with fluorescent properties. No changes in spectral intensities were observed when Fura-2/AM was extracted from cells with acetonitrile.

In preparation for further studies to estimate the intracellular concentrations of Fura-2/AM and Fura-2 acid, we have investigated the stability of Fura-2 in selected organic and inorganic solvents. In the present studies, we have used HPLC coupled to both fluorescence and ultraviolet detection to compare the effects of methanol and acetonitrile on changes in the spectral intensities of Fura-2/AM and a similar ion indicator Mag-Fura AM which is used to estimate intracellular concentrations of free magnesium ions. We have also compared the rates of change of spectral intensities of these ion indicators in glass containers with plastic containers.

2. Experimental

Fura-2/AM, Fura-2 acid and Mag-fura AM were obtained from Molecular Probes (Eugene, OR, USA). Stock solutions of each were prepared in dimethyl sulfoxide and stored in plastic vials at −10°C. Glass vials were 4-ml Wheaton (Millville, NJ, USA) borosilicate screw-capped sample vials (No. 224882). Plastic vials were 2-ml Sarstedt (Newton, NC, USA) screw-capped polypropylene micro centrifuge tubes. Methanol and acetonitrile were Burdick and Jackson (Muskegon, MI, USA) high-purity solvents.

Reactions were initiated by adding 20 μl of the stock solution of the ester (either Fura-2/AM or Mag-Fura AM) to 180 μl of solvent (methanol, acetonitrile, absolute ethanol, dimethyl sulfoxide or distilled water). The vials were capped and allowed to sit at room temperature. At the designated time period, an aliquot (either 5 μl or 10 μl) was drawn directly into a syringe for injection onto the HPLC column.

The HPLC system consisted of a EM Science-Hitachi LiChroGraph Model L-6200 gradient pump, a Varian Model 2050 variable-wavelength ultraviolet spectrometer and a Varian Model 2070 spectrofluorometer. The UV and fluorometric detectors were connected in tandem so that the eluent from the column passed through the UV detector and then immediately through the fluorometer. Chromatographic data, collected on a customized computer data acquisition system, were analyzed by computing both the peak height and the area under the curve for each peak.

A randomized complete block analysis of variance was used to identify difference among groups and a Tukey-Kramer [5] multiple comparison test was performed on all possible combinations to determine significant differences ($p < 0.05$).

3. Results and discussion

Previous studies have shown that Fura-2/AM is unstable in methanol but is very stable in acetonitrile [4]. We undertook studies to further characterize these changes which occur with methanol, especially with regard to the rate of decomposition and the breakdown products formed. Based upon previous studies [4,6], we had expected to observe a decline in the fluorescent properties of the esters as they underwent decomposition when exposed to methanol. Instead, we noted a two fold increase in fluorescence within 1 to 2 h of mixing the esters with

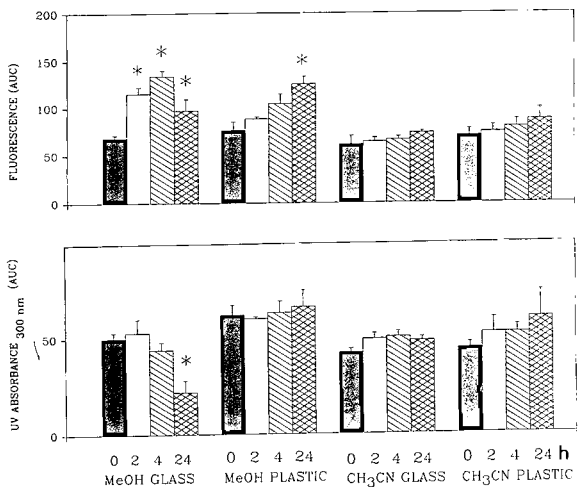

Fig. 1. Changes in spectral intensities of Fura-2/AM in different solvents and different containers. The eluate from the HPLC was monitored by fluorescence detection with excitation at 340 nm and emission at 500 nm and by UV detection at 300 nm. The data represent the mean ± S.D. ($n = 6$–10). The asterisk indicates significant differences ($p < 0.05$) from time zero. AUC = area under the curve.

methanol (Fig. 1). Acetonitrile did not change the fluorescence properties of the ester, even after 24 h of contact. This increased fluorescence with methanol was not accompanied by a change in retention time or in the shape of the ester peak. Although it is unlikely, it is possible that the presence of methanol changes the structure of the compound without altering the retention time. Thus, these changes in fluorescence which occur with methanol appear to represent a change in the fluorescent properties of Fura-2/AM rather than decomposition.

The enhanced fluorescence observed with Fura-2/AM in the presence of methanol is more pronounced when the Fura-2/AM is in contact with glass compared to plastic. The chromatograms illustrated in Fig. 2 indicate that the enhanced fluorescence was not accompanied by a change in retention time or in the shape of the Fura-2/AM peak. An indicated above, these changes in fluorescence were not accompanied by changes in UV absorbency. Acetonitrile had no effect on either the fluorescence or the ultraviolet absorbency of Fura-2/AM, even after 24 h in contact with glass (Fig. 1). As indicated in Fig. 3, the height and shape of the peak remained consistent over 24 h for both fluorescence and ultraviolet absorbency when Fura-2/AM was dissolved in acetonitrile.

A number of studies were performed in an attempt to further characterize the changes caused by methanol and by glass. One possible cause of the increased fluorescence which we considered was initial binding of the ester to glass with subsequent release over a period of time. Our results suggest that this was not the case. Methanol (without Fura-2/AM), when added to glass vials for 10 min and then transferred to a plastic vial containing Fura-2/AM produced a pattern of changes in spectral intensities similar to that observed when Fura-2/AM was added directly to glass (Fig. 4). Fluorescence increased more than two fold by 2 h while no changes were observed in ultraviolet absorbency, even after 24 h. Similar changes were observed when Fura-2/AM was added to a glass vial and immediately transferred to another glass vial (Fig. 4). When glass vials were prewashed with methanol prior to the addition of Fura-2/AM, there were no changes observed in either the fluorescence or the ultraviolet properties of the fluorescent dye. To further prove that adsorption was not occurring, we connected an ultraviolet detector immediately before or immediately after the fluorescence detector. Ultraviolet absorbency did not change in the ester peak during the first 4 h despite a two fold increase in fluorescence. Finally, we were able to demonstrate similar changes in fluorescence occur when a wavelength of excitation of 360 nm was used rather than 340 nm (data not shown).

Fura-2 acid appears to be more stable in methanol than is the ester and is unaffected by glass (Fig. 5). However, there were changes in fluorescence when methanol was transferred from glass to plastic and in ultraviolet absorption when Fura-2 was dissolved in water in a glass container.

Mag-fura exhibited a much different pattern of changes. When Mag-fura was dissolved in methanol in glass vials, rather than an increase in fluorescence as seen with Fura-2/AM, there was a rapid decline with more than 90% of the

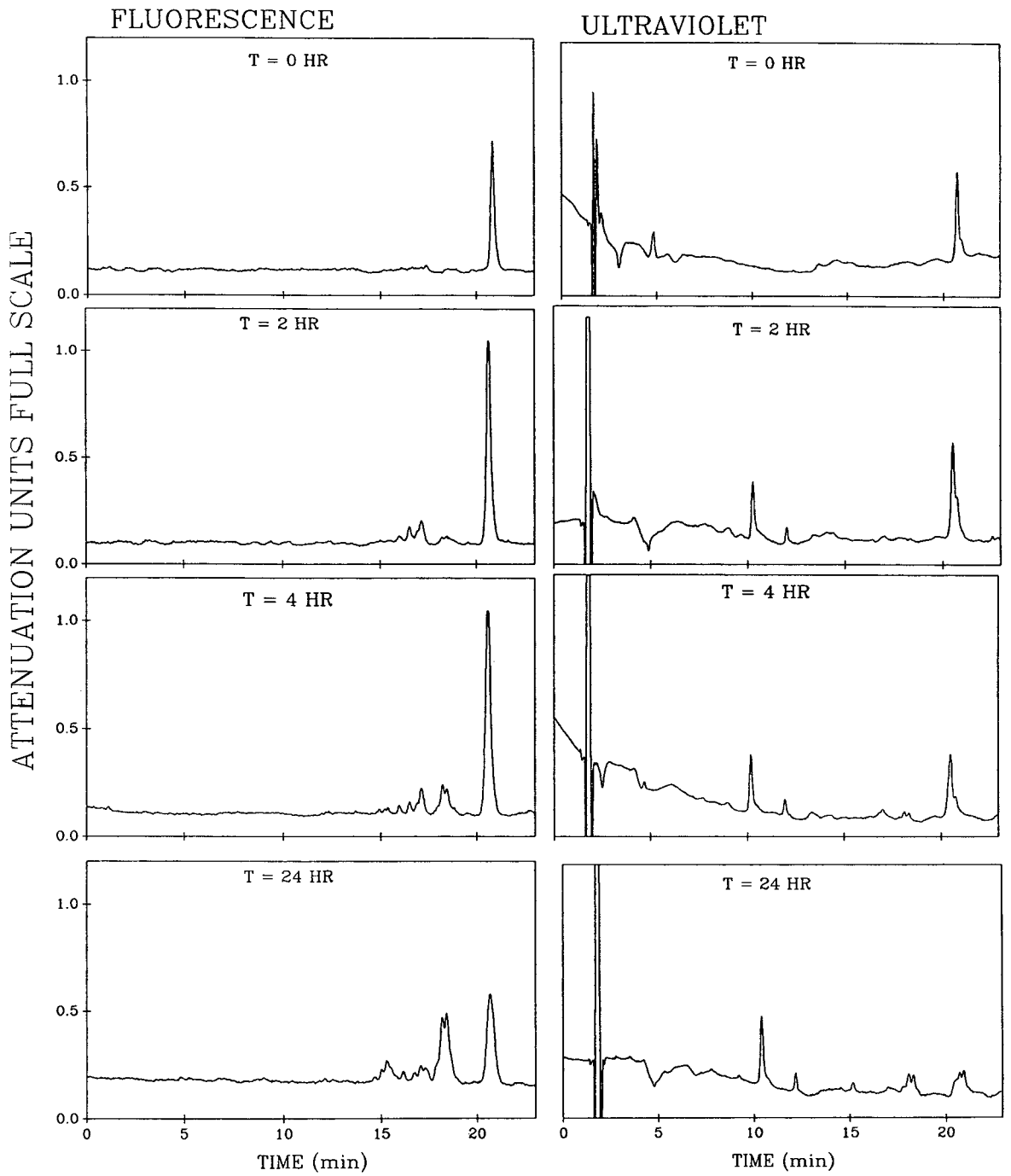

Fig. 2. HPLC of Fura-2/AM at various times after dissolving in methanol in glass vials. The column was a Phenomenex (Torrance, CA, USA) Ultramex C_{18}, 250 × 4.6 mm, containing 5 μM packing material. The mobile phase (1.5 ml/min) consisted of a linear gradient (3.33% per min) from 20 to 70% acetonitrile in buffer (10 mM NaH_2PO_4, 5 mM tetrabutylammonium hydroxide and 0.1 mM $CaCl_2$, pH 5.3). The eluate from the HPLC was monitored by fluorescence detection with excitation at 340 nm and emission at 500 nm and by ultraviolet detection at 300 nm.

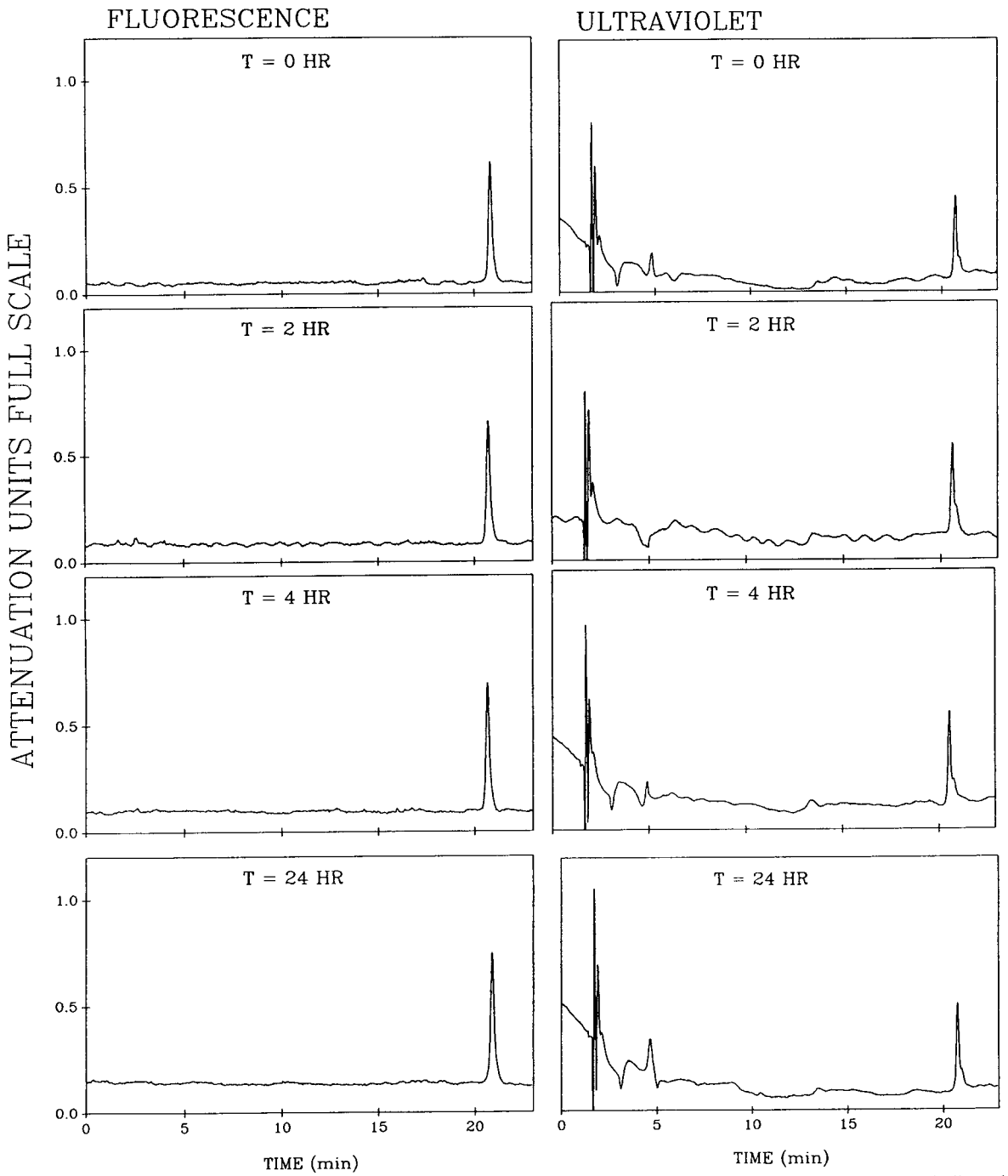

Fig. 3. HPLC of Fura-2/AM at various times after dissolving in acetonitrile in glass vials. Conditions were the same as indicated in Fig. 2. The eluate from the HPLC was monitored by fluorescence detection with excitation at 340 nm and emission at 500 nm and by ultraviolet detection at 300 nm.

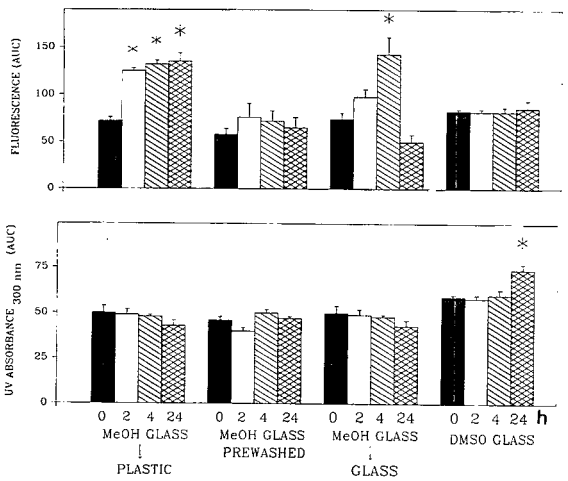

Fig. 4. Changes in spectral intensities of Fura-2/AM in different solvents and different containers. The eluate from the HPLC was monitored by fluorescence detection with excitation at 340 nm and emission at 500 nm and by ultraviolet detection at 300 nm. The data represent the mean ± S.D. ($n = 6$–10). The asterisk indicates significant differences ($p < 0.05$) from time zero. DMSO = dimethylsulfoxide.

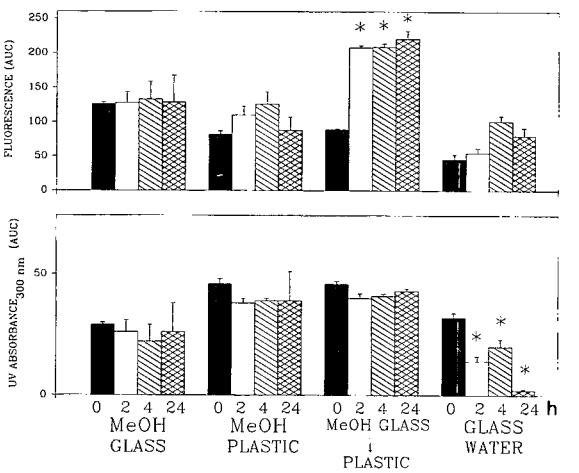

Fig. 5. Changes in spectral intensities of Fura-2 acid in different solvents and different containers. The eluate from the HPLC was monitored by fluorescence detection with excitation at 340 nm and emission at 500 nm and by ultraviolet detection at 300 nm. The data represent the mean ± S.D. ($n = 6$–10). The asterisk indicates significant differences ($p < 0.05$) from time zero.

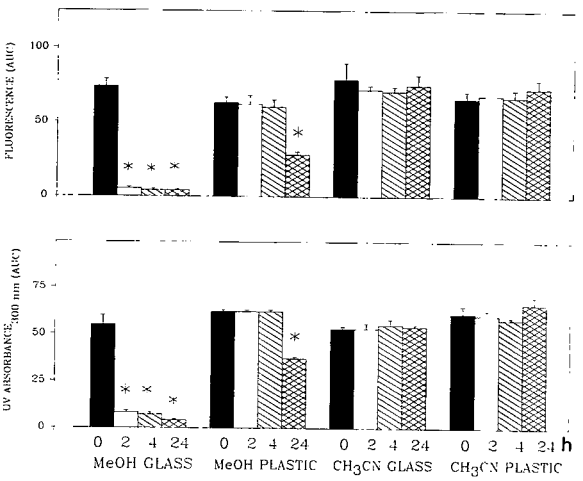

Fig. 6. Decomposition of Mag-Fura in different solvents and different containers. The eluate from the HPLC was monitored by fluorescence detection with excitation at 340 nm and emission at 500 nm and by ultraviolet detection at 300 nm. The data represent the mean ± S.D. ($n = 6$–10). The asterisk indicates significant differences ($p < 0.05$) from time zero.

fluorescence lost within 2 h (Fig. 6). Ultraviolet absorbency followed a similar pattern (Fig. 6). Most of the decomposition which occurred when

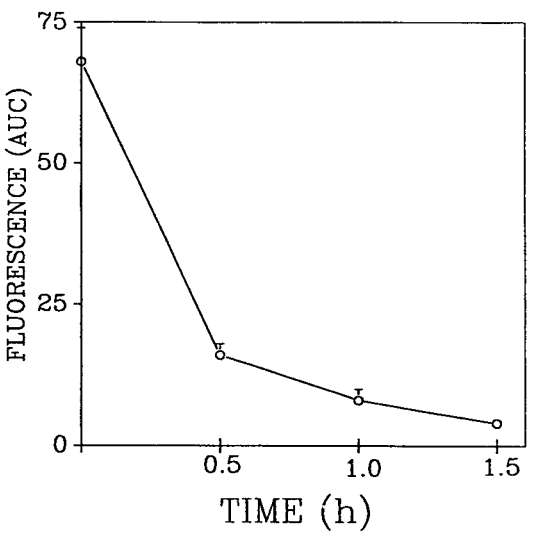

Fig. 7. Decomposition of Mag-Fura dissolved in methanol in glass vials. The eluate from the HPLC was monitored by fluorescence detection with excitation at 340 nm and emission at 500 nm and by ultraviolet detection at 300 nm. The data represent the mean ± S.D. ($n = 6$–10).

Mag-Fura was dissolved in methanol in glass vials occurred within the first 30 min after mixing (Fig. 7). When Mag-fura was dissolved in methanol in a plastic vial no changes were observed over the first 4 h and approximately 50% of the initial fluorescence and ultraviolet absorption remained after 24 h (Fig. 6). Mag-fura was more stable in acetonitrile with no evidence of decomposition during the first 4 h in either glass or plastic containers.

These results confirm previous studies which suggest that acetonitrile is preferable to methanol for sample preparation and chromatographic analysis of Fura-2 and Mag-Fura. Our data also indicate that glass vials contain an extractable substance which markedly enhances the spectral intensities of Fura-2/AM.

References

[1] M.W. Roe, J.J. Lemasters and B. Herman, *Cell Calcium*, 11 (1990) 63.
[2] R.Y. Tsien, *Ann. Rev. Neuro.*, 12 (1989) 227.
[3] G. Grynkiewicz, M. Poenie and R.Y. Tsien, *J. Biol. Chem.*, 260 (1985) 3440.
[4] S.G. Oakes, W.J. Martin II, C.A. Lisek and G. Powis, *Anal. Biochem.*, 169 (1988) 159.
[5] R.E. Kirk, *Experimental Design*, Wadsworth, Belmont, CA, 1982, p. 119.
[6] F. Lattanzio, S.G. Oakes and M.C. Castle, *FASEB J.*, 4 (1990) A1208.

ELSEVIER

Journal of Chromatography A, 696 (1995) 101–112

JOURNAL OF CHROMATOGRAPHY A

Gas chromatographic study of the inclusion properties of calixarenes
I. *p-tert.*-Butylcalix[4]arene in a micropacked column

Petr Mňuk, Ladislav Feltl*

Department of Analytical Chemistry, Charles University, Albertov 2030, 128 40 Prague 2, Czech Republic

First received 1 March 1994; revised manuscript received 2 December 1994; accepted 7 December 1994

Abstract

Quantitative structure–retention relationships (QSRR) in gas–solid chromatography (GSC) were employed as an auxiliary method to study the inclusion properties of *p-tert.*-butylcalix[4]arene. Selected experimental retention data were studied thermodynamically. The sorbates involved homologous series of aliphatic and alicyclic alkanes and alkenes, aromatics, halo derivatives, alcohols and ethers. It is presumed that *p-tert.*-butylcalix[4]arene forms inclusion complexes with benzene, its lower *n*-alkyl derivatives (toluene to *n*-butylbenzene), *p*-dialkylbenzenes (*p*-xylene, *p*-ethyltoluene), *m*-xylene, di- and trichloromethane, methanol and ethanol under GSC conditions.

1. Introduction

Calixarenes, i.e., cyclic phenol–formaldehyde polycondensates (Fig. 1), are capable of selective interactions with many metal ions and organic molecules. X-ray structural analysis and ^{1}H NMR spectroscopy have demonstrated that *p-tert.*-butylcalix[4]arene forms inclusion complexes with benzene [1], toluene [2], *p*-xylene [1], phenol [3], anisole [1,4] and chloroform [5]. There also exist complexes of *p-tert.*-butylcalix[4]arene derivatives with acetonitrile [6], pyridine [7] and ethanol [8], complexes of *p*-isopropyldihomooxacalix[4]arene with *o*-xylene [9], *p-tert.*-butyldihomooxacalix[4]arene with 1,3,5-trimethylbenzene [10] and a complex of a bis-*p-tert.*-butylcalix[4]arene derivative with dichloromethane [11].

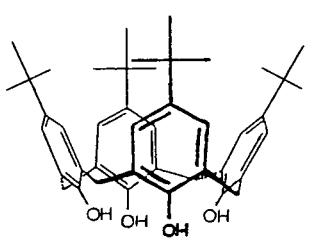

Fig. 1. The most stable conformation (cone) of *p-tert.*-butylcalix[4]arene (schematic).

Preparation of crystals suitable for X-ray structural analysis from a convenient solvent and ^{1}H NMR studies of calixarene complexes in solution bring about certain problems. Unsubstituted calixarenes are very poorly soluble in most organic solvents. The weak intermolecular interactions predominating in molecular complexes of calixarenes with neutral organic molecules are often insufficient for competitive displacement of

* Corresponding author.

0021-9673/95/$09.50
SSDI 0021-9673(94)01218-0

solvent molecules from the calixarene cavity. The cavities in solvated calixarenes are not rigid and are subject to rapid processes leading to a conformational inversion of the molecule. In a mass spectrometric study of the formation of inclusion complexes in the gaseous phase, only a complex of *p-tert.*-butylcalix[4]arene with benzene was demonstrated [12].

In this study we applied a non-traditional approach to study the inclusion properties of calixarenes, which is based on the low-temperature deposition of calixarenes on the surface of a suitable support. The structure of calixarene molecules is thus conformationally stabilized and is exposed to a stream of an inert carrier gas containing active low-molecular-mass components. The first experiments of this type were carried out in 1982 at Charles University in Prague [13] and at Parma University, Italy [14]. This relatively well defined system was used for the specification of group of substances that selectively interact with *p-tert.*-butylcalix[4]arene under gas chromatographic conditions. On the basis of the retention behaviour of selected homologous series, we tried to characterize the kind of intermolecular interactions taking part in the gas chromatographic separation process. This is the first effort concerning the systematic investigation of the selectivity of calixarenes in gas chromatography.

2. Theoretical

The following non-specific interactions, described by their potential energies E, can be expected to occur in molecular complexes of the calixarene–electroneutral organic molecule type under gas–solid chromatographic (GSC) conditions:

Dispersion interactions:

$$E_{\mathrm{d}} = -\left(\frac{1}{4\pi\epsilon_0}\right)^2 \cdot \frac{3}{2} \cdot \frac{I_1 I_2}{I_1 + I_2} \cdot \frac{\alpha_1 \alpha_2}{\epsilon r^6} \tag{1}$$

Dipole–dipole interactions:

$$E_{\mathrm{d-d}} = -\left(\frac{1}{4\pi\epsilon_0}\right)^2 \cdot \frac{2}{3kT} \cdot \frac{\mu_1^2 \mu_2^2}{\epsilon r^6} \tag{2}$$

Dipole–induced dipole interactions:

$$E_{\mathrm{d-id}} = -\left(\frac{1}{4\pi\epsilon_0}\right)^2 \cdot \frac{\alpha_1 \mu_2^2 + \alpha_2 \mu_1^2}{\epsilon r^6} \tag{3}$$

where I denotes the ionization energies of the interacting molecules, α their polarizabilities, ϵ the relative permittivity of the surroundings, r the distance between the interacting molecules, k the Boltzmann constant, T the absolute temperature and μ the dipole moments of the interacting molecules.

Among specific interactions, inclusion, induced fit, hydrogen bonding, electron pair donor–acceptor, electron pair repulsive interactions and entropic effects can be assumed. The terms T (constant column temperature) and $I_1 I_2 / (I_1 + I_2)$ in general, and the terms α and μ^2 for calixarene, in Eqs. 1–3 can be considered to be constant. The gas chromatographic retention data ($\log k$, $\log V_g$) can be considered to be directly proportional to the interaction energy between the sorbates and the stationary phase. Using the method of quantitative structure–retention relationship (QSRR [15]) it is thus possible to study, in congeneric series, the course of the sorbate–stationary phase dispersion interactions on the basis of retention data dependences on the analyte polarizabilities (α) and molar volumes (MV), and the course of electrostatic interactions from retention data dependences on the analyte dipole moments (μ) or the $\alpha + \mu^2$ values, provided that the required data are available. The effect of the sum of Van der Waals interactions can then be found from retention data dependences on the analyte boiling points (b.p.) or enthalpies of vaporization. The deviations from these standard dependences refer to the presence of certain specific interactions. For quantitative evaluation of these deviations in a congeneric series of sorbates, the quantity IRT_s^D has been defined by the equation

$$IRT_s^D = \frac{t'_{\mathrm{r,X}} - t'_{\mathrm{r,H}}}{t'_{\mathrm{r,H}}} \cdot 100 \tag{4}$$

where D is a defined molecular descriptor and S a reference homologous series, $t'_{\mathrm{r,X}}$ is the experimental adjusted retention time for sorbate X

and $t'_{r,H}$ is a calculated adjusted retention time obtained by regression analysis for a hypothetical sorbate that elutes in agreement with the given homologous series and whose physico-chemical data are identical with those of sorbate X. The quantity IRT_s^D can be handled in the same way as retention data.

Thermodynamic data are calculated using the equations

$$\Delta G^0 = -RT \ln K \quad (5)$$

$$K = V_g \cdot \frac{M}{T_0 R} \quad (6)$$

$$\Delta G^0 = \Delta H^0 - T\,\Delta S^0 \quad (7)$$

where K is the distribution coefficient, V_g the specific retention volume, M the molar mass of the stationary phase (calixarene) and T the column absolute temperature. It follows from Eqs. 5–7 that

$$\log V_g = -\frac{\Delta H^0}{2.3R} \cdot \frac{1}{T_c} + \frac{\Delta S^0}{2.3R} - \log\left(\frac{M}{T_0 R}\right) \quad (8)$$

The log V_g vs. $1/T_c$ dependence permits the determination of the mean differential molar enthalpy for the sorbate–stationary phase interaction, ΔH^0, and an estimation of the mean differential molar entropy, ΔS^0, of the process. The mean differential Gibbs energy, ΔG^0, can be found from Eqs. 5 and 6 for a given column temperature. Using the relationships valid between the activity coefficients and the ΔH^0 and ΔS^0 values under certain conditions [16], the above interactions can also be evaluated from so-called compensation graphs of enthalpy and entropy [17].

3. Experimental

The stationary phase was prepared by dissolving *p-tert.*-butylcalix[4]arene (Shinkai Chemirecognics Project, Japan) in dichloromethane (the solubility is 130 mg per 100 ml at 20°C), mixing the solution with silanized Chromosorb W (100–120 mesh) (Carlo Erba) and allowing the solvent to evaporate freely at atmospheric pressure; the temperature was maintained below 23°C during the whole procedure. The thermal stability of the prepared phase was assessed from thermogravimetric analysis and a limiting temperature of 280°C was obtained. The stationary phase, containing 3.2% (w/w) of *p-tert.*-butylcalix[4]arene, was transferred into a glass micropacked column (1.64 m × 1 mm I.D.). A reference column (1.65 m × 1 mm I.D.), containing pure silanized Chromosorb W (100–120 mesh) (Carlo Erba), was prepared analogously. A reference column (0.62 m × 1 mm I.D.) was packed with silanized Porapak P (Waters). The structure of the cross-linked divinylbenzene–styrene copolymer represents the dense network of the aromatic (π-electron-donor) centres.

The stationary phase containing *p-tert.*-butylcalix[4]arene was conditioned at temperatures from 70 to 280°C for 120 h; the progress of the conditioning procedure was checked on the basis of the retention behaviour of cyclohexane, benzene, toluene, xylenes, methanol, ethanol and *n*-propanol.

The measurements were carried out on a Chrom 61 gas chromatograph with a flame ionization detector (Laboratorní Přístroje, Prague, Czech Republic), maintaining the thermostat temperature within ±0.1°C and the carrier gas flow-rate within ±0.02 ml min^{-1}. The column temperature was varied from 50 to 130°C and the carrier gas (nitrogen) flow-rate from 7.5 to 20.0 ml min^{-1}. The retention times were measured with a Casio digital stop-watch with a precision of 0.01 s. The analytes were injected using the headspace method with Hamilton microsyringes; the vapour volume varied from 10 to 100 μl at 25°C.

4. Results and discussion

The formation of inclusion compounds of *p-tert.*-butylcalix[4]arene was studied with homologous series of aliphatic and alicyclic alkanes and alkenes, aromatics, alcohols, ethers and halogenated hydrocarbons. The retention behaviour of the homologous series on the reference Porapak P column indicates that dispersion inter-

actions predominate (even with alcohols, ethers and halo derivatives); specific $\pi-\pi$ interactions complement dispersion interactions for aromatics. The homologous series are eluted within a relatively narrow time interval in the order alcohols < ethers < alkanes/alkenes < halo derivatives < aromatics. The retention behaviour on silanized Chromosorb W is affected by the residual OH active sites remaining after silanization. Hydrogen bonding predominates for alcohols, ethers and halo derivatives, whereas orientation dipole–dipole interactions are dominant for aromatics and alkenes. The microporous structure of the pure support probably also plays a role. The homologous series are eluted over a wide time interval, in the order alkanes < alkenes < aromatics, halo derivatives < ethers < alcohols. The retention behaviour of the homologous series on *p-tert.*-butylcalix[4]arene indicates a strong influence of the phenolic hydroxyls in calixarene on the overall interaction mechanism for the sorbates. The homologous series are eluted over a wide time interval, the order being alkanes < alkenes < halo derivatives < aromatics < ethers < alcohols.

4.1. Retention behaviour of saturated and unsaturated aliphatic and alicyclic hydrocarbons

The retention data for lower (up to C_8) and higher (C_9–C_{13}) *n*-alkanes and *n*-alkenes on the *p-tert.*-butylcalix[4]arene column exhibit linear dependences on selected molecular descriptors, namely the boiling point (b.p.), molar volume (*MV*), polarizability (α) and enthalpy of vaporization. Electrokinetic dispersion interactions predominate. *p-tert.*-Butylcalix[4]arene behaves selectively toward the π-electron systems in alkenes and cycloalkenes, depending on the position and number of double bonds in the sorbate hydrocarbon skeleton. Similarly to the reference stationary phases (Chromosorb W, Porapak P), electrostatic orientation interactions are also important in this case. In contrast to the reference phases, cyclic hydrocarbons are retarded substantially less than the corresponding linear homologues on *p-tert.*-butylcalix[4]arene phase ($IRT^{\text{b.p.}}_{n\text{-alkanes}} = -10$ to -26.2) owing to a certain specific non-dispersion interaction. In agreement with the reference phases, branched alkanes are retarded less than the linear isomers.

4.2. Retention behaviour of aromatic hydrocarbons

The measurements yielded linear dependences of the retention data on selected molecular descriptors for toluene, ethylbenzene, *n*-propylbenzene and *n*-butylbenzene on the *p-tert.*-butylcalix[4]arene stationary phase (Table 1). A similar behaviour is also exhibited by *m*-xylene and *p*-ethyltoluene. On the basis of these results, stereochemical calculations and published work [1,2], a reference homologous series (RHS) was formulated including lower *n*-alkylbenzenes (toluene, ethylbenzene, *n*-propylbenzene and *n*-butylbenzene). This series meets the condition of a defined sorbate–stationary phase interaction mechanism that is the same in character for all the members of the series [the correlation coefficient is 0.999998 for the $-\Delta H = f(-\Delta S)$ dependence]. It can be assumed that the predominating interaction for RHS is guest inclusion into the *p-tert.*-butylcalix[4]arene cavity, involving CH_3(host)–π(guest) interactions and possibly also CH_3(guest)–π(host) interactions. The increased retardation of benzene ($IRT^{\text{b.p.}}_{\text{RHS}} = +29.4$), as the "zero" RHS member, is probably also caused by a high probability of a suitable

Table 1
Linear dependences of the retention data obtained on *p-tert.*-butylcalix[4]arene on selected molecular descriptors for toluene, ethylbenzene, *n*-propylbenzene and *n*-butylbenzene

Functional dependence	$y = A + Bx$		
	A	*B*	*r*
Log *k* = f (b.p.)	−2.5055	0.0151	0.9999
Log *k* = f (*MV*)	−3.1890	0.0223	0.9994
Log *k* = f (α)	−3.2715	0.0016	0.9999
ΔH = f (b.p.)	−1.7355	0.2756	0.9993
ΔS = f (b.p.)	9.1010	0.2428	0.9993
$\Delta G_{60.0°C}$ = f (b.p.)	−4.7675	0.1947	0.9993

Column temperature, 60.0°C; nitrogen flow-rate, 7.5 ml min^{-1}; volume of sample, 70 μl (vapour).

steric arrangement of the benzene molecule during its entry into the calixarene cavity. This specific interaction mechanism for benzene on a phase containing *p-tert.*-butylcalix[4]arene permits complete separation of benzene (b.p. = 80.1°C) from aliphatic and alicyclic hydrocarbons (hexane and cyclohexane, b.p. = 69–81°C) (Fig. 2).

Linear dependences of the retention data for RHS and xylenes on Chromosorb W and Porapak P (Fig. 3) on selected molecular descriptors and their comparison with the retention behaviour on *p-tert.*-butylcalix[4]arene demonstrate that *o*-xylene is retarded significantly less than RHS ($IRT^{b.p.}_{RHS} = -12.5$) and that *m*-xylene elutes in agreement with RHS ($IRT^{b.p.}_{RHS} = -3.9$), as can be seen in Fig. 4. *p*-Xylene is retarded significantly more strongly than the other isomers (Table 2).

The retention of ethyltoluenes was primarily evaluated with respect to the Porapak P reference phase. Whereas *p*-ethyltoluene is eluted in agreement with RHS on the *p-tert.*-butylcalix-[4]arene phase ($IRT^{b.p.}_{RHS} = -1.6$), *m*- and *o*-ethyltoluene are retarded significantly less (the respective $IRT^{b.p.}_{RHS}$ values are −11.5 and −23.3; see Fig. 4).

A decreased retardation was found for isopropylbenzene ($IRT^{b.p.}_{RHS} = -12.9$), 1,3,5- and 1,2,4-trimethylbenzenes ($IRT^{b.p.}_{RHS} = -18.7$ and −22.2, respectively), *tert.*-butylbenzene ($IRT^{b.p.}_{RHS} = -35.6$), *sec.*-butylbenzene ($IRT^{b.p.}_{RHS} = -25.7$) and *p*-cymene ($IRT^{b.p.}_{RHS} = -15.1$).

The experimental thermodynamic data relating to the sorbate–stationary phase interaction are given in Table 3. The magnitude of the enthalpy ΔH (the mean differential molar enthalpy) corresponds to weak bonding interactions. The relatively high magnitude of entropy ΔS (the mean differential molar entropy) suggests a significant contribution of the degree of ordering in the system to the overall interaction mechanism. A comparison of the thermodynamic data for cyclohexane and benzene (or RHS) demonstrates that the presence of an aromatic system in the guest causes an increase in ΔH of ca. 3.5 kJ mol^{-1} and in ΔS of 3.0 J mol^{-1} K^{-1}.

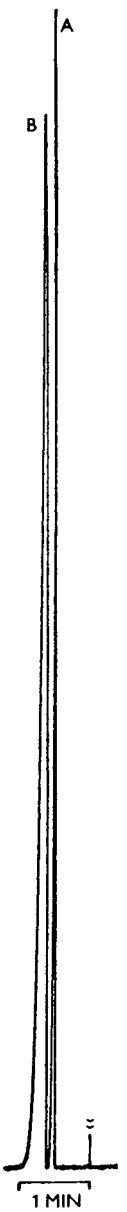

Fig. 2. Chromatogram of separation of benzene from hexane and cyclohexane. Micropacked column (1.64 m × 1 mm I.D.) containing *p-tert.*-butylcalix[4]arene, $T_c = 31.0$°C. Peaks: A = hexane (b.p. = 69.0°C) and cyclohexane (b.p. = 80.7°C); B = benzene (b.p. = 80.1°C).

The reference homologous series for the thermodynamic measurements consisted of toluene, ethylbenzene and *p*-ethyltoluene [for

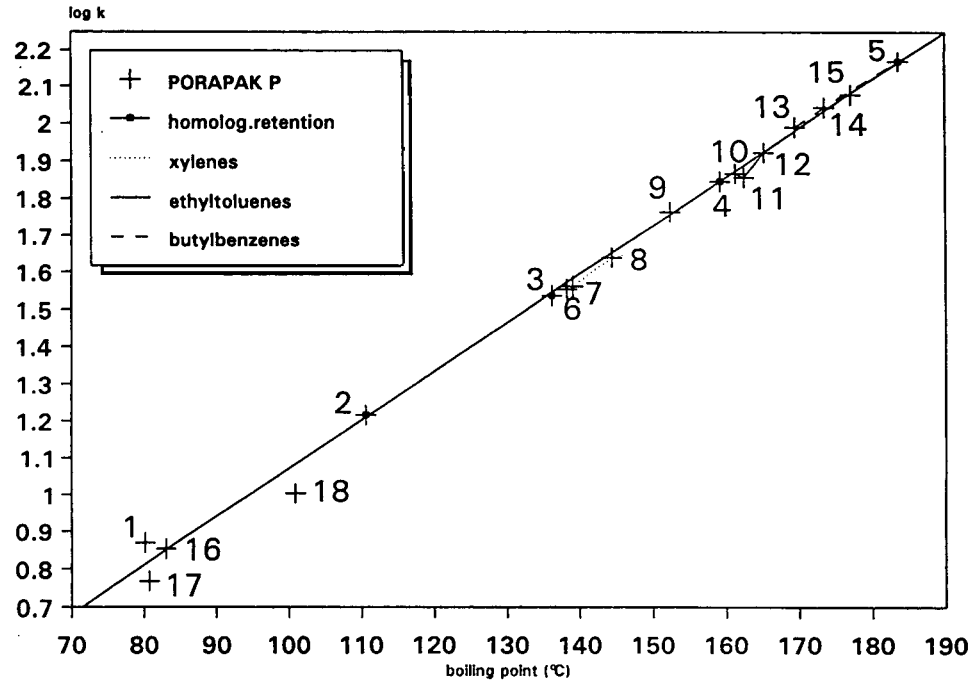

Fig. 3. Retention behaviour of aromatics on the Porapak P stationary phase: log (capacity factor) dependence on boiling point. Column temperature, 130.0°C; nitrogen flow-rate, 20.0 ml min^{-1}; volume of sample, 50 μl (vapour). 1 = Benzene; 2 = toluene; 3 = ethylbenzene; 4 = *n*-propylbenzene; 5 = *n*-butylbenzene; 6 = *p*-xylene; 7 = *m*-xylene; 8 = *o*-xylene; 9 = isopropylbenzene; 10 = *m*-ethyltoluene; 11 = *p*-ethyltoluene; 12 = *o*-ethyltoluene; 13 = *tert.*-butylbenzene; 14 = *sec.*-butylbenzene; 15 = *p*-cymene; 16 = cyclohexene; 17 = cyclohexane; 18 = methylcyclohexane.

the dependence $\Delta H = A + B$ (b.p.) it was calculated that $A = -1.7355$, $B = 0.2756$, $r = 0.9993$]. It can be seen from Fig. 5 that there is a significant increase in ΔH (in comparison with RHS) for *p*-xylene [$\Delta(\Delta H) = +1.4$ kJ mol^{-1}], which corresponds to an increased entropy [$\Delta(\Delta S) = +1.8$ J mol^{-1} K^{-1}] and retardation in the column ($IRT^{b.p.}_{RHS} = +5.6$). This is probably caused by an increased probability of a suitable spatial orientation of the molecule during interaction with the *p-tert.*-butylcalix[4]arene cavity compared with, e.g., toluene. The significant enthalpy decreases for *o*-xylene [$\Delta(\Delta H) = -2.2$ kJ mol^{-1}], *m*-ethyltoluene [$\Delta(\Delta H) = -2.4$ kJ mol^{-1}] and *o*-ethyltoluene [$\Delta(\Delta H) = -4.8$ kJ mol^{-1}] correspond to the retention behaviour of these compounds, as discussed above. Differences have been found between the experimental thermodynamic data and the retention behaviour for benzene and isopropylbenzene. The same holds for the entropy changes.

Whereas the thermodynamic data for ethyltoluene isomers are in agreement with their elution order, there is disagreement for xylene isomers.

It follows from the above findings that benzene, lower *n*-alkyl derivatives (toluene to *n*-butylbenzene), *p*-dialkylbenzenes (*p*-xylene, *p*-ethyltoluene) and *m*-xylene are probably included in the *p-tert.*-butylcalix[4]arene cavity. Steric hindrances to inclusion probably appear for *o*-dialkylbenzenes (*o*-xylene, *o*-ethyltoluene), *m*-ethyltoluene in the presence of at least one isopropyl or a more voluminous substituent on the benzene ring and for trisubstituted benzenes.

It should be pointed out that the selectivity of

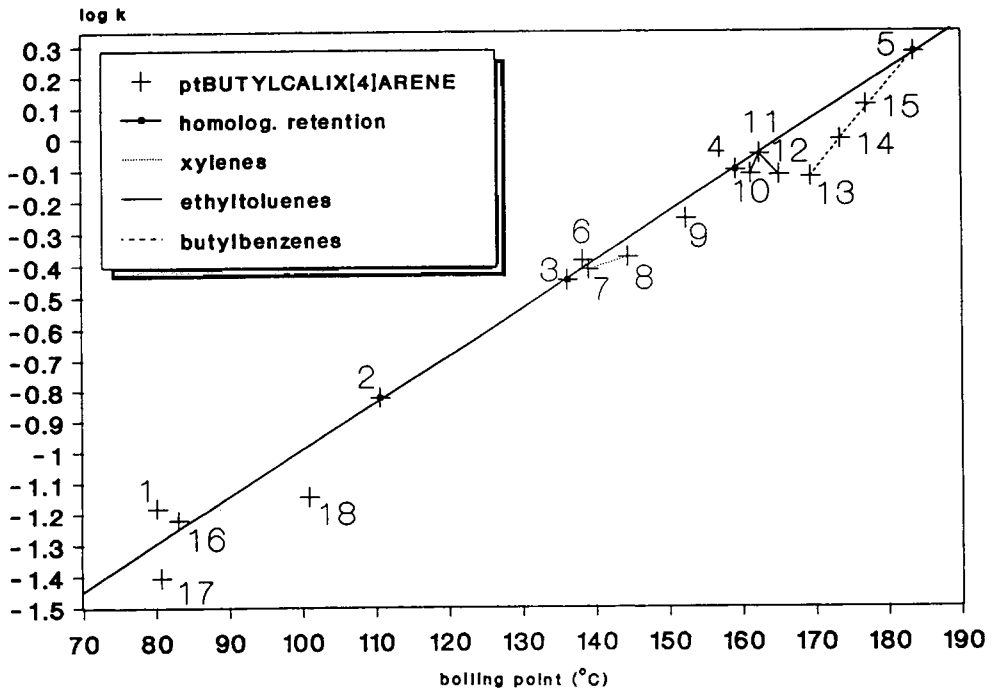

Fig. 4. Retention behaviour of aromatics: log (capacity factor) dependence on boiling point. Column temperature, 60.0°C; nitrogen flow-rate, 7.5 ml min^{-1}; volume of sample, 70 μl (vapour). 1 = Benzene; 2 = toluene; 3 = ethylbenzene; 4 = *n*-propylbenzene; 5 = *n*-butylbenzene; 6 = *p*-xylene; 7 = *m*-xylene; 8 = *o*-xylene; 9 = isopropylbenzene; 10 = *m*-ethyltoluene; 11 = *p*-ethyltoluene; 12 = *o*-ethyltoluene; 13 = *tert.*-butylbenzene; 14 = *sec.*-butylbenzene; 15 = *p*-cymene; 16 = cyclohexene; 17 = cyclohexane; 18 = methylcyclohexane.

Table 2
Linear dependences of the retention data for xylenes on some molecular descriptors

Column	Functional dependence	$y = A + Bx$			$IRT_{xylenes}$ value for *p*-xylene
		A	*B*	*r*	
Chromosorb W	Log *k* = f (b.p.)	−1.7703	0.0084	0.9991	−1.0
	Log *k* = f (*MV*)	1.7763	−0.0194	1.0000	+0.6
	Log *k* = f (α)	8.9566	−0.6705	0.9989	−0.4
Porapak P	Log *k* = f (b.p.)	−0.4182	0.0142	0.9990	+2.0
	Log *k* = f (*MV*)	5.6015	−0.0329	0.9970	+2.2
	Log *k* = f (α)	17.7024	−1.1318	0.9914	+0.6
p-tert.-Butylcalix[4]arene	Log *k* = f (b.p.)	−1.4658	0.0075	–	+8.5
	Log *k* = f (*MV*)	1.7845	−0.0179	–	+8.9
	Log *k* = f (α)	1.8428	−0.6494	–	+9.2

On *p-tert.*-butylcalix[4]arene stationary phase, *IRT* value according to *m*-/*o*-xylene retention level. Column temperature, 60.0°C (Chromosorb W and *p-tert.*-butylcalix[4]arene) and 130°C (Porapak P); nitrogen flow-rate, 7.5 ml min^{-1}; volume of sample, 70 μl (vapour).

Table 3
Experimental values of the thermodynamic properties of some aromatics on the *p-tert.*-butylcalix[4]arene stationary phase

Sorbates	$-\Delta H \pm L_{1,2}$ (kJ mol^{-1})	$-\Delta S \pm L_{1,2}$ (J mol^{-1} K^{-1})	$-\Delta G \pm L_{1,2}$ (333.1 K) (kJ mol^{-1})
Cyclohexane	17.1 ± 0.3	25.2 ± 0.1	8.7 ± 0.4
Methylcyclohexane	22.9 ± 0.3	31.1 ± 0.3	12.5 ± 0.6
Cyclohexene	17.4 ± 0.3	24.8 ± 0.3	9.1 ± 0.6
Benzene	20.6 ± 0.2	28.2 ± 0.1	11.2 ± 0.3
Toluene	28.9 ± 0.2	36.1 ± 0.7	16.9 ± 0.9
Ethylbenzene	35.5 ± 0.2	41.9 ± 0.1	21.5 ± 0.3
p-Xylene	37.8 ± 0.3	44.5 ± 0.1	23.0 ± 0.4
m-Xylene	35.5 ± 0.2	41.8 ± 0.1	21.6 ± 0.3
o-Xylene	35.9 ± 0.2	41.8 ± 0.0	22.0 ± 0.2
Isopropylbenzene	39.6 ± 0.2	45.7 ± 0.1	24.4 ± 0.3
m-Ethyltoluene	40.3 ± 0.3	45.3 ± 0.1	25.2 ± 0.4
p-Ethyltoluene	43.2 ± 0.3	48.7 ± 0.1	27.0 ± 0.4
o-Ethyltoluene	39.0 ± 0.2	43.6 ± 0.1	24.5 ± 0.3

Column temperature range, 50.0–100.0°C; nitrogen flow-rate, 7.5 ml min^{-1}; volume of sample, 70 μl (vapour).

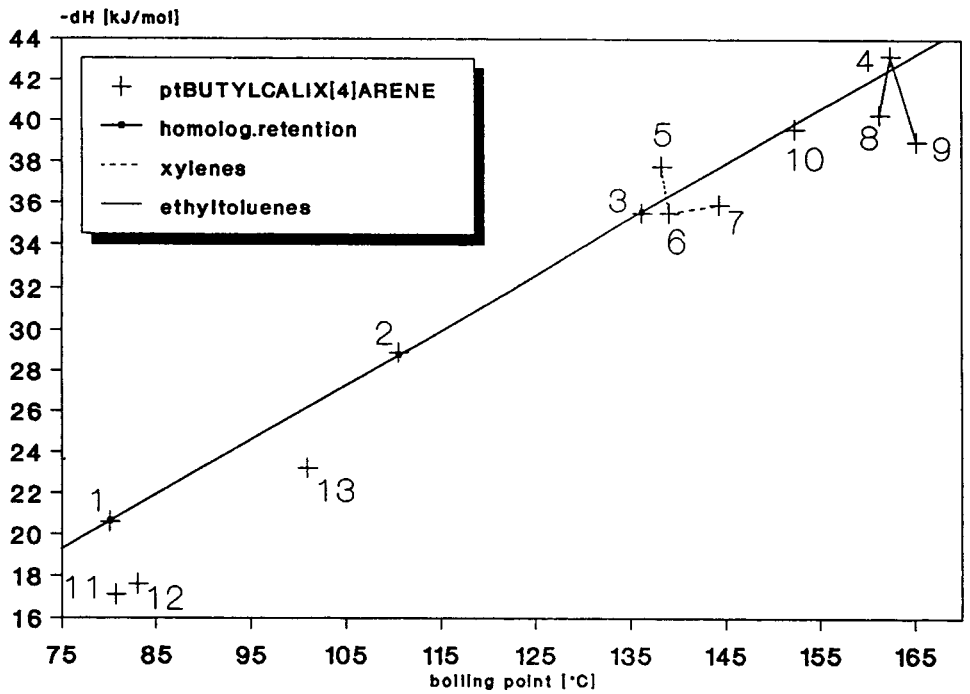

Fig. 5. Thermodynamic properties of aromatics: dependence of mean differential molar enthalpy (ΔH) on boiling point. Column temperature, 50.0–100.0°C; nitrogen flow-rate, 7.5 ml min^{-1}; volume of sample, 70 μl (vapour). 1 = Benzene; 2 = toluene; 3 = ethylbenzene; 4 = *p*-ethyltoluene; 5 = *p*-xylene; 6 = *m*-xylene; 7 = *o*-xylene; 8 = *m*-ethyltoluene; 9 = *o*-ethyltoluene; 10 = isopropylbenzene; 11 = cyclohexane; 12 = cyclohexene; 13 = methylcyclohexane.

p-tert.-butylcalix[4]arene towards *p*-xylene found here is in agreement with the published results for selective extraction [18].

4.3. Retention behaviour of halo derivatives

The dependences between the retention data and selected molecular descriptors for *n*-chloroalkanes (C_4–C_8) on both the Porapak P reference phase and the *p-tert.*-butylcalix[4]arene phase are linear (Table 4). The interaction mechanism involves dispersion and orientation dipole interactions.

The bromo, iodo and chloro derivatives elute together according to a single retention dependence on the Porapak P reference phase, but retardation increases in the order I < Br < Cl on the *p-tert.*-butylcalix[4]arene phase. Halocycloalkanes are retarded more than the linear isomers on Porapak P ($IRT^{b.p.}_{C_4-C_8Cl}$ = +6.5 to +10.7), but significantly less on *p-tert.*-butylcalix[4]arene ($IRT^{b.p.}_{C_4-C_8Cl}$ = −41.7 to −50.9). Dibromobutanes elute over a narrow time interval on Porapak P, in agreement with *n*-haloalkanes ($IRT^{b.p.}_{C_4-C_8Cl}$ = −0.4 to +7.2), whereas on *p-tert.*-butylcalix[4]arene they are retarded significantly less and over a wide time interval ($IRT^{b.p.}_{C_4-C_8Cl}$ = −51.0 to −5.7). The elution order is identical with the order of boiling points.

There exists a group of molecules, including iodomethane, diiodomethane, iodoethane and bromoethane, whose molar volumes do not exceed 95 cm^3 mol^{-1} and that are retarded, with respect to *n*-haloalkanes, significantly more on *p-tert.*-butylcalix[4]arene than on Porapak P. It is probable that inclusion of these molecules in the calixarene cavity contributes significantly to the overall interaction.

The experimental retention data for di-, tri- and tetrachloromethane on Chromosorb W exhibit roughly linear dependences of log k on selected molecular descriptors (b.p., MV, α, $1/\epsilon$, μ^2, $\alpha + \mu^2$). The retardation of tetrachloromethane on Porapak P is decreased, probably owing to a decrease in electrostatic interaction between the sorbate and the aromatic system of Porapak P. A further decrease in tetrachloromethane retention compared with di- and trichloromethane was observed on *p-tert.*-butylcalix[4]arene. In view of data published earlier [5,11], it is probable that the molecules of di- and trichloromethane are included in the *p-tert.*-butylcalix[4]arene cavity. The decrease in the tetrachlormethane retardation is apparently caused by non-existence of CH–π interactions between the tetrachloromethane molecule and the calixarene aromatic system, which seems to be an important factor for inclusion of this sorbate in the *p-tert.*-butylcalix[4]arene cavity.

Table 4
Linear dependences of the retention data on some molecular descriptors for *n*-haloalkanes (1-chlorobutane to 1-chlorooctane) on selected stationary phases

Column	Functional dependence	$y = A + Bx$		
		A	B	r
Porapak P	Log k = f (b.p.)	−0.3973	0.0136	1.000
	Log k = f (MV)	−1.6318	0.0220	0.9999
	Log k = f (α)	−1.3145	0.1968	0.9999
p-tert.-Butylcalix[4]arene	Log k = f (b.p.)	−2.6274	0.0161	0.9994
	Log k = f (MV)	−4.0711	0.0260	0.9996
	Log k = f (α)	−3.6972	0.2325	0.9996

Column temperature, 60.0°C (*p-tert.*-butylcalix[4]arene) and 130.0°C (Porapak P); nitrogen flow-rate, 7.5 ml min^{-1}; volume of sample, 70 μl (vapour).

4.4. Retention behaviour of alcohols

The dependences of the retention data on selected molecular descriptors for *n*-alkanols from methanol to *n*-octanol on the Porapak P reference phase are linear (Table 5) and dispersion interactions predominate. In contrast to Porapak P, where hydroxyl groups apparently do not participate in the interaction mechanism, on the *p-tert.*-butylcalix[4]arene phase strong interactions of hydroxyl groups with phenolic hydroxyls are exhibited.

Methanol and ethanol deviate significantly from linear dependences between the retention data and selected molecular descriptors for *p-tert.*-butylcalix[4]arene (Table 5): $IRT^{b.p.}_{C_3-C_6OH}$ = +98.6 and +41.5, respectively, $IRT^{MV}_{C_3-C_6OH}$ = +254.2 and +49.2, respectively, $IRT^{\alpha}_{C_3-C_6OH}$ = +229.9 and +50.8, respectively (Fig. 6). It can be assumed that this pronounced retardation is caused by inclusion of the methanol and ethanol molecules in the *p-tert.*-butylcalix[4]arene cavity.

In contrast to the Porapak P reference phase, branched alkanols are retarded significantly less than the isomeric *n*-alkanols on *p-tert.*-butylcalix[4]arene ($IRT^{b.p.}_{C_3-C_6OH}$ = −27.4 to −47.9), see Fig. 6, except for *tert.*-butanol ($IRT^{b.p.}_{C_3-C_6OH}$ = +4.0). Thus, *p-tert.*-butylcalix[4]arene permits the complete separation of butanol isomers, compared with Chromosorb W (resolution *iso-*/*n-* = 1.4 compared with 0.6 and *tert.*-/*iso-* = 1.5 compared with 0.9). In contrast to Porapak P, alcohols with a hydroxyl group inside the alkyl chain are retarded significantly less than the isomeric 1-alkanols ($IRT^{b.p.}_{C_3-C_6OH}$ = −26.6 to −83.5), see Fig. 6.

4.5. Retention behaviour of ethers

On the reference phases, di-*n*-alkyl ethers (C_4–C_{12}) exhibit linear dependences of the retention data on b.p., *MV*, α and $\alpha + \mu^2$ (Table 6). Diisopropyl ether is retarded less on both phases ($IRT^{b.p.}_{C_4-C_{12}O}$ = −11.9 on Chromosorb W, and −48.0 on Porapak P), tetrahydrofuran is retarded significantly more on Porapak P ($IRT^{b.p.}_{C_4-C_{12}O}$ = +30.8). On *p-tert.*-butylcalix[4]-arene, di-*n*-alkyl ethers (C_4–C_{14}) yield linear dependences of the retention data on b.p., *MV*, α and $\alpha + \mu^2$ (Table 6). Cyclic ethers are eluted in agreement with *n*-alkyl ethers. Diisopropyl ether is retarded perceptibly less than the isomeric di-*n*-propyl ether ($IRT^{b.p.}_{C_4-C_{14}O}$ = −36.0).

5. Conclusions

The results obtained indicate that the QSRR method for treatment of GSC retention data is

Table 5
Linear dependences of the retention data on some molecular descriptors for *n*-alkanols on selected stationary phases

Column	Functional dependence	$y = A + Bx$		
		A	*B*	*r*
Porapak P (methanol to *n*-octanol)	Log *k* = f (b.p.)	−1.3240	0.0181	0.9998
	Log *k* = f (*MV*)	−1.0603	0.0206	0.9993
	Log *k* = f (α)	−0.8232	0.1869	0.9995
	Log *k* = f (μ)	42.1156	24.8532	0.9897
	Log *k* = f ($\alpha + \mu^2$)	−1.3338	0.1844	0.9965
p-tert.-Butylcalix[4]arene (*n*-propanol to *n*-hexanol)	Log *k* = f (b.p.)	−3.0838	0.0291	0.9984
	Log *k* = f (*MV*)	−2.8509	0.0374	0.9985
	Log *k* = f (α)	−2.4428	0.3150	0.9985
p-tert.-Butylcalix[4]arene (methanol to *n*-butanol)	Log *k* = f (μ)	53.1336	31.8010	0.9984

Column temperature, 60.0°C (*p-tert.*-butylcalix[4]arene) and 130.0°C (Porapak P); nitrogen flow-rate, 7.5 ml min^{-1}; volume of sample, 70 μl (vapour).

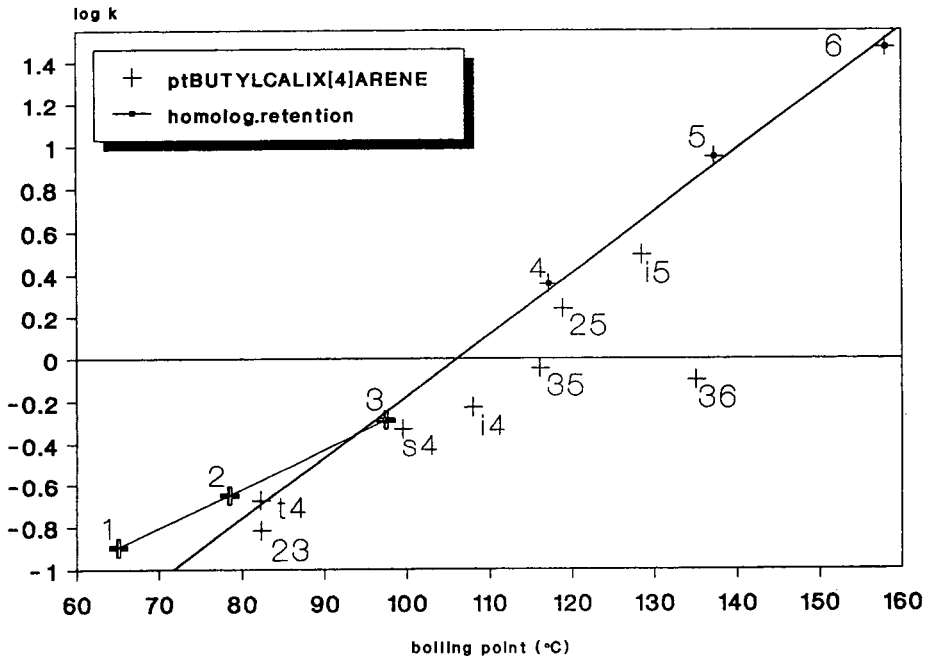

Fig. 6. Retention behaviour of alcohols: dependence of log (capacity factor) on boiling point. Column temperature, 60.0°C; nitrogen flow-rate, 7.5 ml min^{-1}; volume of sample, 70 μl (vapour). 1 = Methanol; 2 = ethanol; 3 = 1-propanol; 4 = 1-butanol; 5 = 1-pentanol; 6 = 1-hexanol; t4 = *tert.*-butanol; s4 = *sec.*-butanol; i4 = isobutanol; i5 = isopentanol; 23 = 2-propanol; 25 = 2-pentanol; 35 = 3-pentanol; 36 = 3-hexanol.

Table 6
Linear dependences of the retention data on some molecular descriptors for *n*-alkyl ethers (diethyl ether to di-*n*-heptyl ether) on selected stationary phases

Column	Functional dependence	$y = A + Bx$		
		A	B	r
Chromosorb W	Log k = f (b.p.)	−2.1605	0.0137	0.9978
	Log k = f (MV)	−3.9829	0.0221	0.9980
	Log k = f (α)	−3.4455	0.1973	0.9974
	Log k = f ($\alpha + \mu^2$)	−3.7026	0.1962	0.9985
Porapak P	Log k = f (b.p.)	−0.3660	0.0130	0.9998
	Log k = f (MV)	−2.1310	0.0213	0.9996
	Log k = f (α)	−1.6152	0.1903	0.9998
	Log k = f ($\alpha + \mu^2$)	−1.8586	0.1888	0.9992
p-tert.-Butylcalix[4]arene	Log k = f (b.p.)	−2.1670	0.0146	0.9993
	Log k = f (MV)	182.8840	50.8050	0.9988
	Log k = f (α)	24.5802	8.9153	1.0000
	Log k = f ($\alpha + \mu^2$)	2.1039	9.6772	0.9993

Column temperature, 60.0°C (Chromosorb W and *p-tert.*-butylcalix[4]arene) and 130.0°C (Porapak P); nitrogen flow-rate, 7.5 ml min^{-1}; volume of sample, 70 μl (vapour).

suitable for studying the selective properties of *p-tert.*-butylcalix[4]arene under gas chromatographic conditions. The newly introduced quantity IRT_s^D permits the quantitative evaluation of deviations in the retention behaviour within homologous series. It is probable that *p-tert.*-butylcalix[4]arene forms, under GSC conditions, inclusion complexes with benzene, its lower *n*-alkyl derivatives (toluene to *n*-butylbenzene), *p*-dialkylbenzenes (*p*-xylene, *p*-ethyltoluene), *m*-xylene, dichloromethane, trichloromethane, methanol and ethanol. Steric hindrance to inclusion in the *p-tert.*-butylcalix[4]arene cavity presumably arises with *o*-dialkylbenzenes (*o*-xylene, *o*-ethyltoluene), *m*-ethyltoluene in the presence of at least one isopropyl or a more bulky substituent on the benzene ring and trisubstituted benzenes. It is probable that the presence of CH–π interactions is decisive for the formation of *p-tert.*-butylcalix[4]arene inclusion complexes with the studied neutral organic molecules under GSC conditions, as follows from the example of tetrachloromethane. In addition, phenolic hydroxyls located at the narrower edge of the calixarene molecule participate strongly in the overall interaction mechanism. A more detailed mechanism of the sorbate–calixarene interactions is still unknown. Our statements about probable inclusion complexes should be complemented by further more exact methods (NMR spectroscopy, X-ray crystallography); work on these problems is in progress.

Acknowledgements

We are indebted to Professor Seiji Shinkai (Kyushu University, Japan) and Mr. Toru Sakaki (Research Development Corporation of Japan) for kindly providing calixarene samples. P.M. thanks Professor E. Smolková-Keulemansová for useful advice. This work was supported by a grant from Charles University, No. 180/93.

References

[1] M. Coruzzi, G.D. Andreetti, V. Bocchi, A. Pochini and R. Ungaro, *J. Chem. Soc., Perkin Trans. 2*, (1982) 1133.
[2] G.D. Andreetti, R. Ungaro and A. Pochini, *J. Chem. Soc., Chem. Commun.*, (1979) 1005.
[3] G.D. Andreetti, in J. Vicens and V. Böhmer (Editors), *Calixarenes, a Versatile Class of Macrocyclic Compounds*, Kluwer, Dordrecht, 1991, p. 111.
[4] R. Ungaro, A. Pochini, G.D. Andreetti and P. Domiano, *J. Chem. Soc., Perkin Trans. 2*, (1985) 197.
[5] C.D. Gutsche, B. Dhawan, K.H. No and R. Muthukrishnan, *J. Am. Chem. Soc.*, 103 (1981) 3782.
[6] M.A. McKervey, E.M. Seward, G. Ferguson and B.L. Ruhl, *J. Org. Chem.*, 51 (1986) 3581.
[7] G.D. Andreetti, O. Ori, F. Ugozzoli, C. Alfieri, A. Pochini and R. Ungaro, *J. Inclus. Phenom.*, 6 (1988) 523.
[8] K.-E. Bugge, W. Verboom, D.N. Reinhoudt and S. Harkema, *Acta Crystallogr., Sect. C*, 48 (1992) 1848.
[9] K. Suzuki, A.E. Armah, S. Fujii, K. Tomita, Z. Asfari and J. Vicens, *Chem. Lett.*, 10 (1991) 1699.
[10] M. Perrin and S. Lecocq, *J. Crystallogr. Spectrosc. Res.*, 22 (1992) 619.
[11] J.L. Atwood, S.G. Bott, C. Jones and C.L. Raston, *J. Chem. Soc., Chem. Commun.*, (1992) 1349.
[12] T.-M. Liang, K.K. Laali, M. Cordero and C. Wesdemiotis, *J. Chem. Res. (S)*, (1991) 354.
[13] E. Smolková-Keulemansová and L. Feltl, presented at the *2nd International Symposium on Clathrate Compounds and Molecular Inclusion Phenomena, Parma, Italy, 1982*, abstracts, p. 45.
[14] A. Mangia, A. Pochini, R. Ungaro and G.D. Andreetti, *Anal. Lett.*, 16 (1983) 1027.
[15] R. Kaliszan, *Quantitative Structure–Chromatographic Retention Relationships*, Wiley, New York, 1987.
[16] J.R. Conder and C.L. Young, *Physicochemical Measurements by Gas Chromatography*, Wiley, New York, 1986.
[17] E.L. Arancibia, C.R. de Schaefer and M. Katz, *Chromatografia*, 33 (1992) 41.
[18] J. Vicens, A.E. Armah, S. Fujii and K.-I. Tomita, *J. Inclus. Phenom.*, 10 (1991) 159.

ELSEVIER

Journal of Chromatography A, 696 (1995) 113–122

JOURNAL OF CHROMATOGRAPHY A

Determination of methylmercury in fish and river water samples using in situ sodium tetraethylborate derivatization following by solid-phase microextraction and gas chromatography–mass spectrometry

Yong Cai, Josep M. Bayona*

Environmental Chemistry Department, C.I.D.-C.S.I.C., Jordi Girona 18–26, E-08034 Barcelona, Spain

First received 20 October 1994; revised manuscript received 28 November 1994; accepted 29 November 1994

Abstract

A solid-phase microextraction (SPME) analytical procedure is described for the quantitative determination of methylmercury and labile Hg^{2+} in fish and river water matrices. The analytical procedure involves aqueous-phase derivatization of ionic mercury species with sodium tetraethylborate in a sample vial and subsequent extraction with a silica fiber coated with poly(dimethylsiloxane). The mercury derivatives are desorbed in the splitless injection port of a gas chromatograph and subsequently analyzed by electron impact mass spectrometry. Both headspace SPME and aqueous-phase SPME are studied, and the linear range of the method spans several orders of magnitude for both procedures. The detection limits of the headspace SPME procedure for a 20-ml sample are 7.5 and 3.5 ng/l as Hg for CH_3Hg^+ and Hg^{2+}, respectively. The detection limits of aqueous-phase SPME for a 1.5-ml sample are 6.7 and 8.7 ng/l as Hg for CH_3Hg^+ and Hg^{2+}, respectively. Analyses of standard reference materials and river water sample demonstrate the suitability of this method for the determination of methylmercury and labile Hg^{2+}.

1. Introduction

Mercury pollution has become a global problem because of its occurrence from natural and anthropogenic sources, and its biogeochemical processes. The determination and monitoring of mercury is a special concern in the field of heavy metal analysis. A number of publications have reported the presence of mercury in a variety of environmental and biological samples [1–3]. It has been demonstrated that mercury can be methylated in the environment and bioconcentrated in biota [4,5]. Ingestion of fish muscle is an important exposure pathway of mercury to humans. The high toxicity of methylmercury has been well recognized. As a result, the US Food and Drug Administration (FDA) has set an Action Level of 1 μg/g (wet mass) for concentration of mercury in fish. Fish containing concentrations of mercury above this level are considered to be hazardous for human consumption and cannot be sold in interstate commerce. Canada and several US States have developed consumption advisories of 0.5 μg/g for mercury in fish [3]. In addition, the European Union (EU) has set environmental quality objectives of 0.3 μg/g (wet mass) for fish, 1 μg/l for continental water, 0.5 μg/l for estuarine water, and 0.3

* Corresponding author.

0021-9673/95/$09.50
SSDI 0021-9673(94)01177-X

μg/l for coastal water as total mercury [6]. As public awareness regarding the toxicity and the environmental impact of mercury contamination increases, the demand for a simple, accurate, reliable speciation analytical method, which can distinguish between organic and inorganic forms of mercury, also increases.

Traditionally, gas chromatography (GC) with electron-capture detection (ECD) was widely used for the determination and speciation of organomercury in many environmental and biological samples [7–9]. The classic method for extracting and separating methylmercury is based on a procedure originally devised by Gage [10] and later modified by Westöö [11], which involves liberation, isolation by multiple liquid–liquid extraction with benzene or toluene, and subsequent analysis by GC–ECD. However, organomercury halides are noted for their poor chromatographic characteristics including severe tailing, decomposition, and low column efficiency. In addition, the halogen-bearing compounds coextracted with methylmercury can interfere with the determination because of the non-specificity of ECD. To overcome these problems, many efforts have been made, involving column passivation using a concentrated organic solution of mercury(II) [8], butylation of methylmercury by a Grignard reagent [9,12] and the coupling of chromatography (gas or liquid) with atomic spectrometry [13]. Most of these methods, however, are time-consuming, require tedious liquid–liquid extraction with organic solvent prior to chromatographic separation and detection, and often lead to the final determination of only the CH_3Hg^+ species. An alternative method has recently been developed for CH_3Hg^+ and Hg^{2+} analysis by using aqueous ethylation with sodium tetraethylborate ($NaBEt_4$), followed by purge and trap and detection by atomic absorption spectrometry (AAS) [14,15] or by atomic fluorescence spectrometry (AFS) [16,17]. The use of $NaBEt_4$ as an ethylation reagent has significant advantages since the derivatization reaction can be performed in the aqueous phase, subsequently reduces the analytical time and eliminates the need for organic solvent extraction.

Recently, a novel analytical technique, solid-phase microextraction (SPME), has been developed by Pawliszyn and co-workers [18–20]. This technique involves the extraction of volatile or semivolatile organic compounds directly from aqueous or gaseous samples onto a fused-silica fiber that is coated with an appropriate stationary phase. While the fiber is exposed to the sample, the analytes partition from the sample matrix into the stationary phase until equilibrium is reached. The fiber is then directly transferred into a GC injector for thermal desorption and analysis. Such a fast, simple technique has been used for the determination of a number of organic pollutants [18–24]. Recently, a procedure has also been reported for the extraction of bismuth(II) from aqueous nitric acid solution using a fused-silica fiber coated with poly(dimethylsiloxane), which was modified to contain ion-exchanging functions [25]. In the present study, we report an analytical procedure for the determination of CH_3Hg^+ and labile Hg^{2+} using in situ aqueous ethylation with $NaBEt_4$, subsequent SPME sampling and then GC–MS detection. This is, to our knowledge, the first application of SPME to the determination of organometallics. Both aqueous-phase and headspace SPME extraction procedures were studied. This analytical process is much simpler than the methods previously reported, and does not require organic solvent extraction. It is free from chromatographic complications, since the CH_3Hg^+ and Hg^{2+} are derivatized to fully alkylated species before analysis. Compared with the conventional purge and trap method, this procedure eliminates the use of large amounts of liquid nitrogen and the possible blockage of column due to water condensation. Applications to standard reference materials, Dorm-1 and Dorm-2, and river water sample are also presented.

2. Experimental

2.1. Apparatus

SPME device

The SPME fiber holder for manual use and the fiber coated with 100 μm thickness of poly(di-

methylsiloxane) were obtained from Supelco (Bellefonte, PA, USA). This holder was designed to be used with a reusable, replaceable, Supelco SPME fiber assembly. The 25 or 1.5 ml of glass vial were used for headspace and aqueous-phase SPME extraction, respectively. The silicone rubber septa coated with PTFE were used for both vials. The SPME extractions were performed with magnetic stirring to ensure the proper mixing of the sample solution, and a 15×6 mm or a 4×2 mm PTFE-coated magnetic stirring bar was used in headspace or aqueous-phase extraction.

GC–MS

The analysis was performed using a GC 8000 series gas chromatograph coupled with an MD 800 mass spectrometer (Fisons Instruments, Milan, Italy) at 70 eV of ionization energy. Transfer line and ion source temperatures were maintained at 280 and 200°C, respectively. A mass range from m/z 50–450 was recorded in the scan mode, and four ions [m/z 217 and 246 for $CH_3HgC_2H_5$, m/z 231 and 260 for $Hg(C_2H_5)_2$)] were chosen in the selective ion monitoring mode (SIM). A split/splitless injector was used in the splitless mode and maintained at 220°C. A 30-s desorption time was used for all fiber injections. The analytical column used for all experiments was 30 m × 0.32 mm I.D. fused silica coated with 1.8 μm film thickness of DB-624 (J & W Scientific). The column temperature program is given in the chromatograms. Helium at a head pressure of 7.5 p.s.i. (1 p.s.i. = 6894.76 Pa) was used as carrier gas.

2.2. Reagents and materials

Two standard reference materials, Dorm-1 and Dorm-2 (dogfish muscle), were obtained form the National Research Council of Canada (NRCC), Ottawa, Canada. The certified values of CH_3Hg^+ in Dorm-1 and Dorm-2 are 0.731 ± 0.060 and 4.47 ± 0.32 μg/g as Hg, respectively. A subsurface (0.5 m) river water sample was collected from Llobregat river adjacent to Barcelona, Spain.

Methylmercuric chloride (99%), mercury dichloride (99.9995%), and sodium tetraethylborate were purchased from Strem Chemicals (Newburgport, MA, USA). Analytical-grade potassium hydroxide pellets were from Merck (Darmstadt, Germany). Sodium acetate (analytical grade) and acetic acid (analytical grade) were obtained from Aldrich (Steinheim, Germany). All other chemicals were of analytical grade or better.

Stock standards at 1000 mg/l as Hg for methylmercury and inorganic mercury were prepared in acetone and 5% (v/v) nitric acid, respectively. A mixed working solution was prepared weekly by diluting the stock solution with acetone to a range of 0.05–50 mg/l as Hg. A fresh $NaBEt_4$ solution of 1% (w/v) was prepared daily in deionized water and passed through a 0.5-μm FH filter (Millipore, Bedford, MA, USA). Both mercury working solution and $NaBEt_4$ were stored at 4°C. A buffer at pH 4.5 was prepared by mixing appropriate amount of sodium acetate (0.2 *M*) and acetic acid (0.2 *M*).

2.3. Procedure

The liberation of mercury from biological samples was performed using a procedure reported by Fisher et al. [15]. Briefly, 100–200 mg sample of fish tissue was placed in a 50-ml glass bottle. Then 10–20 ml of 25% (w/v) methanolic KOH solution were added, and the sample was shaken in an ultrasonic bath for 3 h. The dissolved sample was stored at 4°C before analysis.

For headspace SPME sampling, the magnetic stirring bar, 17 ml of deionized water and 3 ml of acetate buffer solution (pH 4.5) were placed in a 25-ml glass vial. A 100-μl aliquot of the fish extract or 1-μl aliquot of mixed mercury standards (0.5–50 mg/l as Hg), and 200 μl of 1% $NaBEt_4$ solution were added, and the vial was then closed immediately. The fiber was drawn into the needle of the holder, and the needle was used to pierce the septum of the sample vial. The fiber was then lowered into the headspace by depressing the plunger. The fiber within the vial headspace was situated about 0.3 cm above the surface of the aqueous phase, and never came into contact with the liquid. After a predetermined sampling time, the fiber was retracted into the needle and immediately inserted into the GC

injector for thermal desorption. The depth of the fiber in the injection port was 4.4 cm (measured from the holder), which was about 1.5 cm above the column. This position was suggested by the manufacturer for conventional syringe injection, and was found to be suitable in this study. For analysis of the river water sample, 17 ml of real sample was placed in the vial instead of deionized water.

For aqueous-phase SPME sampling, the magnetic stirring bar, 1.0 ml of deionized water, 0.5 ml of acetate buffer solution, 20 μl aliquot of the fish extract or 1 μl of mixed mercury standards (0.05–10 mg/l as Hg), and 20 μl of $NaBEt_4$ were added to the 1.5-ml sample vial. Only about 100 μl of headspace were left in the vial, which prevented the loss of analyte due to the formation of a large headspace. The other steps for aqueous-phase SPME sampling were as described above for SPME sampling of the headspace except that the entire fiber was placed in the solution.

3. Results and discussion

3.1. Development of SPME procedure and GC–MS determination

The SPME procedure, including headspace and aqueous-phase sampling, has been studied extensively for the analysis of organic pollutants [18–24]. SPME, unlike most conventional extraction techniques, is not based on exhaustive extraction of the sample, but on an equilibrium between the analyte concentration in the sample (and/or in the headspace) and that in the solid-phase fiber coating [18]. In the present study, the CH_3Hg^+ and Hg^{2+} were derivatized to ethylmethylmercury and diethylmercury, respectively, and then extracted by the fiber. The derivatization procedure can significantly improve the partitioning of the analytes between fiber coating and sample matrix, since the fully alkylated mercury species have greater affinity for the poly(dimethylsiloxane) coating. As this derivatization reaction can be carried out rapidly in aqueous phase [15,16] and the ethylated products are volatile (b.p. of $Hg(C_2H_5)_2$ = 159°C), it was expected that the extraction equilibration would be reached quickly. Fig. 1 shows the time profile of the in situ ethylation and extraction of CH_3Hg^+ and Hg^{2+} obtained by using the headspace SPME technique. The results indicate that the reaction and extraction equilibration time is approximately 10 min for both compounds at room temperature (25°C). Higher temperature (50°C) of reaction and extraction was investigated, but no significant enhancement in the amount extracted by the fiber was found. The reaction and extraction equilibrium time for the aqueous-phase SPME sampling technique was also estimated. It was found that the equilibration time was extended to approximately 20 min. The reduced sampling time given by the headspace technique can be explained by the fact that the diffusion of analytes is much faster in vapor phase than in aqueous phase. This result agrees with the determination of organic pollutants reported by Zhang and Pawliszyn [20]. To test the effect of salting out as a means of enhancing the amount extracted by the fiber, 1.0 ml of saturated NaCl was added to the vial and a similar procedure to that described for headspace SPME sampling was performed. In contrast to the results obtained for some organic compounds [23], the extraction efficiency for mercury species by the fiber was decreased by the addition of salt. The decreased absorption could be attributed to the high concentration of chloride, which hampers the ethylation reaction of organometallics with $NaBEt_4$ [16,26]. To confirm this explanation, an experiment was performed by injecting 1 ml of saturated NaCl through the septum of the vial after the reaction had been carried out for 5 min, and the result was similar to that obtained without addition of salt. The amount of salt injected to the vial was limited due to the closed system used in this study, and the addition of 1 ml of saturated NaCl did not enhance the amount extracted by the fiber for either $CH_3HgC_2H_5$ or $Hg(C_2H_5)_2$.

A suitable desorption temperature is critical, since the thermal decomposition of mercury derivatives in the process of desorbing from a

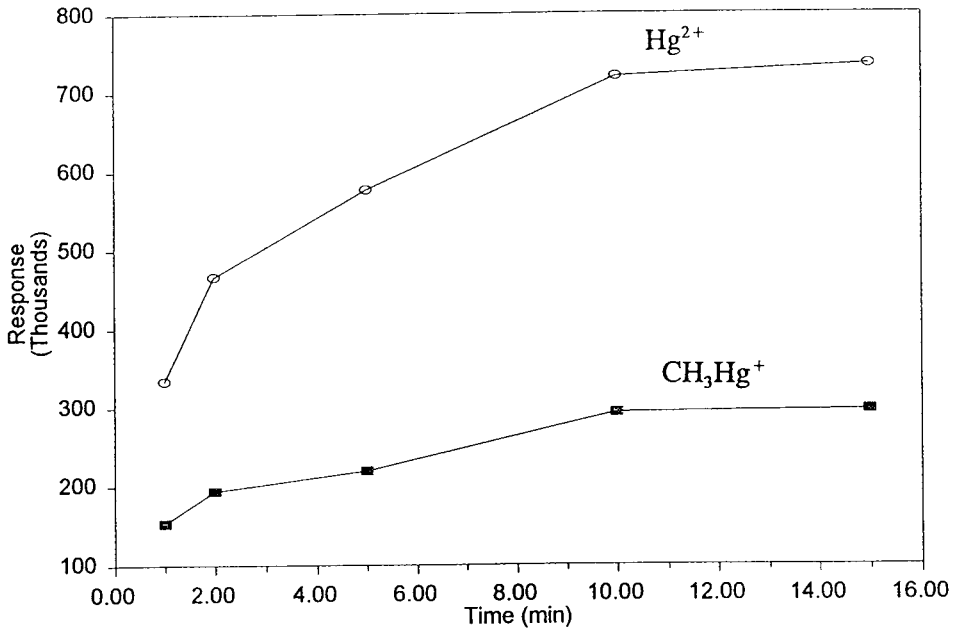

Fig. 1. Time profile of the in situ ethylation and absorption of CH_3Hg^+ and labile Hg^{2+} obtained by using headspace SPME technique with an initial concentration of 0.5 μg/l as Hg.

Carbotrap column has been observed [17]. We found that at 220°C fast desorption of the analytes can be ensured and the decomposition can be eliminated. A significant advantage of this analytical procedure is that the fiber is directly exposed to the high-temperature injection port for desorption. This is in contrast to the conventional purge-and-trap technique, in which the analyte on the trap column is desorbed by heating the column with a resistance wire. Rapid desorption has been shown to eliminate the thermal decomposition [17].

Carryover or memory effect is a common problem encountered in the analysis of mercury using conventional techniques [13,15]. It was also observed in the determination of organic compound by the SPME method [21,23]. To determine whether the analytes remained on the fiber after desorption, two types of carryover experiment were performed for both the headspace and aqueous-phase SPME sampling procedures. The first consisted of running a second desorption of the same fiber after the initial desorption, following exposure to a standard solution. The second involved running a blank using a same procedure, except that no standard was added, after the initial desorption of the same fiber. In the first case, no memory effect was observed for either headspace or aqueous-phase sampling procedures. This result suggests that the ethylated mercury absorbed on the fiber can be efficiently desorbed under the experimental conditions used. In the latter experiment, neither compound showed any sign of carryover when the headspace SPME method was used. For the aqueous-phase SPME sampling procedure, however, an evident peak of diethylmercury was found. This can be attributed to Hg^{2+}, which was absorbed in the first sampling, but remained in the coating after desorption. It was ethylated during the next sampling, then desorbed with the subsequent injection. The extent of carryover relies mainly on the type and thickness of the fiber, and the concentration of analyte. When 100-μm thickness fiber coated with poly(dimethylsiloxane) was used, and a 0.67 μg/l solution was sampled, the carryover was less than 1% for a subsequent blank. The mem-

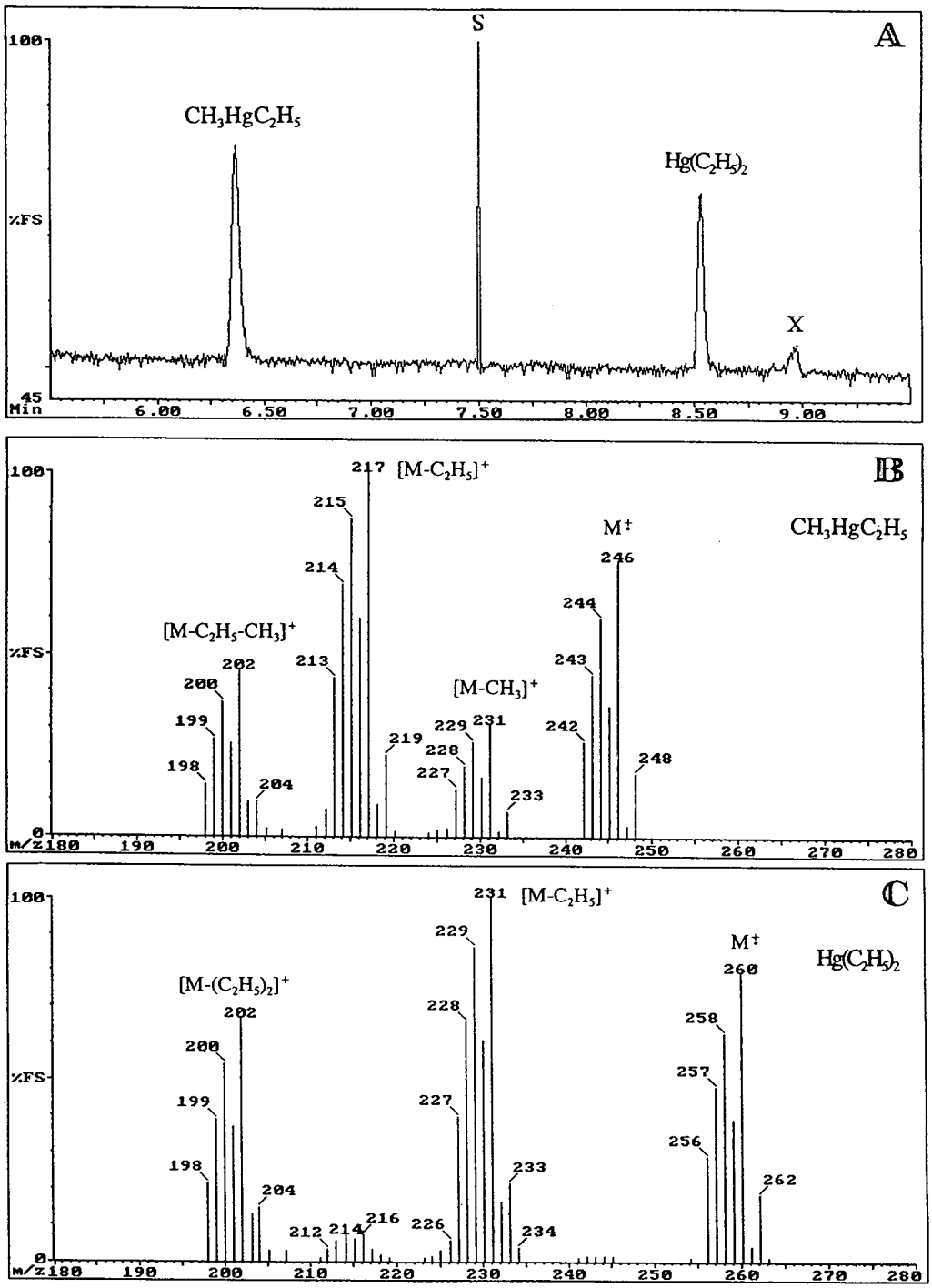

Fig. 2. (A) Selected ion mode GC–MS chromatogram for CH_3Hg^+ and labile Hg^{2+} spiked at 0.25 μg/l as Hg in water using headspace SPME. The unidentified peak X was from blank. Peak S was an electric noise resulting from changing the retention window of the acquisition pragram. The column temperature was initially held at 30°C, programmed at 10°C/min to 80°C, then increased to a final temperature of 260°C at a rate of 15°C/min, and held there for 2 min. (B, C) Electron impact mass spectra of $CH_3HgC_2H_5$ and $Hg(C_2H_5)_2$, respectively, obtained at 70 eV.

Table 1
Detection limits and linear range for the determination of CH_3Hg^+ and Hg^{2+} by SPME

	Absolute detection limits (ng as Hg)		Concentration detection limits: Water sample (ng/l as Hg)		Concentration detection limits: Fish tissue (μg/g as Hg)[b]		Linear range[a] (ng/l as Hg)	
	CH_3Hg^+	Hg^{2+}	CH_3Hg^+	Hg^{2+}	CH_3Hg^+	Hg^{2+}	CH_3Hg^+	Hg^{2+}
Headspace	0.15	0.07	7.5	3.5	0.15	0.07	25–2500	25–2500
Aqueous phase	0.01	0.013	6.7	8.7	0.1	0.13	30–6700	30–6700

[a] Correlation coefficients ranged from 0.9959 to 0.9999.
[b] Dry mass.

ory effect can be significantly reduced by using a longer desorption time, or by running blanks. In contrast to the aqueous-phase SPME sampling, the fiber did not contact the liquid solution in headspace SPME sampling and only the ethylated mercury species escaping to the headspace were extracted. This greatly reduces the possibility of Hg^{2+} carryover, and consequently eliminates interference in the analysis of subsequent samples.

A thicker stationary phase column (DB-624, 1.8 μm film thickness) was employed, and in this study the desorption temperature was high enough (220°C) for the desorption to be fast. This eliminated the need for a cryofocusing step, which is often included to refocus the analytes onto the capillary column, and to avoid band broadening when volatile compounds are analyzed by SPME [20]. Fig. 2A shows a GC–MS chromatogram in SIM mode for determination of CH_3Hg^+ and Hg^{2+} spiked at 0.25 μg/l as Hg in deionized water, using headspace SPME sampling. Mass spectra of $CH_3HgC_2H_5$ and $Hg(C_2H_5)_2$ in scan mode are shown in Fig. 2B and C for confirmation of the ethylation products.

The headspace SPME and the aqueous-phase SPME techniques were calibrated with a series of CH_3Hg^+ and Hg^{2+} standard. The linearity ranges for both CH_3Hg^+ and Hg^{2+} are at least from 0.025 to 2.5 μg/l and from 0.03 to 6.7 μg/l for headspace and aqueous-phase SPME procedures, respectively. Detection limits were determined for both sampling methods. The linear ranges and absolute detection limits, calculated as three times the baseline noise are shown in Table 1. The concentration detection limit is a function of the sample size that can be used in

Table 2
Results of mercury speciation in fish tissue and river water samples

	Measured values (μg/g as Hg)		Certified CH_3Hg^+ (μg/g as Hg)
	CH_3Hg^+	Hg^{2+}	
Dorm-1[a]	0.77 ± 0.03 (n = 2)	0.38 ± 0.078 (n = 2)	0.731 ± 0.060
Dorm-2[b]	4.41 ± 0.55 (n = 5)	0.13 ± 0.01 (n = 5)	4.47 ± 0.32
River sample[b,c]	ND	9.30 ± 0.03 (n = 2)	NC

ND = Not detectable; NC = not certified.
[a] Using aqeuous-phase SPME.
[b] Using headspace SPME.
[c] Values given in ng/l as Hg.

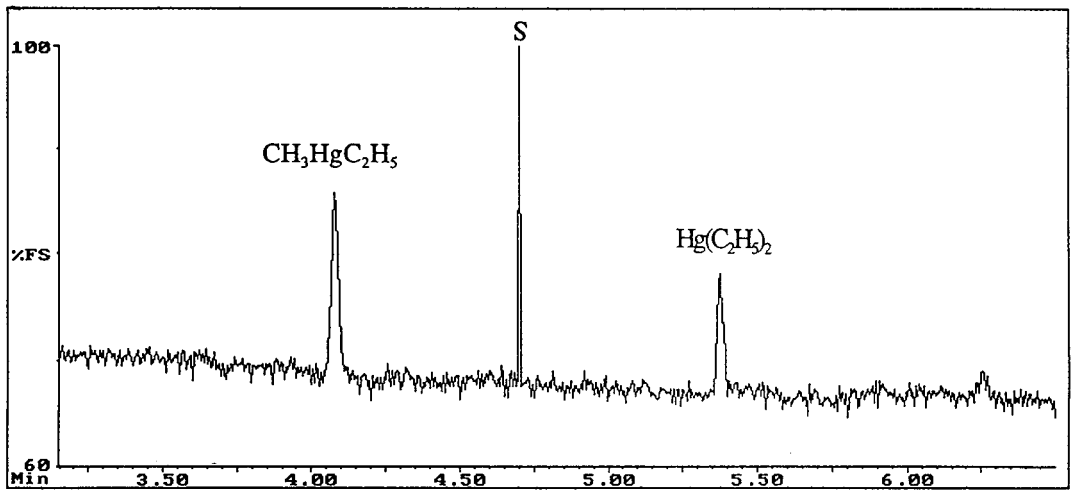

Fig. 3. GC–MS chromatogram in SIM mode for Dorm-1 analysis with aqueous-phase SPME technique. The column temperature was initially held at 30°C, programmed at 25°C/min to 90°C, then increased to a final temperature of 260°C at a rate of 20°C/min, and held there for 2 min. Peak S was an electric noise resulting from changing the retention window of the acquisition program.

the experiment. In the present study, 1.5 ml for aqueous-phase sampling and 20 ml for headspace sampling were used. For analysis of biological samples, 100 mg of sample was dissolved in 20 ml of methanolic KOH solution and from this solution 200 μl (headspace SPME) and 20 μl (aqueous-phase SPME) were analyzed. The concentration detection limits calculated for water sample and biological sample are also listed in Table 1. These detection limits are adequate to meet the requirements of FDA and EU for monitoring mercury in fish or water samples. The relative standard deviation (R.S.D.) of the signal (peak area) was also examined. For headspace SPME, the R.S.D.s for a 0.25 μg/l as Hg of CH_3Hg^+ and Hg^{2+} standards were 4.8 and

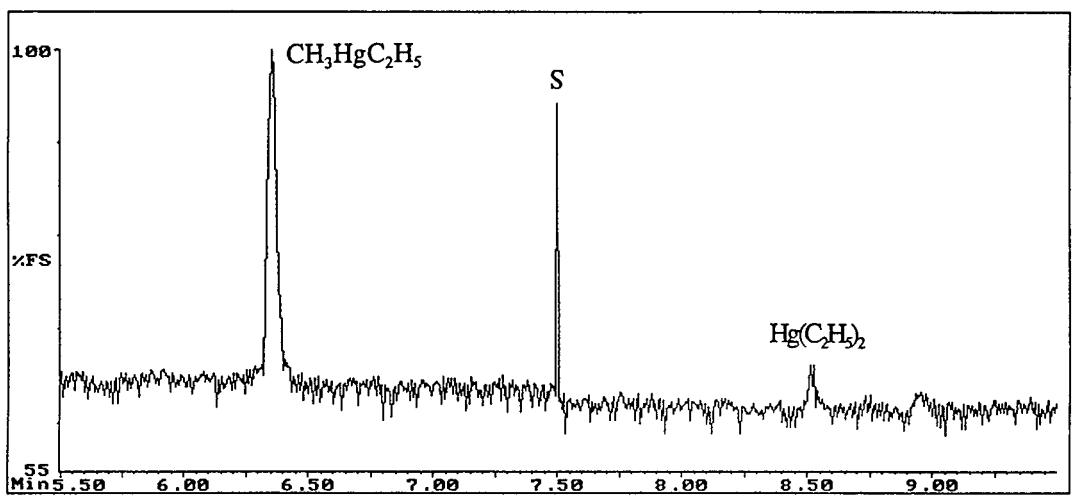

Fig. 4. GC–MS chromatogram in SIM mode for Dorm-2 analysis with headspace SPME technique. Column temperature program as in Fig. 2. Peak S was an electric noise resulting from changing the retention window of the acquisition program.

2.4% ($n = 3$). For aqueous-phase SPME the R.S.D.s for a 0.67 μg/l as Hg of CH_3Hg^+ and Hg^{2+} standards were 3 and 11% ($n = 3$), respectively.

3.2. Application to real samples

To evaluate the reliability of the analytical technique developed for the analysis of real-world samples, two standard reference materials and a river water sample were analysed. The method of standard addition was used to account for the matrix effects. The analytical results are listed in Table 2. Typical GC–MS chromatograms in SIM mode for Dorm-1 analysis with aqueous-phase SPME procedure and for Dorm-2 analysis with headspace SPME procedure are presented in Figs. 3 and 4, respectively. The analytical result for Dorm-2 indicates that the mercury present in this material is almost entire-

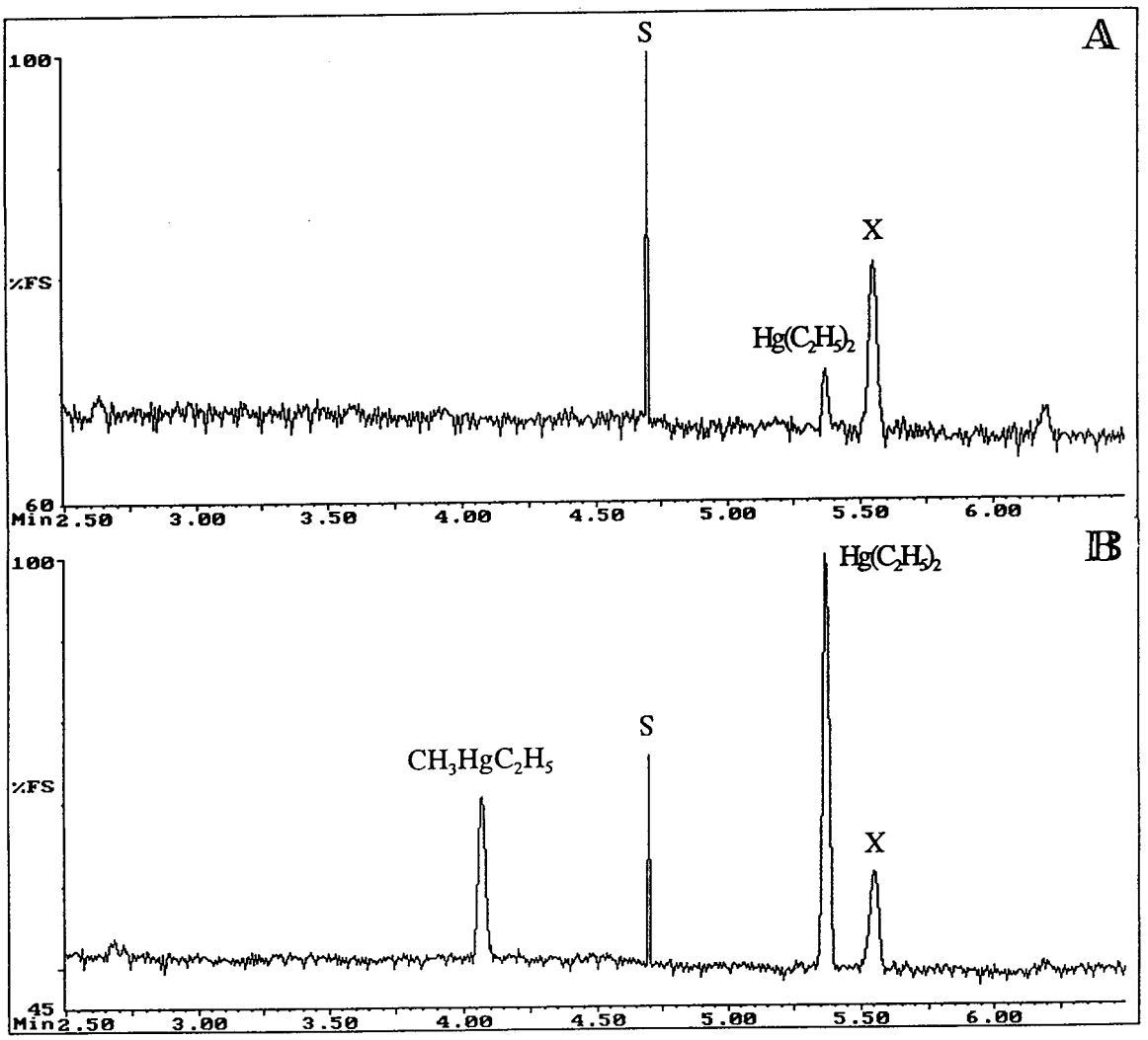

Fig. 5. GC–MS chromatogram in SIM mode for river Llobregat sample analyses with headspace SPME technique. (A) Unspiked, (B) spiked at 100 ng/l as Hg for both CH_3Hg^+ and Hg^{2+}. The unidentified peak X was from blank. Peak S was an electric noise resulting from changing the retention window of the acquisition program. Column temperature program as in Fig. 3.

ly methylmercury. This is in good agreement with the NRCC's report for this certified reference material. No methylmercury was found in the Llobregat river sample. The inorganic mercury, however, was measured at a concentration of 9.3 ng/l as Hg. Fig. 5 shows the GC–MS chromatograms of the river sample in SIM mode for the samples unspiked and spiked at 100 ng/l as Hg for CH_3Hg^+ and Hg^{2+} using headspace SPME techniques.

In summary, the results of this study demonstrate that the quantitative, simultaneous determination of CH_3Hg^+ and labile Hg^{2+} from fish and water samples can be achieved using an in situ aqueous derivatization followed by SPME and GC–MS detection. Compared with the direct SPME sampling from aqueous phase, the headspace SPME sampling procedure is more suitable since it eliminates the memory effects of Hg^{2+}. This analytical method is simple, rapid, solvent-free, and cost-effective. It uses an existing GC injector, and hence could be extended for use with other hyphenated techniques. Taking these advantages into account, this technique could be used to monitor and screen mercury species in the environment.

Acknowledgements

Financial support was obtained from the Commission of the European Communities (grant EV5V-CT94-0357). Y.C. acknowledges the fellowship provided by the Spanish Ministry of Science and Education. We are thankful to Dr. S. Rapsomanikis and Mr. R. Fischer, Max Planck Institute for Chemistry, Mainz, Germany for providing some of the certified reference materials.

References

[1] R.P. Mason and W.F. Fitzgerald, *Nature (London)*, 347 (1990) 457.
[2] G.A. Gill and K.W. Bruland, *Environ. Sci. Technol.*, 24 (1990) 1392.
[3] C.T. Driscoll, C. Yan, C.L. Schofield, R. Munson and J. Holsapple, *Environ. Sci. Technol.*, 28 (1994) 136A.
[4] P.J. Graig, in P.J. Craig (Editor), *Organometallic Compounds in the Environment*, Longman, Harlow, 1986, p. 66.
[5] M. Bernhard, M. Filippelli, in G.P. Gabrielides (Editor), *Proceedings of the FAO/UNEP/IAEA Consultation Meeting on the Accumulation and Transformation of Chemical Contaminants by Biotic and Abiotic Processes in the Marine Environment, La Spezia, Italy, 24–28 September 1990*, UNEP, Athens, 1991, p. 99
[6] *Off. J. Eur. Commun.*, 3 (1982) 142.
[7] M. Horvat, A.R. Bryne and K. May, *Talanta*, 37 (1990) 207.
[8] J.E. O'Reilly, *J. Chromatogr.*, 238 (1982) 433.
[9] E. Bulska, D.C. Baxter and W. Frech, *Anal. Chim. Acta*, 249 (1991) 545.
[10] J.C. Gage, *Analyst (London)*, 86 (1961) 457.
[11] G. Westöö, *Acta Chem. Scand.*, 20 (1966) 2131.
[12] R.D. Wilken, *Fresenius' J. Anal. Chem.*, 342 (1992) 795.
[13] S. Rapsomanikis, in R.M. Harrison and S. Rapsomanikis (Editors), *Environmental Analysis Using Chromatography Interfaced with Atomic Spectroscopy*, Ellis Horwood, Chichester, 1989, Ch. 10.
[14] S. Rapsomanikis, O.F.X. Donard and J.H. Weber, *Anal. Chem.*, 58 (1986) 35.
[15] R. Fisher, S. Rapsomanikis and M.O. Andreae, *Anal. Chem.*, 65 (1993) 763.
[16] N. Bloom, *Can. J. Fish. Aquat. Sci.*, 46 (1989) 1131.
[17] L. Liang, M. Horvat and N.S. Bloom, *Talanta*, 41 (1994) 371.
[18] C.L. Arthur and J. Pawliszyn, *Anal. Chem.*, 62 (1990) 2145.
[19] D. Louch, S. Motlagh and J. Pawliszyn, *Anal Chem.*, 64 (1992) 1187.
[20] Z. Zhang and J. Pawliszyn, *Anal. Chem.*, 65 (1993) 1843.
[21] D.W. Potter and J. Pawliszyn, *Environ. Sci. Technol.*, 28 (1994) 298.
[22] B.D. Page and G. Lacroix, *J. Chromatogr.*, 648 (1993) 199.
[23] K.D. Buchholz and J. Pawliszyn, *Anal. Chem.*, 66 (1994) 160.
[24] S.B. Hawthorne, D.J. Miller, J. Pawliszyn and C.L. Arthur, *J. Chromatogr.*, 603 (1992) 185.
[25] E.O. Otu and J. Pawliszyn, *Mikrochim. Acta*, 112 (1993) 41.
[26] Y. Cai, S. Rapsomanikis and M.O. Andreae, *Talanta*, 41 (1994) 589.

ELSEVIER

Journal of Chromatography A, 696 (1995) 123–130

JOURNAL OF CHROMATOGRAPHY A

Gas chromatographic determination of incurred chloramphenicol residues in eggs following optimal extraction

M. Humayoun Akhtar[a,*], Claude Danis[a], Andre Sauve[b], Carla Barry[b]

[a]*Centre for Food and Animal Research, Research Branch, Agriculture and Agri-Food Canada, Ottawa, Ontario K1A 0C6, Canada*

[b]*Laboratory Services Division, Food Production and Inspection Branch, Agriculture and Agri-Food Canada, Ottawa, Ontario K1A 0C6, Canada*

First received 30 August 1994; revised manuscript received 20 December 1994; accepted 21 December 1994

Abstract

The existing method for analysis of chloramphenicol (CAP) residues in animal tissues was optimized to extract spiked-labelled and unlabelled chloramphenicol from freeze-dried egg albumen and yolks. Although recoveries of CAP were essentially the same for both albumen and yolk, the standard deviation was narrow for albumen compared to yolk. There was no statistical difference in recoveries of spiked CAP from whole liquid or freeze-dried (powdered) eggs. The method was validated with eggs of chickens given CAP in drinking water. No loss of CAP occurred during freeze-drying. The method has the potential of being used routinely for monitoring CAP in eggs and egg products.

1. Introduction

Although chloramphenicol (CAP), a broad-spectrum antibiotic, has no reported adverse effect on animal health, it has been shown to be toxic to humans. CAP causes dose-related suppression of bone marrow which results in many related diseases such as leucopenia [1,2]. Two potentially fatal adverse effects of CAP are aplastic anemia and gray syndrome [3]. There is also evidence that prolonged topical use of CAP in the human eye causes aplastic anemia [3–5]. In one documented case, a daily dose of 2 mg over 40 days caused death [4]. These and many other cases are of major concern to consumers and regulatory officials since the effect(s) of consuming small amounts of CAP via food is unknown.

CAP is a very effective veterinary drug and is used to control diseases such as salmonellosis [6], mastitis and other cattle diseases [7–9]. Further, CAP is also used to treat diseases of animal pathogen, which have become resistant to other commonly used antibiotics [10,11]. In poultry, CAP has been recommended for the treatment of *Salmonella* infections [12] and prevention of secondary infections associated with chronic respiratory diseases and "blue-comb" [13].

In view of the high toxic effects of CAP to humans, it has been subject to strict control in many countries around the world. In some countries, it is still used under very controlled conditions. The USA [14] and Canada [15] have banned the use of CAP for food-producing

* Corresponding author.

SSDI 0021-9673(94)01284-9

animals. The World Health Organization recommended that CAP not be used for treatment of food animals [16].

Various chromatographic techniques have been developed to detect and quantitate CAP residues in food products including eggs. The methods employ gas chromatography (GC), liquid chromatography (LC), thin-layer chromatography (TLC), and involve many clean-up steps prior to analysis. Methods developed up to 1984 have been reviewed by Allen [17]. In recent years, modification of previous methods and employment of immunoassay techniques have been reported [18,19]. Capillary GC [20] and GC–mass spectrometry (MS) [21], LC and LC–MS [23–25] have been used as confirmatory tools.

Most of the reported methods for analysis of CAP residues are for spiked samples, and not validated fully for actual (incurred) samples [26,27]. As our work was near completion, Samouris et al. [25] reported a high-performance liquid chromatography technique for detection of incurred CAP residues in eggs of chickens given chloramphenicol in feed at a concentration of 800 mg/kg for 1 day. Our work in poultry involves 9 CAP drinking water concentrations over 10 consecutive days.

This paper details an optimum condition for the extraction of chloramphenicol residues from incurred eggs. The validity of the extraction technique is supported by the use of ^{14}C-labelled chloramphenicol. Data are provided which show that freeze-drying of liquid eggs caused no loss of CAP residues.

2. Experimental

2.1. Reagents and solutions

The solvents ethyl acetate, methanol, hexane and cyclohexane (distilled-in-glass grade or equivalent) were purchased from Caledon Labs. (Georgetown, Canada).

Chloramphenicol (unlabelled) was purchased from Aldrich (Milwaukee, WI, USA) and [^{14}C]Chloramphenicol (dichloroacetyl 1,2-^{14}C, >98% radio purity) was obtained from NEN Products, a Division of DuPont.

The derivatizing reagent Sylon HTP (No. 3-3403) was purchased from Supelco Canada (Toronto, Canada) and consisted of hexamethyldisilazane (HMDS)–chlorotrimethylsilane(TMCS)–pyridine (3:1:9).

Sodium chloride solution (4%) was prepared by dissolving the appropriate amount of NaCl (ACS grade) in filtered/distilled deionized water.

The scintillation cocktail was ICN Biomedicals' (Irvine, CA, USA) CytoScint, a ready-to-use, environmentally safe preparation.

2.2. Preparation and storage of standard solutions

Stock solutions were prepared by dissolving a known amount of CAP in methanol in an acid-rinsed volumetric flask and stored at 0°C. Similarly, intermediate and analytical standard solutions of CAP were prepared by appropriate dilution of stock and intermediate solutions, respectively. The concentration of analytical CAP solutions ranged from 12.5 to 250 pg/ml.

Supplier's [^{14}C]CAP solution (in ethanol) was diluted with methanol to give a working solution of 222 dpm/μl (0.650 ng CAP/μl). A calculated volume of the working solution was added to the sample to study the solvent extraction efficiency and the effect of freeze-drying on the residue level in eggs.

2.3. Animal treatment

Adult White Leghorn hens (1.6 to 2.1 kg body mass) had free access to drinking water containing CAP at 0, 1, 5, 10, 25, 50, 100, 150 and 200 mg/ml for 10 consecutive days followed by a withdrawal period of 10 days. Eggs were collected daily and stored at 4°C until analyzed after freeze-drying (powdered).

2.4. Processing of eggs

Eggs from individual treatment group were divided into two groups of 5–6 eggs each. One group was set aside for development and valida-

tion of a Robotic sample preparation technique (this will be reported separately). The second set of eggs were broken, separated into albumen and yolk, combined on group and date basis. The separated and pooled albumen and yolk were mixed thoroughly with a spatula and freeze dried before analysis. Freeze dryer, a Virtis Model 50 SRC (Fisher), was operated at 450 mTorr vacuum (1 Torr = 133.322 Pa), shelf temperature 20°C, condenser temperature −55°C and drying time 7 days.

2.5. Extraction of CAP from powdered eggs

The first step in the existing method ([28–30]; Fig. 1A) is the extraction of samples with 4% NaCl and ethyl acetate. However, in our hands, this step caused heavy emulsion formation resulting in considerable difficulties with separation and delays in analysis time. Steps shown in Fig. 1B did not form emulsion. Incurred freeze-dried samples were extracted by steps shown in Fig. 1B, which is a slight modification of the existing method for tissues.

2.6. Preparation of powdered spiked samples

A 1-g amount of freeze-dried control albumen or yolk, after mixing with a spatula, was weighed into a 50-ml Falcon centrifuge tube. Samples were spiked with the appropriate volume of unlabelled or labelled [^{14}C]CAP solution to produce samples containing 2, 10, 25 and 50 ng/g (ppb). Samples were mixed gently for even distribution and allowed to stand for 60 min prior to extraction. Spiked samples were extracted by the method detailed in Fig. 1B. Extracts containing [^{14}C]CAP were analyzed first by LSC followed by GC. Similarly, the whole liquid egg (albumen and yolk mixed together) was spiked with a known amount of unlabelled CAP and recovery studies were conducted. Recovery study was repeated with powdered whole eggs as well.

Liquid albumen and yolk of control eggs were spiked with a known amount of [^{14}C]CAP and freeze-dried as detailed above to observe any loss of ^{14}C during this process.

2.7. Derivatization

Derivatization conditions were established using [^{14}C]CAP. [^{14}C]CAP (equivalent to 2, 10, 50 ppb) was transferred to a centrifuge tube, Sylon HTP (200 μl) added to the tube, tube heated at 65°C for 20 min, volume reduced under gentle stream of nitrogen, residue redissolved in hexane and radioactivity measured before analysis by GC. Data showed that very little radioactivity was lost during the entire derivatization process. This procedure was used to derivatize extracts from spiked and actual samples.

2.8. Gas chromatograph and accessories

A Model 8500 Perkin-Elmer gas chromatograph equipped with (i) a DB-1701 column (30 m × 0.32 mm I.D., 25 μm film thickness), (ii) splitless injector with silanized glass insert, (iii) an electron-capture detector, (iv) a data handling system (PE Nelson 900 Series interface), and an autosampler (PE AS-100) was used. GC operating conditions were: injector at 280°C; detector at 330°C; oven temperature programmed from 100°C (0.5 min equilibrium time) to 250°C (at 20°C/min) and finally to 280°C (at 5°C/min) and hold for 15 min; carrier gas P-5 (methane–argon, 5:95) flow-rate 3 ml/min plus 57 ml/min make-up gas for a total of 60 ml/min.

2.9. Liquid scintillation counter

A Beckman scintillation System Model LS 3801 was used for radioactivity measurement using an external standard and correction for quenching.

2.10. Statistical analysis

All data were statistically analyzed using Microsoft Excel software (Version 5.0, Analysis ToolPak; Microsoft, Redmond, WA, USA). The relative standard deviation (R.S.D.) was calculated using the formula: standard deviation × 100/mean.

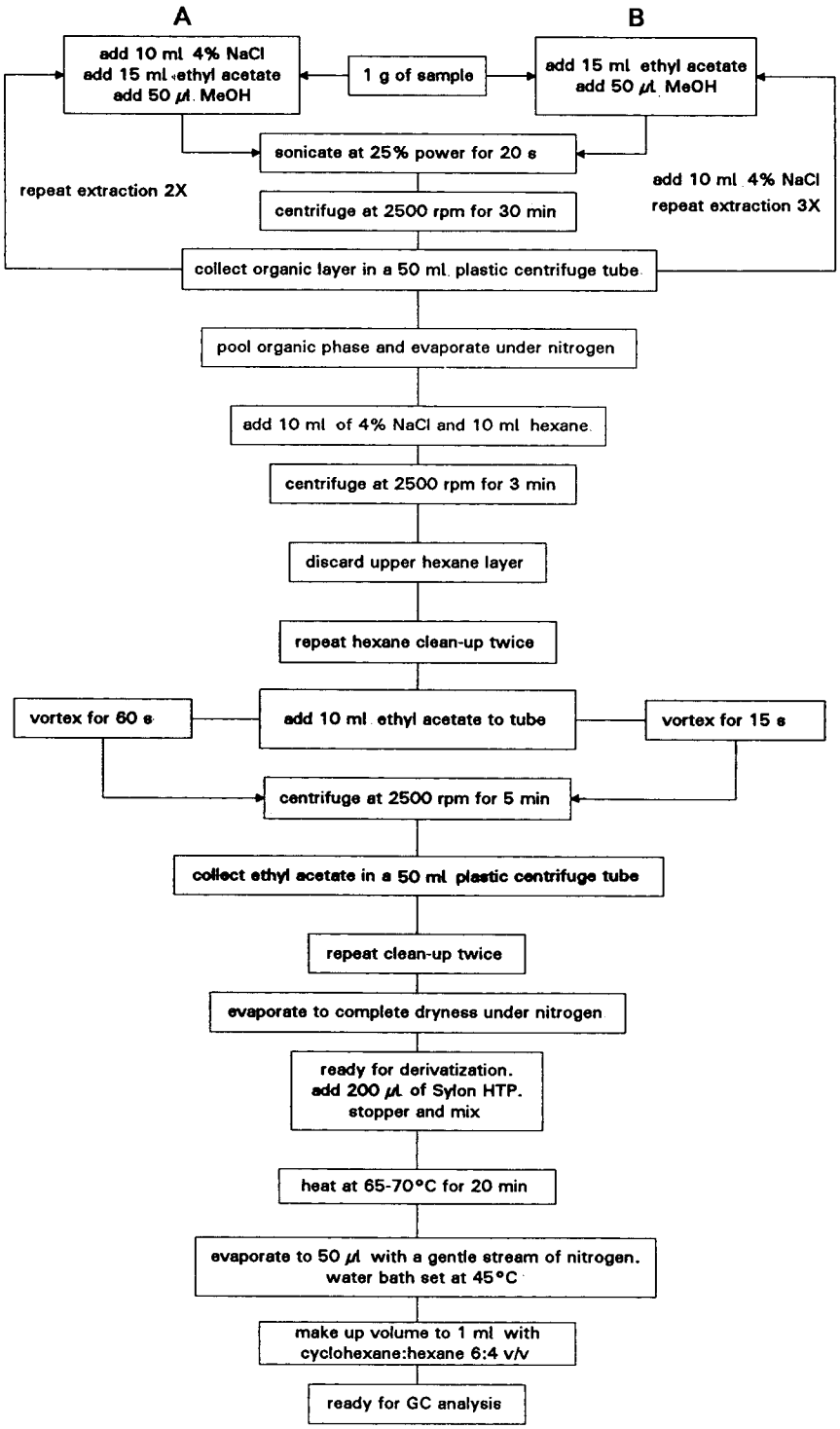

Fig. 1. Techniques for the extraction, isolation and derivatization of chloramphenicol from eggs. (A) Existing method; (B) modified method.

2.11. Miscellaneous supplies

Further supplies used were: (a) glassware: volumetric flasks, pipettes, disposable pipettes, 15-ml centrifuge tubes; (b) polypropylene centrifuge tubes; (c) autosampler vials/caps/crimper; (d) microsyringes: Hamilton various sizes; (e) solvent evaporator N-Evap Model 111 (Organomation Associates); (f) mixer: Vortex, Braun adjustable; (g) centrifuge: IEC clinical; (h) balances: (Mettler AE 160, BB 2400).

3. Results and discussion

CAP is a broad-spectrum antibiotic which is highly effective in treating many diseases of farm animals. However, CAP showed adverse reactions in humans and was banned (USA and Canada) from use on milk, meat and egg-producing animals. Since CAP is less expensive and possesses high efficacy for treatment of animal diseases that are not resistant to other registered antibiotics, there exists a situation where CAP can be misused and/or abused. In recent years, considerable efforts have been made world-wide to develop efficient and cost-effective methods to monitor CAP residues in milk, meat and eggs to protect humans from its severe adverse effect.

Currently, CAP in eggs and egg products are analyzed following the method described for determination of CAP in milk and tissues [28–30]. As part of the ongoing effort of monitoring drug residues in eggs, we reviewed all available techniques. One of the major difficulties of the existing solvent extraction technique is the formation of heavy emulsion. This step is difficult, tedious and time consuming.

In our hands, the use of the existing extraction technique as detailed in Fig. 1A gave poor and inconsistent recoveries of spiked CAP from powdered eggs (freeze-dried). It is assumed that this was, in part, due to the formation of heavy emulsion during extraction. To overcome the emulsion formation, we investigated various alternatives and observed that emulsion formation can be eliminated, if the first extraction is done with ethyl acetate without 4% NaCl, followed by further extraction with 4% NaCl. When our investigation was already completed, Kijak [21] and Munns et al. [31] also reported extraction of CAP from milk and shrimp first with ethyl acetate without the use of 4% NaCl. In addition, the extraction for 15 s is sufficient rather than 1 min. The modified method is shown in Fig. 1B. Recoveries of spiked [^{14}C]CAP from powdered albumen and yolk by two methods are recorded in Table 1. The recoveries of spiked CAP from

Table 1
Recoveries of [^{14}C]CAP from spiked powdered eggs by methods described in Fig. 1A and B

Sample	Spiked at ng/g (ppb)	Recoveries (%)[a]			
		Fig. 1A		Fig. 1B	
		LSC	GC	LSC	GC
Albumen	50	52.7 ± 9.1	104.5 ± 15.3	86.5 ± 5.2	70 ± 4.1
	25	45.4 ± 3.3	39.9 ± 9.3	79.7 ± 3.0	73.7 ± 10.9
	10	72.0 ± 11.1	51.4 ± 10.1	85.3 ± 6.0	73.1 ± 7.0
	2	54.3 ± 28.7	70.0 ± 30.3	101.5 ± 12.7	94.7 ± 11.3
Yolk	50	86.1 ± 2.4	71.5 ± 17.6	79.1 ± 11.0	70.3 ± 5.8
	25	58.2 ± 3.5	33.7 ± 4.5	70.6 ± 6.1	68.2 ± 20.1
	10	87.3 ± 1.5	86.0 ± 14.7	87.6 ± 3.0	72.3 ± 3.5
	2	82.6 ± 3.8	142.4 ± 10.1	74.3 ± 2.7	76.5 ± 13.1

[a] Mean ± R.S.D., $n = 3–5$.

Table 2
Recoveries of spiked CAP from the whole egg (liquid and powdered)

Sample	Spiked at ng/g	Recoveries (%)[a]
Liquid	25	79.0 ± 3.5
	10	84.0 ± 6.7
	5	77.5 ± 7.7
	2	106.0 ± 22.0
Powder	25	73.0 ± 7.0
	10	79.0 ± 6.0
	5	92.0 ± 3.0
	2	87.0 ± 7.0

[a] Mean ± R.S.D., $n = 6$.

Table 3
Effect of freeze-drying of eggs on [^{14}C]CAP residues

Sample	Spiked at ng/g[a]	Recoveries (%)[b]
Albumen	50	103.5 ± 5.1
	25	100.6 ± 7.6
	10	99.6 ± 7.2
	5	82.9 ± 12.1
	2	109.1 ± 5.9
Yolk	50	109.1 ± 6.6
	25	108.9 ± 5.9
	10	90.5 ± 9.0
	5	94.5 ± 9.8
	2	96.6 ± 2.7

[a] Liquid albumen and yolk were spiked with a known amount of [^{14}C]CAP, mixed with a glass pipette and freeze-dried in a commercial freeze-drier for 4 days.
[b] Mean ± R.S.D., $n = 5$ or 6.

powdered egg samples shown in Table 2 have greater reproducibility (R.S.D.) for the modified method (Fig. 1A). The data from two procedures, when compared used an *F*-test-two-samples for variance (Microsoft Excel, 1993), show a significant difference $p = 0.084$ and 0.003 for albumen and yolk, respectively. The calibration curves, representing mean peak areas versus concentration, show excellent linearity for concentration from 2 to 200 pg. The correlation coefficient (r) was 0.9995, and the limit of detection was established at 0.5 ppb (twice the noise level).

Recoveries of CAP (Table 2) from liquid and powdered whole eggs show no significant difference in the two types of egg handling. However, the advantage of powdered eggs is that they can be stored for a long period and be used for quality control.

No information is available on the stability of CAP during the freeze-drying process. Our data in Table 3 showed that there was no loss of CAP during the freeze-drying process.

Chromatograms of standard CAP and extracts of blank albumen and yolk after derivatization with Sylon HTP are shown in Fig 2. Silylated CAP elutes in a reasonable time of under 15 min. The blank samples (albumen and yolk) did not exhibit significant interferences (less than twice the baseline noise level) in that region.

A few pooled powdered eggs (albumen and yolk separately) were analyzed to check the validity of the modified method (Fig. 1B). Data shown in Table 4 are based on liquid eggs. The average water content in albumen was 70.5%, and that in yolk was 42.3%. These values were used in recalculating the concentration of CAP in incurred liquid eggs. The literature value for water content is 88 and 56% for albumen and yolk, respectively [32]. Data in Table 4 showed that residues in yolk were considerably higher than albumen. It also appears that residues of CAP in albumen decreased rapidly when treated water supply was removed. However, the residues in yolk appeared to persist. A similar result was reported by Samouris et al. [25]. This may, in part, be due to lipid content of yolks. It is well documented that lipophilic substances, such as pesticides having halogen moiety, are deposited preferentially in yolk [33,34].

A Robotic extraction technique was developed with spiked samples which was validated by analysis of 60 albumen and yolk samples containing incurred residues from the feeding trial. Data will be reported separately [35].

4. Conclusions

On the basis of data compared here for the existing and modified extraction techniques, it is

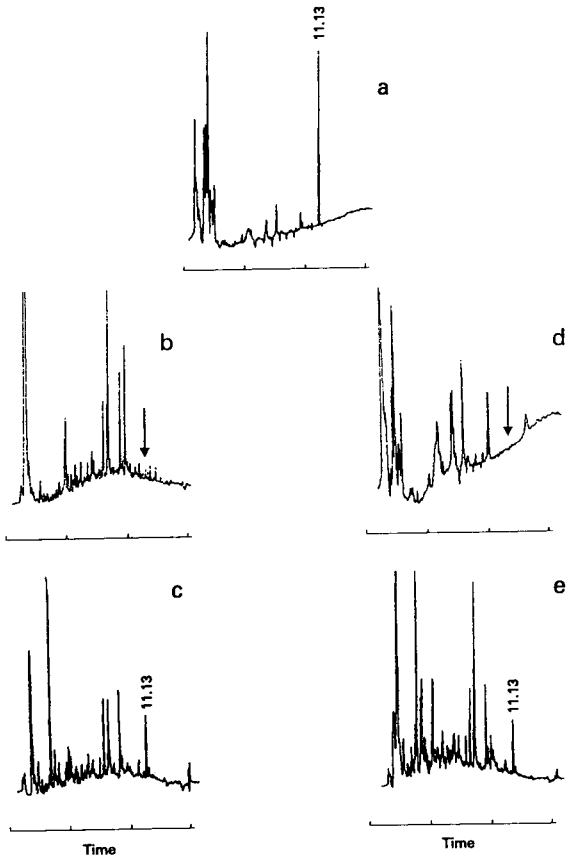

Fig. 2. Gas chromatograms after treatment with silylating agents: (a) CAP standard; extract of (b) blank albumen, (c) incurred albumen; extract of (d) blank yolk, (e) incurred yolk.

concluded that the modified technique is superior and is reproducible. Any advancement leading to fast, accurate, reproducible, environmentally friendly and less costly method will always be welcomed. One factor which is very important in any method development is the availability and affordability of the analytical system by developing countries for monitoring food supplies before they are exported, thus safeguarding the health of consumers globally. We believe that the modified method has the potential for being employed routinely to monitor CAP residues in eggs and other biological samples worldwide.

References

[1] H.C. Meissner and A.L. Smith, *Pediatrics*, 64 (1979) 348.
[2] A.G. Gilman, L.S. Goodman and A. Gilman, in L.S. Goodman and A.S. Gilman (Editors), *The Pharmacological Basis of Therapeutics*, McMillan, New York, 6th ed., 1980.
[3] H.M. Feder Jr., C. Osler and E.G. Maderazo, *Rev. Infec. Disease*, 3 (1981) 479.
[4] F.T. Fraunfelder, G.C. Bagby, Jr. and D.J. Kelly, *Am. J. Opthalmol.*, 93 (1982) 356.
[5] J.A. Settepani, *J. Am. Vet. Med. Assoc.*, 184 (1984) 930.
[6] R.H. Whitlock, *J. Am. Vet. Med. Assoc.*, 185 (1984) 210.
[7] C.S. Sisodia, R.H. Dunlop, V.S. Gupta and L. Taksas, *Am. J. Vet. Res.*, 34 (1973) 1147.

Table 4
Concentration of CAP in albumen and yolk (liquid basis)[a] of eggs from laying hens given CAP in water

Day[b]	Concentration in water (mg/ml)	Albumen (ng/kg)[c]	Yolk (ng/kg)[c]
8	25	26.55 ± 4.14	78.02 ± 4.90
7	50	65.55 ± 0.23	166.28 ± 6.63
8	100	271.89 ± 2.77	477.81 ± 7.73
− 2[d]	200	26.69 ± 9.78	1834.65 ± 7.35

[a] Data from analysis of powdered incurred albumen and yolk were converted to liquid basis.
[b] Refers to number of days from the start of treatment of CAP in water.
[c] Mean ± R.S.D., $n = 4$.
[d] Refers to days after water was removed. Laying hens had free access to drinking water containing CAP for 10 continuous days.

[8] K.J. Varma, B.S. Paul and R.C. Gupta, *J. Vet. Pharm. Ther.*, 3 (1980) 151.
[9] G.E. Burrows, P.B. Barto, B. Martin and M.L. Tripp, *Am. J. Vet. Res.*, 44 (1984) 1053.
[10] A.P. Knight, *J. Am. Vet. Med. Assoc.*, 178 (1981) 309.
[11] H. Trolldenier, *Monatsh. Veterinaemed.*, 39 (1984) 505.
[12] G.C. Brander and D.M. Pugh, *Veterinary Applied Pharmacology and Therapeutics*, Edition II, Baillière Tindall, London, 1971, Ch. 22.
[13] C.S. Sisodia and R.H. Dunlop, *Can. Vet. J.*, 13 (1972) 263.
[14] L.M. Crawford, *Mod. Vet. Pract.*, 65 (1984) 419.
[15] D. Walter-Toews, S.W. Martin and A.H. Meek, *Can. Vet. J.*, 27 (1986) 17.
[16] Joint FAO/WHO Expert Committee on Food Additives, *12th Report; Specifications for the Identity and Purity of Food Additives and Their Toxicological Evaluation: Some Antibiotics (WHO Tech. Rep. Ser.*, No. 430), World Health Organization, Geneva, 1969.
[17] E.W. Allen, *J. Assoc. Off. Anal. Chem.*, 68 (1985) 990.
[18] M. Ashton, *J. Liq. Chromatogr.*, 12 (1989) 1719.
[19] C. van der Water, D. Tebbal and N. Haagsma, *J. Chromatogr.*, 428 (1989) 208.
[20] L. Weber, *J. Chromatogr. Sci.*, 28 (1990) 501.
[21] P.J. Kijak, *J. Assoc. Off. Anal. Chem. Int.*, 77 (1994) 34.
[22] L.A. van Ginkel, H.J. van Rossum, P.W. Zoontjes, H. van Blitterswijk, G. Ellen, E. van der Heeft, A.P.J.M. de Jong and G. Zomer, *Anal. Chim. Acta*, 237 (1990) 61.
[23] W.J. Blanchflower, A. Cannavan, R.J. McCracken, S.A. Hewitt and D.G. Kennedy, *Proceedings of the EuroResidue II Conference, Veldhoven, Netherlands, 3–5 May 1993*, p. 196.
[24] B. Delepine, P. Saunders, M. Dagorn and M. Laurentie, *Proceedings of the EuroResidue II Conference, Veldhoven, Netherlands, 3–5 May 1993*, p. 261.
[25] G. Samouris, B. Nathanael, H. Tsoukali-Papadapoulou and N. Papadimitriou, *Vet. Human Toxicol.*, 35 (1993) 406.
[26] M. Ramos, Th. Reuvers, A. Aranda and J. Gomez, *J. Liq. Chromatogr.*, 17 (1994) 385.
[27] M. Gips, M. Bridzy, S. Barel and S. Soback, *Proceedings of the EuroResidue II Conference, Veldhoven, Netherlands, 3–5 May 1993*, p. 313.
[28] US Department of Agriculture, Food Safety and Inspection Services, *Chemistry Laboratory Guidebook, Section 5.023*, US Government Printing Office, Washington, DC, 1986, pp. 5-127 and 5-128.
[29] *Methods Manual, Method CHL-SP0332*, Health of Animals Laboratory, Agriculture and Agri-Food Canada, Saskatoon, 1990.
[30] *Internal Report Validation of Method for Chloramphenicol in Eggs and Egg Products*, Laboratory Services Division, Agriculture and Agri-Food Canada, Ottawa, 1991.
[31] R.K. Munns, D.C. Holland, J.E. Roybal, J.M. Storey, A.R. Long, G.R. Stehly and S.M. Plakas, *J. Assoc. Off. Anal. Chem. Int.*, 77 (1994) 596.
[32] O.J. Cotterill, in W.J. Stadelman and O.J. Cotterill (Editors), *Egg Science and Technology*, Food Products Press (The Howarth Press), New York, 3rd ed., 1990, p. 219.
[33] M.R. Redshaw and B.K. Follet, in B.M. Freeman and P.E. Lake (Editors), *Poultry Science Symposium 8, Egg Formation and Production*, British Poultry Science, Edinburgh, 1972, p. 35.
[34] M.H. Akhtar, R.M.G. Hamilton and H.L. Trenholm, *J. Agric. Food Chem.*, 33 (1985) 610.
[35] A. Sauve, C. Barry and M.H. Akhtar, in J.R. Strimaitis and J.P. Helfrich (Editors), *Advances in Laboratory Automation —Robotics*, Zymark, Hopkinton, MA, 7 (1995) 137.

ELSEVIER

Journal of Chromatography A, 696 (1995) 131–138

JOURNAL OF CHROMATOGRAPHY A

Determination of the relative amounts of the B and C components of neomycin by thin-layer chromatography using fluorescence detection

E. Roets*, E. Adams, I.G. Muriithi, J. Hoogmartens

Laboratorium voor Farmaceutische Chemie en Analyse van Geneesmiddelen, Faculteit Farmaceutische Wetenschappen, Katholieke Universiteit Leuven, Van Evenstraat 4, B-3000 Leuven, Belgium

First received 20 September 1994; revised manuscript received 19 December 1994; accepted 20 December 1994

Abstract

The determination of the relative amounts of the B and C components of neomycin sulphate by thin-layer chromatography using silica gel plates from Whatman as the stationary phase is described. The mobile phase consisted of methanol–20% (m/v) sodium chloride solution (15:85). Fluorescence detection was performed after derivatization with 4-chloro-7-nitrobenzo-2-oxa-1,3-diazole. The influence of different parameters on the separation was investigated. A number of commercial samples was analysed using this method and the results were compared with results obtained with ion-exchange chromatography and ninhydrin colorimetric detection, which is the official method prescribed by the European Pharmacopoeia. The described method is much easier to perform than the official method.

1. Introduction

Neomycin is a widely used broad spectrum water-soluble aminoglycoside antibiotic produced during fermentation of *Streptomyces fradiae* [1]. It inhibits the growth of Gram-positive and Gram-negative bacteria. It has a narrow therapeutic range, is potentially toxic like other aminoglycosides and may cause ototoxicity and nephrotoxicity.

Neomycin sulphate is mainly composed of a mixture of neomycin B (Fig. 1) and its stereoisomer neomycin C [2]. Neomycin with a content of less than 3% neomycin C is called framycetin. Another minor component, neomycin A, which was isolated from the mixture [3] and proved to be identical with neamine, can be obtained by partial hydrolysis of neomycins B or C [4,5]. Small amounts of other constituents, less than 1%, are also present in commercial samples. These impurities, formerly called neomycins D, E and F were identified as paromamine, paromomycin I and paromomycin II, respectively [6]. The antimicrobial potency of neomycin C is lower than that of neomycin B and it varies with the microorganism and experimental conditions used in the microbiological assay. The difference in activity necessitates a limit and control of neomycin C in commercial samples [7]. Neamine has no antimicrobial activity. The

* Corresponding author.

0021-9673/95/$09.50
SSDI 0021-9673(94)01272-5

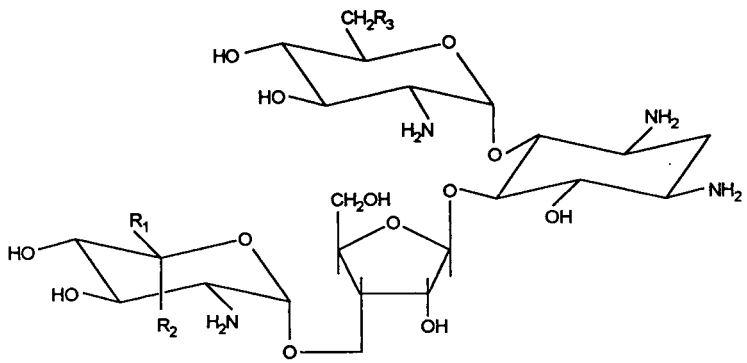

	R_1	R_2	R_3
Neomycin B :	H	CH_2NH_2	NH_2
Neomycin C :	CH_2NH_2	H	NH_2
Paromomycin I :	H	CH_2NH_2	OH
Paromomycin II :	CH_2NH_2	H	OH

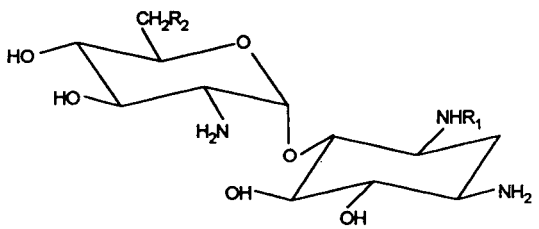

	R_1	R_2
Neamine	H	NH_2
Paromamine	H	OH

Fig. 1. Structures of different neomycin components.

European Pharmacopoeia limits the amount of neomycin C to 3–15% [8]. The United States Pharmacopeia does not distinguish neomycin and framycetin and therefore does not limit neomycin C in a separate test [9].

Chromatographic separation of the stereoisomers neomycins B and C is quite difficult. Ion-exclusion liquid chromatography (IELC) [10], liquid chromatography (LC) on normal phase after dinitrophenylation [11] or gas–liquid chromatography after trimethylsilylation [12] have been described for determination of neomycins

B and C. The IELC method was further studied by Decoster et al. [13] and this method was finally chosen by the European Pharmacopoeia to determine the neomycin C content [8]. More recently LC methods on normal phase combined with pre-column derivatization [14,15] and on reversed phase with post-column derivatization [16] were published. Meanwhile the European Pharmacopoeia [8] method proved to be very laborious and difficult to perform: the column must be packed in the laboratory, the stationary phase is not easily available, the stationary phase is not stable, the efficiency is low, the separation time is about 2 h and the derivatization of the fractions with ninhydrin is carried out manually. Thin-layer chromatographic (TLC) separation was first described on acid-treated carbon black plates, detection was performed by autobiography [17]. Kovacs-Hadady [18] reported on the influence of the interaction of silica gel with metal ions. When the acidic silanol sites were partially saturated with metal ions from the mobile phase, the aminoglycosides migrated while by developing with water no migration occurred. The separation of the components depended on the degree of saturation of the silanol groups by the metal ions [18]. Quantitative densitometric TLC which requires no prederivatization has not been reported until very recently [19]. Quantitative results for different neomycins were not reported in this paper. When this method was tried out in our laboratory, the separation was not as good as shown and it was impossible to determine small amounts of neomycin C (3% and less) which is necessary to distinguish neomycin and framycetin.

In this work a TLC method is described for the quantitative determination of the relative amounts of neomycins B and C. The method is based on that described by Kovacs-Hadady [18]. A wide-pore silica gel was used as the stationary phase. The mobile phase consisted of methanol–20% (m/v) sodium chloride solution (15:85). Detection was performed after derivatization with 4-chloro-7-nitrobenzo-2-oxa-1,3-diazole (NBD-Cl). The different components were quantified by densitometry using the fluorescence mode. The results for the different samples are compared with those obtained with the official European Pharmacopoeia method.

2. Experimental

2.1. Chemicals

Methanol and acetone, *n*-hexane and liquid paraffin, sodium chloride of analytical grade and NBD-Cl were all from Janssen Chimica (Beerse, Belgium). Water was distilled twice from glass apparatus. Precoated silica gel layers on glass (20×20 cm) 150A K5 and 60A K6 were obtained from Whatman (Maidstone, UK). Other precoated silica gel layers were: DC-fertigplatten Kieselgel 60 (Merck, Darmstadt, Germany), Alugram SilG and DC-fertigplatten SilG 25 (Macherey–Nagel, Düren, Germany), Si 250 (Baker, Phillipsburg, NJ, USA), Silica platten (Woelm, Eschwege, Germany) and Stratocrom SIF_{254} (Carlo Erba, Milan, Italy). Silanized silica gel layers, DC-fertigplatten Kieselgel 60 silanisiert, were obtained from Merck.

2.2. Standards and samples

Neomycin B sulphate, neomycin C sulphate and neamine hydrochloride standards were prepared in the laboratory from commercial samples, as described [20]. Mixtures of the neomycins B and C laboratory standards ranging from 1% (m/m) to 50% neomycin C (m/m) in neomycin B were prepared. Commercial samples were obtained from Sifa (Paris, France), Roussel-Uclaf (Romainville, France), Upjohn (Kalamazoo, MI, USA) and Takeda (Osaka, Japan). Other aminoglycoside antibiotics used in the development of the TLC method were: paromomycin sulphate from Carlo Erba (Italy), gentamicin sulphate from Pierrel (Milan, Italy), kanamycin sulphate from Continental Pharma (Brussels, Belgium), kanamycin B sulphate from the European Pharmacopoeia (Strasbourg, France), tobramycin from Alcon (Puurs, Bel-

gium), apramycin from Eli Lilly (Indianapolis, IN, USA) and amikacin from Myers Squibb (Syracuse, NY, USA). The structures of these aminoglycosides can be found in some reviews [21,22].

2.3. TLC method

The TLC plates were used as received. A narrow band of the layer was removed from both sides of the plate, supposed to be in vertical position during development. Samples were dissolved in water in a concentration of 4.0 mg/ml. Aliquots of 1.0 μl were applied to the TLC plate with a microsyringe (Hamilton, Bonaduz, Switzerland) starting at 10 mm from the edge and at 20 mm from the bottom of the plate. The distance between the lanes was 10 mm. The chromatographic chamber was lined with paper and equilibrated with the mobile phase methanol–20% (m/v) sodium chloride solution (15:85) for at least 1 h prior to use. The plate was developed over a distance of 12 cm with a migration time of about 2 h. After development the plate was dried in an oven at 105–110°C (30 min). Detection of the spots was performed by dipping horizontally for 4 s in a laboratory-made container, filled with a solution of 60 mg NBD-Cl in 300 ml of methanol–acetone (1:1). The plate was allowed to dry on the bench for 5 min and was heated in an oven at 80°C for 30 min to complete the derivatization reaction. The excess reagent was removed by developing the plate twice in methanol–acetone (1:1) over a distance of 12 cm. The plate was dried in an oven at 80°C for 5 min. The sensitivity was enhanced by dipping the plate for 1 s in a 30% (v/v) solution of liquid paraffin in *n*-hexane. The plate was dried in an oven at 80°C for 5 min. Greenish-yellow fluorescent spots on a colourless background were obtained.

The chromatograms were analysed with a CS-990 TLC scanner (Shimadzu, Kyoto, Japan) using the following parameters: linear scan, scan step in the *y*-direction 0.05 mm, beam size 6 mm × 0.4 mm, fluorescence mode with emission at $\lambda = 475$ nm and filter 4; linearizer off, background correction on; drift-line integration 0.05. The ratio of the peak areas of the two isomers was compared to the ratios obtained for the mixtures of the house standards.

3. Results and discussion

3.1. Influence of the brand of silica gel

The different brands of silica gel plates were examined for their selectivity towards the separation of neomycins B and C. Precoated plates from Macherey–Nagel and Carlo Erba gave insufficient retention and the spots moved close to the front. The layers from Merck and Baker gave separation with considerable streaking. Both the silica gels from Whatman gave good separation of the two isomers. Since the separation and spot shape on Whatman K5 plates with 150 Å pores were better, these plates were preferred. Experiments with silica gel from Merck with pore sizes of 60, 200 and 1000 Å indicated that the use of silica gel with wider pores did not improve the separation.

The silanized silica gel layers from Merck gave results comparable to those obtained with bare silica gel. The difference in result between the different brands of plates may be due to the quality of the silica gel and the nature of the binder.

3.2. Composition of the mobile phase

Different salts such as sodium chloride, sodium bromide, sodium fluoride, lithium chloride, sodium bromide and triethylammonium acetate were used to prepare the mobile phase. Sodium chloride was found to be the best in terms of symmetry of the spots and retention characteristics. Decreasing the sodium chloride concentration deteriorated the symmetry, but with higher concentrations the baseline noise increased. A final concentration of 20% was adopted. An explanation for the mechanism was given by Kovacs-Hadady. The retention is connected with the adsorption of the metal ions on the surface of the stationary phase. As long as the surface of the silica gel layer is not saturated by adsorbed

metal ions, the free silanol groups interact strongly with the basic aminoglycosides [18]. The R_F values decreased with increase of the methanol content but the resolution decreased at the same time. A final concentration of 15% was selected. Substitution of methanol by ethanol did not improve the separation. Good separations were obtained after a saturation time of the chromatographic chamber for at least 1 h prior to use. Activation of the plate at 105°C for 30 min did not improve the separation. Predevelopment of the plate with methanol, followed by drying at 105°C for 30 min did affect neither the separation nor the noise during scanning. The plates were always developed at room temperature over a distance of 12 cm. Table 1 shows the R_F values for different neomycins and some related aminoglycoside antibiotics. With the described method the relative amount of paromomycin II in commercial samples of paromomycin sulphate can also be determined.

3.3. Resolution and peak symmetry

The resolution between the peaks of neomycins B and C and their symmetry factors were measured using a mixture of equal amounts of both components. The resolution was 1.7 and the symmetry factor of the peak of neomycin B was 1.2 and that of neomycin C 1.1.

Table 1
R_F values of the different neomycins and some related aminoglycoside antibiotics

Aminoglycoside antibiotic	R_F
Neomycin A	0.33
Neomycin B	0.24
Neomycin C	0.16
Paromamine	0.59
Paromomycin I	0.51
Paromomycin II	0.40
Kanamycin A	0.47
Kanamycin B	0.21
Amikacin	0.68
Tobramycin	0.30
Apramycin	0.47
Gentamicin	0.53, 0.57, 0.62

3.4. Detection method

Since fluorescence is more sensitive and gives higher slopes than colorimetric procedures, a fluorogenic technique was investigated. Fluorescamine was not investigated as the fluorescence decays rapidly. NBD-Cl, which reacts only with primary and secondary amines, while yielding a non-fluorescent hydrolysis product, was found to be the fluorogenic reagent of choice [23]. The NBD-Cl solution used may be stored in the dark at room temperature for at least two months. Horizontal dipping using a 0.02% solution of NBD-Cl in methanol–acetone (1:1) and a dipping time of 4 s, was determined to be optimal. The heating time to complete the derivatization was varied from 20 to 60 min at 80°C. A reaction time of 30 min was proved satisfactory. Higher temperature did not increase the response. Spraying the plate instead of dipping has the drawback that unstable baselines are obtained and integration is difficult to standardize. The excess NBD-Cl was removed by developing the plate twice in a mixture methanol–acetone (1:1). Treatment of the plate with sodium acetate or sodium carbonate as buffer before reaction with NBD-Cl was described to enhance the sensitivity [24]. However, the loading of more salt on the plate increased the baseline noise during the scanning procedure and therefore this technique was not retained. Measurements at 475 nm afforded the highest response. By immersing the plate for 1 s in a hexane solution of liquid paraffin, the fluorescence was enhanced by a factor of about 1.5 [25]. When stored in the dark and protected from dust the fluorescence remained stable for several months.

3.5. Linearity and detection limits

A calibration curve was prepared from mixtures containing 1% neomycin C up to 50% neomycin C. The linearity was examined and the following results were found: $y = -0.10860 + 1.007699x$; $r = 0.9988$; $S_{y,x} = 0.1247$, where $y =$

ratio neomycins C/B prepared; x = ratio neomycins C/B found; r = coefficient of correlation; $S_{y,x}$ = standard error of estimate; number of concentrations examined = 11; number of scans per concentration = 3. These experiments were performed on one single plate. In the assay of commercial samples, a calibration curve was not used, but standard mixtures, applied on the same plate, were used in a single-point calibration.

For an application of 4 μg of the sample to the plate, the limit of detection was about 1% (m/m) (0.04 μg), which is similar to that obtained with the official European Pharmacopoeia method.

3.6. Assay of commercial samples

Several samples of neomycin and framycetin were assayed using the described method. A typical chromatogram is shown in Fig. 2. To calculate the percentage of neomycin C, the nearest chromatogram of a standard mixture was used. The C/B ratio of the standard mixtures were adapted to the ratio present in the samples. The results are shown in Table 2, which also contains figures calculated by normalisation and figures which were mentioned previously [13] for a number of the neomycin samples, using the European Pharmacopoeia method: IELC, detection with ninhydrin and calculation by normalization. For the TLC method, the values obtained by normalisation are smaller than those obtained by calculation against a standard. The latter correspond well with the figures obtained with the official method. This would suggest that the derivatization reaction on the plate is less complete for neomycin C than for neomycin B. The amount of neomycin C in older neomycin samples varies from 9.4 to 39.9%. In more recent neomycin samples the neomycin C content is between 7 and 13%. The relative standard deviation (R.S.D.) for $n = 10$ is 6–8%. In experiments with the official method [8] the R.S.D. for a framycetin sample containing 1.4% of neomycin C was 16% ($n = 3$). The neomycin samples comply with the European Pharmacopoeia limits (3–15% C). The framycetin samples examined also comply with European Pharmacopoeia limits (<3% C).

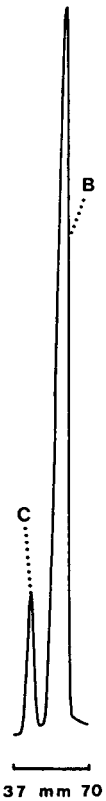

Fig. 2. Fluorescence scan of a typical chromatogram of commercial neomycin sulphate.

4. Conclusions

Neomycins B and C can be separated by TLC on Whatman plates. The method allows to determine the composition of commercial samples. The results show that the qualitative composition may vary over a wide range. The results confirm the need for a limit test for the composition in official texts such as pharmacopoeias. The proposed method can be used as an alternative to IELC followed by ninhydrin colorimetry, which is the official method prescribed by the European Pharmacopoeia.

Table 2
Relative amounts of neomycin C in commercial samples

Sample	Method		
	TLC–fluorescence detection		IELC–ninhydrin detection [13]
	With standards	With normalization	
Old neomycin samples			
U.XZ-336	10.3	7.8	9.8
S. 52001	39.9	30.9	37.8
U. TRO-32	9.4	6.9	9.6
R. 7S-1251	10.2	7.9	10.0
R. 9S0581	15.0	11.6	15.3
St. Nat.	29.8	23.1	27.0
G. 58510	18.5	14.1	19.1
G. S.51009	32.4	25.1	30.0
T. H5XHTN4	15.4	11.9	16.9
Recent neomycin samples			
04/0393 A	8.3	6.4	
30/062 A	10.6	9.0	
939006 A	10.4	10.0	
939005 A	8.7	8.3	
40/418 A	11.3	8.9	
30/042 A	12.2	10.7	
Framycetin samples			
93/0420 A	1.8	1.1	
940/370 A	1.8	1.9	
7SO2224 B	1.3	0.7	
9SO238	1.1	0.6	
9SO425	1.1	0.6	

Acknowledgements

Mrs. A. Decoux is acknowledged for skillful secretarial assistance. The Belgian National Fund for Scientific Research is acknowledged for financial support.

References

[1] S.A. Waksman and H.A. Lechevalier, *Science*, 109 (1949) 305.
[2] J.D. Dutcher, N. Hosansky, M. Donin and O. Wintersteiner, *J. Am. Chem. Soc.*, 73 (1951) 1384.
[3] R.L. Peck, C.E. Hoffine, P. Gale and K. Folkers, *J. Am. Chem. Soc.*, 71 (1949) 2590.
[4] J.D. Dutcher and M.N. Donin, *J. Am. Chem. Soc.*, 74 (1952) 3420.
[5] B.E. Leach and C.M. Teeters, *J. Am. Chem. Soc.*, 74 (1952) 3187.
[6] E.J. Hessler, H.K. Jahnke, J.H. Robertson, K. Tsuji, K.L. Rinehart and W.T. Shier, *J. Antibiot., Ser. A*, 23 (1970) 464.
[7] H. Maehr and C.P. Schaffner, *Anal. Chem.*, 36 (1964) 104.
[8] *European Pharmacopoeia*, Maisonneuve, Sainte Ruffine, France, 2nd ed., 1983.
[9] *United States Pharmacopeia XXII*, United States Pharmacopeial Convention, Rockville, MD, 1989.
[10] S. Inouye and H. Ogawa, *J. Chromatogr.*, 13 (1964) 536.
[11] K. Tsuji, J.F. Goetz, W. Van Meter and K.A. Gusciora, *J. Chromatogr.*, 175 (1979) 141.
[12] M. Margosis and K. Tsuji, *J. Pharm. Sci.*, 62 (1973) 1836.

[13] W. Decoster, P. Claes and H. Vanderhaeghe, *J. Chromatogr.*, 211 (1981) 223.
[14] P. Helboe and S. Kryger, *J. Chromatogr.*, 235 (1982) 215.
[15] K. Tsuji and K.M. Jenkins, *J. Chromatogr.*, 369 (1986) 105.
[16] J.A. Apffel, J. Van der Louw, K.R. Lammers, W.Th. Kok, U.A.Th. Brinkman, R.W. Frei and C. Burgess, *J. Pharm. Biomed. Anal.*, 3 (1985) 259.
[17] T.F. Brodasky, *Anal. Chem.*, 35 (1963) 343.
[18] K. Kovacs-Hadady, *J. Planar Chromatogr.*, 2 (1989) 211.
[19] W. Funk, T. Küpper, A. Wirtz and S. Netz, *J. Planar Chromatogr.*, 7 (1994) 10.
[20] G. Nominé and L. Penasse, *US Pat.*, 3 062 807 (1962); *Chem. Abstr.*, 58 (1963) 3277.
[21] K.L. Rinehart and L.S. Shield, in K.L. Rinehart and T. Suami (Editors) , *Aminocyclitol Antibiotics*, American Chemical Society, Washington, DC, 1980.
[22] D.A. Cox, K. Richards and B.C. Ross, in P. Sammes (Editor), *Topics in Antibiotic Chemistry*, Vol. I, Ellis Horwood, Chichester, 1977.
[23] D.M. Benjamin, J.J. McCormack and D.W. Gump, *Anal. Chem.*, 45 (1973) 1531.
[24] P. Kabasakalian, S. Kalliney and A.W. Magatti, *Anal. Chem.*, 49 (1977) 953.
[25] S. Uchiyama and M. Uchiyama, *J. Chromatogr.*, 153 (1978) 135.

ELSEVIER

Journal of Chromatography A, 696 (1995) 139–148

JOURNAL OF CHROMATOGRAPHY A

Fluorescence, photodestruction, photoionization and thermal degradation of *o*-phthalaldehyde/β-mercaptoethanol-labelled aliphatic α-oligopeptides

Owe Orwar[a,*], Stephen G. Weber[b], Mats Sandberg[c], Staffan Folestad[a], Anna Tivesten[a], Mikael Sundahl[d]

[a]*Department of Analytical and Marine Chemistry, Göteborg University and Chalmers University of Technology, S-412 96 Göteborg, Sweden*

[b]*Department of Chemistry, University of Pittsburgh, Pittsburgh, PA, USA*

[c]*Institute of Neurobiology, Faculty of Medicine, Göteborg University, Göteborg, Sweden*

[d]*Department of Organic Chemistry, Chalmers University of Technology, Göteborg, Sweden*

First received 28 September 1994; revised manuscript received 2 December 1994; accepted 2 December 1994

Abstract

Photophysical and photochemical properties of *o*-phthalaldehyde/β-mercaptoethanol-labelled aliphatic α-peptides were investigated. It is found that α-peptide derivatives have lower fluorescence quantum yields, higher photodestruction quantum yields and lower yields for formation of solvated electrons as compared to amino acid and simple alkylamine derivatives in aqueous alkaline solution. These properties of the α-peptide derivatives sets narrow limits for their utilization in laser-based (high light intensity) detector systems. In contrast, the thermal stability of the peptide derivatives was found to be severalfold higher than for the parent amino acid derivatives. The differential rates of thermal derivative degradation could be utilized in a new approach towards selective determination of peptides.

1. Introduction

o-Phthalaldehyde/β-mercaptoethanol (OPA/βME) is well suited as a fluorogenic reagent for both pre- and post-separation labelling of amino acids in liquid chromatographic (LC) and capillary electrophoretic (CE) analyses [1–5]. The fluorescence intensity from OPA/βME-labelled α-peptides is weaker than for labelled amino acids [3,6], which in part is explained by the lower fluorescence quantum yields (Φ_f) of the α-peptide-containing chromophores [3]. However, even if corrected for differences in fluorescence quantum yields, the fluorescence signal obtained from α-peptide derivatives, also with conventional detectors (low light intensity), are much lower than expected. Thus, there must exist some process for depletion of ground state

* Corresponding author. Present address: Department of Chemistry, Stanford University Stanford, CA 94305-5080, USA.

0021-9673/95/$09.50
SSDI 0021-9673(94)01200-8

molecules that is favoured for peptide as compared to amino acid derivatives. The identity of this pathway has, hitherto, not been demonstrated. Further, it has not been established if laser-induced fluorescence (LIF) detection (high light intensity) will enable highly sensitive detection of α-peptide derivatives because the key photophysical and photochemical parameters required to optimize LIF detection [7] have not been fully characterized for these chromophores.

In the present study we determined photophysical and photochemical properties of OPA/βME α-peptide and amino acid derivatives that are of fundamental value for optimization of LIF detection. It is found that photodestruction quantum yields for α-peptide derivatives could be as high as 0.5. This, in combination with low fluorescence quantum yields, explains the weak fluorescence yielded even with low intensity excitation sources. Less than 0.2 photon/Ala peptide derivative and 13 photons/Ala derivative are expected at the most at high laser irradiances. At this level, a 80–90-fold detection selectivity for amino acid over peptide derivatives is yielded. As previously shown for certain OPA/βME-amino acid derivatives and cyclodeca[*a*]indene derivatives [8], also the derivatives in the present investigation were ionized upon excitation. The formation of solvated electrons correlated with the fluorescence lifetimes, hence α-peptide derivatives yielded fewer solvated electrons than did amino acid and alkylamine derivatives. We further describe two related ways to introduce selectivity over amino acids in peptide determinations. These approaches take advantage of the superior thermal stability in solution of the peptide derivatives. Degradation at basic pH is the most selective against amino acids, but is rather time consuming (several hours). In acidic solution, most amino acids could be degraded in less than 10 min, however, with a concomitant increased decay rate of peptide derivatives. Any fluorescent by-products could not be observed. This procedure could substantially aid in order to clean up samples from amino acids to more favourably detect peptides.

2. Experimental

2.1. Apparatus

Electrophoresis experiments in 780 mm × 50 μm I.D fused-silica capillaries (Polymicro Technologies, Phoenix, AZ, USA) were performed using a laboratory-built apparatus based on a Bertan 2462 power supply (Bertan, Hickswill, NY, USA). The working potentials applied were unless otherwise noted 27 kV and currents were about 40 μA. Injections were done by raising the injection end of the capillary 6.5 cm above the negative end for 30 s. A 1-cm portion of the capillary polyimide layer was removed by a butane flame to serve as a detection window. A Shimadzu RF 530 (Kyoto, Japan) HPLC fluorescence detector fitted with a Scott UG11 filter on the excitation side was rebuilt for use with capillaries. The spectral power (340 nm) on the capillary detection window was estimated to be about 0.5 μW (18 nm bandwidth). Electropherograms were recorded using a Perkin-Elmer Model 561 strip chart recorder.

The quantum yields of photodestruction (Φ_D) were measured in an optical bench arrangement comprising a Xe arc lamp and a monochromator from Applied Photophysics (Leatherhead, UK) as described previously [8]. Azobenzene [9] calibrated against ferrioxalate [10] was used as an actinometer. Laser-flash photolyses were performed on continuously stirred and deoxygenated solutions using the 355 nm line (frequency-tripled 1064 nm line) of a Spectron Nd:YAG laser Model SL 803 G (Spectron Laser Systems, Rugby, UK). The pulse duration and energy were 7 ns (full width at half maximum) and 45 mJ, respectively. A commercially available laser-flash photolysis spectrometer from Applied Photophysics was used. Uncorrected fluorescence spectra were recorded on derivatized 10–50 μ*M* standard solutions at pH 9.5 (2 min reaction time, at least 150-fold molar excess of reagent) using a Shimadzu RF5001 PC spectrofluorimeter. Corrected fluorescence spectra of the derivatives in 50 m*M* borate buffer (pH 9.5) were recorded using an Aminco SPF-500

spectrofluorimeter. Fluorescence quantum yields, corrected for differences in solvent refractive indices, were calculated using 9,10-diphenylanthracene in cyclohexane as a reference compound ($\Phi_f = 0.9$) [11]. UV absorption spectra were obtained on a Varian CARY 4 UV–Vis spectrophotometer (Varian, Australia). For reaction kinetics 160 μM standard solutions were derivatized using a 150-fold molar excess reagent. Molar absorptivities (corrected for a derivatized water blank) were obtained for derivatized 160–250 μM standards (2 min reaction time, 150-fold molar excess of reagent) against a distilled water blank. Thermal degradation kinetics were monitored using CE. Here, a derivatized sample was injected on the capillary after a controlled period of time as detailed below.

2.2. Standard solutions

Stock solutions were prepared in distilled deionized water with the occasional addition of HCl in order to properly dissolve the peptides. The standards were stored at −20°C. Ala, Gly, Gly_2 to Gly_5 and Ala_2 to Ala_5 were obtained from Sigma (St. Louis, MO, USA), and H–Ala_4–Glu_4–OH, Gly_6, Ala_6, Val–Val and Val–Ala from Bachem (Bubendorf, Switzerland). The combined amino acid standard AA-S-18 (Sigma) contains: Ala, NH_3, Arg, Asp, cystine, Glu, Gly, His, Ile, Leu, Lys, Met, Phe, Pro, Ser, Thr, Tyr and Val in 0.1 M HCl. This was neutralized with an equal volume 0.1 M NaOH to yield a final concentration of 1.25 mM of each amino acid (except cystine, 0.625 mM).

2.3. Reagents and derivatization procedures

The borate buffer (ionic strength 54 mM, pH 9.6) used in the CE experiments was prepared by mixing 50 ml of 40 mM disodiumtetraborate (Merck, Darmstadt, Germany), 14.1 ml of 0.1 M NaOH and 35.9 ml of distilled deionized water. A borate buffer for use with reagents was prepared by dissolving boric acid in distilled deionized water to a final concentration of 0.8 M. The pH was adjusted to 9.5–10.5 with 5.0 M NaOH. The OPA/βME reagent solutions were prepared by dissolving 100–333 mg OPA (99%, Sigma) in 1 ml of MeOH and adding to this solution 100–333 μl of βME (99%). This was made up to 10 ml with the borate buffer. The hydrochloric acid (0.5 M) was glass distilled. βME (Sigma) was used as received. Derivatizations were performed in polypropylene vials washed in HNO_3 (1 M) and thereafter rinsed with distilled deionized water and ethanol. In the derivatization reactions, 1:1 to 1:8 reagent to standard volume ratios were typically used. In some experiments 0.5 M HCl was added to accelerate the degradation of amino acid derivatives. After a controlled period of time, as detailed in the proceeding text, the solution was injected on the capillary. In the laser-flash photolysis and photodegradation experiments, stoichiometric amounts of reactants were used. The completion of the derivatization reactions were then ascertained by absorption measurements at 340 nm.

3. Results and discussion

3.1. Derivative formation

In reactions of amino acids with OPA/βME, 1-alkylthio-2-alkylisoindoles are formed in less than 1 min, provided that the reagent is held at millimolar concentrations [2,3]. With many reagents, peptides requires lengthy reaction times and sometimes also heating. Here, however, the reaction was brought to completion in 2 min even with hexa- and octapeptides (Fig. 1). Such rapid reaction rates are favourable, in particular for post-separation derivatization schemes, where short reaction times are sought.

3.2. Photophysical and photochemical properties

Qualitatively, OPA/βME-amino acid and -peptide derivative fluorescence spectra were similar to each other. The maxima of the excitation spectra and the maxima of the emission spectra were centered around 336 and 450 nm,

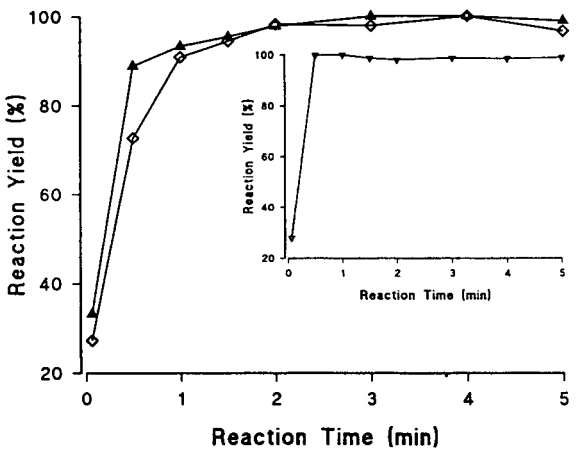

Fig. 1. Influence on reaction time for formation of OPA/βME-peptide derivatives. Gly_6 (◇), Ala_6 (▲) and inset; Ala_4–Glu_4. The reactions were followed by UV absorption measurements at 340 nm.

respectively. For all derivatives molar absorptivities were in the range $6000 \pm 300\ M^{-1}\ cm^{-1}$ at an absorption wavelength of 336 nm. The fluorescence quantum yields, however, depend significantly on the structure of the analyte (Table 1). Our results for the Ala, Gly_2, Gly_3 and Ala_3 derivatives are in agreement with those of Chen et al. [3]. Within the respective series, the largest decrement in fluorescence quantum yield occurs between the amino acid and the dipeptide, whereas further extension of the peptide backbone has little influence. It has been shown previously that OPA/βME-labelled peptides and amino acid amides have, in addition to lower fluorescence quantum yields, significantly shorter excited state lifetimes as compared to amino acid derivatives [3]. The peptide derivatives thus have an increased rate of some nonradiative process.

We previously showed that certain OPA/βME-amino acid and cyclodeca[*a*]indene derivatives undergo facile photochemical decomposition with quantum yields, Φ_D, in the range 0.01–0.14 [8]. Here, we determined the Φ_D values for the *n*-propylamine, Ala and the peptide derivatives in the Ala series (Table 1). With Φ_D values as high as 0.5, α-peptide derivatives are the most photolabile of OPA/βME derivatives determined so far. It is interesting to note that photodestruction is the major pathway and considerably more important than fluorescence for deexcitation of α-peptide derivatives while the

Table 1
Fluorescence quantum yields, fluorescence lifetimes, photodestruction quantum yields and photodestruction lifetimes of OPA/βME derivatives

Amine	Φ_f [a]	τ_f/ns [b]	Φ_D [c]	τ_d/ns
n-Propyl-NH_2	0.52	–	0.023	–
Ala	0.40	18.4	0.031	593.5
Ala_2	0.085	–	0.49	–
Ala_3	0.061	4.0	0.45	8.9
Ala_4	0.057	–	0.41	–
Ala_5	0.055	–	0.39	–
Ala_6	0.050	–	0.34	–
Gly_2	0.173	7.3		
Gly_3	0.094	6.7		
Gly_4	0.088			
Gly_5	0.086			
Gly_6	0.079			
Val–Val	0.050			
Val–Ala	0.063			

Φ_f = fluorescence quantum yield; τ_f = fluorescence lifetime; Φ_D = photodestruction quantum yield; τ_d = photodestruction lifetime.
[a] Corrected fluorescence spectra were recorded with the derivatives dissolved in a 50 m*M* borate buffer (pH 9.5).
[b] Data taken from Chen et al. [3].
[c] The Φ_D values were obtained for derivatives dissolved in a 50 m*M* borate buffer (pH 8.8).

reverse is true for amino acid and alkylamine derivatives.

Apart from fluorescence and photodestruction, photoionization is an important route for OPA/βME-amino acid and cyclodeca[*a*]indene-peptide derivatives following excitation [8]. Pulsed-laser excitation ($\lambda = 355$ nm) of the derivatives in the present study also yielded spectra characteristic for solvated electrons [12] (Fig. 2). The yield of the solvated electrons increased linearly with the laser intensity in the range 5–45 mJ, indicating a one-photon process as is usually the case for photoejection of electrons from aromatic chromophores in water solution [13]. However, bi-photonic processes might be important at higher light intensities. Decay curves for solvated electrons in equimolar Ala and Ala_4 derivative solutions, respectively, are shown in Fig. 3. The yield of the solvated electron in Ala and *n*-propylamine solutions were twice as high as for Ala_2 and Ala_4 solutions. We note that the formation of the solvated electrons correlates rather well with the excited state lifetime for amino acid and peptide derivatives, respectively (Table 1). The radical cation of the isoindole chromophores was observed at shorter absorption wavelengths than that of the solvated electron (Fig. 4).

In conclusion, the α-peptide derivatives have different excited state behavior compared to the Ala and *n*-propylamine derivatives. They give fewer solvated electrons, they have higher photodestruction quantum yields, they have lower fluorescence quantum yields and they have shorter fluorescence lifetimes. It is thus clear that photoionization and photodestruction are two different pathways. However, another deactivation channel for the excited states might be various degrees of intramolecular electron transfer (see below). Any triplet absorption could not be detected in the present experiments. This is consistent with our previous results and with findings on the indole and tryptophan systems in polar solvents [8,14].

Both with regard to substituent and solvent effects on fluorescence quantum yields, there are

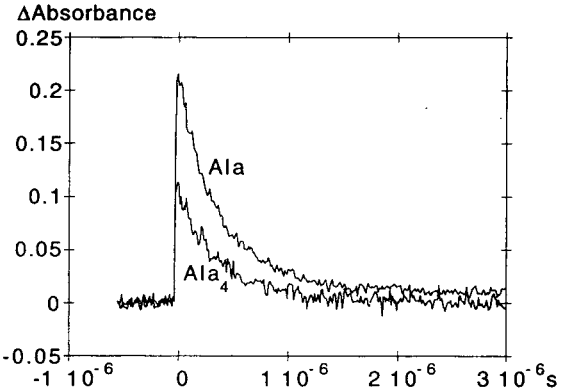

Fig. 3. Decay curves at 700 nm for solvated electrons ejected from Ala and Ala_4 derivatives (120 μ*M* in 50 m*M* borate buffer, pH 8.8).

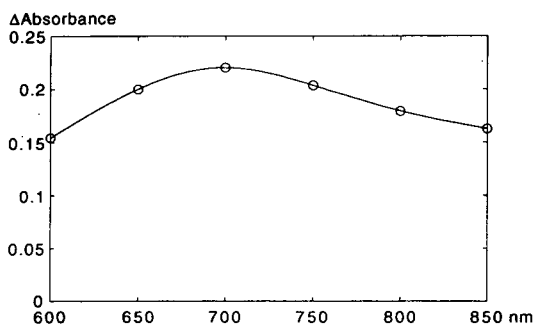

Fig. 2. Difference absorption spectrum of solvated electrons obtained by laser irradiation of an Ala solution (initially 120 μ*M* in 50 m*M* borate buffer, pH 8.8). The traces were sliced 100 ns after the laser pulse.

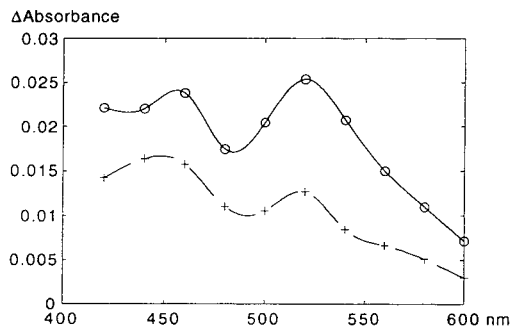

Fig. 4. Difference absorption spectra obtained by slicing traces 4 μs after the laser pulse at different detection wavelengths. OPA/βME-Ala solution (○) and OPA/βME-Ala_4 solution (+). The derivatives were initially 120 μ*M* in 50 m*M* borate buffer, pH 8.8.

some analogies between the isoindole derivatives in this study and various tryptophan derivatives [3,14–16]. In tryptophan and some analogues it is postulated that an important deexcitation process, in addition to fluorescence, results from an intramolecular excited state electron transfer reaction where the indole excited singlet states are electron donors and nearby functional groups are electron acceptors [17,18]. The amide functional group is a better electron acceptor than the carboxylate, which in turn is a better electron acceptor than the methylene group, thus it more effectively quenches the isoindole fluorescence (compare Φ_f for the *n*-propylamine, Ala and peptide derivatives in Table 1). In prior work, we have shown that β-Asp dipeptide derivatives, apparently, fluoresce as intensively as amino acid derivatives [19]. Thus, moving the peptide bond one C–C bond away from the isoindole nucleus reduces the quenching efficiency considerably. The factor of 3–4 increase in excited state lifetime brought about by separating the isoindole from the amide by one C–C bond is consistent with current estimates of the distance dependence (number of bonds) of electron transfer [20,21].

3.3. Implications for LC–LIF detection

To be able to optimize LIF detection, knowledge about the photodegradation rate of the fluorescent species is important. The ratio Φ_f/Φ_D describes the mean maximal number of fluorescent photons that can be expected from a fluorophore when going to the limit of infinite laser irradiances [7,22]. These values are compiled in Table 2 together with the relative fluorescence intensity (peak height) for each derivative in CE experiments where a conventional low intensity light source is used (Fig. 5). If only fluorescence and photodestruction are taken into consideration, these data suggest that each chromophore on the average absorbs roughly two photons with this detector configuration. Further, at high light intensities, a 80–90-fold detection selectivity for amino acid over peptide derivatives is yielded (Table 2). OPA/βME- and fluoresceinisothiocyanate (FITC)-labelled amino acids are detected in a low-light-intensity regime with approximately the same sensitivity [4]. However, in LIF detection schemes where several hundreds or thousands of photons may be available to excite the chromophore, the detection limits for FITC-labelled amino acids can be 10^2–10^5 superior to OPA/mercaptopropionate-labelled amino acids [23,24]. The difference is most likely primarily due to a higher photostability of the FITC-amino acid chromophores.

Table 2
Calculated ratio between fluorescence quantum yields and photodestruction quantum yields and relative fluorescence intensity

Amine	Φ_f/Φ_D	RFI[a]
n-Propyl-NH_2	22.6	–
Ala	12.9	10 ± 0.5
Ala_2	0.17	1.0 ± 0.06
Ala_3	0.14	0.7 ± 0.06
Ala_4	0.14	0.7 ± 0.06
Ala_5	0.14	0.5 ± 0.09
Ala_6	0.15	0.4 ± 0.06
Gly_2	–	0.7 ± 0.05
Gly_3	–	0.3 ± 0.04
Gly_4	–	0.2 ± 0.04
Gly_5	–	0.3 ± 0.02
Gly_6	–	0.3 ± 0.02

[a] RFI = Relative fluorescence intensity, obtained from peak height measurements in CE experiments.

The choice of using OPA/βME for labelling of α-peptides must not be to achieve ultra-sensitive

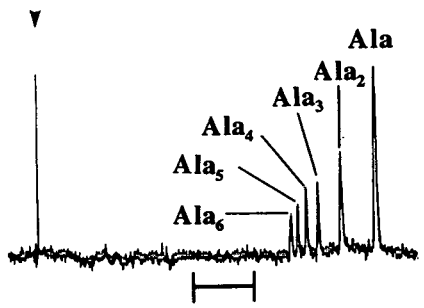

Fig. 5. Separation of a mixture of Ala and Ala peptide standards. A 510-μl volume of standard (100 μ*M* of each peptide and 20 μ*M* Ala) was derivatized with 60 μl of reagent (OPA, 500 m*M* and βME, 250 m*M*). Following a 2-min reaction time the solution was injected. CE conditions; potential 25 kV, current ca. 40 μA. Time bar is 1 min.

LIF detection as the derivatives are extremely light sensitive. However, these derivatives have some attractive features that would enable their selective determination. As an example, phase-modulated detection would enable highly selective determination of OPA/βME-labelled α-peptides over amino acid derivatives owing to their significantly shorter excited state lifetimes. Further, the high thermal stability of labelled α-peptides may be used to enhance the detection selectivity against amino acids (see below).

3.4. Thermal stability of OPA/βME-peptide derivatives in solution

It is well known that several OPA/βME-amino acid derivatives decay rapidly [25]. Particularly unstable are Gly and Orn, whereas Ala belongs to an intermediate group while under the same conditions, the most stable are Val and Ile [26]. Here, both the Ala peptide and the Gly peptide derivatives were found to be severalfold more stable than their parent amino acid derivative. The peptide derivatives in the Ala series were considerably more stable than those in the Gly series, and the two Val dipeptides were by far the most stable (Table 3). Thus, the structural features of the N-terminal amino acid residue has a

Table 3
Apparent first-order decay constants and half lives for OPA/βME-derivatized amino acids and peptides (1 m*M*) with different concentrations of OPA in borate buffer (pH 10)

Amine	k_{app}/min^{-1}	$t_{1/2}$/min	[OPA]/m*M*
Gly	0.43	1.6	150
Gly_2	0.15	4.7	150
Gly_6	0.12	5.7	150
Ala	0.026	26.6	150
Ala_2	0.016	43.3	150
Ala_6	0.015	46.2	150
Val–Ala	0.0029	239	150
Val–Val	0.0032	217	150
Ala	0.058	11.9	495
Ala_2	0.019	36.5	495
Ala_6	0.017	40.8	495

The derivatives were generated by adding 60 μl of a reagent solution (150 or 495 m*M* OPA) to 65 μl of a mixed standard containing Ala 77 μ*M*, Ala_2 308 μ*M* and Ala_6 615 μ*M*. Separate experiments were performed for the Gly series, Val–Ala and Val–Val. Following a 2-min reaction time the derivatives were injected into the capillary and thereafter at 5–7-min intervals until 50 or 70 min ($n = 5$–7 in each experiment, except for Gly: $n = 3$).

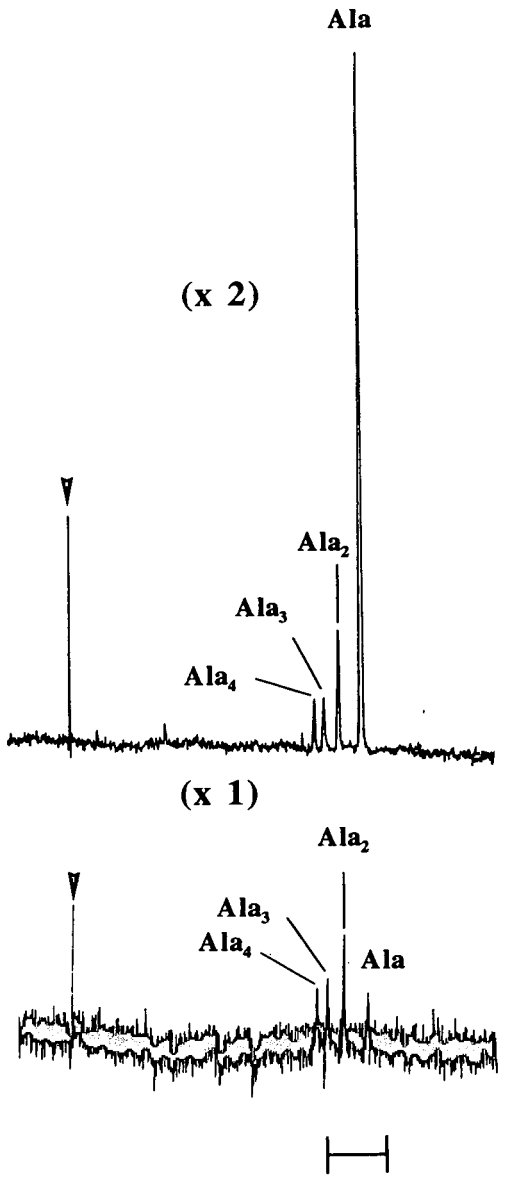

Fig. 6. Electropherograms of a derivatized standard. A 180-μl volume of Ala_2, Ala_3 and Ala_4 (278 μ*M* of each), Ala (167 μ*M*) and 60 μl reagent (OPA, 150 m*M* and βME, 75 m*M*), injected after a 2-min reaction time (upper trace) and following acidification for 6.5 min with 50 μl HCl (0.5 *M*) yielding pH 1.8. Time bar is 1 min.

large impact on the stability of the OPA/βME-peptide derivative which also is obvious when comparing the stability of the Val–Val and Val–Ala derivatives (Table 3). Thus, it appears safe to say that for peptides with aliphatic sidegroups, the derivative stability can be estimated from the identity of the N-terminal residue alone and ranked Val peptide > Ala peptide > Gly peptide. Extremely stable derivatives have been obtained with OPA/βME-labelled Leu–Ala and Phe–Ala (less than 3% absorbance drop after 24 h, borate buffer pH 9.7) [27]. This corroborates the above reasoning as the OPA/βME derivatives of Leu and Phe are among the most stable obtained with amino acids [26,27]. It has earlier been shown that the stability of 1-alkylthio-2-alkylisoindoles is largely dependent on the thiol and amine structure [28,29]. Extensive branching and increased steric bulk at C-10 (α-C in the native amino acid or peptide), and increased chain length renders derivatives with a higher stability [28,29]. The derivative stability ranking obtained in the present study are consistent with these observations. However, increasing the length of the peptide backbone does not produce any profound effects as realized for simple linear–CH_2–extensions, where an approximate 2-fold higher stability is observed per each methylene group incorporated [28].

Isoindole degradation rates are strongly dependent on the concentration of *cis*- and *trans*-phthalandiols (hydrated OPA), [29]. These authors postulated that degradation occurs by two parallel routes:

$$k_{app} = k_0 + k_1[\mathrm{OPA}]$$

where k_{app} is the apparent first-order decay constant, k_0 and k_1 are the rate constants for the OPA-independent and OPA-dependent processes, respectively. Under most analytical conditions this appears over all first order and the OPA-dependent process is by far the most important [28,29]. The observed differential rate of degradation comparing amino acid and peptide derivatives provides a possible avenue to achieve improved selectivity for peptides over amino acids. It was found that the degradation of the peptide derivatives is less dependent on the OPA concentration than the amino acid derivatives (Table 3). Further, OPA/βME derivative degradation is augmented following acidification [8,28,30,31]. We previously used acidification in order to degrade various amino acid and peptide

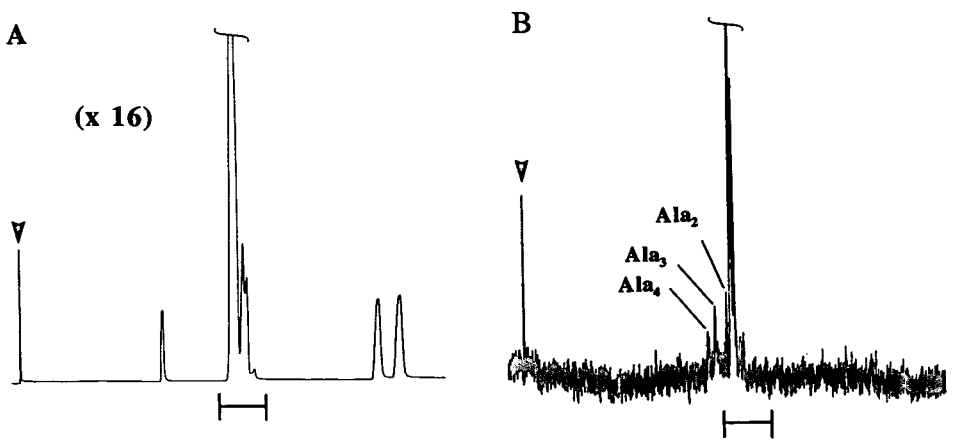

Fig. 7. Electropherogram of a derivatized standard. A 120-μl volume of Ala_2, Ala_3 and Ala_4 (250 μ*M* of each) and 312 μ*M* of each amino acid in a combined amino acid standard AA-S-18 was derivatized with 60 μl reagent (OPA, 150 m*M* and βME, 75 m*M*) injected after a 2-min reaction time (A) and the same standard following acidification for 6.5 min with 50 μl HCl (0.5 *M*) yielding pH 1.8 (B). Time bar is 1 min.

derivatives to enable selective determination of highly stable glutathione and γ-glutamylcysteine derivatives [8]. However, upon acidification (HCl, pH ≈ 1.8) after the completion of the derivatization reaction, the degradation rates increasingly diverged, and the decay of the Ala derivative was estimated to be approximately six times faster than for Ala_2 and Ala_6 derivatives, using merely a 45-fold excess OPA (Fig. 6). Selectivity-enhanced detection of peptides in certain types of samples should thus be feasible by this approach. This was tested in an amino acid standard spiked with three Ala peptides where most of the amino acids could be completely degraded after a 6.5-min acid treatment (Fig. 7). At the same time, the peptide derivatives were destroyed to a lesser extent and are clearly visible in the electropherogram in Fig. 7B. Certain thermally stable peptide derivatives, e.g. those with N-terminal Val residues may be favourably detected using that approach. As an example A-VI-5, a bradykinin potentiating peptide seems to be a suitable for such purposes.

4. Conclusions

It is shown that thermal and photoinduced degradation of OPA/βME-amino acid and -peptide derivatives are unrelated. In addition to fluorescence, photoionization and photodestruction are important pathways for deactivation of the first excited singlet state. α-Peptide derivatives are the most light sensitive and with high irradiances of the excitation light, a 80–90-fold detection selectivity for amino acid derivatives over peptide derivatives is yielded. Furthermore, our results show that a given OPA/βME-α-peptide derivative has higher thermal stability compared to the derivative obtained where the N-terminal amino acid in the peptide is reacted as a free amino acid.

Acknowledgements

This work was supported by the Swedish Natural Science Research Council (Nos. 1905-308 and 9709-300), the NIH (GM 44842) the Knut and Alice Wallenberg Foundation, the Torsten and Ragnar Söderbergs Foundation, the Åke Wiberg Foundation, the O.E. and Edla Johansson foundation, the Åhléns Foundation and the Erna and Victor Hasselblad Foundation. We are grateful to Dr. Kjell Sandros and Dr. Svante Eriksson for kind help.

References

[1] M. Roth, *Anal. Chem.*, 43 (1971) 880.
[2] P. Lindroth and K. Mopper, *Anal. Chem.*, 51 (1979) 1667.
[3] R.F. Chen, C. Scott and E. Trepman, *Biochim. Biophys. Acta*, 574 (1979) 440.
[4] M. Albin, R. Weinberger, E. Sapp and S. Moring, *Anal. Chem.*, 63 (1991) 417.
[5] S.L. Pentoney, X. Huang, D.S. Burgi and R.N. Zare, *Anal. Chem.*, 60 (1988) 2625.
[6] M.H. Joseph and P. Davies, *J. Chromatogr.*, 277 (1983) 125.
[7] R.A. Mathies, K. Peck and L. Stryer, *Anal. Chem.*, 62 (1990) 1786.
[8] O. Orwar, M. Sundahl, M. Sandberg and S. Folestad, *Anal. Chem.*, 66 (1994) 4474.
[9] G. Gauglitz and S. Hubig, *J. Photochem.*, 30 (1985) 121.
[10] C.G. Hatchard and C.A. Parker, *Proc. R. Soc. London A*, 235 (1956) 518.
[11] S. Hamai and F. Hirayama, *J. Phys. Chem.*, 87 (1983) 83.
[12] M.S. Matheson and L.M. Dorfman, *Pulse Radiolysis*, M.I.T. Press, Cambridge, MA, 1969.
[13] R. Lesclaux and J. Joussot-Dubien, in J.B. Birks (Editor), *Organic Molecular Photophysics*, Wiley, New York, 1973.
[14] Y. Hirata, N. Murata, Y. Tanioka and N. Mataga, *J. Phys. Chem.*, 93 (1989) 4527.
[15] R.W. Cowgill, *Arch. Biochem. Biophys.*, 100 (1963) 36.
[16] R.W. Cowgill, *Biochim. Biophys. Acta*, 133 (1966) 6.
[17] J. Teraoka, P.A. Harmon and S.A. Asher, *J. Am. Chem. Soc.*, 112 (1990) 2892.
[18] S. Arnold, L. Tong and M. Sulkes, *J. Phys. Chem.*, 98 (1994) 2325.
[19] O. Orwar, S. Folestad, S. Einarsson, P. Andiné and M. Sandberg, *J. Chromatogr.*, 556 (1991) 39.
[20] J.J. Hopfield, *Proc. Natl. Acad. Sci. U.S.A.*, 71 (1974) 3640.
[21] S. Priyadarshy, S.M. Risser and D.N. Beratan, submitted for publication.

[22] T. Hirschfeld, *Appl. Optics*, 15 (1976) 3135.
[23] B. Nickerson and J.W. Jorgenson, *J. High. Resolut. Chromatogr. Chromatogr. Commun.*, 11 (1988) 878.
[24] S. Wu and N. Dovichi, *J. Chromatogr.*, 480 (1989) 141.
[25] M.C.G. Alvarez-Coque, M.J.M. Hernandez, R.M.V. Camanas and C.M. Fernandez, *Anal. Biochem.*, 178 (1989) 1.
[26] V.-J.K. Svedas, I.J. Galaev, I.L. Borisov and I.V. Berezin, *Anal. Biochem.*, 101 (1980) 188.
[27] R. Rowlett and J. Murphy, *Anal. Biochem.*, 112 (1981) 163.
[28] W.A. Jacobs, M.W. Leburg and E. Madaj, *Anal. Biochem.*, 156 (1986) 334.
[29] J.F. Stobaugh, A.J. Repta, L.A. Sternson and K.W. Garren, *Anal. Biochem.*, 135 (1983) 495.
[30] S.S. Simons, Jr. and D.F. Johnson, *Anal. Biochem.*, 82 (1977) 250.
[31] S.S. Simons, Jr. and D.F. Johnson, *Anal. Biochem.*, 90 (1978) 705.

ELSEVIER

Journal of Chromatography A, 696 (1995) 149–152

JOURNAL OF CHROMATOGRAPHY A

Short communication

Application of polarimetric detector for the high-performance liquid chromatographic determination of the optical purity of 5(4*H*)-oxazolones

Z. Wodecki, M. Ślebioda, A.M. Kołodziejczyk*

Department of Organic Chemistry, Technical University of Gdańsk, 80-952 Gdańsk 6, Poland

First received 19 August 1994; revised manuscript received 8 December 1994; accepted 12 December 1994

Abstract

An HPLC procedure for monitoring one of the reactive intermediates in peptide synthesis, 5(4*H*)-oxazolone, was developed. The reversed-phase mode made it possible not only to monitor the formation and consumption of oxazolone, but also to determine the concentration of other components of the reaction mixture. Moreover, with polarimewtric and UV detectors coupled in series it was possible to determine the content of both oxazolone enantiomers in the reaction mixture. Hence with the achiral chromatographic system employed, the enantiomeric excess of the crucial component of the mixture could be monitored.

1. Introduction

The main objective of peptide synthesis is the preparation of peptides not only chemically pure but also of defined chiral identity. The well known thalidomide tragedy [1] still remains a classic warning of how dangerous a drug contaminated with its diastereomeric counterpart can be. Taking into consideration the large production scale of some peptides, any improvement in the reaction yield and the purity of the product is of great economic importance. A great deal of effort has been devoted to trying to define the circumstances under which racemization can be eliminated or minimized. In general, any activation of an N-protected amino acid or a peptide indispensible for peptide bond formation is accompanied by a risk of the loss of chiral purity of the activated moiety. As the formation of 2-alkyl-5(4*H*)-oxazolones intermediate is commonly regarded as one of the main roots of the racemization process, an analytical technique for monitoring their transformation in peptide synthesis is very desirable. 5(4*H*)-Oxazolones easily undergo base-catalysed racemization and their subsequent aminolysis by the amino component contributes to peptide racemization. Our previous findings [2], along with many other results [3,4], indicate that aminolysis of racemized 5(4*H*)-oxazolones is responsible for slow peptide racemization with a prolonged reaction time, but the question arises of whether they are formed already racemized or whether they are initially chirally pure and racemize during the reaction. This paper describes the application of

* Corresponding author.

0021-9673/95/$09.50
SSDI 0021-9673(94)01223-7

an HPLC method for monitoring the formation of oxazolone and its transformation.

2. Experimental

2.1. Apparatus and reagents

An HP 1090A chromatograph equipped with a diode-array UV detector and a system consisting of a Pye Unicam PU 410 pump, PU 4020 variable-wavelength UV detector, Knauer Chiralyser 2 polarimetric detector and Kipp Zonen BD 41 recorder were employed. Separations of 5(4*H*)-oxazolones and other components of the investigated reaction mixtures were performed on a Nucleosil ODS 100-5 column (Macherey–Nagel) with aqueous acetonitrile or methanol as the mobile phase. Tetrahydrofuran (THF) was distilled from above Na–K alloy. Water was distilled twice in glass apparatus. Methanol and acetonitrile (Baker, chromatographic grade) were used as received. For detailed chromatographic conditions, see Figs. 1 and 2.

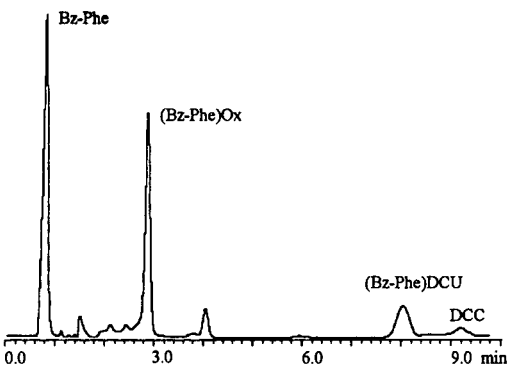

Fig. 1. Chromatogram of the reaction mixture of Bz-Phe with DCC. Reagent concentrations: Bz-Phe, 5.2 m*M*; DCC, 5.1 m*M*. Column, Nucleosil ODS 100-5 (100 × 4.6 mm I.D.); mobile phase, methanol–water (75:25); flow-rate 1.0 ml/min; temperature, 35°C; detection, UV at 220 nm. Reaction:

$$\text{Bz-Phe} + \text{DCC} \xrightarrow{\text{THF, 20°C}} \text{(Bz-Phe)Ox} + \text{(Bz-Phe)DCU}$$

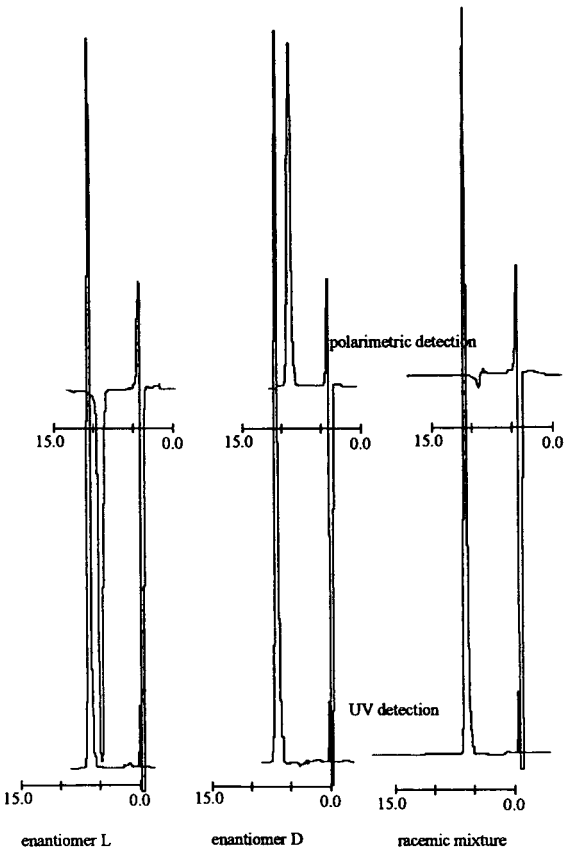

Fig. 2. Chromatograms of the enantiomers of 2-phenyl-4-benzyl-5(4*H*)-oxazolone. Column, Nucleosil ODS 100-5 (100 × 4.6 mm I.D.); mobile phase, acetonitrile–water (60:40); flow-rate 1.0 ml/min; detection, UV at 285 nm and polarimetric.

2-Phenyl-4-benzyl-5(4*H*)-oxazolone (Bz-Phe)-Ox was obtained from N-benzoylphenylalanine and 2-ethoxy-1-ethoxycarbonyl-1,2-dihydroquinoline according to the published procedure [5]. Both the D and L-enantiomers were prepared.

Owing to the possibility of oxazolone autoracemization [6], the oxazolone standards for detector calibration were prepared by dissolving the pure enantiomers in acetonitrile just before use.

N - Benzoylphenylalanyl - N,N′ - dicyclohexylurea (Bz-Phe)DCU was obtained from N-benzoylphenylalanine (Bz-Phe) and N,N′-dicyclo-

hexylcarbodiimide (DCC) according to the published procedure [7]. Both the D- and L-enantiomers were prepared.

2.2. Reaction conditions

The reactions were carried out in thermostated vessels with magnetic stirring. All the reagents were added as solutions in an appropriate solvent (for the initial concentrations and the reaction temperature, see Fig. 4). The resulting reaction mixtures were injected directly in the HPLC system.

3. Results and discussion

Previously, we reported the use of Pirkle and Oi chiral stationary phases for the normal-phase separation of protected dipeptides and N-acyl-N,N′-dicyclohexylurea enantiomers in carbodiimide-mediated peptide synthesis [7,8]. An attempt to apply those stationary phases to the separation of 2-alkyl-5(4*H*)-oxazolone enantiomers failed and prompted us to search for a different method for their rapid analysis.

Although 2-alkyl-5(4*H*)-oxazolones are susceptible to hydrolysis, they are stable under the conditions of reversed-phase chromatography. Good resolution of all chemical species present in the reaction mixture was achieved using the conditions applied (Fig. 1) and, together with the use of polarimetric and UV detectors coupled in series, enabled us to measure the enantiomer ratio in the 5(4*H*)-oxazolone mixture. To make this possible, the UV and polarimetric signals had to be evaluated simultaneously [9] as the UV detector provided information on the total oxazolone concentration whereas the polarimetric detector gave the signal proportional to the enantiomeric excess (Fig. 2).

The reliability of such a chromatographic system was successfully tested by comparison of the data on the chiral purity of 5(4*H*)-oxazolone standards obtained using HPLC and conventional polarimetric methods. The straight regression line of the experimental data ($R^2 = 0.995$) proved that the oxazolone remains chemically

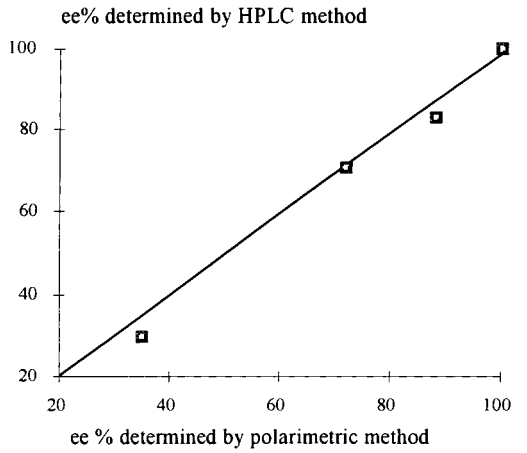

Fig. 3. Comparison of the data on chiral purity of 5(4*H*)-oxazolone standards obtained using HPLC and conventional polarimetric methods. ee = Enantiomeric excess.

and chirally intact under the chromatographic conditions applied (Fig. 3). The detection limit for each of the 2-phenyl-4-benzyl-5(4*H*)-oxazolone enantiomers was 2 μg on-column and the linear response range was 0.5–20 m*M*.

The method was applied to the investigation of the reaction of dicyclohexyl carbodiimide with benzoylphenylalanine as a model reagent. The compound was chosen for its racemization-prone properties and the fact that crystalline 2-phenyl-4-benzyl-5(4*H*)-oxazolone derived from benzoylphenylalanine is chemically and chirally stable and its physico-chemical and optical data are well known. As the oxazolone concentration was very low at the beginning of the reaction, the first determination of its chiral purity could be performed not earlier than a few minutes after the start of the reaction. A specific interdependence was observed: the longer the reaction time, the lower was the chiral purity of the oxazolone. Extrapolation of the experimental data gave a 100% optical purity of the initially formed oxazolone (Fig. 4). Although this value has no direct physical meaning, it allows for the deduction that 2-alkyl-5(4*H*)-oxazolones are formed during peptide synthesis without altering the chirality of the α-C atom of the activated

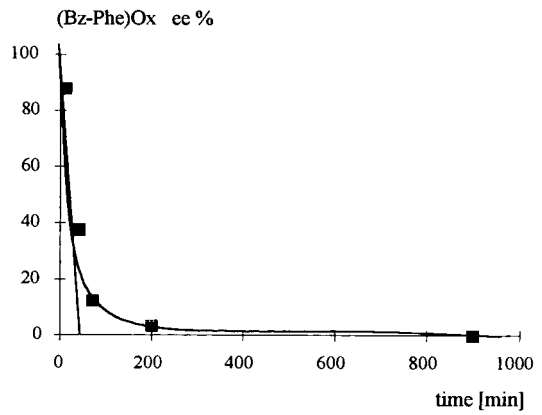

Fig. 4. Change in chiral purity of 2-phenyl-4-benzyl-5(4*H*)-oxazolone during the course of the reaction of DCC with Bz-Phe. Reagent concentrations: Bz-Phe, 15.1 m*M*, DCC, 14.8 m*M*. Reaction:

$$\text{Bz-Phe} + \text{DCC} \xrightarrow{\text{THF,20°C}} \text{(Bz-Phe)Ox} + \text{(Bz-Phe)DCU}$$

N-acylamino acids and they racemize slowly in the course of the reaction.

Acknowledgements

We thank Professor Lamparczyk, Head of the Medical Centre of Postgraduate Education, Department of Biopharmaceutics, Bydgoszcz, for making the polarimetric detector available. Support of this work by Grant KBN 2 0859 91 01 is greatly appreciated.

References

[1] G. von Blaschke, H.P. Kraft, K. Fickentscher and F. Kohler, *Arzneim.-Forsch.*, 29 (1979) 1640.
[2] M. Ślebioda and A.M. Kołodziejczyk, *Int. J. Pept. Protein Res.*, 28 (1986) 444.
[3] D.S. Kemp, in E. Gross and J. Meienhofer (Editors), *The Peptides*, Vol. 1, Academic Press, New York, 1979, p. 315.
[4] N.L. Benoiton, in E. Gross and J. Meienhofer (Editors), *The Peptides*, Vol. 5, Academic Press, New York, 1983, p. 216.
[5] C. Griehl and H. Jaschkeit, *Z. Chem.*, 28 (1988) 439.
[6] I.Z. Siemion and A. Dżugaj, *Roczn. Chem.*, 40 (1966) 1699.
[7] M. Ślebioda, Z. Wodecki and A.M. Kołodziejczyk, *Int. J. Pept. Protein Res.*, 35 (1990) 359.
[8] Z. Wodecki, M. Ślebioda and A.M. Kołodziejczyk, *J. Chromatogr.*, 477 (1989) 454.
[9] D.K. Lloyd and D.M. Goodall, *Chirality*, 1 (1989) 251.

ELSEVIER

Journal of Chromatography A, 696 (1995) 153–159

JOURNAL OF CHROMATOGRAPHY A

Short communication

Occasional sub-ambient temperature programming performed in two "isothermal" gas chromatographs☆

Hameraj Singh, Liguo Chen, Walter A. Aue*

Department of Chemistry, Dalhousie University, Halifax, Nova Scotia B3H 4J3, Canada

First received 27 October 1994; accepted 14 December 1994

Abstract

By temporarily inserting large thermal masses into the column baths of existing "isothermal" gas chromatographs, linear temperature ramps have been obtained from constant energy inputs. Typically, the rise of temperature could be held linear (within ±3°C) over a more than 100°C range. Since the metal inserts can be cooled before insertion, this approach extends thermal programming to subambient temperatures (e.g. down to −130°C in one case of this study). While such a temporary arrangement cannot compete in speed and convenience with gas chromatographs specifically designed for electronic control and liquid nitrogen cooling, it offers the occasional user an alternative that is inexpensive to assemble and simple to use.

1. Introduction

Gas chromatographs (GCs) that can be programmed at subambient temperatures are available from several GC manufacturers. These should obviously be employed if subambient temperature programming is the prime analytical task.

For most GCs, it is not. Yet occasions do arise when the analyst would like an innately isothermal GC to perform subambient and/or superambient temperature programming, say in order to accommodate an infrequent but insistent customer, or to meet an unusual but unavoidable research demand. Two typical cases from our group —whose main concern is detector development and trace organic analysis— may illustrate the point.

In the first case, the GC —a recently acquired, dedicated Shimadzu Model GC-8AIE— carried an electron-capture detector and had therefore little need and indeed no facility for temperature programming. After using it for some studies of electron-capture mechanisms [1], we connected its column to a laboratory-made sequential three-detector [1] combination (existing electron-capture plus reactive-flow luminescence [2] plus flame ionization detector). To test this tridector's performance in multi-channel correlation chromatography, we wanted to observe the behavior of some highly volatile analytes; and we also wanted to trace these analytes in a complex matrix such as gasoline. This obviously required a thermal program —and one that would start at subambient temperature.

In the second case, the GC —a Hewlett-Pac-

* Corresponding author.

☆ Part of graduate programs of H.S. and L.C.

0021-9673/95/$09.50
SSDI 0021-9673(94)01226-1

kard Model 700 with flame ionization detector—hailed from so early a chromatographic time that, although it already sported a fan, it still lacked a thermostat. Consequently, the isothermal temperatures of its column bath had to be slowly established as steady-state outcomes of the contest between the heat gain from its constant-voltage resistance coil and the heat loss to its walls and the lab environment. For a student project [3] involving volatile air pollutants, we decided to press this surplus item from our undergraduate organic chemistry laboratory into service, and lend it subambient-temperature programming capability.

The question was how. Modern GCs have very small heat capacities to permit fast temperature adjustment with shallow gradients in the air of the column bath. If they lack a temperature-programming controller, the only possibility to introduce a thermal ramp is to go "ballistic". (Despite this historic name, a "ballistic program" is really no "program" at all: the operator simply aims at some high isothermal setting and allows the temperature to shoot up.) In most isothermal instruments, therefore, the available ballistic program is too fast, not capable of a change in rate, and severely non-linear. In other words, it is of little or no practical value.

Despite the non-linearity of a ballistic program, its heat *input* is still roughly constant (and usually going at full tilt). The *non*-linearity of its temperature rise thus derives from the increasing temperature differential —and hence the increasing rate of heat transfer— from the inside (column-bath) air to the *low* thermal-capacity surrounding walls with associated structures and on to the outside air. However, if the column bath could be given a *high* thermal capacity, the "ballistic" temperature rise should come closer to being linear. In other words, most of the heat input could then enter a massive thermal sink (which would be part of, or would be situated in, the column bath); provided that heat transfer to this sink were made a reasonably fast process.

Simpler expressed, it should be possible to insert large pieces of metal into the column bath, with enough structure in the metal so the circulating air could heat them fast and efficiently. If these pieces of metal were precooled, a subambient temperature program would result.

Is such a procedure feasible? Is it cheap to install and easy to run? How large is its linear temperature range? How low a temperature can it conveniently reach?

2. Experimental

In order to answer these and other questions, larger pieces of structured, blackened aluminum were strung together in a form that, cold or hot, could be easily moved in and out of the column bath. The assembled piece for the Shimadzu weighed about 8 kg, the three pieces for the Hewlett-Packard together 4.5 kg. That seemed adequate for a first try. It also allowed us to compare two substantially dissimilar thermal sink capacities operating in two roughly similar column-bath volumes.

The Hewlett-Packard's isothermal temperature is *not* under thermostatic control; it is the steady-state, slowly attained outcome of a constant voltage being imposed on the heater. Setting a higher voltage would therefore increase the slope of the ballistic or thermal-sink-moderated temperature ramp: a feature that conveniently coincided with what we had in mind for the instrument.

In contrast, the Shimadzu's isothermal temperature is controlled by a thermostat with full-voltage input to the resistance heater: if left alone this would allow only *one* heating rate (short of changing the mass of the aluminum insert). The Shimadzu's resistance heater was therefore connected to an external Variac (variable autotransformer) such that either the instrument's thermostat controlled the time, or the external Variac controlled the magnitude, of the voltage imposed on the heater. Even nowadays, Variacs are occasionally used as GC inputs, although they usually serve a different purpose (cf. Ref. [4] and references cited therein). Just to be on the safe side, a laboratory-made digital thermometer was set up to cut off all power to

the heater if the column bath temperature should rise beyond a given threshold.

The aluminum inserts were cooled by solid water or liquid nitrogen. The Shimadzu column was an 80 cm × 2.5 mm I.D. borosilicate tube filled with 5% OV-101 on Chromosorb W, 45–60 mesh; the Hewlett-Packard column a similar 160 cm-long tube filled with 5% OV-101 on Chromosorb W AW, 100–120 mesh. Other conditions were similarly crude and conventional.

3. Results and discussion

It is obvious that, during the program, the temperature of the aluminum inserts will lag that of the constantly heated air circulating in the column bath. The extent of the lag must depend on the thermal mass of the aluminum and on the rate of its heat exchange (as well as on the power input). Clearly, the structure of the aluminum heat sink —its surface area and radiative ef-

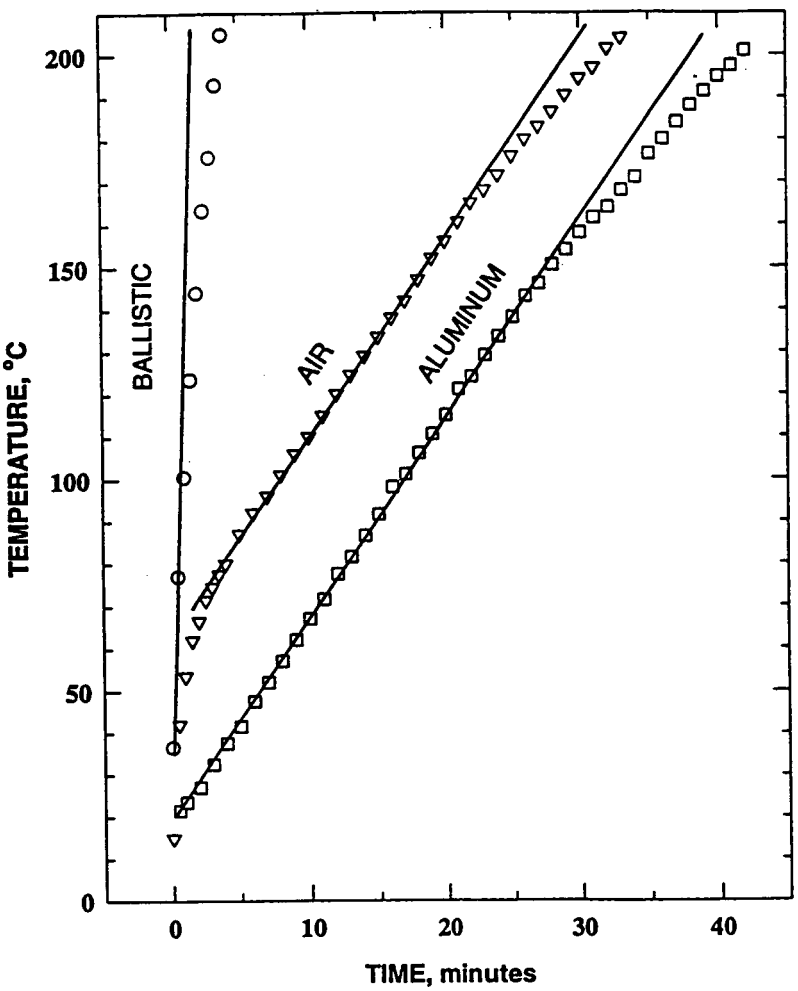

Fig. 1. Temperature rise in column bath air and aluminum insert (at an arbitrarily chosen location), as compared to a "ballistic" program (i.e. without aluminum insert). The 8-kg aluminum insert was cooled with ice cubes in the sink. Power input: 90% of line voltage (Variac). Shimadzu gas chromatograph.

ficiency, its local thickness, its extent of interaction with the air stream, etc.— will all influence the overall thermal exchange rate.

Given the but occasional task the aluminum inserts have to perform, we did not attempt to optimize their mass, surface, interactions with the air flow, etc. We simply assembled various pieces of aluminum, subjected them to some milling and drilling (to improve air-aluminum contact), and blackened them. Partly due to available bath geometry and partly due to experimental design, the Shimadzu's insert was far heftier than the Hewlett-Packard's.

For general interest, the temperature lag between the aluminum insert and the bath air was determined in both instruments, with a relatively high programming rate ensuring a pronounced lag. Figs. 1 and 2 show the results obtained with ice-cooled inserts from the Shimadzu and the Hewlett-Packard, respectively. They offer no surprises. The thermal lag is about 42°C in the Shimadzu, about 15°C in the Hewlett-Packard. The difference between the two relates mainly to the different mass of the aluminum inserts (8 kg in the Shimadzu and 4.5 kg in the Hewlett-Packard) and to the different power output of the heaters.

Figs. 1 and 2 also illustrate the limits of linear behavior. The straight (and parallel) lines show that the air temperature rises in a linear manner over about 100°C in both instruments. For the occasional need of programmed chromatography —and only the *occasional* need we want to address here— this range should be more than adequate. Where the heat-sink moderated programs do deviate from linearity, the deviation —as long as it is reproducible— is unlikely to hurt most analytical tasks. In view of the lower

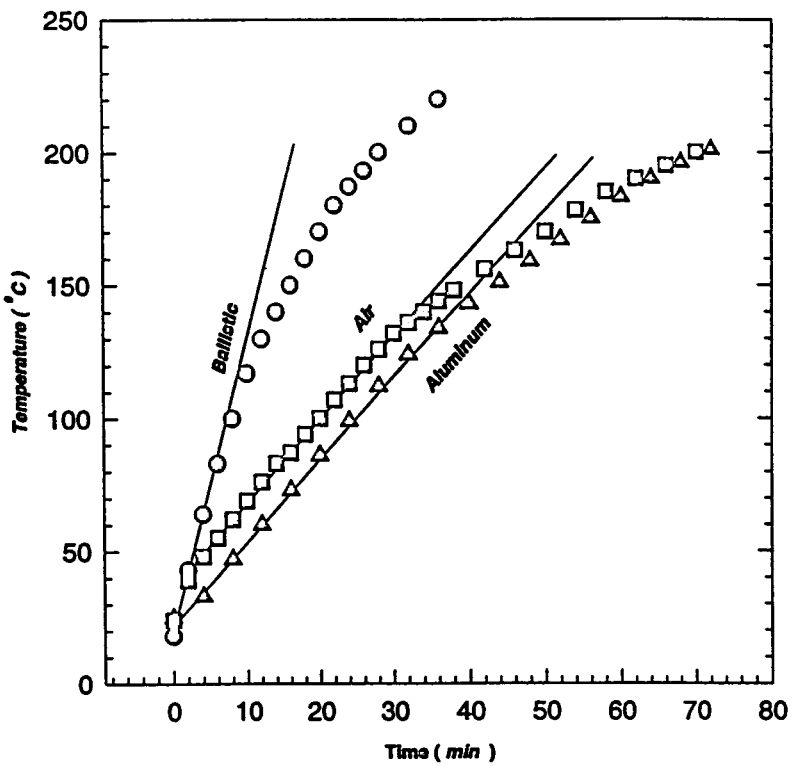

Fig. 2. Similar to Fig. 1, but Hewlett-Packard gas chromatograph. Power setting "8" (on a scale of 10). Three aluminum inserts of total mass 4.5 kg were used.

separation numbers ("Trennzahlen") at higher temperatures, a gradual slackening of the temperature rise may sometimes be even desirable.

For special needs it is possible to obtain lower temperatures and an even longer linear range. Fig. 3 shows an example. The Hewlett-Packard column bath and the inserts are cooled with liquid nitrogen. The program starts at −130°C and proceeds in linear fashion over a 150°C range.

It should be mentioned, however, that such heroic measures can have side effects. If sizeable amounts of water from the atmosphere freeze on exposed metal parts (as they are wont to do in the Shimadzu), the temperature rise will kink at 0°C and possibly even at 100°C.

Since this study was designed to satisfy temporary needs by a make-shift approach, no constructive measure was taken to cope with the problem of water condensation; nor was any sort of mechanical or procedural optimization attempted. Similarly, no attempt was made to measure or modify any —possibly even pronounced— temperature differences in different regions of the circulating column bath air (which could lower the resolution of high-performance columns).

The make-shift procedure did indeed satisfy our temporary need. Fig. 4 presents as a typical example the rough separation of gasoline. Gasoline is used here as a model hydrocarbon matrix under low-resolution conditions (i.e. on an 80-cm column packed with 45–60-mesh particles), which can potentially interfere with the response of highly volatile analytes in the tridector [1]. The early hydrocarbon peaks are well spread out, as desired.

While such separations can be more easily and

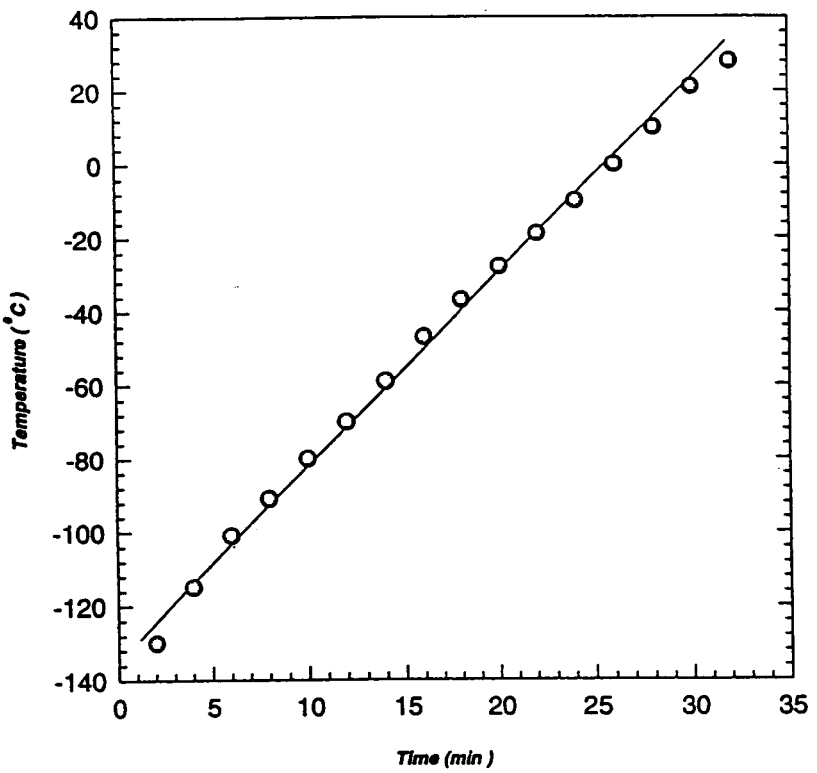

Fig. 3. Subambient temperature ramp in the Hewlett-Packard gas chromatograph. Column bath and aluminum inserts precooled by liquid nitrogen. Power input setting: 8.

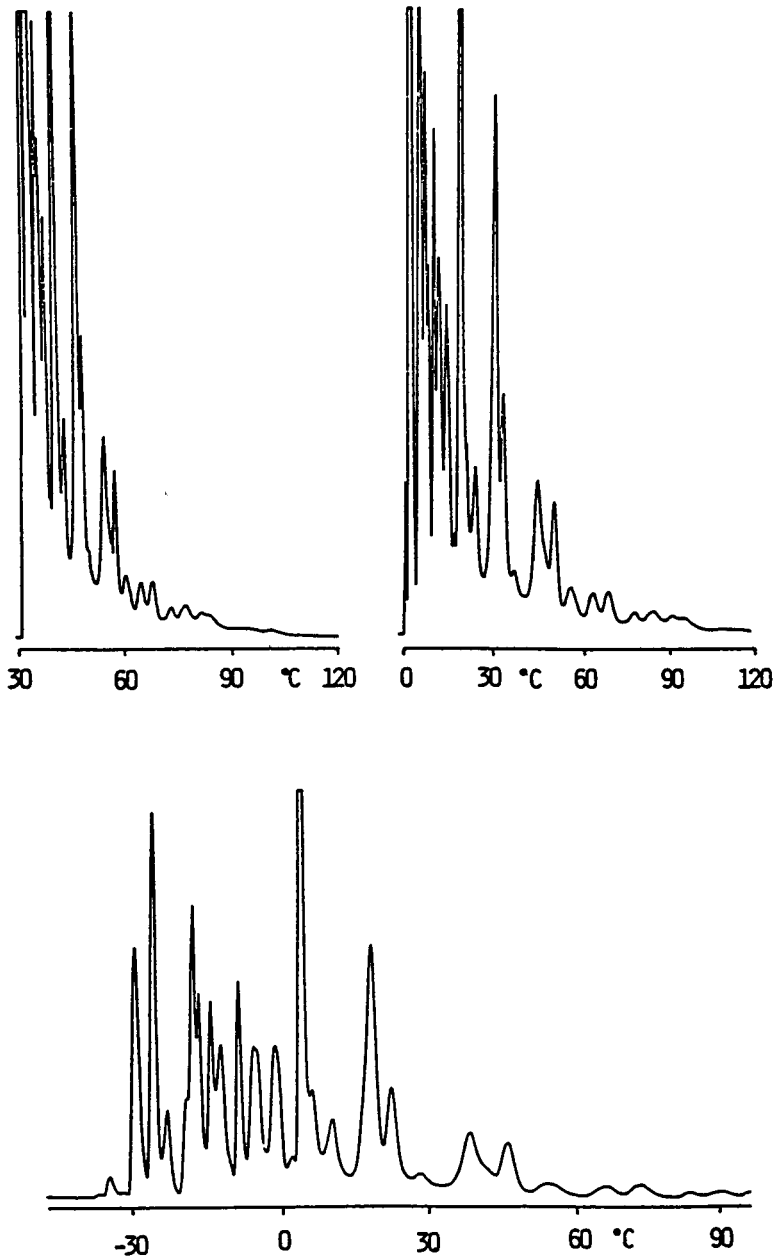

Fig. 4. Temperature-programmed chromatographies of "regular"-brand gasoline in the Shimadzu gas chromatograph, starting at different temperatures. Power input: 90% of line voltage.

more efficiently (though also more expensively) carried out on a liquid nitrogen-cooled commercial GC, inserting a thermal sink into an existing isothermal (or even programmable) GC provides an easy way out for the analyst who faces an unexpected but temporary requirement for subambient programming. Beyond analysis, the dampening effect of the large thermal mass may come in handy if the operator should want to avoid, for whatever purpose, the short-term

discontinuities (cycling) of conventional heating controls. A further and —at least in our labs— major advantage of using a heat sink designed to be inserted and removed for each subambient or superambient temperature-programmed run is that *one* insert can serve the occasional needs of *several* similarly dimensioned gas chromatographs. To wit, we use the same insert on three different Shimadzu model-8 units carrying different detectors and associated equipment. One heat sink thus provides both programming capability to an electron-capture instrument and subambient capabilities to two (temperature programmed) flame-photometric instruments. Furthermore, a typical heat sink can be designed to serve even differently sized and shaped column baths.

We should add that metal inserts of high cooling capacity are such a "natural" that it would come as no surprise to us if similar units had been used before— in chromatography, analytical chemistry, or other scientific disciplines. Searching a vast literature for devices of a self-evident nature can, however, take a long time. Worse, it can produce false negatives and, in turn, induce false notions of novelty. We prefer therefore —just in case— to pre-emptorily extend our apologies to kindred tinkerers for any unintentional failure on our part to recognize their earlier contributions.

Acknowledgements

This study was supported by NSERC Individual Research Grant A-9604. Thanks are also due to our Departmental shops, particularly to B. Millier in electronics and C.G. Eisener in engineering.

References

[1] H. Singh, unpublished Ph.D. research, Dalhousie University, 1993–1994.
[2] K. Thurbide and W.A. Aue, *J. Chromatogr. A*, 684 (1994) 259.
[3] L. Chen, unpublished M.Sc. research, Dalhousie University, 1993–1994.
[4] R.I. Meacham, B.A. Buffham, D.W. Drott and G. Mason, *J. Chromatogr. A*, 659 (1994) 205.

ELSEVIER

Journal of Chromatography A, 696 (1995) 160–163

JOURNAL OF CHROMATOGRAPHY A

Short communication

Measurement of binding constants by capillary electrophoresis

Donald J. Winzor

Centre for Protein Structure, Function and Engineering, Department of Biochemistry, University of Queensland, Brisbane, Queensland 4072, Australia

First received 4 October 1994; revised manuscript received 10 January 1995; accepted 20 January 1995

Abstract

The assumptions inherent in a capillary electrophoresis procedure for evaluating binding constants for interactions between lectins and charged polysaccharides [S. Honda et al., *J. Chromatogr.*, 597 (1992) 377] have been reappraised. Whereas the results were originally interpreted on the basis that the lectin–carbohydrate interaction was restricted to 1:1 complex formation, a more plausible interpretation is shown to be that an approximately constant incremental difference separates the mobilities of the successive complexes formed as the result of saccharide binding to equivalent and independent sites on the lectin. The parameter that is determined by capillary electrophoresis should thus be regarded as the intrinsic binding constant.

1. Introduction

Recent articles [1–6] have drawn attention to the potential of capillary zone electrophoresis as a method of evaluating binding constants for interactions between proteins and charged ligands. In that regard the first-mentioned two investigations [1,2] were concerned with the interactions of lectins with charged saccharides; and both investigations are therefore open to criticism on the grounds that the multivalence of the lectins in their interactions with carbohydrates has been ignored. Indeed, conformity of the experimental results with the quantitative expressions developed on the basis of 1:1 stoichiometry was taken to imply the operation of the lectin in monovalent mode. The aim of the present communication is to examine more closely the theoretical aspects of the quantification; and hence to identify the actual assumptions that were inherent in the analyses.

2. Theory

In both quantitative applications of capillary zone electrophoresis the interaction of the lectin with a charged saccharide has been quantified by determining the effect of ligand concentration upon the electrophoretic mobility of the protein (acceptor, A). The parameter being measured is the constituent electrophoretic mobility, $\bar{\mu}_A$, defined [7,8] by

$$\bar{\mu}_A = \left[\mu_A C_A + \sum_1^p \left(\mu_{AS_i} C_{AS_i} \right) \right] / \bar{C}_A \qquad (1a)$$

$$\bar{C}_A = C_A + \sum_1^p C_{AS_i} \qquad (1b)$$

0021-9673/95/$09.50
SSDI 0021-9673(95)00097-6

a system in which acceptor, A, characterized mobility μ_A and present at free molar con- ıtration C_A, possesses p sites for interaction :h ligand (saccharide), S. Complexes AS_i nere $1 \leq i \leq p$), characterized by mobilities s_i, are present at molar concentrations C_{AS_i}, ;ereupon the total acceptor concentration, $\bar{C}_A$, obtained by summing the concentrations of all :eptor-containing species (Eq. 1b). As noted eviously [1–6], the binding constant for a stem restricted to 1:1 complex formation ($p =$ is readily determined from the dependence of upon C_S, the concentration of saccharide cluded in the electrophoretic medium. How- er, the decision [1,2] to ascribe p a value of ıity is in conflict with the quaternary structure hibited by the various lectins investigated.

For acceptors with more than one binding site r ligand ($p > 1$), an analytical solution to Eq. 1 quires specification of μ_{AS_i}, the electrophoretic obility of each acceptor–ligand complex, AS_i $\leq i \leq p$), as well as its equilibrium concen- ation. Even under circumstances where all :eptor–ligand interactions are governed by a ngle intrinsic binding constant [9], K_A, the roblem of its determination is intractable with- ut invoking a formal relationship between the ıagnitudes of the various μ_{AS_i}. By making the :asonable approximation [8] that each succes- ıve attachment of a charged ligand to a protein ives rise to a constant incremental change in rotein migration rate, the constituent mobility $\bar{\mu}_A$) is related to the mobility of free acceptor μ_A) by the expression [10,11]

$$(\bar{\mu}_A/\mu_A) - 1] = (p\delta)K_A C_S/(1 + K_A C_S) \quad (2)$$

In this equation $\delta = (\mu_{AS_i} - \mu_{AS_{i-1}})/\mu_A$ is the ncremental change in mobility expressed as a raction of the mobility of free A. The two arameters that emanate from the rectangular ıyperbolic dependence of $[(\bar{\mu}_A/\mu_A) - 1]$ upon ree ligand concentration, C_S, thus define the ntrinsic binding constant, K_A, and $(p\delta) =$ $[(\mu_{AS_p}/\mu_A) - 1]$. Multiplication of the latter parameter by μ_A yields the difference between the mobilities of ligand-saturated and free acceptor species. Because no account is taken in Eq. 2 of the consequences of endosmotic flow through the capillary, the mobilities incorporated into the analysis must be corrected for such effects.

In the original measurement of binding constants for lectin–carbohydrate interactions by capillary zone electrophoresis [1] the migration rate was defined in terms of time taken by the acceptor zone to migrate from the point of application to the detection point. On the grounds that the time taken to migrate a fixed distance is inversely proportional to mobility, the analogue of Eq. 2 becomes

$$[1 - (t_A/\bar{t}_A)] = [1 - (t_A/t_{AS_p})]K_A C_S/(1 + K_A C_S) \quad (3)$$

where $\bar{t}_A$ is the retention time for acceptor in the presence of a given ligand concentration, C_S; and where t_A and t_{AS_p} are the corresponding retention times for free and ligand-saturated acceptor. Like their electrophoretic mobility counterparts in Eq. 2, these retention times need to be corrected for variations in endosmotic flow.

3. Applications

Because the fundamental quantitative expressions are initially derived in terms of electrophoretic mobilities, the first capillary electrophoresis study of ligand binding to be considered employs results presented in that format. Fig. 1a summarizes results obtained by capillary electrophoresis for the interaction of fucose 1-phosphate with the slowest-migrating component of *Tetragonolobus purpureas* lectin [2]. Non-linear regression analysis of the experimental results in terms of Eq. 2 yields an intrinsic association constant (± 2 standard error of the mean, SEM) of 5600 (± 800) M^{-1} and a value of 0.094 (± 0.001) for $p\delta$. If, for example, the lectin were tetrameric ($p = 4$), the latter parameter would imply that the incremental change in mobility for each successive ligand attachment is 2.35% of the mobility of free lectin.

The second illustration of the present approach (Fig. 1b) employs retention time data for

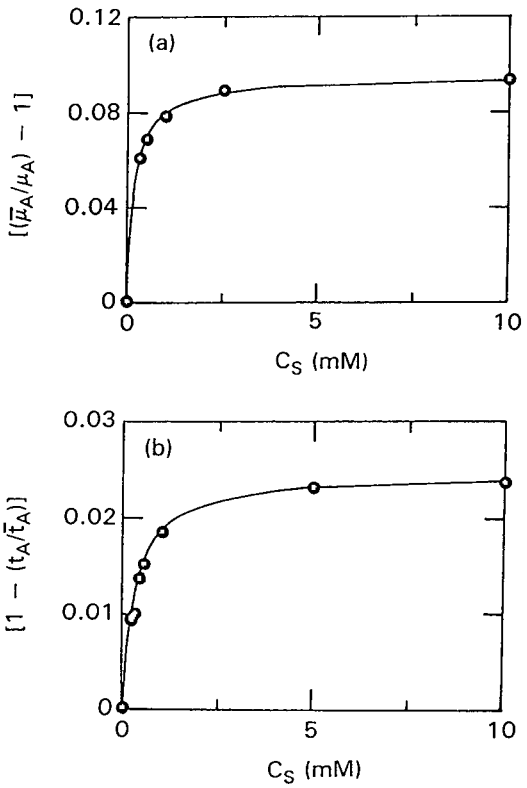

Fig. 1. Evaluation of binding constants by capillary zone electrophoresis. (a) Plot, in accordance with Eq. 2, of published electrophoretic mobility data [2] for the interaction of fucose 1-phosphate with the slowest-migrating component of *T. purpureas* lectin. (b) Plot, in accordance with Eq. 3, of published retention time data [1] for the interaction of lactobionic acid with *R. communis* agglutinin.

the interaction of lactobionic acid with *Ricinus communis* agglutinin, the results being taken from the original study of ligand binding by capillary electrophoresis [1]. Values (± 2 SEM) of 2900 (± 500) M^{-1} and 0.025 (± 0.001) are obtained for the intrinsic binding constant and $(t_A - t_{AS_p})$, respectively, by non-linear regression analysis of the results in terms of Eq. 3.

4. Discussion

The present consideration of the use of capillary electrophoresis for the characterization of interactions between lectins and charged saccharides has eliminated the invalid assumption, inherent in the earlier analyses [1,2], that the lectins exhibit univalence towards carbohydrates. Nevertheless, despite its elimination of this undesirable feature of the earlier analyses, the present approach is readily shown to differ very little from its predecessors. Although linear transformation of rectangular hyperbolic expressions is not recommended because of the consequent statistical distortion of the data distribution that results from such transformation [12], Eqs. 2 and 3 may be written in double-reciprocal format as

$$\frac{1}{[(\bar{\mu}_A/\mu_A) - 1]} = \frac{1}{[(\mu_{AS_p}/\mu_A) - 1]} + \frac{1}{K_A[(\mu_{AS_p}/\mu_A) - 1]C_S} \quad (4a)$$

$$\frac{1}{[1 - (t_A/\bar{t}_A)]} = \frac{1}{[1 - (t_A/t_{AS_p})]} + \frac{1}{K_A[1 - (t_A/t_{AS_p})]C_S} \quad (4b)$$

to conform with the practices adopted earlier [1,2]. As required, these equations are essentially identical with the expressions deduced in those publications if a value of unity is assigned to p. Indeed, the magnitudes of the binding constants deduced from the present analysis must also duplicate those reported in the original publications [1,2]. However, whereas conformity of the results with these expressions was taken to justify an assumption that the lectin–carbohydrate interactions were restricted to 1:1 complex formation, a more plausible interpretation is that the linear double-reciprocal plots (Figs. 3 and 2 of [1] and [2], respectively) signify an approximately constant incremental difference between the mobilities of successive AS_i complexes. On that basis the constants reported for the binding of lactobionic acid to *R. communis* agglutinin, peanut agglutinin and soybean agglutinin [1], and of fucose 1-phosphate to *T. purpureas* lectins [2] should simply be regarded as intrinsic association constants for the interactions of the charged saccharides with equivalent and independent binding sites on the various lectins. In other

words, the importance of this reappraisal of the earlier quantitative investigations [1,2] is its identification of the parameter (the intrinsic binding constant) that is actually measured; and its identification of the assumptions inherent in the application of capillary electrophoresis [1–6] as well as conventional gel electrophoresis [13] to the quantitative characterization of interactions between charged ligands and multivalent acceptor systems.

In summary, this reappraisal of the evaluation of binding constants by capillary electrophoresis serves to bring the method into line with earlier electrophoretic procedures [8,10,11], in which the inherent assumptions/approximations associated with the interpretation of constituent migration rates for multivalent acceptors had already been identified. Such strengthening of its theoretical basis adds considerably to the quantitative potential of capillary electrophoresis, which has great advantages over its electrophoretic predecessors from the viewpoints of experiment duration, material requirements, and resolving power.

Acknowledgement

The support of this research by the Australian Research Council is gratefully acknowledged.

References

[1] S. Honda, A. Taga, K. Suzuki, S. Suzuki and K. Kakehi, *J. Chromatogr.*, 597 (1992) 377.
[2] R. Kuhn, R. Frei and M. Christen, *Anal. Biochem.*, 218 (1994) 131.
[3] Y.-H. Chu and G.M. Whitesides, *J. Org. Chem.* 57 (1992) 3524.
[4] Y.-H. Chu, L.Z. Avila, H.A. Biebuyck and G.M. Whitesides, *J. Med. Chem.*, 35 (1992) 2915.
[5] J.L. Carpenter, P. Camilieri, D. Dhanak and D. Goodall, *J. Chem. Soc., Chem. Commun.*, (1992) 804.
[6] L.Z. Avila, Y.-H. Chu, E.C. Blossey and G.M. Whitesides, *J. Med. Chem.*, 36 (19093) 126.
[7] R.A. Alberty and H.H. Marvin, Jr., *J. Phys. Colloid Chem.*, 54 (1950) 47.
[8] R.F. Smith and D.R. Briggs, *J. Phys. Colloid Chem.*, 54 (1950) 33.
[9] I.M. Klotz, *Arch. Biochem.*, 9 (1946) 109.
[10] R.H. Drewe and D.J. Winzor, *Biochem. J.*, 159 (1976) 737.
[11] L.D. Ward and D.J. Winzor, *Arch. Biochem. Biophys.*, 209 (1981) 650.
[12] I.M. Klotz, *Trends Pharm. Sci.*, 4 (1983) 253.
[13] V. Hořejší and M. Tichá, *J. Chromatogr.*, 376 (1986) 49.

1995 International Symposium & Exhibit on

PREPARATIVE CHROMATOGRAPHY

June 11-14, 1995

Washington, DC, USA

Organized by Professor Georges Guiochon
University of Tennessee and Oak Ridge National Laboratory

LECTURE & POSTER PRESENTATIONS
WORKSHOPS
SEMINARS
ROUNDTABLE DISCUSSIONS
CASE STUDIES
INSTRUMENTATION EXHIBIT

Sponsored by the Washington Chromatography Discussion Group

For more information contact: Janet Cunningham, c/o Barr Enterprises
P.O. Box 279, Walkersville, Maryland 21793 USA
(tele. 301-898-3772, fax 301-898-5596)

PRINCIPAL COMPONENTS

By **D.L. Massart** and **P.J. Lewi**

This attractively packaged set, comprising 4 videos, a manual and a software package, is an introduction to the use of principal components analysis (PCA) and related methods in chemometrics. Emphasis has been placed on the use of PCA to display graphically the structure of data sets or to extract graphically information from such a set (display methods). However, links are provided to several other important methods, such as evolving factor analysis, principal component regression and partial least squares.

In order to induce students to learn PCA, and convince them of the usefulness of the methods, several real-life examples have been included. These examples have been chosen to illustrate the generality of the data analysis approach. The data pertain to food, industrial and environmental analysis, animal experimentation, medicinal chemistry, virology and epidemiology. In the software section an additional example concerned with food analysis has been added. Section 3 of the manual contains a complete list of figures. This allows the user to look at some of the figures in a more leisurely fashion or to re-read text which has been heard when viewing the videos. Some of the visuals and some of the texts (occasionally shortened) have been included in this section.

Two types of software augment this series. The first is a tutorial version of a commercial software package called SPECTRAMAP, which has been modified for didactical use. SPECTRAMAP is a performant software for methods derived from PCA that gives excellent display quality.

The other type of software is a listing of a MATLAB® program. In order to understand completely a mathematical algorithm or method, the authors recommend the user to program it himself, using MATLAB®. In this way the user can also obtain all the intermediate results, thereby understanding what happens with a data set when analyzed by PCA. This section also contains an additional data set with which the user can experiment with the software. Some hints are given in to teachers and self-learners on how to use the material to optimize results.

Contents: VIDEOS:

Part A: Principal components as display method.
Part B: Display variables and relationships between variables and objects.
Part C: Singular value decomposition; Eigenvalues; Evolving factor analysis; Software and exercises.
Part D: The display of latent variables in tabulated data.

A 25-minute demonstration video, containing a representative selection from all four video tapes is available at cost price.

ELSEVIER

An imprint of Elsevier Science

MANUAL:

1. Introduction.
2. Proposed didactical concepts.
3. List of Visuals.
4. Software Section.

4A. SPECTRAMAP (P.J. Lewi, J. Van Hoof, M. Nijs).

4B. A MATLAB program for principal components analysis (M. Massart).

©1994 Complete set VHS PAL
Price: Dfl. 1750.00 (US$1000.00)
ISBN 0-444-81622-4
Complete set VHS NTSC
Price: Dfl. 1750.00 (US$1000.00)
ISBN 0-444-81655-0
Manual
Price: Dfl. 65.00 (US$37.00)
ISBN 0-444-81653-4
Demonstration copy
VHS PAL Video
Price: Dfl. 50.00 (US$28.50)
ISBN 0-444-81980-0
Demonstration copy
VHS NTSC Video
Price: Dfl. 50.00 (US$28.50)
ISBN 0-444-81979-7

Additional copies of the manual may be ordered separately.

ORDER INFORMATION

ELSEVIER SCIENCE B.V.
P.O. Box 330
1000 AH Amsterdam
The Netherlands
Fax: +31 (20) 5862 845

For USA and Canada
P.O. Box 945
Madison Square Station
New York, NY 10159-0945
Fax: +1 (212) 633 3680

US$ prices are valid only for the USA & Canada and are subject to exchange rate fluctuations; in all other countries the Dutch guilder price (Dfl.) is definitive. Customers in the European Union should add the appropriate VAT rate applicable in their country to the price(s). Books are sent postfree if prepaid.

PUBLICATION SCHEDULE FOR THE 1995 SUBSCRIPTION

Journal of Chromatography A and *Journal of Chromatography B: Biomedical Applications*

MONTH	1994	J	F	M	A	M	
Journal of Chromatography A	Vols. 683–688	689/1 689/2 690/1 690/2	691/1 + 2 692/1 + 2 693/1 693/2	694/1 694/2 695/1 695/2	696/1 696/2 697/1 + 2 698/1 + 2	699/1 699/2 700/1 + 2 702/1 + 2	The publication schedule for further issues will be published later.
Bibliography Section				713/1			
Journal of Chromatography B: Biomedical Applications		663/1 663/2	664/1 664/2	665/1 665/2	666/1 666/2	667/1 667/2	

INFORMATION FOR AUTHORS

(Detailed *Instructions to Authors* were published in *J. Chromatogr. A*, Vol. 657, pp. 463–469. A free reprint can be obtained by application to the publisher, Elsevier Science B.V., P.O. Box 330, 1000 AH Amsterdam, Netherlands.)

Types of Contributions. The following types of papers are published: Regular research papers (full-length papers), Review articles, Short Communications and Discussions. Short Communications are usually descriptions of short investigations, or they can report minor technical improvements of previously published procedures; they reflect the same quality of research as full-length papers, but should preferably not exceed five printed pages. Discussions (one or two pages) should explain, amplify, correct or otherwise comment substantively upon an article recently published in the journal. For Review articles, see inside front cover under Submission of Papers.

Submission. Every paper must be accompanied by a letter from the senior author, stating that he/she is submitting the paper for publication in the *Journal of Chromatography A* or *B*.

Manuscripts. Manuscripts should be typed in **double spacing** on consecutively numbered pages of uniform size. The manuscript should be preceded by a sheet of manuscript paper carrying the title of the paper and the name and full postal address of the person to whom the proofs are to be sent. As a rule, papers should be divided into sections, headed by a caption (*e.g.*, Abstract, Introduction, Experimental, Results, Discussion, etc.). All illustrations, photographs, tables, etc., should be on separate sheets.

Abstract. All articles should have an abstract of 50–100 words which clearly and briefly indicates what is new, different and significant. No references should be given.

Introduction. Every paper must have a concise introduction mentioning what has been done before on the topic described, and stating clearly what is new in the paper now submitted.

Experimental conditions should preferably be given on a *separate* sheet, headed "Conditions". These conditions will, if appropriate, be printed in a block, directly following the heading "Experimental".

Illustrations. The figures should be submitted in a form suitable for reproduction, drawn in Indian ink on drawing or tracing paper. Each illustration should have a caption, all the *captions* being typed (with double spacing) together on a *separate sheet*. If structures are given in the text, the original drawings should be provided. Coloured illustrations are reproduced at the author's expense, the cost being determined by the number of pages and by the number of colours needed. The written permission of the author and publisher must be obtained for the use of any figure already published. Its source must be indicated in the legend.

References. References should be numbered in the order in which they are cited in the text, and listed in numerical sequence on a separate sheet at the end of the article. Please check a recent issue for the layout of the reference list. Abbreviations for the titles of journals should follow the system used by *Chemical Abstracts*. Articles not yet published should be given as "in press" (journal should be specified), "submitted for publication" (journal should be specified), "in preparation" or "personal communication".

Vols. 1–651 of the *Journal of Chromatography*; *Journal of Chromatography, Biomedical Applications* and *Journal of Chromatography, Symposium Volumes* should be cited as *J. Chromatogr.* From Vol. 652 on, *Journal of Chromatography A* (incl. Symposium Volumes) should be cited as *J. Chromatogr. A* and *Journal of Chromatography B: Biomedical Applications* as *J. Chromatogr. B.*

Dispatch. Before sending the manuscript to the Editor please check that the envelope contains four copies of the paper complete with references, captions and figures. One of the sets of figures must be the originals suitable for direct reproduction. Please also ensure that permission to publish has been obtained from your institute.

Proofs. One set of proofs will be sent to the author to be carefully checked for printer's errors. Corrections must be restricted to instances in which the proof is at variance with the manuscript.

Reprints. Fifty reprints will be supplied free of charge. Additional reprints can be ordered by the authors. An order form containing price quotations will be sent to the authors together with the proofs of their article.

CALL FOR PAPERS

Fourth International Symposium on

HYPHENATED TECHNIQUES IN CHROMATOGRAPHY
HYPHENATED CHROMATOGRAPHIC ANALYZERS
(HTC 4)

The Saint John's Conference Center, Bruges (Belgium), February 6 - 9, 1996

The purpose of this fourth symposium will again be to highlight and treat in-depth recent developments and progress in the field of chromatographic hyphenations. It will cover all fundamental aspects, instrumental developments and applications of the various hyphenated chromatographic techniques e.g. coupling of LC to LC,GC and SFC ; MS, FTIR, AED and other techniques coupled with GC, (HP)LC, SFC and CZE; on-line air traps GC; purge-and-trap-GC, etc. Emphasis will also be placed on the design of hyphenated, on-line and at-line chromatographic analyzers.

The **scientific programme** will include oral presentations in plenary and parallel sessions, poster presentations and discussion sessions with prominent scientists. A **technical exhibition** will give an overview of instruments, books and accessories. The latest developments in instrumentation will be presented during workshop type **seminars**. Finally, a social and an accompanying persons programme including optional tours in Bruges and Northern Belgium will be offered.

The symposium will be preceeded by **workshops** on February 5 and 6, 1996.

A special volume of the *Journal of Chromatography* will be dedicated to the accepted and reviewed papers, which will be channelled through the usual refereeing system.

Participants who wish to present a paper are hereby invited to submit an abstract. Deadline for abstracts : **June 30, 1995** and for last minute posters : **December 15,1995**.

Submission forms for papers, enquiries about the technical exhibition and all other information may be obtained from the HTC 4-Congress Secretariate, Lucas Henninckstraat 18, B-2610 Wilrijk (Belgium), tel.: + 32 (3) 561.28.31, fax : + 32 (3) 828.89.61

0021-9673(19950407)696:1;1-I